5-2013

Constraining Ice Advance and Linkages to Paleoclimate of Two Glacial Systems in the Olympic Mountains, Washington and the Southern Alps, New Zealand

Cianna E. Wyshnytzky
Utah State University

CONSTRAINING ICE ADVANCE AND LINKAGES TO PALEOCLIMATE OF TWO GLACIAL SYSTEMS IN THE OLYMPIC MOUNTAINS, WASHINGTON AND THE SOUTHERN ALPS, NEW ZEALAND

by

Cianna E. Wyshnytzky

A thesis submitted in partial fulfillment
of the requirements for the degree

of

MASTER OF SCIENCE

in

Geology

Approved:

UTAH STATE UNIVERSITY
Logan, Utah

2013

ABSTRACT

Constraining Ice Advance and Linkages to Paleoclimate of Two

Glacial Systems in the Olympic Mountains, Washington

and the Southern Alps, New Zealand

by

Cianna E. Wyshnytzky, Master of Science

Utah State University, 2013

Major Professor: Tammy M. Rittenour
Department: Geology

This thesis investigated marine isotope stage (MIS) 3-2 glacial sequences in the South Fork Hoh River Valley, Washington and the Lake Hawea Valley, New Zealand. Research objectives were to reconstruct the style and timing of ice advance in both areas and to assess the viability of luminescence dating of glacial sediments in various depositional facies and distances from the ice front. This thesis focused on the sedimentology and stratigraphy of surficial and older glacial sequences in the South Fork Hoh and Lake Hawea areas and used OSL and radiocarbon dating techniques to establish age control for the deposits. Specifically, this research identified, described, and dated the stratigraphy of glacial sequences in order to reconstruct ice dynamics. This work also presents updated geomorphic maps for both study areas as an additional way to show ice advance and retreat events recorded in deposited sediment and geomorphic surfaces.

The glacial sequence expressed in the Lake Hawea moraine exposure shows four distinct depositional events that represent retreat from an ice position down-valley, re-advance to the

Hawea moraine position, and subsequent retreat and deglaciation broadly spanning ~32-18 ka. These results document the terminal glacial advance and subsequent retreat in the Lake Hawea Valley and contribute to the wider swath of research studying the last phase of glacial retreat and its connections to climate on the South Island of New Zealand. The Hawea chronology corresponds to other glacial records and paleoclimate reconstructions from the South Island that collectively suggest the commencement of deglaciation at ~18 ka.

Three late Pleistocene ice positions are preserved in the South Fork Hoh River Valley, here referred to as South Fork 1-3 (SF 1-3). One of these positions has not previously been recognized in this valley or in the mainstem Hoh River Valley. Optically stimulated luminescence (OSL) and radiocarbon (^{14}C) ages are generally consistent throughout the valley. These findings advocate for a detailed sedimentologic and stratigraphic approach to glacial deposits and questions whether a similar advance or still-stand occurred in other valleys in the region. If so, this may reveal information regarding climate influences on MIS 2 glaciers in the Olympic Mountains.

This research also assesses the applicability of OSL dating to glacial deposits in both field areas. Quartz OSL dating was used in the South Fork Hoh study area; however, quartz produced unreliable results in the Hawea study area, so samples were therefore assessed using feldspar methods. The results advocate for a facies-based sampling approach in glacial settings, where better sorted sandy facies and more distal deposits produce better bleached and more reliable age results than other deposits.

(206 pages)

PUBLIC ABSTRACT

Constraining ice advance and linkages to paleoclimate of two glacial systems in the Olympic Mountains, Washington and the Southern Alps, New Zealand

by

Cianna E. Wyshnytzky, Master of Science

Utah State University, 2013

Major Professor: Tammy M. Rittenour
Department: Geology

This thesis investigates glacial sediments in the South Fork Hoh River Valley, Washington and the Lake Hawea Valley, New Zealand that were deposited during the last glacial period. Research objectives were to reconstruct the style and timing of glacier advance and retreat in both areas and to assess the viability of luminescence dating of sediments in glacial environments.

Glaciers are influenced primarily by temperature and precipitation. Valley glaciers, like those in the Olympics Mountains and Southern Alps, are thought to respond relatively rapidly to climate fluctuations in comparison to continental ice sheets. Understanding how these glacial systems responded to past climate fluctuations therefore holds importance for understanding how modern glaciers, which are important for water resources and stream-flow habitat, may respond to future climate change.

Fieldwork for this project was conducted over the course of approximately ten weeks, during which sites in the Olympic Mountains and Southern Alps were visited, described, and

sampled. Chronologic constrain on sediment deposition was obtained through radiocarbon and luminescence dating. Radiocarbon samples were sent to the Lawrence Livermore National Laboratory for analysis, whereas luminescence samples were processed and analyzed at the Utah State University Luminescence Laboratory. Funding for this project was obtained from National Science Foundation grants (NSF-EAR 1024657 and 1024850) and awards from the Utah State University Department of Geology.

DEDICATION

Some may find it odd to dedicate a thesis to a furry, four-legged friend. This thesis, however, is dedicated to Geo the dog, who *adopted me* shortly after my arrival in Utah. This boy has forced me to take invaluable breaks from my work, has proven to be an excellent fieldwork companion, and has a remarkable ability to put a smile on my face when needed. He's also the best fieldwork companion a girl could ask for. You, Big G, have played the biggest role in maintaining my sanity, and I look forward to many more years.

ACKNOWLEDGMENTS

I would sincerely like to thank the National Science Foundation, the USU Department of Geology, and the ISU of Department of Geosciences for their generous funding and support of this research project. I would also like to acknowledge and especially thank Michelle Summa Nelson at the USU Luminescence Laboratory for her endless help in sample analysis. I am grateful for my committee members, Glenn Thackray and Joel Pederson, for their help throughout the past two years. Courses with Joel helped me especially refine mapping, field, and writing skills, and his perspective as a non-glacial geomorphologist has been important as a set of eyes and ears outside the project. This project would not have been possible without Glenn's previous work and continued interest in unraveling the history of glaciation in the Olympic Mountains and Southern Alps. His expertise and experience in both field areas has been crucial to fieldwork planning and interpretations. As the biggest proponent of tea time, fine wines and cheeses, and skipping stones in the field, Glenn's presence during trips extended to maintaining positive morale and providing the important perspective of fun and relaxation in any situation.

I would especially like to thank Tammy Rittenour, my primary adviser, for the opportunity to join the graduate program at USU through full funding. Tammy spent countless hours editing grant proposals and thesis drafts, writing references, and discussing data and interpretations associated with my work. Her encouragement and support in presenting my research as various conferences significantly impacted dissemination of my research and confidence in my presenting skills. I will be continually grateful for the opportunity that I have had to work in the Luminescence Lab, and look forward to continued collaboration with Tammy in published chapters of my thesis. I will continue to "take one for the team" with your voice echoing in my head, Tammy.

Many thanks to others that played significant parts in this research. The National Park Service authorized research access and collecting permits for Olympic National Park. Katie Marshall assisted greatly with fieldwork, and her companionship on the coast and in the rainforest was ever-valuable. Jamie Shulmeister, as well as his students Olivia Hyatt and Lucas Evans, and Allan Ashworth provided valuable insight in the field and through email correspondence. Lastly, I would like to thank my family and friends for their support from afar and my friends in Logan for their feedback, adventures, and camaraderie.

Cianna E. Wyshnytzky

CONTENTS

LIST OF TABLES

LIST OF FIGURES

CHAPTER 1

Introduction

This thesis investigated marine isotope stage (MIS) 3-2 glacial sequences in the South Fork of the Hoh River valley, Washington and the Lake Hawea valley, New Zealand. The primary research objective were to reconstruct the style and timing of ice advance in both areas. More specific research goals include: 1) describing and interpreting the sedimentology and stratigraphic architecture of glacial deposits in areas with similar maritime climate settings, yet in opposite hemispheres; 2) establishing a chronology for the deposits; and 3) comparing these glacial sequences and reconstructions of ice dynamics to existing paleoclimate data and regional glacial sequences.

Glacial systems in humid maritime regions remain understudied with respect to ice dynamics and responses to climate forcing. This thesis focuses on the sedimentology and stratigraphy of surficial and older buried glacial sequences in the South Fork Hoh and Lake Hawea areas and uses optically stimulated luminescence (OSL) and radiocarbon (^{14}C) dating techniques to establish age control for the deposits. This work also presents updated geomorphic maps for both study areas in order to help reconstruct ice advance and retreat events recorded in sediment, stratigraphy, and geomorphic surfaces.

Significance of Study Areas

Research areas in the Olympic Mountains, Washington and Southern Alps, New Zealand were chosen because they have maritime climates, are at similar latitudes, and are associated with mountain ranges that capture moisture from Westerlies. These mountain ranges additionally host (and hosted) mountain glaciers. Such glaciers in humid settings are thought to

be highly sensitive to minor climate fluctuations (e.g. Thackray, 2008; Anderson and Makintosh, 2006; Rother and Shulmeister, 2006). Most importantly, preliminary evidence suggests synchronous glacial advances in both study areas during MIS 4-2 (McCarthy et al., 2008; Thackray, 2008; Shulmeister et al., 2010), which is opposite of what is expected given opposed insolation signals between the Northern and Southern Hemispheres.

Ice advances at both locations from 70-60 ka (MIS 4) and 40-30 ka (MIS 3) occurred during Southern Hemisphere insolation minima (and Northern Hemisphere insolation maxima), and ice advances occurred from 25-20 ka (MIS 2) during a Northern Hemisphere insolation minimum (and a Southern Hemisphere insolation maximum) (e.g Williams, 1996; Almond et al., 2001; Thackray, 2001; Preusser et al., 2005; McCarthy et al., 2008; Doughty and Denton, 2009; Thackray et al., 2009; Shulmeister et al., 2010) (Figure 1.1). The synchronous nature of advances between the Olympic Mountains and Southern Alps suggests a possible interhemispheric climate transfer via the Pacific Ocean. However, this is merely a hypothesized linkage, as insolation-driven mechanisms for trans-Pacific precipitation patterns remain poorly understood despite model-based research (Pinot et al., 1999; Khodri et al., 2001) and solar-insolation gradient studies (Raymo and Niscancioglu, 2003; Loutre et al., 2004). Teleconnections specifically directed from the Northern Hemisphere to the Southern Hemisphere are typically hypothesized because of the influence of large Northern Hemisphere continental ice sheets on global albedo and atmospheric circulation. Here we hypothesize a Southern Hemisphere to Northern Hemisphere directed climate transfer due to possible changes in ocean or atmosphere circulation, as Northern Hemisphere glaciers are not expected to advance maximum Northern Hemisphere solar insolation, from 30-40 ka (Figure 1.1).

Temperature and precipitation influence glacial mass balance by modulating ablation and accumulation, which in turn influence ice volume, glacial dynamics, and ice-margin position

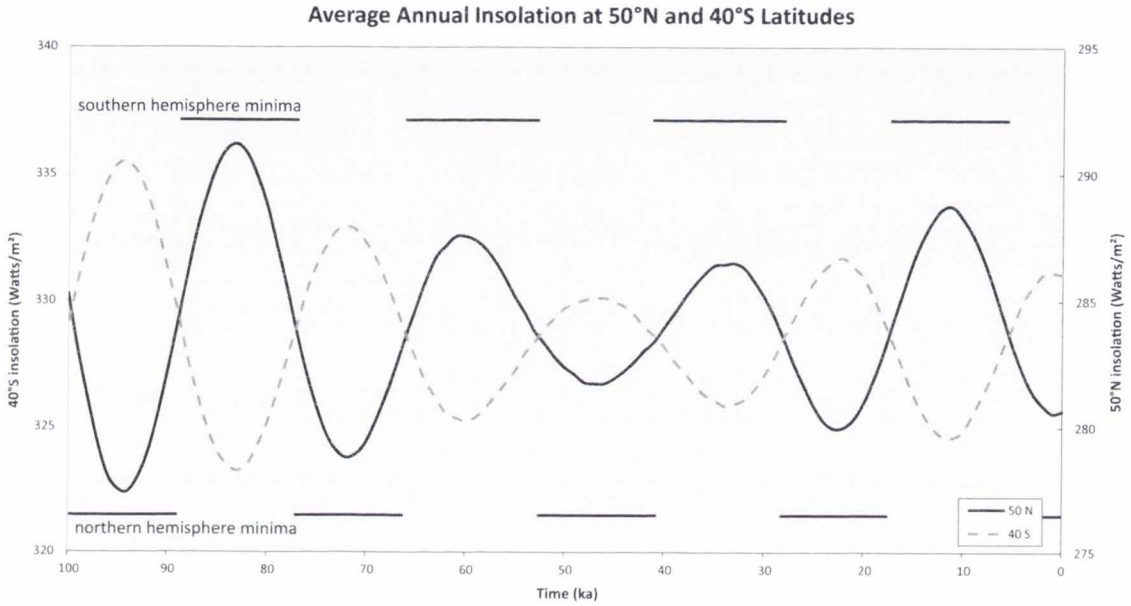

Figure 1.1 Approximate average annual insolation values, based on mid-month insolation for each month, for 50°N (Olympic Mountains, Northern Hemisphere) and 40°S (Southern Alps, Southern Hemisphere) from Berger and Loutre (1991). Black bars indicate insolation minima.

(Paterson, 1994). Valley glaciers respond relatively rapidly to climatic fluctuations in comparison to continental ice sheets due to their small size (Gillespie and Molnar, 1995). In the Olympic Mountains, coalescing glaciers extended radially from the central Olympic Mountains, while in New Zealand, valley glaciers were fed by a regional ice cap extending northeast-southwest along the Southern Alps. Large valley glaciers reached both study areas, which contain well-exposed sedimentary sequences, allowing detailed stratigraphic descriptions and analyses. Furthermore, more recent advances over-rode older glacial deposits, rendering traditional geomorphic mapping, analyses, and dating techniques (such as cosmogenic nuclide methods) of limited value in determining the long-term glacial histories of these areas.

This research is part of a larger National Science Foundation funded project that focuses on the style and timing of glacial advances in the Olympic Mountains and Southern Alps and their paleoclimate implications (NSF grants EAR 1024657 and 1024850). The Olympic-New Zealand Glacial and Paleoclimate (ONZGAP) project is designed to test the hypothesis that Pleistocene glacial advances are synchronous between study areas, due to some interhemispheric climate transfer, as previously suggested by Lowell et al. (1995), Denton et al. (1999), and Vandergoes et al. (2005). Temperature-based reconstructions from chironomids and beetles can help determine the influence of temperature on these glacial environments, and improved chronologies in both areas are crucial to test the hypothesis of the project.

Several scenarios suggest climate teleconnections between the Northern and Southern Hemispheres:

- An ice advance in the Olympic Mountains and Southern Alps during a Northern Hemisphere insolation minimum ~25-20 ka (and therefore Southern Hemisphere insolation maximum) (Thackray, 2001) (Figure 1.1) suggests a transfer of Northern

Hemisphere cooling to the Southern Hemisphere, as expected to some extent due to the strong influence from Northern Hemisphere ice sheets (Gillespie and Molnar, 1995).

- A possible advance on the Olympic Peninsula at ~30-40 ka may suggest a transfer of Southern Hemisphere cooling associated with a Southern Hemisphere insolation minimum to the Northern Hemisphere (Vandergoes et al., 2005; Sutherland et al., 2007) (Figure 1.1). Conversely, a Northern Hemisphere insolation maximum may drive increased Westerly circulation and moisture delivery to the coastal maritime climate of the Olympic Mountains while a Southern Hemisphere insolation minimum at this time may not be directly related. Therefore, controls on the major glacial advances may be a result of either interhemispheric climate teleconnections or more local influences. We would expect, however, to see Olympic glaciers retreat during Northern Hemisphere maxima based on assumed warmer Northern Hemisphere temperatures alone, i.e. without taking the influence of increased insolation on precipitation into account.
- Furthermore, the Olympic Mountain glacial system is unique in that the MIS 4-3 ice extents were greater than during MIS 2. This contrasts with other more continental records in North America, where MIS 2 ice extents were greatest primarily due to the influence of temperature (i.e. insolation changes) and secondarily due to the influence of moisture, particularly from more localized sources (Munroe et al., 2006; Thackray, 2008). This difference suggests a potential stronger linkage to Pacific Ocean circulation and/or the influence of Westerlies on orographically induced precipitation of the Olympic Mountains.

This thesis research focuses on glacial sequences from the South Fork Hoh River, Washington (~47°47' N) and Lake Hawea, New Zealand (~44°35'S), which lie at similar maritime Pacific latitudes in opposite hemispheres, and therefore may reveal details about the timing and

style of ice advance in the two study areas. If results confirm that advances are synchronous between the study areas, then mechanisms for this synchrony can be proposed. Correlation, however, may not necessarily connect these advances to the same forcing mechanism. More sites beyond the scope of this project will be investigated to confirm any apparent correlations.

Research Objectives and Goals

The research in this thesis aims to provide greater resolution on mountain glacier ice dynamics prior to and during the global LGM ice of the western Olympic Mountains of Washington and the eastern Southern Alps of New Zealand. The broader significance of this project lies in understanding the timing and dynamics of ice and connections to paleoclimate forcings in these humid mountain-valley glacial systems. This research, combined with chronologies from ice-marginal records in these regions, may help to reconstruct the larger image of interhemispheric climate teleconnections. It is expected that if the same global climate changes force glacial cycles in both hemispheres, the timing of ice advance will be within the error of dating techniques (typically ± 10-20%). This research also seeks to assess the application of OSL dating to glacial deposits in the two study areas.

Thesis Structure

To summarize, the goals of this thesis are to develop a chronostratigraphy of glacial deposits in order to reconstruct the glacial history of both study areas. The framework includes five chapters and is designed so that each of the three main chapters is prepared as an individual paper for publication. Chapter 2 describes the sedimentology and geomorphology of the most recent glacial advances in the Hawea River valley, New Zealand, and is intended for the journal *Quaternary Research*. The authors of this chapter additionally include Tammy M.

Rittenour, Glenn D. Thackray, and Jamie Shulmeister. Chapter 3 assesses the style and timing of ice dynamics during the global last glacial maximum, including three periods of ice re-advance and moraine formation, in the South Fork Hoh River valley, Washington, and is intended for the journal *Quaternary Science Reviews*. The authors of this chapter additionally include Tammy M. Rittenour and Glenn D. Thackray. As explained in Chapter 4, OSL dating of glacial sediments is riddled with complications. Results suggest that although difficulties do exist, they may be lessened with careful sampling procedures and laboratory protocol, and can therefore be used to extend the use of OSL dating in similar glacial environments. This chapter is intended for the journal *Quaternary Geochronology*. The authors of this chapter additionally include Tammy M. Rittenour and Michelle C. Summa-Nelson. Finally, Chapter 5 draws conclusions from the research project overall and discusses potential future work.

References Cited

Almond, P. C., Moar, N. T., and Lian, O. B., 2001, Reinterpretation of the glacial chronology of South Westland, New Zealand. New Zealand Journal of Geology & Geophysics 44: 1-15.

Anderson, B. and Mackintosh, A., 2006, Temperature change is the major driver of late-glacial and Holocene glacier fluctuations in New Zealand. Geology 34(2): 121-124.

Berger, A. and Loutre, M. F., 1991, Insolation values for the climate of the last 10 million years. Quaternary Science Reviews 10: 297-317.

Denton, G. H., Lowell, T. V., Heusser, C. J., Moreno, P. I., Andersen, B. G., Heusser, L. E., Schlüchter, C., and Marchant, D. R., 1999, Interhemispheric Linkage of Paleoclimate during the Last Glaciation. Geografiska Annaler 81(2): 107-153.

Doughty, A. and Denton, G., 2009, ^{10}Be Cosmogenic exposure ages of Late Pleistocene moraines near the Maryburn Gap of the Pukaki Basin (abstract). Past Climates Symposium and Workshop, Wellington, New Zealand, 15-17 May, 2009.

Gillespie, A. and Molnar, P., 1995, Asynchronous maximum advances of mountain and continental glaciers. Reviews of Geophysics 33: 311-364.

Khodri, M., Leclainche, Y., Ramstein, G., Braconnot, P., Marti, O., and Cortijo, E., 2001, Simulating the amplification of orbital forcing by ocean feedbacks in the last glaciation. Nature 410: 570-574.

Loutre, M., Paillard, D., Vimeux, F., and Cortijo, E., 2004, Does mean annual insolation have the potential to change the climate? Earth and Planetary Science Letters 221: 1-14.

Lowell, T. V., Heusser, C. J., Andersen, B. G., Moreno, P. I., Hauser, A., Heusser, L. E., Schlüchter, C., Marchant, D. R., and Denton, G. H., 1995, Interhemispheric Correlation of Late Pleistocene Glacial Events. Science 269: 1541-1549.

McCarthy, A., Mackintosh, A., Reiser, U., and Fink, D., 2008, Mountain Glacier Chronology from Boulder Lake, New Zealand, Indicates MIS 4 and MIS 2 Ice Advances of Similar Extent. Arctic, Antarctic, and Alpine Research 40(4): 695-708.

Munroe, J. S., Laabs, B. J. C., Singer, B. S., Mickelson, D. M., Refsnider, K. A., and Caffee, M. W., 2006. Latest Pleistocene advance of alpine glaciers in the southwestern Uinta Mountains, Utah, USA: Evidence for the influence of local moisture sources. Geology 34(10): 841-844.

Paterson, W. S. B., 1994, *Physics of Glaciers*. Pergamon, Tarrytown, N. Y., 480.

Pinot, S., Ramstein, G., Harrison, S. P., Prentice, I. C., Guiot, J., Stute, M., Joussaume, S., 1999, Tropical paleoclimates at the Last Glacial Maximum: comparison of Paleoclimate Modeling Intercomparison Project (PMIP) simulations and paleodata. Climate Dynamics 15: 857-874.

Preusser, F., Andersen, B. G., Denton, G. H., and Schlüchter, C., 2005, Luminescence chronology of Late Pleistocene glacial deposits in North Westland, New Zealand. Quaternary Science Reviews 24: 2201-2227.

Raymo, M. E. and Nisancioglu, K., 2003, The 41 kyr world: Milankovitch's other unsolved mystery. Paleoceanography 18(1): 1101-1106.

Rother, H., and Shulmeister, J., 2006, Synoptic climate change as a driver of late Quaternary glaciations in the mid-latitudes of the Southern Hemisphere. Climate of the Past 2: 11-19.

Shulmeister, J., Thackray, G. D., Rieser, U., Hyatt, O. M., Rother, H., Smart, C. C., and Evans, D. J. A., 2010, The stratigraphy, timing and climatic implications of glaciolacustrine deposits in the middle Rakaia Valley, South Island, New Zealand. Quaternary Science Reviews 29: 2362-2381.

Sutherland, R., Kim, K., Zondervan, A., and McSaveney, M., 2007, Orbital forcing of mid-latitude Southern Hemisphere glaciation since 100 ka inferred from cosmogenic nuclide ages of moraine boulders from the Cascade Plateau, southwest New Zealand. Geological Society of America Bulletin 119: 443-451.

Thackray, G. D., 2001, Extensive Early and Middle Wisconsin Glaciation on the Western Olympic Peninsula, Washington, and the Variability of Pacific Moisture Delivery to the Northwestern United States. Quaternary Research 55: 257-270.

Thackray, G. D., 2008, Varied climatic and topographic influences on Late Pleistocene mountain glaciation in the western United States. Journal of Quaternary Science 23(6-7): 671-681.

Thackray, G. D., Shulmeister, J., and Fink, D., 2009, Evidence for expanded Middle and Late Pleistocene glacier extent in northwest Nelson, New Zealand. Geografiska Annaler 91 A (4): 291-311.

Vandergoes, M. J., Newnham, R. M., Preusser, F., Hendy, C. H., Lowell, T. V., Fitzsimons, S. J., Hogg, A. G., Kasper, H. U., and Schlüchter, C., 2005, Regional insolation forcing of late Quaternary climate change in the Southern Hemisphere. Nature 436: 242-245.

Williams, P. W., 1996, A 230 ka record of glacial and interglacial events from Aurora Cave, Fiordland, New Zealand. New Zealand Journal of Geology and Geophysics 39: 225-241.

CHAPTER 2

THE STRATIGRAPHY AND TIMING OF LATE PLEISTOCENE GLACIAL ADVANCES IN THE LAKE HAWEA VALLEY, SOUTH ISLAND, NEW ZEALAND

Abstract

This research documents the marine isotope stage (MIS) 3-2 glacial sequence in the Lake Hawea valley and contributes to greater research efforts on late Pleistocene glaciation and connections to climate on the South Island of New Zealand. The lake bluff stratigraphy and geomorphology of the Hawea moraine at the southern margin of the Lake Hawea valley, South Island, New Zealand permit reconstruction of early MIS 2 history of the valley. The glacial sequence is interpreted to represent four depositional episodes. Basal gravels with sand lenses represent a braided outwash system are overlain by lacustrine sediments (sub-aqueous ice-contact fan deposits and proglacial gravel deltas) that represent an ice-contact glaciolacustrine environment. A subsequent re-advance sculpted the underlying sequence into mega-flute-shaped forms, and then ice stagnation and retreat from this position deposited a weakly stratified diamicton, forming the Hawea moraine at the southern margin of Lake Hawea. The capping glaciolacustrine silts and sands are locally deformed and represent local ponding between the ice front and the Hawea moraine during the final phase of ice retreat. Infrared-stimulated luminescence constrains the age of the basal glaciofluvial outwash to ~29 ka, and external ages constrain deglaciation to ~18 ka, indicating that the Hawea moraine formed between 29-18 ka. The Hawea moraine chronology is similar to other glacial records from the South Island that record MIS 3 and MIS 2 glacial advances and collectively suggest the commencement of deglaciation at ~18 ka. However, in contrast to other South Island records that suggest a broad period of stagnant ice during the global last glacial maximum, the Hawea valley chronology shows a dynamic and fluctuating ice margin during this time.

Introduction

The research presented here focuses on describing the sedimentology and stratigraphy of the deposits underlying the Hawea moraine and establishing the Late Pleistocene chronology of glacial sequences in the Lake Hawea valley. More specifically, this study documents the ice margin dynamics and positions leading up to and following the global last glacial maximum (gLGM). Ice advances in this area were previously named by Thomson (2009); Deposits related to the Albertown, Mt. Iron, and Hawea stable ice positions are presumably recorded during the MIS 4-2 time period. The purpose of this research is to document the timing and style of events leading up to and following the development of the Hawea moraine and to compare these results with the records of other valley glacier sequences on the South Island in order to reconstruct a regional picture.

Background

Late Pleistocene Glaciation of the Southern Alps, South Island, New Zealand

Glacial volume and ice-margin position are modulated by glacier mass balance, which is primarily controlled by climate variations. More specifically, winter snow accumulation and temperatures during summer ablation typically control ice advance and retreat (e.g. Paterson, 1994). The relative roles of precipitation versus temperature changes on ice dynamics in the late Pleistocene are debated, however, especially in New Zealand. For example, maximum ice extent of the Southern Alps on the South Island of New Zealand (Figure 2.1) may not correspond to the coldest time there because of reduced moisture delivery (Williams, 1996). However, moderate cooling can generate large glaciers by converting rain to snow in the accumulation zone of this humid setting (Rother and Shulmeister, 2006). Some researchers suggest that enhanced precipitation delivery controlled glacial advance during the gLGM (e.g. Williams, 1996;

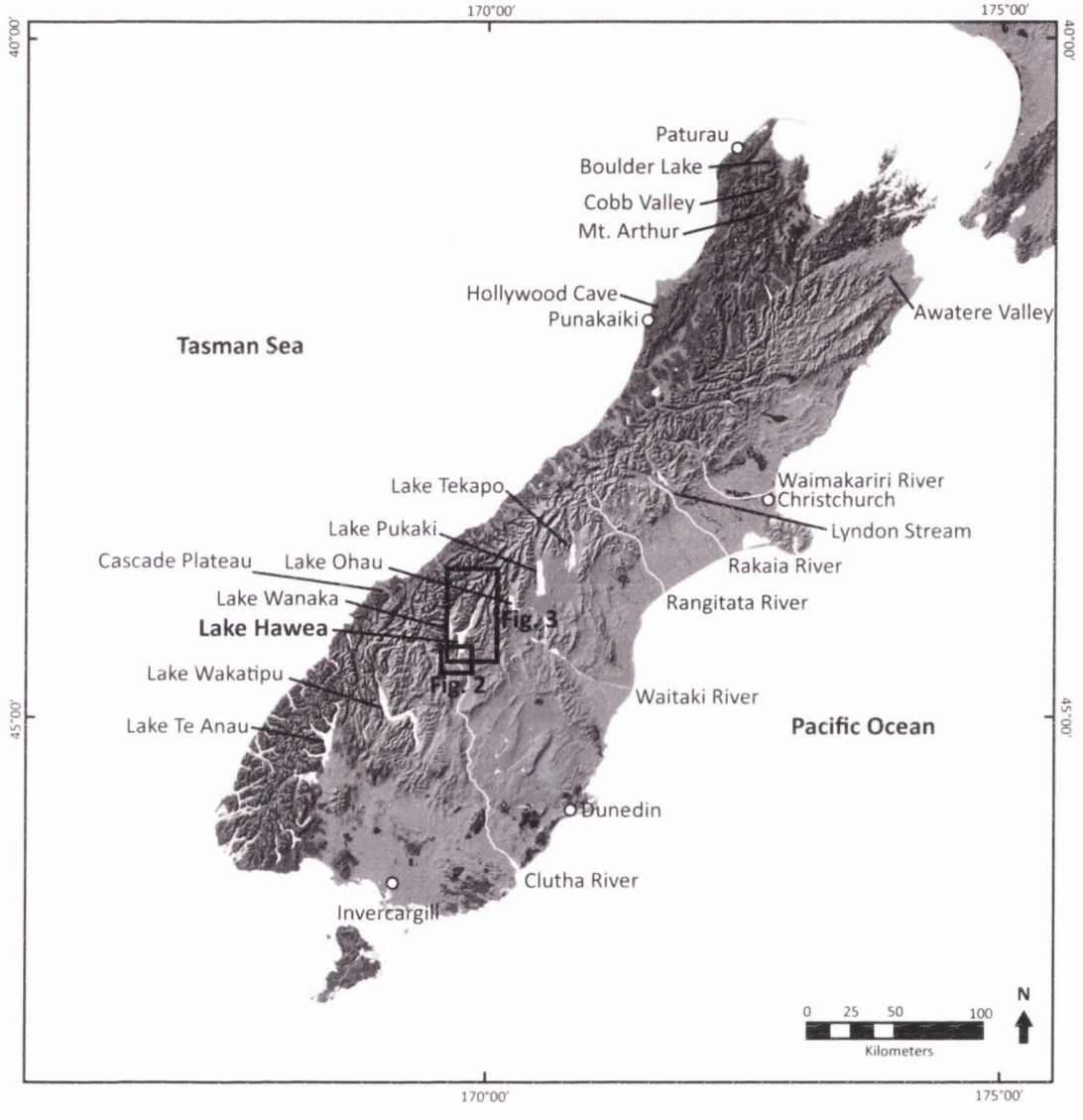

Figure 2.1 Map of the South Island, New Zealand with major lakes, rivers, cities, and other geographic features labeled on a 100 m DEM hillshade. Inset boxes show locations of Figure 2.2 and Figure 2.4. Elevation data from Geographx.

Shulmeister et al., 2005; Rother and Shulmeister, 2006), whereas others suggest temperature was the dominant influence (e.g. Denton et al., 1999; Anderson and Mackintosh, 2006; Schaefer et al., 2006; McCarthy et al., 2008; Golledge et al., 2012). A recent study paired an energy-balance and ice-flow model, based on relationships to the field record of ice extent, with chironomid data from the South Island to suggest that both temperature and precipitation drivers of the glacial behavior on the South Island during the Antarctic Cold Reversal (ACR) (Doughty et al., 2012).

Previous researchers recognized nine glaciations in the Southern Alps during the last 0.7 Ma, the most recent of which coincide with MIS 10, 8, 6, and 4-2 (Suggate, 1990). The last glaciation, which broadly spans MIS 4-2, is regionally called the Otira glaciation (Table 2.1). The timing of the last glacial advance on the South Island is broadly constrained to ~25-17 ka (Suggate, 1965; Suggate and Moar, 1970; Mansergh, 1973; Ricker et al., 1992; Williams, 1996; Shulmeister et al., 2005, 2010a; Schaefer et al., 2006), and deglaciation broadly recorded at ~23-16 ka (Williams, 1996; Williams et al., 2005; Shulmeister et al., 2005, 2010a; Putnam et al., 2013).

The glacial chronology of the upper Clutha River area (Lake Wanaka and Lake Hawea valleys) of the central South Island (Figure 2.1) is poorly constrained. Current age constraints are based on correlation of landforms and a limited number of radiocarbon (^{14}C) ages on the younger deposits. Thomson (2009) identified the ice advances of the upper Clutha River area as the Northburn (MIS 26), Lowburn (MIS 16), Lindis (MIS 12), Queensbury (MIS 10), Luggate (MIS 6), Albertown (MIS 4), Mt. Iron (MIS 2 early), and Hawea (MIS 2 late) advances, with moraines and heads of outwash marking most advances (Thomson, 2009) (Figure 2.2). These advances represent progressive reduced ice extent. For example, the Albertown MIS 4 ice position reached farther down-valley than the MIS 2 (and global LGM) ice position(s). The Mt. Iron

Table 2.1 Examples of documented MIS 2 and MIS 3 ice advances of glacial systems on the South Island of New Zealand discussed in the text. Ages reported are approximate and have been converted to calendar years using the IntCal09 calibration curve (Riemer et al., 2009) where applicable. Locations are arranged from north to south and location in relation to the spine of the Southern Alps is noted as west (W) or east (E).

Location	Southern Alps	Age (ka)	Methods	MIS	Researchers
NW South Island	W	18.2-17.2	δ180, δ13C	2	Williams et al., 2005
Cobb-Takaka Valley	W	>18	TCN	2	Shulmeister et al., 2005
North Westland	W	>25	OSL, 14C	2	Preusser et al., 2005
Waimakariri valley	E	18.4, 23.3-21	weathering rind	2	Ricker et al., 1992
Rakaia River valley	E	24-17.4	OSL, TCN	2	Shulmeister et al., 2010a
Rangitata River valley	E	24	TCN	2	Evans, 2008
Lake Pukaki valley	E	>17.4	TCN	2	Schaefer et al., 2006
Cascade Plateau	W	22-19	TCN	2	Sutherland et al., 2007
Ohau River valley	E	22.5, 18.2	TCN	2	Putnam et al., 2013
Lake Hawea valley	**E**	**<18**	**14C; TCN**	**2**	**McKellar, 1960; Graham et al., 1998; this study**
Lake Te Anau valley	E	20-18	U-series	2	Williams, 1996
Cobb-Takaka Valley	W	59-28	TCN	3 (or late 4)	Thackray et al., 2009
North Westland	W	>32	OSL	3	Preusser et al., 2005
Waimakariri valley	E	29	weathering rind	3	Ricker et al., 1992
Rakaia River valley	E	48, 40	OSL, IRSL	mid-3, late-3	Shulmeister et al., 2010
Rangitata River valley	E	59	TCN	3	Evans, 2008
Lake Pukaki valley	E	36.4	TCN	3	Mansergh, 1973
Cascade Plateau	W	31	TCN	3	Sutherland et al., 2007
Ohau River valley	E	32.5, 27.4	TCN	3	Putnam et al., 2013
Lake Hawea valley	**E**	**>29**	**OSL**	**3**	**this study**
Lake Te Anau valley	E	51.7- 40.3	U-series	3	Williams, 1996

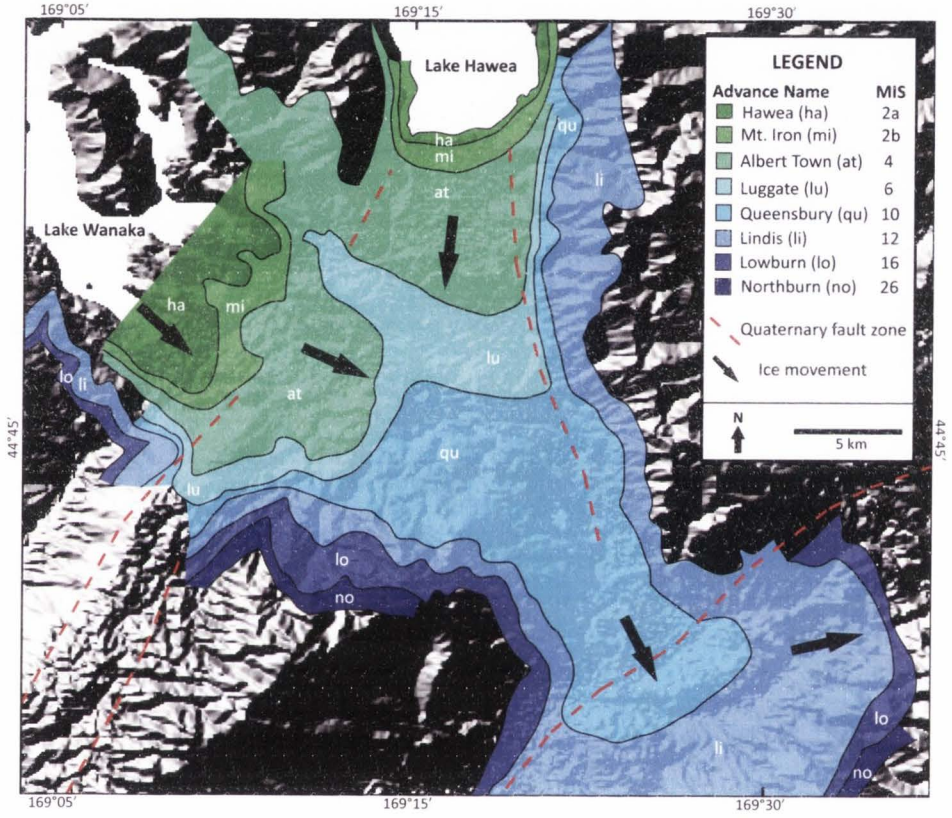

Figure 2.2 Map of glacial events in the Wanaka-Hawea area, New Zealand. For more specific locations of this study, see Figure 2.1 and Figure 2.4. Modified from Thomson, 2009.

advance probably marks the global LGM correlative position in this area, although age control and geomorphic evidence of this advance are limited. The youngest advance is represented by a moraine at the southern margin of Lake Hawea. Radiocarbon ages from peat overlying outwash in an abandoned channel at the southern outlet of Lake Hawea constrain the minimum age of this moraine to 15.1 ± 0.2 ^{14}C ka (~17.8-18.7 ka cal. years, 2 σ error[1]) (McKellar, 1960). Cosmogenic surface exposure dating (^{10}Be) of a biotite schist with quartz veins exposed in thesame outwash channel produced an age of ~17.5 ka (Graham et al., 1998). Additionally, samples have been collected for cosmogenic dating of boulders in the upper Clutha River area, but these results are not yet available (Rother, personal communication).

Late Pleistocene Paleoclimate of the Southern Alps, South Island, New Zealand

Speleothem-, pollen-, and beetle-based paleoclimate records are available for MIS 4-3 on the South Island (Figure 2.3). Most climate reconstructions for the South Island focus on the LGM period and the transition to interglacial conditions. Paleoclimate data during MIS 3 on the South Island, in contrast, is sparse. MIS 4 conditions were cold and wet, based on δ^{18}O and δ^{13}C speleothem dated with U-series techniques record from Hollywood Cave in the northwestern Southern Alps (Figure 2.1) (Whittaker et al., 2011). More broadly, Whittaker et al. (2011) suggest that MIS 4 was wetter than MIS 3 and MIS 2, although both later stages were punctuated by periods of increased precipitation that could have promoted ice advance.

---

[1] Calibrated using IntCal09 calibration curve: Reimer, P. J., Baillie, M. G. L., Bard, E., Bayliss, A., Beck, J. W., Blackwell, P. G., Bronk Ramsey, C., Buck, C. E., Burr, G. S., Edwards, R. L., Friedrich, M., Grootes, P. M., Guilderson, T. P., Hajdas, I., Heaton, T. J., Hogg, A. G., Hughen, K. A., Kaiser, K. F., Kromer, B., McCormac, F. G., Manning, S. W., Reimer, R. W., Richards, D. A., Southon, J. R., Talamo, S., Turney, C. S. M., van der Plicht, J., Weyhenmeyer, C. E., 2009. Radiocarbon 51:1111-1150.

Figure 2.3 Summary of climate data pertaining to the South Island of New Zealand spanning MIS 4 to MIS 1. A represents the oxygen isotope record from the Greenland GRIP ice core (Blunier and Brook, 2001). Three oxygen isotope speleothem records from the South Island are presented: B (Hellstrom et al., 1998; MD3), C (Williams et al., 2005; data published in Williams et al., 2010), and D (Whittaker et al., 2011). E is the combined record of the Antarctica Taylor Dome CO_2 record (Smith et al., 1999; Indermühle et al., 1999), with some overlap. Raw data is plotted in light grey under 10-year moving average smoothed data. Interpretations regarding temperature, precipitation, and flora of the South Island, as discussed in the text, are also plotted. Lighter grey zone mark broad interpretations presented by the authors, whereas darker zones mark more specific data . The timing of the Lake Hawea valley glacial advances, as constrained by this research, are also plotted.

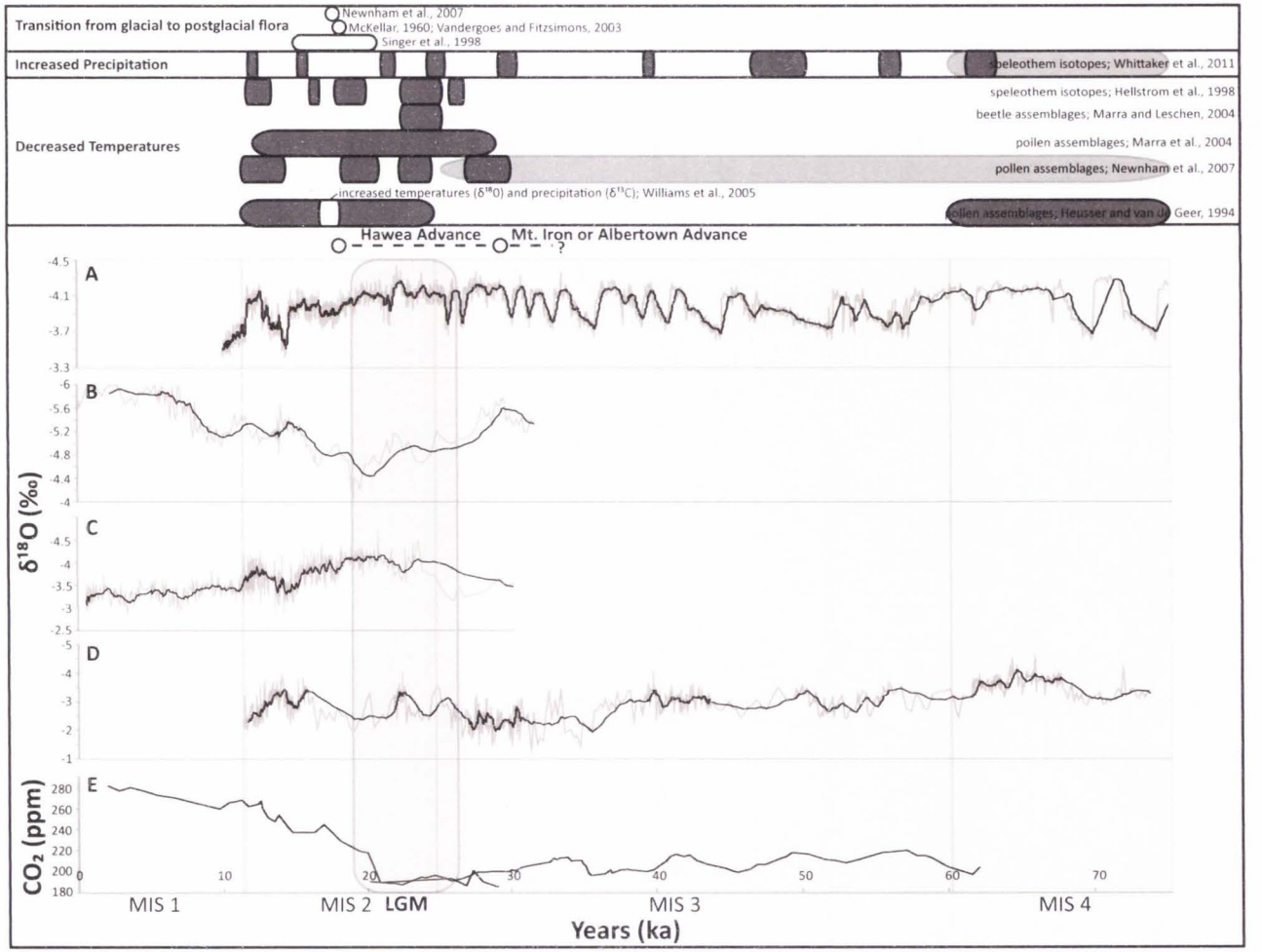

Research comparing terrestrial and marine pollen-based paleoclimatic records of the South Island suggests that temperatures were decreased during MIS 4 and MIS 2 (Heusser and van de Geer, 1994) (Figure 2.3). Another pollen-based study suggests colder climates during MIS 4-2, but that MIS 4 was warmer than MIS 3-2 (Newnham et al., 2007) (Figure 2.3).

The pollen data presented by Newnham et al. (2007) suggest that MIS 3 was cooler than MIS 4, and this data corresponds to the ice advances and speleothem and uranium-series and oxygen ($\delta^{18}O$) and carbon ($\delta^{13}C$) isotope records of glaciation produced by Williams (1996). Several prominent negative excursions in the $\delta^{18}O$ record presented by Whittaker et al. (2011) punctuate the MIS 3-2 dry period (Figure 2.3), and are interpreted to relate to enhanced westerly atmospheric flow (Whittaker et al., 2011). Positive $\delta^{18}O$ excursions recorded in MIS 3-2 speleothems from the Mt. Arthur area (Figure 2.1) are interpreted to be related to enhanced westerly flow and subsequent lowered temperatures in central and southern New Zealand, and more specifically to migration of the Subtropical Front in the Tasman Sea northward (Hellstrom et al., 1998) (Figure 2.3). The collective paleoclimate reconstructions (Figure 2.3) suggest that decreased temperatures and a short period of enhanced precipitation may mark the transition from MIS 3 to MIS 2 and associated LGM glacial advances on the South Island.

As previously stated, Whittaker et al. (2011) interpret that negative $\delta^{18}O$ excursions during MIS 2 in their speleothem record relate to enhanced westerly atmospheric flow bringing increased precipitation to the South Island. Hellstrom et al. (1998) interpret positive $\delta^{18}O$ excursions recorded in speleothems from the Mt. Arthur area (Figure 2.1) to be related to enhanced westerly flow and subsequent lowered temperatures in central and southern New Zealand, and more specifically to migration of the Subtropical Front in the Tasman Sea northward (Figure 2.3). In the Awatere valley (Figure 2.1), subalpine beetle taxa indicate cold temperatures from ~25-22 ka (Marra and Leschen, 2004), which have been modeled to

represent winter temperatures 3.5-6.0°C colder than today (Marra et al., 2004; Figure 2.3). The pollen data from this area indicate grassland conditions from 29-12 ka, indicating cooler than modern temperatures (Marra and Leschen, 2004; Figure 2.3). The beetle-derived temperature reconstruction from Lyndon Stream in the Rakaia Valley (Figure 2.1) instead suggests milder winter temperatures during the LGM, only 1-2.2°C cooler than modern (Marra et al, 2006; Figure 2.3). These results, however, may not be representative of the greater South Island, as the site may have felt lesser effects of southerly and easterly winds (Marra et al., 2006). The beetle assemblage suggests a forest habitat, whereas the pollen assemblage from the same site suggests dominance of grasses and shrubs. Together, these assemblages are interpreted to support the reconstructed relatively mild conditions during MIS 2 (Marra et al., 2006).

More specific research focuses on paleoclimate during the peak of MIS 2 glaciation and deglaciation. The isotope records of glaciations produced by Williams (1996) suggest the peak of Otiran glaciations occurred ~19 ka and lasted from 20-18 ka. A comparison of this record to oxygen isotope analyses from a marine sediment core ~300 km east of the South Island reveals that this was probably not the coldest period of MIS 2, suggesting a strong role of precipitation driving glacial advance (Williams, 1996). Regarding deglaciation, oxygen ($\delta^{18}O$) and carbon isotope ($\delta^{13}C$) analyses from stalagmites in limestone caves on the northwest South Island (four near Punakaiki and five near Paturau, Figure 2.1) more specifically record late-Otiran climate signatures that show warmer temperatures between 18.2 and 17.2 ka, marking the onset of deglaciation (Williams et al., 2005) (Figure 2.3). The data and flora assemblages presented on Figure 2.3 suggest a transition from glacial to interglacial conditions at ~18 ka, indicating deglaciation across the South Island. Shulmeister et al. (2010a), however, argue that deglaciation began ~25 ka and continued gradually until ~15 ka. In summary, paleoclimate reconstructions support the idea that climatic changes to wetter and cooler conditions

prompted the MIS 4-2 glacial periods on the South Island and that warmer temperatures commenced subsequent deglaciation.

Stratigraphy of Glacial Environments

Traditional glacial chronologies in the Southern Alps are based on geomorphic mapping and dating of landforms and sediments (primarily outwash and moraines) (e.g. Schaefer et al., 2006; Thomson, 2009; Putnam et al., 2013). The importance of understanding the sedimentology and stratigraphic architecture of glacial deposits for reconstructing regional glacial histories has recently been emphasized in New Zealand (e.g. Evans et al., 2010; Shulmeister et al., 2010a, 2010b; Hyatt et al., 2012; Evans et al., 2013). These detailed studies can provide more information about processes of formation than simply geomorphic and chronologic analyses (e.g. Evans and Benn, 2004).

The emphasis on detailed sedimentologic and stratigraphic studies of glacial landforms is especially important for sediment deposited leading up to and during the LGM in New Zealand. Several studies document LGM glacial advances on the South Island based foremost on the glacial geomorphic features present in the study areas (e.g. Suggate and Almond, 2005; Schaefer et al., 2006; Shulmeister et al., 2010a; Putnam et al., 2013). These studies do not, however, address the degree of recession before readvance to the LGM position or the ice dynamics associated with sediment deposition and formation of geomorphic features that differentiate ice positions. This study relies not only on geomorphic relations, but also heavily upon the descriptions and interpretations of the internal sedimentology and stratigraphy exposed in the Hawea lake bluffs to provide information on the style and sequence of MIS 3-2 ice advances and deglaciation in the Lake Hawea valley. Facies descriptions are especially important, as the physical characteristics of individual facies are related to their processes of

formation. The interpretations of their origins therefore comprise an important step in unraveling the history of glacial deposits, as facies may connect glacial environments to the same advance and retreat events and/or provide detail crucial to reconstructions of sediment transport- and depositional-dynamics. This level of detail is especially important and novel in comparison to previous Southern Alps studies during the LGM. This research consequently helps better understand the nature of South Island ice dynamics during a globally important glacial and climatic period.

Luminescence Dating of Glacial Sediments

Optically stimulated luminescence (OSL) dating of quartz and feldspar (Huntley et al., 1985) provides an age estimate of the last time sediment was exposed to sufficient sunlight (or heat) to zero (bleach) the luminescence signal from the sediment. This bleaching must occur to release the latent luminescence signal acquired during the previous burial history. Upon deposition and burial, the sediment is removed from sunlight and exposed to radiation from the surrounding sediment and incoming cosmic rays. The sediment acquires a stored charge, the magnitude of which depends on the length of burial and dose-rate environment. The most widely used and accepted method to determine the equivalent dose (or "paleodose") of the sediment is the single-aliquot regenerative-dose (SAR) method (Murray and Wintle, 2000, 2003; Wallinga et al., 2000; Wintle and Murray, 2006).

Researchers have successfully employed OSL dating techniques to glacial deposits in a number of settings. However, glacial deposits pose challenges to luminescence dating. Problems include incomplete bleaching (e.g. Klasen et al., 2007), poor luminescence properties (e.g. Preusser et al., 2006), high thermal transfer (e.g. Alexanderson, 2007), and feldspar contamination of quartz samples (e.g. Lukas et al., 2007). Previous work specifically discusses

problems with OSL dating of quartz on the South Island of New Zealand (e.g. Preusser et al., 2006; Klasen et al., 2007). These complications, however, have not fully thwarted researchers, and recent work has demonstrated success with quartz OSL dating on the eastern coast of the South Island (Rowan et al., 2012). This study applies feldspar infrared stimulated luminescence (IRSL) dating of basal glacial outwash underlying the Hawea moraine to establish a glacial chronology in the Lake Hawea valley and maximum age on the global LGM represented in the Southern Alps.

Study Area

The Southern Alps span ~450 km and trend roughly north-south along the South Island of New Zealand (Figure 2.1). Oblique convergence along the Alpine Fault created the Southern Alps, and the fault marks the boundary between the Pacific and Indo-Australian Plates. Resulting peaks extend higher than 3,700 m (Mount Cook) and decrease west to the Tasman Sea and east to central Otago mountain ranges and the Canterbury Plains, and eventually the South Pacific Ocean. During the last and previous glaciations, a regional ice cap extending along the Southern Alps fed valley glaciers, including the Hawea glacier (McKellar, 1960).

Lake Hawea lies on the eastern side of the Southern Alps drainage divide in northwestern Otago, South Island, New Zealand (Figure 2.1). The lake occupies ~140 km^2 of a northeast-southwest trending valley and spans ~35 km along its long axis (Figure 2.4). Lake Hawea formed in the over-deepened trough excavated by glacial ice extending from the headwaters of the Hunter River and water impoundment from damming by glacial deposits and outwash at the southern margin of the basin. The eastern flank of the Southern Alps hosts many other similar glacial lakes (Gage and Suggate, 1958) (Figure 2.1). The Hunter River to the north feeds the Lake Hawea, while the Hawea River on the southwestern shore drains the lake and

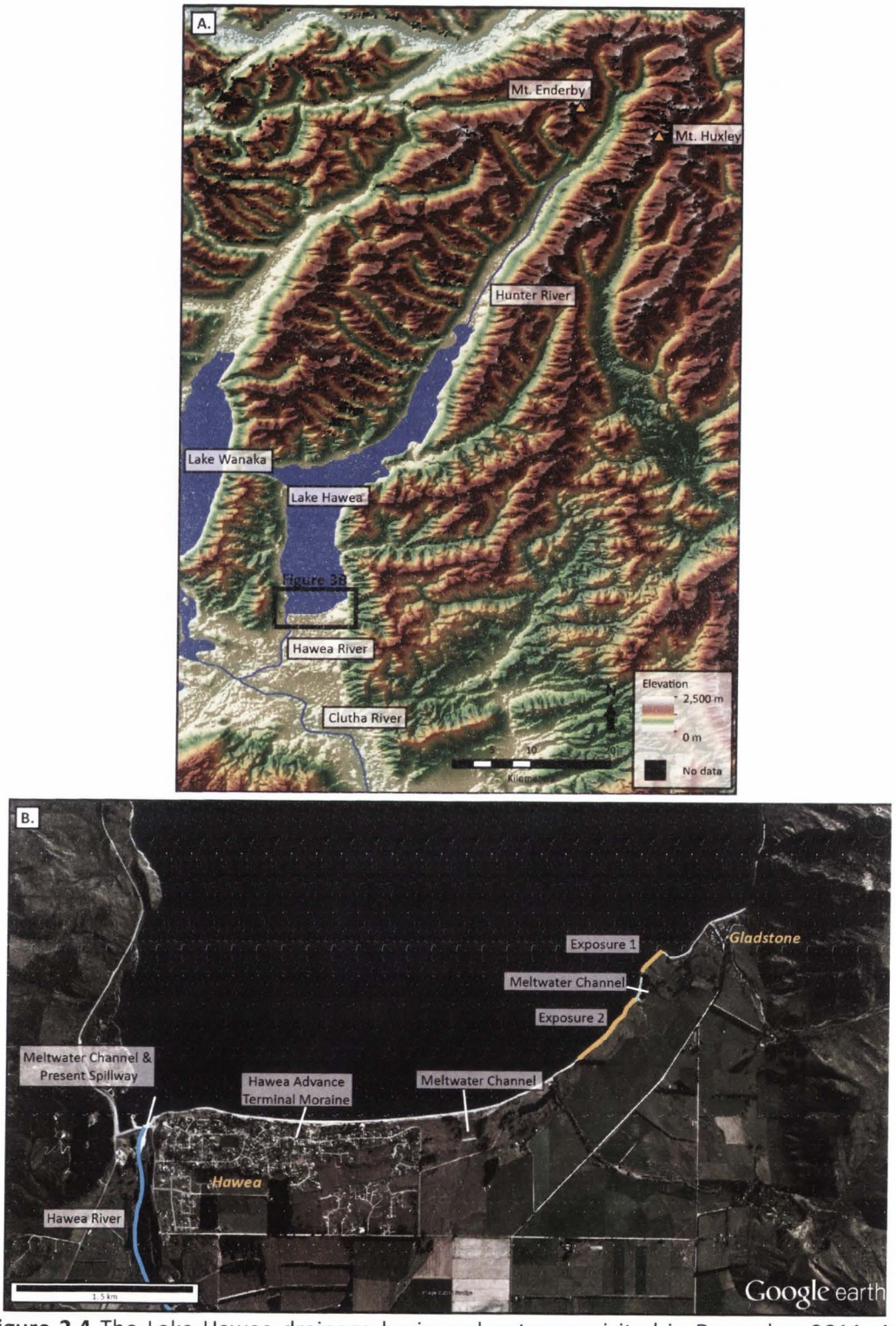

Figure 2.4 The Lake Hawea drainage basin and outcrops visited in December 2011; A. Image covers extent of the Hawea drainage basin and surrounding area, as bound and labeled in Figure 1. Black bounding box shows location of Figure B below. Elevations basen on 30 m SRTM data; B. Exposures studied labeled as Exposure 1 and Exposure 2. Blue line shows paths of the Hawea River. Imagery obtained from Google Earth, 2012 Digital Globe, 2012 GeoEye.

becomes a tributary to the Clutha River ~15 km downstream. The bluffs along the southern shoreline of Lake Hawea, near the town of Gladstone, contain vertical, well-exposed outcrops of the glacial sediment (~2-9 m tall, ~1.3 km long) under the Hawea moraine, referred to by Kirk et al. (2000) as the Grandview Cliffs.

The Hawea exposures were previously described in a M.S. thesis focusing on glaciotectonism of the sediments exposed at the time (Armstrong, 2010). The sediments described varied somewhat from those presented in this research paper, due to the continued erosion of the cliffs (Kirk et al., 2000). Previous descriptions by Armstrong (2010) suggest that the bluffs were taller in the past and three units were exposed (basal outwash overlain by a massive diamicton unit and capped by lacustrine sediments). McKellar (1960) studied an exposure along the eastern wall of the meltwater channel separating Exposure 1 and Exposure 2 in this study, which he refers to as "the gorge." The descriptions by McKellar (1960) note two units: a basal pebble-cobble unit with irregular boulders and bedding dipping to the south, overlain by stratified silt and sand with occasional boulders.

New Zealand experiences a maritime climate dominated by the Southern Hemisphere Westerlies, which deliver moisture from the northwest and southeast. The climate of New Zealand is influenced by sea-surface temperature gradients between subtropical and sub-Antarctic surface water masses. Regional climate is also influenced by variations in the Antarctic Oscillation, El Niño-Southern Oscillation, and Pacific Decadal Oscillation (e.g. Alloway et al., 2007). Due to orographic precipitation and rain shadow effects caused by the Southern Alps, there are differences in precipitation between the western and eastern flank of the mountain range; mean annual precipitation reaches 16,000 mm at the crest and is locally less than 350 mm/yr to the east (e.g. Alloway et al., 2007). The median annual rainfall for the southern shores of Lake Hawea is 700-800 mm (1970-2001, Otago Regional Council).

Methods

Geomorphology and Stratigraphy

Detailed geomorphic mapping of the area was conducted using field observation and aerial imagery in Google Earth recorded on a topographic base map (Lake Hawea, NZTopo50-CA13, 1:50 000). The section of lake bluff studied here has an eastern and a western portion, (labeled as "Exposure 1" and "Exposure 2") in Figure 2.4, separated by a meltwater channel. These exposures were previously described in a M.S. thesis focusing on glaciotectonism of the sediments exposed at the time (Armstrong, 2010). The sediments described therein vary somewhat from those presented in this research paper, due to the different purpose, lower level of detail, and continued erosion of the cliffs (as described in Kirk et al., 2000).

Exposures were logged using detailed sedimentary and stratigraphic measurements and descriptions of unit thickness, bedding, structures, grain size, fabric, and color. Detailed facies photographs were taken and larger photographs were stitched together to form outcrop-scale panels. Table 2.2 contains all facies codes used in unit descriptions. Facies can be interpreted in terms of physical processes of their transport, deposition, and deformation. The collection of facies into units helps describe and interpret larger-scale sediment-ice dynamics of various transport and depositional environments.

Data collected in clast counts provide information about provenance areas, energy regimes, and mechanisms of erosion, transportation, and deposition. Clast morphology (shape, roundness, size) may differ between different depositional and transport processes. Clast counts therefore included recording a-, b-, and c-axis lengths (long, intermediate, and short, respectively) and roundness (very angular, angular, sub-angular, sub-rounded, rounded, and well-rounded). Ternary diagrams record the shapes of clasts based on the length of the three major axes (Benn and Ballantyne, 1993), with the three end members being block (a = b = c),

Table 2.2 Facies and their codes and descriptions found in the stratigraphy of the Lake Hawea exposures. Codes adapted from Evans and Benn (2004).

Code	Description	Interpretation
Fl	Silt and clay; fine lamination often with minor fine sand and very small ripples	glaciolacustrine deposition
Sh	Sand; horizontally bedded	glaciolacustrine deposition
Sfo	Sand; foresets	glaciolacustrine deltaic deposition
Sr	Sand; ripple cross-laminated	glacial outwash
Sr(w)	Sand; ripple cross-laminated with dewatering structures	glacial outwash
Go	Gravel; openwork	glacial outwash
Gm	Gravel; clast-supported gravels massive	glacial outwash
Gh	Gravel; horizontally bedded	glacial outwash
Gfo	Gravel; foresets	glaciolacustrine deltaic deposition
Dml	Diamicton; matrix-supported, laminated	sub-aqueous deposition at an ice margin

slab (a = b; c = 0), and elongate (a > 0; b= c = 0) clasts. The C_{40} index records the percentage of clasts with c:a axis ratios ≤0.4 (elongate) and can help distinguish between actively-transported (or subglacially modified) and passively-transported (i.e. englacial, supraglacial, subaerial) glacial sediment (Evans and Benn, 2004). However, neither this index nor the ternary diagrams assist in differentiating between subglacially- and glaciofluvially-transported sediment, as neither environment readily preserves angular clasts and shape may be primarily influenced by clast lithology. Clast roundness is more useful to distinguish between these two environments, as fluvially-transported clasts are generally more rounded than glacially-transported clasts (Evans and Benn, 2004).

Luminescence Dating

Two samples for luminescence dating (USU-910 and USU-1090) were obtained by pounding a steel tube into sandy strata after the outcrop face was scraped to obtain a fresh surface. A representative sediment sample from a 30 cm radius around each sample tube was collected for dose-rate analysis. A smaller sample was collected in an airtight container to maintain accurate water content at the time of sample collection.

Samples for dose-rate determination were split and the concentrations of K, Rb, Th, and U were analyzed using ICP-MS and ICP-AES techniques at ALS CHEMEX. Moisture content was determined by weighing samples while moist and again when dry, immediately after returning from fieldwork. Chemistry (Guérin et al., 2011), moisture content, and cosmic contribution (Prescott and Hutton, 1994) were used to calculate the dose rate of the sediment following methods of Aitken (1998).

Sample preparation and analyses were conducted at the Utah State University Luminescence Laboratory under ambient amber light (590 nm) conditions. Samples were sieved to 125-212 μm (USU-910) and 150-250 μm (USU-1090). Hydrocloric acid and bleach were used to dissolve carbonates and organic material. Sodium polytungstate was used to separate potassium feldspar (2.58 g/cm^3) from heavy minerals.

Small aliquots (2 mm) of potassium feldspar were dated following the single-aliquot regenerative method (SAR) of Wallinga et al. (2000) and fading-rate technique of Huot and Lamothe (2003). A preheat and cutheat temperature of 250°C for 60 s were used. Equivalent dose distribution and ages were calculated using the minimum age method (MAM; Galbraith et al., 1999). Ages were corrected for fading or loss of signal with time, referred to as "anomalous fading" of feldspar, using the method of Auclair et al. (2003). More specific details about the quartz and feldspar procedures and a more complete discussion of these results can be found in Chapter 4.

Results and Interpretations

Geomorphology

The most notable geomorphic feature within the Hawea valley map area is the Hawea moraine (Q_m), which constrains the southern shore of Lake Hawea (Figure 2.5). The moraine

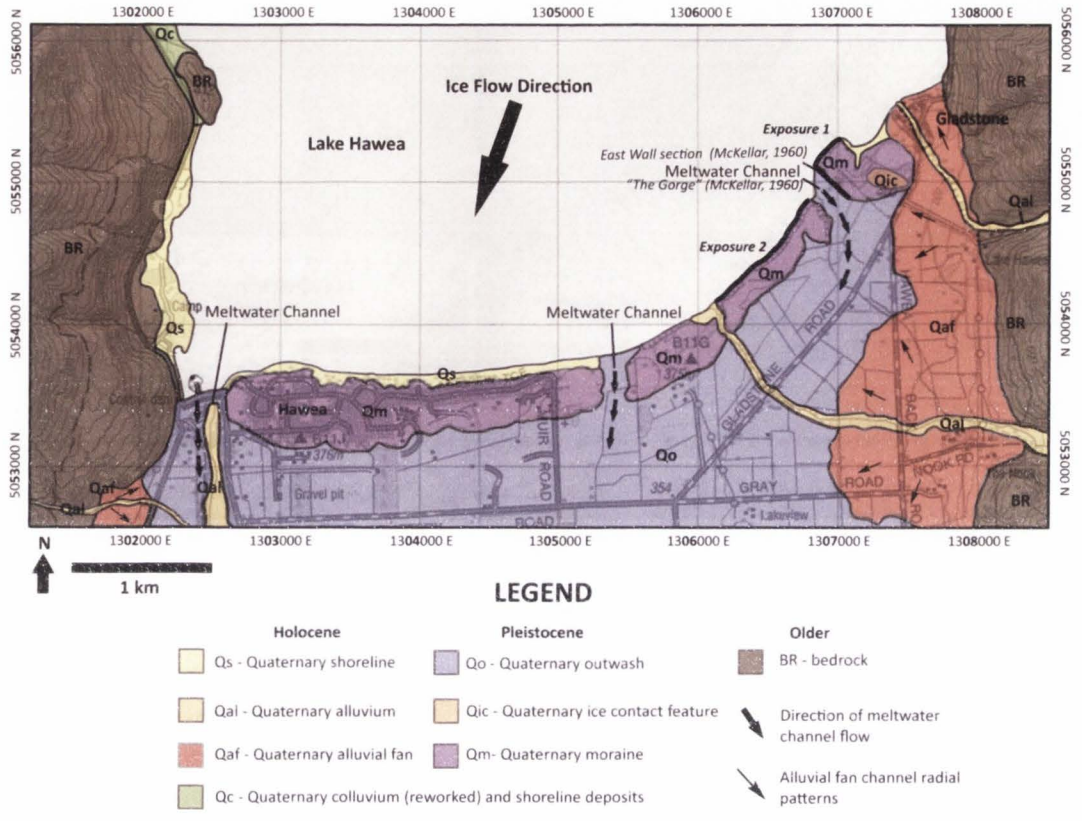

Figure 2.5 Geomorphic map of the southern shore of Lake Hawea, New Zealand.

rises up to 9 m above the Lake Hawea shoreline and is ~1.3 km long and ranges from ~120 to >500 m wide. This recessional moraine marks the most recent stable ice position in the Lake Hawea valley.

A former ice-contact feature manifests itself as a small hill (Q_{ic}) that rises ~20 m above the eastern-most section of the moraine (Figure 2.5). This mound features a distinct east-west trending ridgeline ~265 m long and ranges from ~45-140 m wide. This interpretation as an ice-contact feature is based on limited observations as this landform was not the primary focus of this research and was therefore not studied in depth.

Three meltwater channels cross-cut the Hawea moraine and extend southward onto a braided outwash channel surface (Q_o) (Figure 2.5). These channels range from ~200 to 350 m

wide. Once down-valley of the moraine walls, these channels split and braid away from the lake basin southward. The preservation of this outwash surface and rule of cross-cutting relations suggest that these channels formed during the latest stages of ice retreat and are the most recent geomorphic signature of glaciation in the valley. Additionally, this braided outwash system either covers or removed any geomorphic features created during previous ice advances, such as the Mount Iron position.

Post-glacial geomorphic features include Quaternary colluvium and shoreline deposits (Q_c), alluvial fans (Q_{af}), alluvium (Q_{al}), and shorelines (Q_s). The colluvium and shoreline deposits are differentiated from bedrock (BR) and shore sediment (Q_s) on the western bank of Lake Hawea based primarily on slope and vegetation cover (i.e. lower and shallower slope than the bedrock to the west and more vegetated than the shores). These interpretations, however, are based primarily on observations in Google Earth.

Modern tributaries originating in the surrounding mountains have created alluvial fans (Q_{af}) that have built out onto the valley floor and over the former braided channel surface. Tributary channels are mapped as Quaternary alluvium (Q_{al}). The channels are erosional and in places have incised into alluvial fans and the braided plain surface. One of these tributary channels incises the Hawea moraine to lake level directly west of Exposure 2, creating a gap between this exposure and a section not studied. The sand and gravel shoreline deposits (Q_s) are mapped in two areas based on topographic contours and aerial imagery.

Stratigraphy

The Lake Hawea exposures range from 3-9 m tall. Exposure 1 is ~260 m long, whereas Exposure 2 is ~725 m long (Figure 2.4-2.6). An ~205 m wide meltwater channel separates these exposures. The Lake Hawea bluff exposures can be divided into four stratigraphic units.

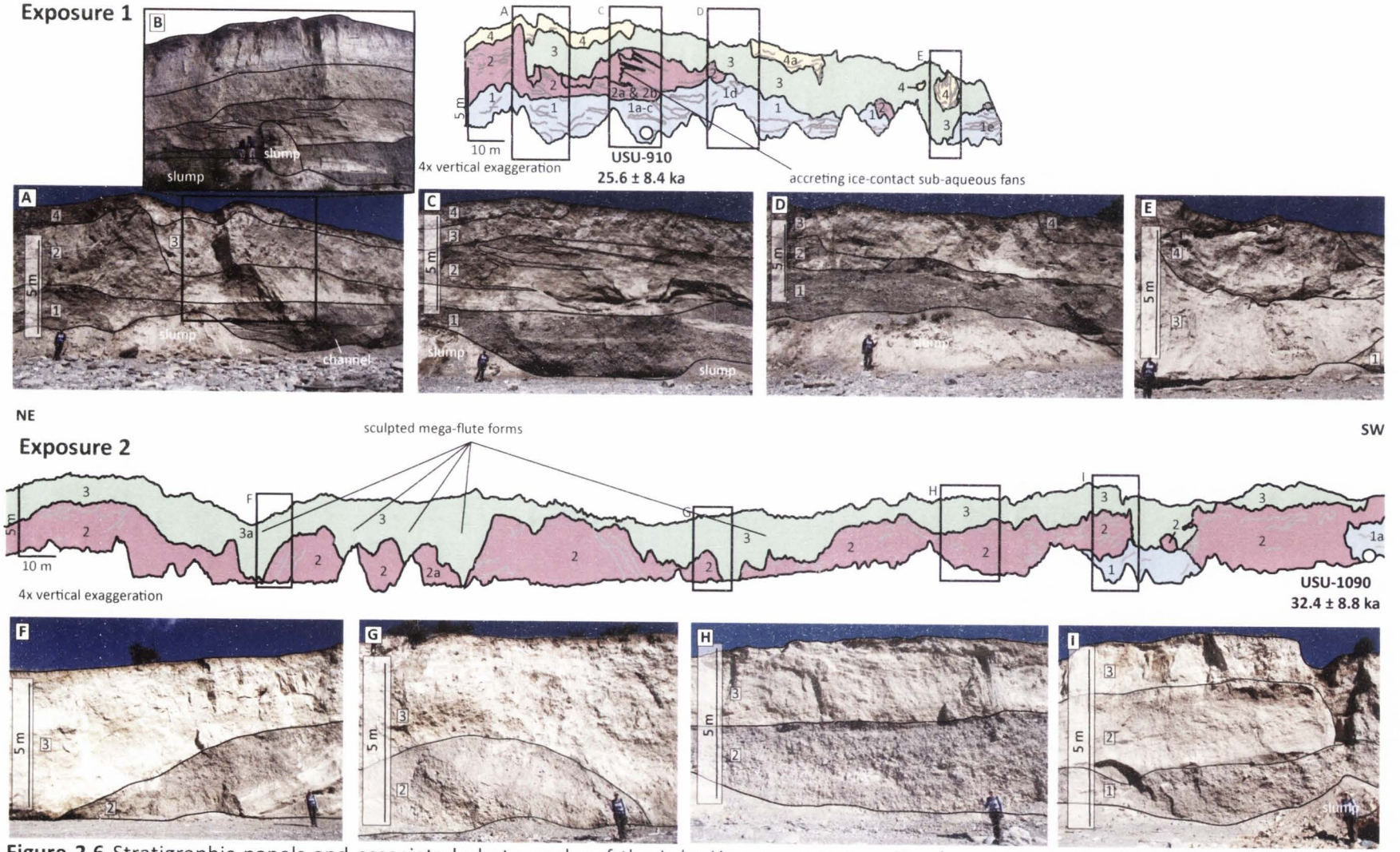

Figure 2.6 Stratigraphic panels and associated photographs of the Lake Hawea exposures. Numbers represent unit labels. Open circles and ages represent luminescence sample locations. Alphanumeric labels represent locations of detailed facies photographs for Exposure 1 (Figure 2.7) and Exposure 2 (Figure 2.8). See text for descriptions. Unit 1 is a gravel outwash with sand lenses, Unit 2 is a gravel outwash with sand lenses and subaqueous depositional features, Unit 3 is a diamicton, and Unit 4 is glaciolacustrine sands and silts.

Although correlation can be easily made between Exposure 1 and Exposure 2, there are differences between the two in geometry, thickness, and presence of units. Exposure 1 contains all four units (Figure 2.6), whereas Exposure 2 only contains Units 1-3. Armstrong (2010), however, noted deposits similar to Unit 4 along Exposure 2 that have since been removed by bluff retreat. The four stratigraphic units were horizontally deposited and are separated by clear contacts. Unit 1 and Unit 2 are composed of predominantly of gravel, with local sand lenses. These are overlain by the diamicton of Unit 3, which is capped by sand and silt of Unit 4.

Within Exposure 1, the exposed thickness of Unit 1 generally decreases from east to west. Unit 2, which is horizontally bedded here, also generally thins from east to west and is truncated by Unit 3 in the middle of the outcrop. Unit 3, on the other hand, generally thickens from east to west across the exposure. Unit 4 is only exposed in the far eastern and western extents of Exposure 1. Within Exposure 2, Unit 1 is exposed only locally in the western part of the exposure and is not only horizontally bedded, but also contains dipping gravel beds. Horizontal beds from Unit 2 are primarily exposed in the western third of the exposure. Previous descriptions by Armstrong (2010) suggest that the bluffs were taller in the past and only three units were exposed (basal outwash overlain by a massive diamicton unit and capped by lacustrine sediments).

Sedimentology

The basal Unit 1 is grey and tan in color and <5 m thick in exposure 1 and ≥2.5 m thick in exposure 2. Unit 1 contains stratified and interbedded sands and pebble gravels with 5-20 cm thick, discontinuous/lenticular, laminated sand beds (Sh) and sand lenses with ripple cross-bedding and dewatering structures (Sr(w)) (Figure 2.7 1a-c). This unit contains decimeter scale, cross-bedded, open-framework (Go) and horizontally bedded, clast-supported (Gh) (and rare

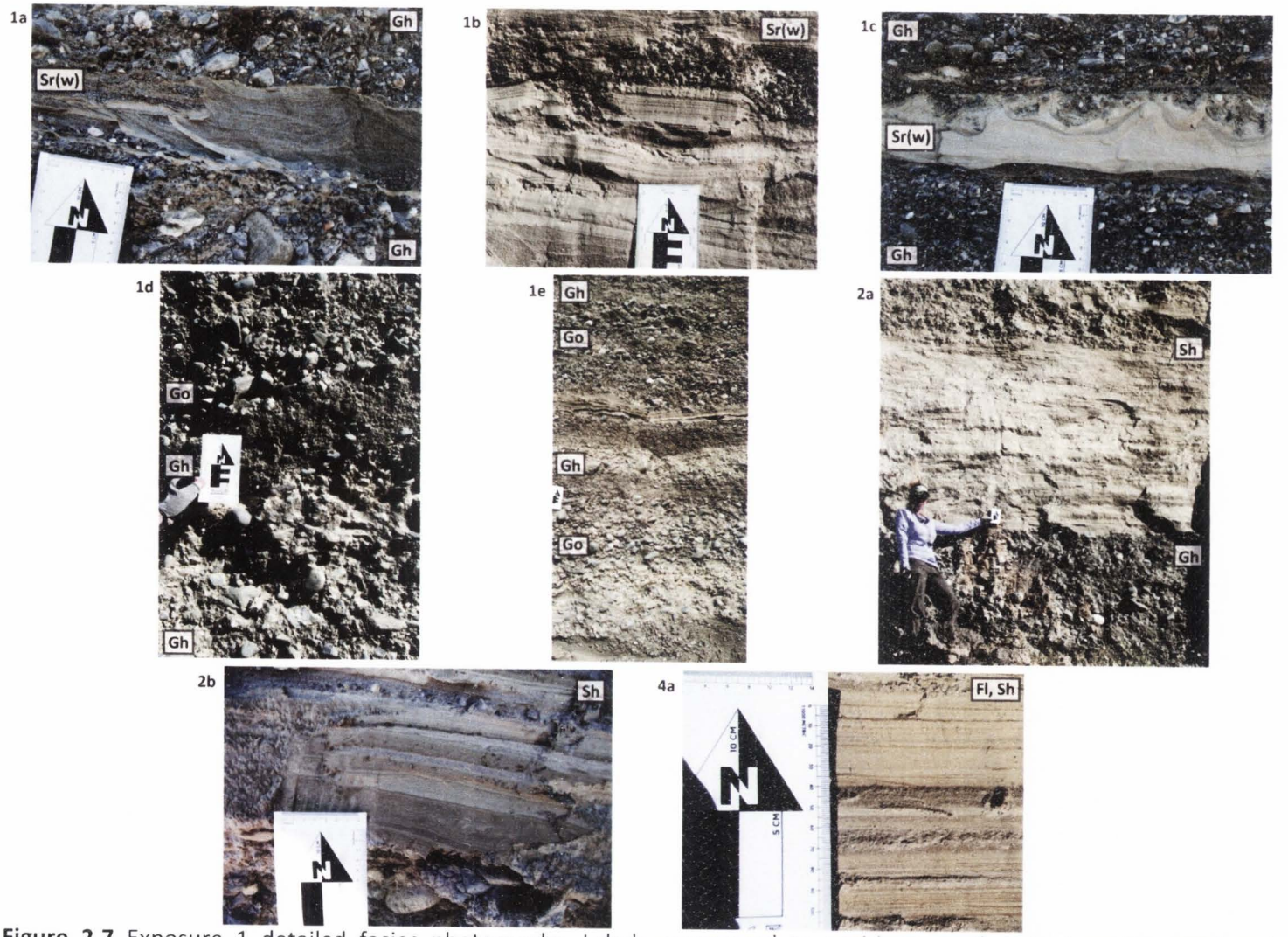

Figure 2.7 Exposure 1 detailed facies photographs. Labels correspond to positions on the stratigraphic panel and numbers refer to units (Figure 2.6). Facies codes (Table 2.2) are presented on the photographs.

matrix supported) pebble gravel (Figure 2.7 1d-e, Figure 2.8 1a). In Exposure 2, clast size (ranging from sand to pebble gravel) defines 5-30 cm thick discontinuous tabular beds, with reverse grading overall. Clasts here are dominantly schist (Figure 2.9). This unit contains a prominent channel (2-3 m deep, 5-7 m wide) cut into underlying sediments in Exposure 1 (Figure 2.6A). This channel is composed of matrix-supported, horizontally bedded gravels ~80 cm thick and a silt-sand matrix dominates the edges of the channel form. Clasts in this unit range from angular to well-rounded, although they are predominantly sub-rounded, as measured in two separate locations (Figure 2.9). Preliminary feldspar IRSL ages from Unit 1 suggest deposition at 25.6 ± 8.4 ka (USU-910, Exposure 1) and 32.4 ± 8.8 ka (USU-1090, Exposure 2) (Table 2.3, Figure 2.6). The sedimentary facies (horizontally bedded, open-framework and clast-support gravels and horizontally bedded sands) and stratigraphic architectures suggest that this unit represents glacial outwash. The debris flow channel fill, dewatering and loading structures in sand lenses, and open-framework gravel suggest rapid deposition in an ice-proximal environment.

Unit 2 is 2-4 m thick in Exposure 1 and 5-7 m thick in Exposure 2, is brownish-grey in color, and contains horizontally laminated and bedded sand (Sh), silt (Fl), and pebble gravel (Gh) in Exposure 1 (Figure 2.7 2a-b), and horizontally bedded and dipping open-framework gravels (Go, Gfo) with sand lenses (Sh, Sfo) in Exposure 2 (Figure 2.8 2a). This unit has a conformable, draping, planar contact with Unit 1 below, where exposed. Sand beds are thin to medium bedded and interbedded with thin to thickly bedded pebble gravel beds, and there are meter thick beds of millimeter- to centimeter-scale laminated silt and sand (Fl) (Figure 2.7 2a, 2b). This unit also contains depositional features in which coarse sand and gravel beds originate in a massive zone and then interfinger and fine into planar sandy and silty beds (Figures 2.6B and 2.6C). The horizontally bedded sand and gravel of Unit 2 is largely replaced by gravel beds with 20-30° depositional dips in Exposure 2. These beds form packages that are 1-3 m thick,

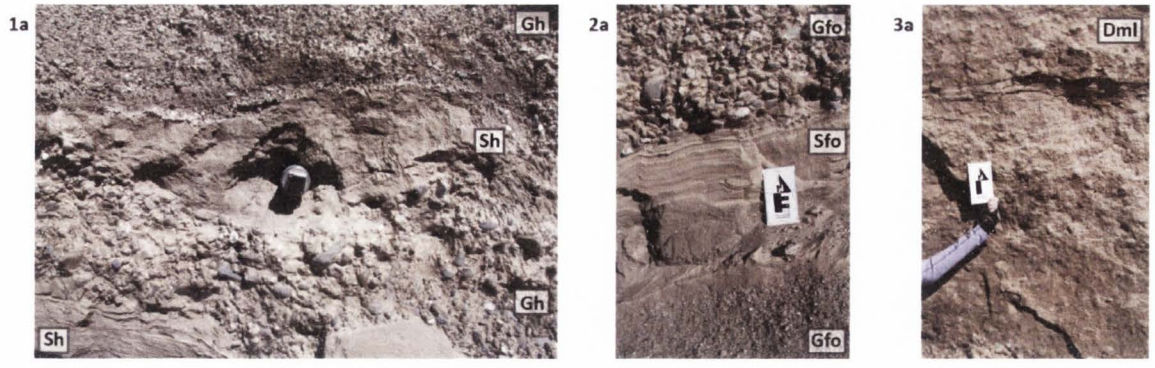

Figure 2.8 Exposure 2 detailed facies photographs. Labels correspond to positions on the stratigraphic panel and numbers refer to units (Figure 2.6). Facies codes (Table 2.2) are present on the photographs.

Table 2.3 Results from IRSL dating of feldspar. The locations of samples can be seen on Figure 2.6.

USU Lab number	Method	OD (%)	Skew	Aliquots Accepted[3]	Dose rate (Gy/ka)	Equivalent dose, De (Gy)[5]	Age (ka)
USU-910	MAM-3[1]	52.7 ± 8.2[2]	0.98 ± 0.51	23(32)	4.10 ± 0.21	72.47 ± 11.16	25.6 ± 8.4
USU-1090	MAM-3[1]	41.3 ± 12.6[2]	1.14 ± 0.74[2]	11(40)	4.71 ± 0.29	150.81 ± 25.41	32.4 ± 8.8

[1] 3-parameter minimum age model (Galbraith et al., 1999)
[2] Significant over-dispersion or positive skew following methods of Bailey and Arnold (2006)
[3] 2-mm mask size; number of aliquots accepted, number of aliquots run in parantheses
[4] Dose rate determined using conversion from concentration data following Guerin et al. (2011), andradioelemental concentration from ICP-MS, which includes the contribution from cosmic sources (Prescott and Hutton, 1994)
[5] Using the single aliquot regenerative dose method (SAR) (Wallinga et al., 2000) with fading correction following Auclair et al. (2003); presented with 2σ uncertainty

composed of pebble-cobble sized clasts and few boulders, and have been sculpted into distinct arcuate forms approximately 10s to 100 m wide and <5 m tall. In Unit 2 overall, clast size differentiates bedding, and clasts tend to be coarser towards the top of the unit. Clasts range from sub-angular to well-rounded and are predominantly sub-rounded (Figure 2.9). The sedimentary facies and stratigraphic architectures of Unit 2 overall suggest that this unit represents ice-proximal sediment aggradation into a subaqueous environment. Horizontally bedded sand and gravel and sand lenses suggest that it was fed by an ice-proximal system. The dipping gravel beds in Exposure 2 are interpreted to be delta foresets, and the aggrading and prograding sands and gravels that interfinger with horizontally bedded sands and silts in Exposure 1 are interpreted to be subaqueous ice-contact fans (e.g. Shulmesiter et al., 2010b).

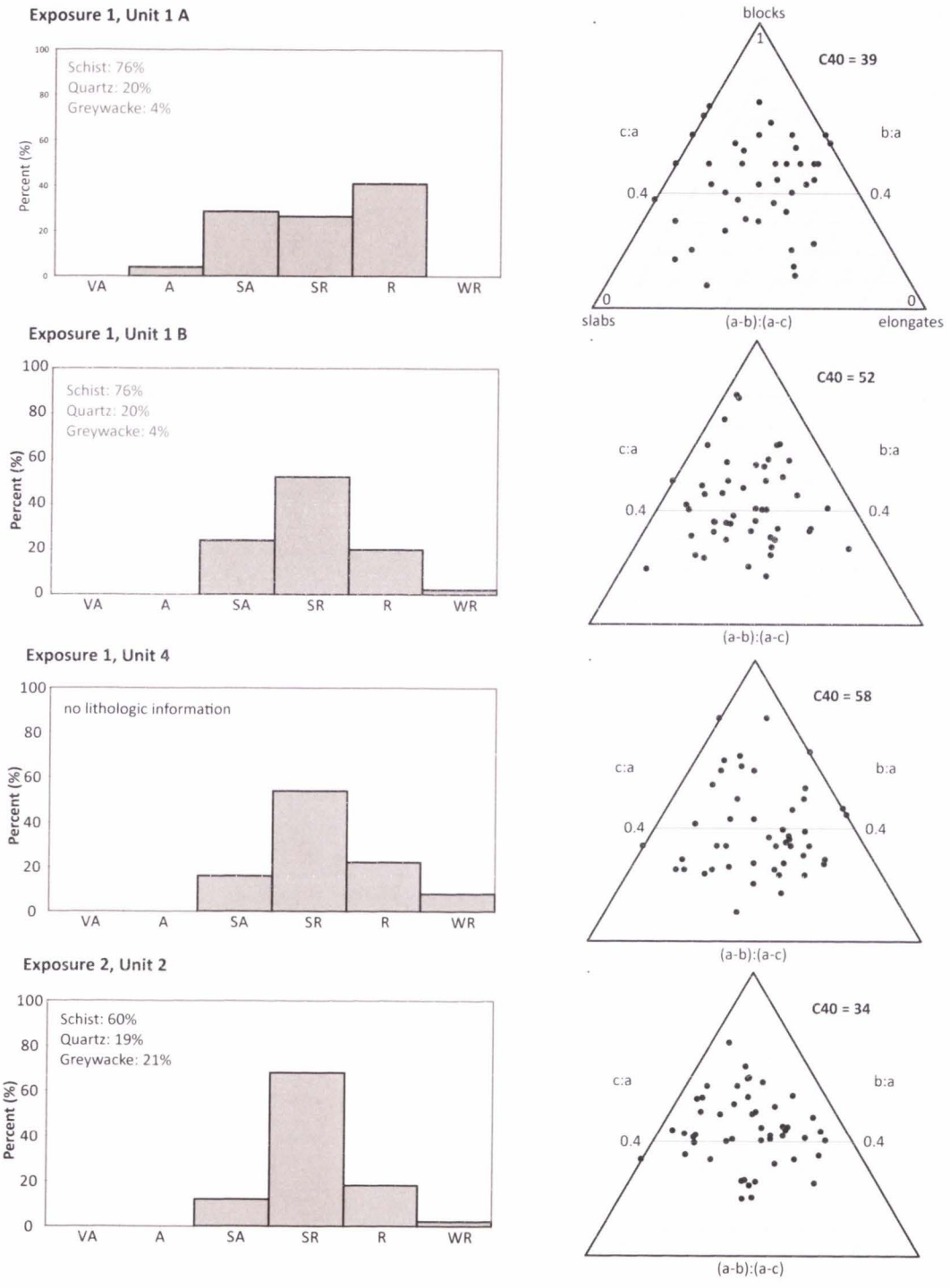

VA = very angular / A = angular / SA = sub-angular / SR = sub-rounded / R = rounded / WR = well-rounded

Figure 2.9 Clast shape data. Individual datasets composed of pebble counts of 50 pebble- to gravel-sized clasts. Lithologic information is present where collected. The lithologic count from Exposure 1 Unit 1 was conducted in a separate location and is therefore represented unassociated with either clast count as a general dataset for Exposure 1 Unit 1, and therefore differentiated by grey font.

McKellar (1960) studied an exposure along the eastern wall of the meltwater channel separating Exposure 1 and Exposure 2, which he refers to as "the gorge," and noted dipping beds of stratified gravels. He similarly interprets these dipping beds to represent delta foresets or ice-contact deposition in local depressions. These facies and depositional features support the interpretation of ice advancing into a lacustrine environment. The sculpted arcuate forms of this unit in Exposure 2 are interpreted to be "mega- flutes," as explained in the interpretation of Unit 3 and summarized by Menzies and Shilts (1996).

Unit 3 is 2-3 m thick in Exposure 1 and 3-4 m thick in Exposure 2. This unit is a light tan, weakly stratified diamicton (Dml) with a silty matrix and silt partings and has a disconformable basal contact that generally drapes scoured, underlying topography (Figure 2.8 3a). This unit also truncates the underlying glaciolacustrine Unit 2 in places in Exposure 2. The basal contact features convex-up structures ~60-85 m wide, separated by areas where the original deposits of Unit 2 (i.e. the interpreted delta foresets) have been removed (Figure 2.6). Evidence for scouring includes truncated beds and small-scale deformation of the underlying Unit 2 below, near the erosional contact. Rounded cobble to boulder clasts are larger towards the bottom of the diamicton creating normally graded sequence, and many boulders are striated.

The erosional basal contact of this diamicton suggests that this unit was deposited following an ice advance that over-rode the underlying ice-proximal sediment. The subsequent deposition of diamicton, with water reworking as interpreted from its weak stratification, is interpreted to have been deposited during an ice still-stand. This depositional unit is interpreted to represent the main Hawea moraine-building event.

Unit 4 is 3-4 m thick, light tan in color, contains weakly bedded silt (Fl) and sand (Sh) (Figure 2.7 4a), and has a conformable basal contact. Bedding is 10-40 cm thick and contains some small ripples (Sr) and coarse sand to small pebble lags. Clasts range from sub-angular to

well-rounded, but are predominantly sub-rounded (Figure 2.9). This unit is laterally discontinuous, found only in Exposure 1, and also contains one noticeable zone of deformation. Originally horizontally bedded sediment appears compressed and is folded upward at the edges and is isoclinally folded (Figure 2.6E). Similar folds and other forms of deformation, i.e. normal and reverse faults, of this unit and the others exposed were noted by Armstrong (2010), who interpreted them as deformation from localized stress exerted by the ice front. Additionally, Armstrong noted cobble- to boulder-sized drop-stones (Armstrong, 2010). McKellar (1960) described this unit in "the gorge" and also noted occasional pebbles and boulders. The sedimentary facies, stratigraphic architecture, and presence of drop-stones and deformation suggest that this unit represents ice-proximal lacustrine sedimentation. Overall, this unit was thicker towards the lake basin prior to its removal by lake bluff retreat, suggesting ponding between the moraine and the retreating ice front (Figure 2.10).

Discussion

Reconstruction of the Last Glacial Advance in the Lake Hawea Valley

Composite stratigraphic columns are shown in Figure 2.10 as a fence diagram and the reconstructed glacial history is summarized in six phases in Figure 2.11. In overview, the study area is an end moraine composed of four stratigraphic units marking the ice-extent of the Hawea advance. The stratified and interbedded sandand gravel with local crossbedding of Unit 1 are interpreted to represent a glacial outwash braided channel network (e.g. Golledge and Phillips, 2008). Sediment size differences between interbeds correspond to variable spatially and temporally variable flow regimes (lower for sand and higher for gravel). The two age estimates from sand beds in Unit 1 indicate it was deposited ~32-26 ka. This braided outwash system likely existed during ice retreat from the Mt. Iron or Albertown position, the next oldest and down-

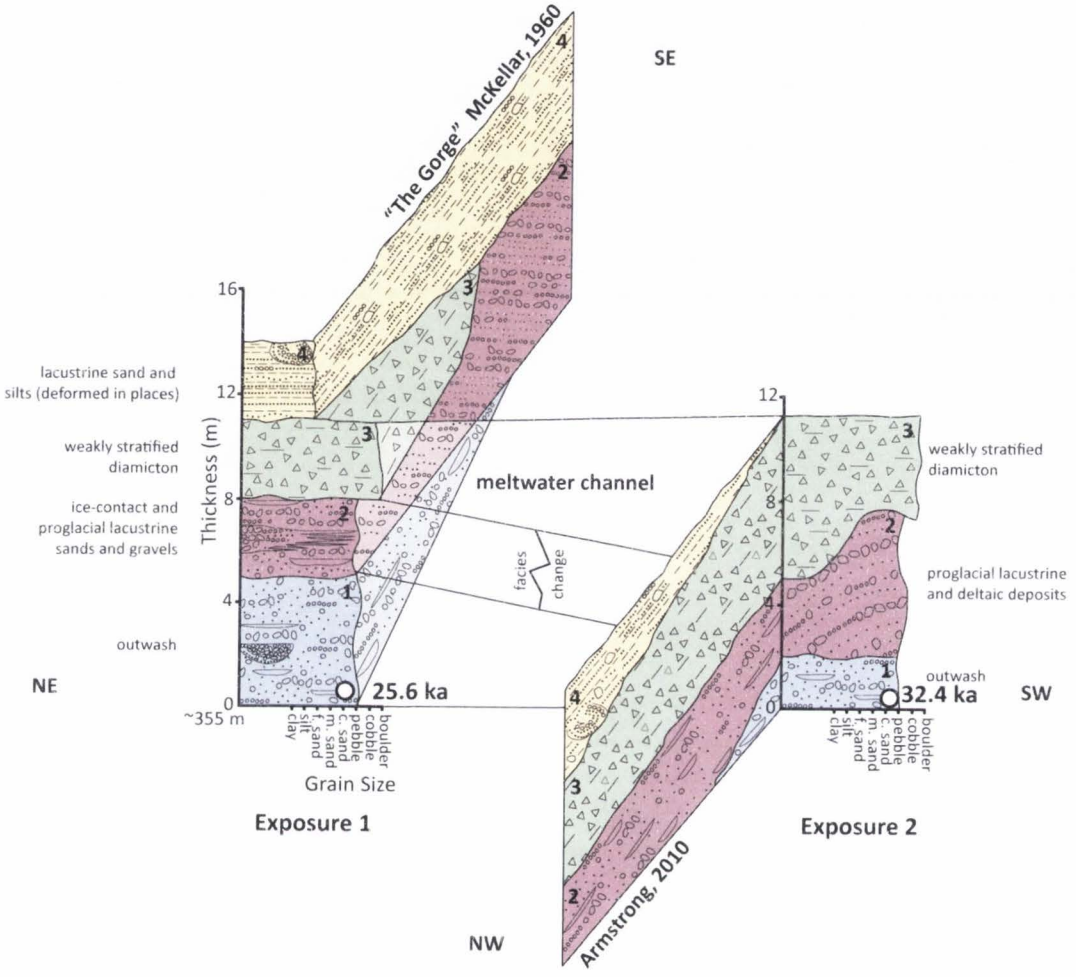

Figure 2.10 Stratigraphic columns presented in a fence diagram illustrating the stratigraphy of the Hawea moraine. The columns representing Exposure 1 and Exposure 2 are derived from this research, and tie lines show relations between units of these two exposures. Open circles and associated ages show OSL sample locations. Unit thicknesses, relations between units, and grain sizes of the McKellar (1960) and Armstrong (2010) sections are not well defined and speculatively depicted here. The length of all four exposures shown does not correspond to length in reality and instead is schematically depicted.

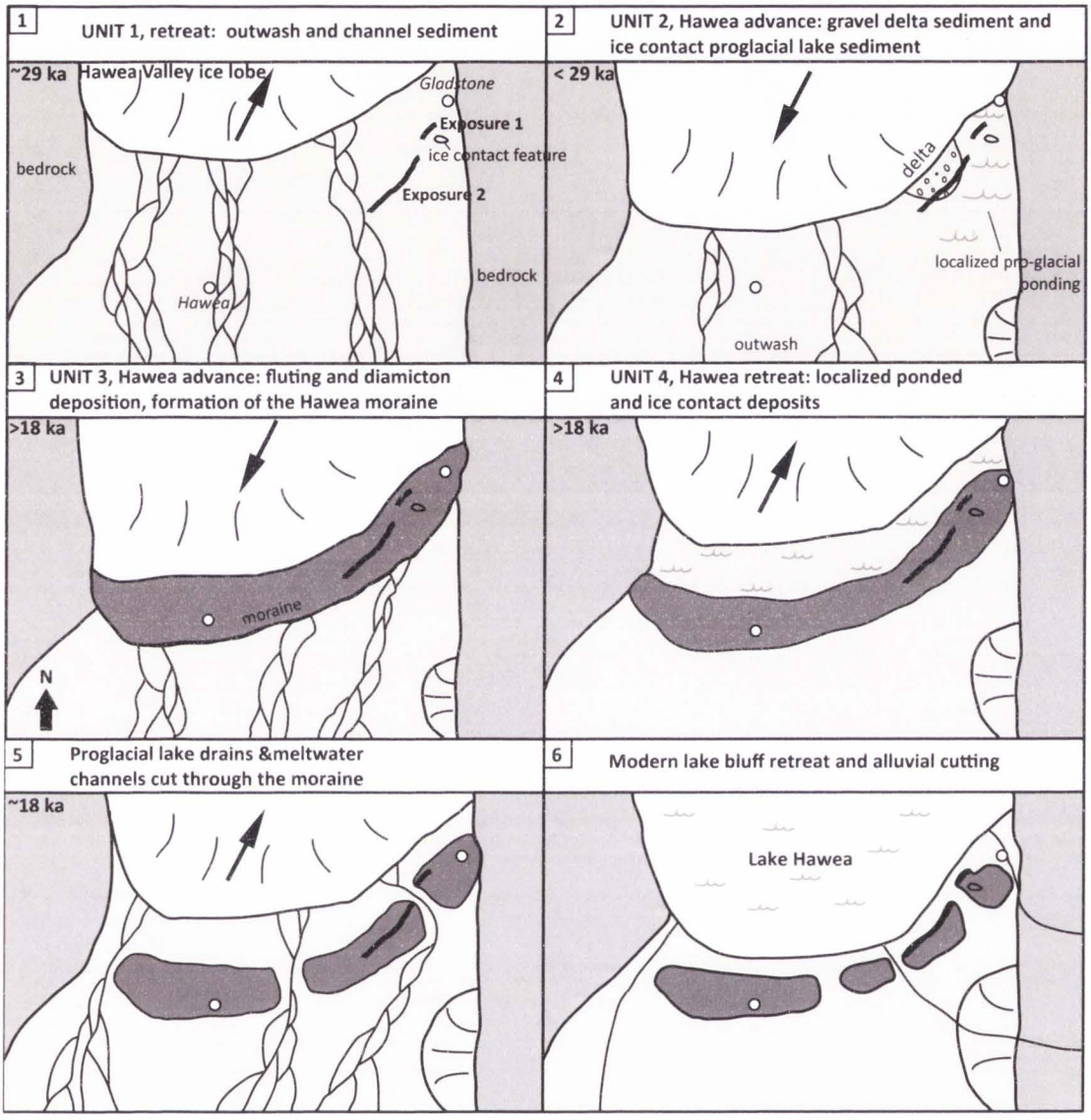

Figure 2.11 The Lake Hawea valley LGM glacial environment and sequence. Arrows show direction of ice movement. Open circles show the towns of Hawea and Gladstone. Thick lines indicate exposure locations. Step 1 shows the proglacial outwash and braided channel environment. Step 2 shows local ponding and associated proglacial gravel delta sedimentation and ice contact proglacial lacustrine sedimentation. Step 3 shows further ice advance, scouring of outwash deposits below producing fluting, and diamicton deposition. Step 4 shows the glacier retreating up valley and the formation of a proglacial lake between the ice front and moraine. Step 5 shows draining of the proglacial lake and meltwater channel cutting of the moraine during ice retreat. The glacier continued to retreat until eventual disappearance during Pleistocene deglaciation. Step 6 shows modern Lake Hawea, lake bluff/moraine retreat, and alluvial cutting of the moraine.

valley ice positions previously recorded in the upper Clutha River valley (Thomson, 2009) based on its position in the stratigraphy below the Hawea moraine-forming diamicton (Unit 3, see below).

The overlying Unit 2 is ice-contact, ponded deposits. Several interpretations of what created this ponding are plausible: 1) localized damming of glacial meltwater by a topographic feature down-valley; 2) pooling in the over-deepened trough created by previous advances; or 3) a local depression. Potential dams include deposits from previous Mt. Iron or Albertown glacial advances. A lack of collapse features suggests that this environment was likely not caused by kettle lake formation. The interpretation of a lacustrine environment is based on horizontally bedded sediments, fine laminations, and the draping character. The interpreted subaqueous ice-contact fans and the dipping pebble-cobble gravel delta foreset deposits further support the interpretation of a glaciolacustrine setting. This proglacial sedimentation likely occurred as the ice advanced before reaching the Hawea position, during the Hawea advance, based on stratigraphic position overlying sediment deposited during ice retreat and underlying the Hawea moraine-forming diamicton.

Further glacial advance caused the Unit 2 lake deposits to be over-ridden, and ice scoured the delta deposits of Exposure 2 into distinctly arcuate flute forms. The ice then stagnated and deposited the weakly stratified diamicton (Unit 3) while the ice was at a stable position. Weak stratification suggests water reworking and therefore an ice-proximal setting, as opposed to subglacial deposition. The surface topography and the extent of the diamicton demark the Hawea moraine.

Retreat from the Hawea moraine produced a local area of ponding in areas, as seen in Exposure 1, and previously recorded lake-ward of Exposure 2 by Armstrong (2010). Sediment

deposited within this ice-contact lake includes laminated and rippled silt and sand and occasional drop-stones, which are most indicative of glaciofluvial transport into a lacustrine setting. These sediments are also locally deformed, and most of Unit 4 was likely deposited up-valley of the current exposures, and these sediments exist only at the top of Exposure 1 and the gorge between Exposure 1 and Exposure 2, suggesting short-lived deposition between the moraine and the retreating ice front, poor preservation, or both.

The Hawea moraine was eventually breached and the lake lowered due to cutting of meltwater channels through the moraine and extended to the braided outwash channel network (Qo) south of the Hawea moraine (Figure 2.5). Meltwater from the ice margin extended down-valley of the moraine as several braided fluvial systems, creating the braided outwash plain, as shown by the preservation of braided outwash channel plain (Q_o) scars on the modern landscape. Linkage of these channels cut into the Hawea moraine to the braided plain to the south suggests that sediment-laden meltwater created these channels. This occurred ~18 ka, based on the peat in the outlet channel described by McKellar (1960). Ice continued to retreat up-valley and did not re-advance past the Hawea moraine.

The timing of events surrounding formation on the Hawea moraine remains preliminary and poorly constrained. The IRSL ages from the base of Unit 1 provide constraint on this outwash unit and retreat from the Mt. Iron position to ~32-26 ka. These samples were collected from near the base of the unit, however, and therefore provide a minimum age on Mt. Iron retreat, based on the stratigraphy and interpreted glacial history. Age control on the timing of ice retreat from the Hawea moraine, after deposition of Unit 4, comes from a ~18 ka radiocarbon age from sediment in a meltwater channel (McKellar, 1960) and ~17.5 ka TCN age from scoured bedrock in a meltwater channel (Graham et al., 1998). These ages provide a minimum constraint on retreat from the Hawea position, formation of Lake Hawea, and

establishment of the current lake outlet. The IRSL and other ages broadly constrain formation of the Hawea moraine to 32-17.5 ka and therefore correlative with the global LGM.

Comparison to Other Southern Alps MIS 2 Glacial Systems and New Zealand Paleoclimate Reconstructions

The glacial chronology and deposits that preceded, formed, and post-dated the Hawea moraine includes retreat from a MIS 3/2 ice-margin position further down valley and readvance during MIS 2 to the Hawea moraine, followed by deglaciation of the valley. This chronology, although only broadly constrained, correlates well with other documented late Pleistocene glacial chronologies and paleoclimate reconstructions (Table 2.1, Figure 2.3) from the South Island of New Zealand (Figure 2.1). The Hawea moraine was formed sometime between 32 ka and 17.5 ka, which corresponds to a period of decreased temperature overall punctuated by periods of increased precipitation (Figure 2.3).

The interpreted glacial history of the Hawea valley records the position of ice here during the gLGM. The emphasis on detailed sedimentologic and stratigraphic analysis of the Hawea moraine reveals a sequence of ice retreat, ice re-advance, and additional ice retreat spanning ~32-17.5 ka, which would not have been traceable through only analysis of spatial relationships of glacial geomorphic features in the valley. Similarly, most studies that rely on cosmogenic nuclide dating of glacial features on the South Island only consider recessional moraines, providing only a glimpse into glacial history. The results of this study show a dynamic ice-margin through the gLGM, as opposed to a static ice position during this period.

The stratigraphic record of the Hawea moraine additionally reveals information about proglacial lacustrine environments. Longitudinal lakes formed in overdeepened glacial troughs, like Lake Hawea, are especially prominent on the eastern side of the Southern Alps (Gage,

1958). Ice-margins interactions with these lakes may affect ice dynamics due to effects of calving and buoyancy of the ice margin, as well as proglacial depositional processes. Although research on this subject in New Zealand is not prolific, the stratigraphic architectures and sedimentology of landforms like the Hawea moraine may elucidate clues to the relationships between proglacial lakes and the dynamics of ice advance and retreat, as speculated by Shulmeister et al. (2010a).

Conclusions

A moraine and outwash composed of sediment associated with the two most recent ice positions constrains modern Lake Hawea. The diamicton unit marks the extent of the late Pleistocene Hawea advance (Thomson, 2009). The lowest braided outwash sediments are inferred to have been deposited during retreat from an ice position further down valley, ~32-26 ka. Subsequent glaciolacustrine sediments were deposited either in a proglacial lake or in the overdeepened trough created by former Hawea valley ice advances. The following ice advance scoured underlying delta gravel deposits. Diamicton deposition and formation of the Hawea moraine was followed by localized lacustrine sedimentation until ice retreated beyond the moraine, allowing meltwater channels to cut through the moraine. Previous age constraint from the modern outlet channel of Lake Hawea suggests ice retreat from the Hawea moraine by 18 ka (^{14}C; McKellar, 1960) and 17.5 ka (TCN; Graham et al., 1998). Chronologic constraint shows that the Hawea moraine formed between 32 and 17.5 ka.

The chronology of the Hawea lobe presented in this research is roughly correlative with other MIS 3 and MIS 2 advances of the South Island and also shows a dynamic ice-margin during the gLGM. Although the debated climatic mechanisms of advance and retreat during this time period cannot be addressed by our data, a review of previous work suggests that and unknown

combination of increased precipitation and decreased temperature leading up to the LGM drove ice advance. This research adds to a growing database of transport and depositional processes of valley glaciers in maritime climate zones and proglacial lacustrine environments by highlighting the dominance of water in all ice-proximal deposits of the Hawea exposures.

References Cited

Aitken, M. J., 1998. An Introduction to Optical Dating: the Dating of Quaternary Sediments by the Use of Photon-stimulated Luminescence. Oxford University Press, Oxford, United Kingdom.

Alexanderson, H., 2007. Residual OSL signals from modern Greenlandic river sediments. Geochronometria 26, 1-9.

Alloway, B. V., Lowe, D. J., Barrell, D. J. A., Newnham, R. M., Almond, P. C., Augustinus, P. C., Bertler, N. A. N., Carter, L., Litchfield, N. J., McGlone, M. S., Shulmeister, J., Vandergoes, M. J., Williams, P. W., 2007. Towards a climate event stratigraphy for New Zealand over the past 30 000 years (NZ-INTIMATE project). Journal of Quaternary Science 22(1), 9-35.

Armstrong, M. H., 2010. Glaciotectonic deformation of the Hawea Moraine. Master of Science Thesis, University of Otago.

Anderson, B., Mackintosh, A., 2006. Temperature change is the major driver of late-glacial and Holocene glacier fluctuations in New Zealand. Geology 34(2), 121-124.

Auclair, M., Lamothe, M., Huot, S., 2003. Measurement of anomalous fading for feldspar IRSL using SAR. Radiation Measurements 37, 487-492.

Bailey, R. M., Arnold, L. J., 2006. Statistical modeling of single grain quartz De distributions and an assessment of procedures for estimating burial dose. Quaternary Science Reviews 25, 2475-2502.

Benn, D. I., Ballantyne, C. K., 1993. The description and representation of particle shape. Earth Surface Processes and Landforms 18, 665-672.

Blunier, T., Brook, E. J., 2001. Timing of millennial-scale climate change in Antarctica and Greenland during the last glacial period. Science 291, 109-112.

Denton, G. H., Lowell, T. V., Heusser, C. J., Moreno, P. I., Andersen, B. G., Heusser, L. E., Schlüchter, C., Marchant, D. R., 1999. Interhemispheric linkage of paleoclimate during the Last glaciation. Geografiska Annaler 81(2), 107-153.

Doughty, A. M., Anderson, B. M., Mackintosh, A. N., Kaplan, M. R., Vandergoes, M. J., Barrell, D. J. A., Denton, G. H., Schaefer, J. M., Chinn, T. J. H., Putnam, A. E., 2012. Evaluation of Lateglacial

temperatures in the Southern Alps of New Zealand based on glacier modeling at Irishman Stream, Ben Ohau Range. Quaternary Science Reviews *in press*.

Evans, D. J. A., Benn, D. I., 2004. *A Practical Guide to the Study of Glacial Sediments*. Hodder Education, London, United Kingdom.

Evans, D. J. A., Shulmeister, J., Hyatt, O., 2010. Sedimentology of latero-frontal moraines and fans on the west coast of South Island, New Zealand. Quaternary Science Reviews 29(27-28), 3790-3811.

Evans, D. J. A., Rother, H., Hyatt, O., Shulmesiter, J., 2013. The glacial sedimentology and geomorphological evolution of an outwash head/moraine-dammed lake, South Island, New Zealand. Sedimentary Geology 284-185, 45-75.

Evans, M. D., 2008. A geomorphological and sedimentological approach to understanding the glacial deposits of the lake Clearwater basin, mid Canterbury, New Zealand. M. S. Thesis, University of Canterbury, Ilam, New Zealand.

Gage, M., 1958. Late Pleistocene glaciations of the Waimakariri Valley, Canterbury, New Zealand. New Zealand Journal of Geology and Geophysics 1(1): 123-155.

Gage, M., Suggate, R. P., 1958. Glacial chronology of the New Zealand Pleistocene. Bulletin of the Geological Society of America 69, 589-598.

Galbraith, R. F., Roberts, R. G., Laslett, G. M., Yoshida, H., Olley, J. M., 1999. Optical dating of single and multiple grains of quartz from Jinmium rock shelter, northern Australia: Part I, experimental design and statistical models. Archaeometry 41, 339-364.

Golledge, N. R., Mackintosh, A. N., Anderson, B. M., Buckley, K. M., Doughty, A. M., Barrell, D. J. A., Denton, G. H., Vandergoes, M. J., Andersen, B. G., Schaefer, J. M., 2012. Last Glacial Maximum climate in New Zealand inferred from a modeled Southern Alps icefield. Quaternary Science Reviews 46, 30-45.

Graham, I.J., Kim, K., McSaveney M.J., Zondervan, A., Webb, P., 1998. Establishment of surface exposure dating methods using ^{10}Be and ^{26}Al at GNS. Institute of Geological and Nuclear Science science report 98/30, Lower Hutt, New Zealand.

Guérin, G., Mercier, N., Adamiec, G., 2011. Dose-rate conversion factors: update. Ancient TL 29, 5-8.

Hellstrom, J., McCulloch, M., Stone, J., 1998. A detailed 31,000-year record of climate and vegetation change, from the isotope geochemistry of two New Zealand speleothems. Quaternary Research 50, 167-178.

Heusser, L. E., van de Geer, G., 1994. Direct correlation of terrestrial and marine paleoclimatic records from four glacial-interglacial cycles—DSDP Site 594 southwest Pacific. Quaternary Science Reviews 13, 273-282.

Huntley, D. J., Godfrey-Smith, D. I., and Thewalt, M. L. W., 1985, Optical dating of sediments. Nature 313, 105-107.

Hyatt, O. M., Shulmeister, J. Evans, D. J. A., Thackray, G. D., Rieser, U., 2012. Sedimentology of a debris-rich, perhumid valley glacier margin in the Rakaia Valley, South Island, New Zealand. Journal of Quaternary Science 27(7), 699-712.

Indermühle, A., Monnin, E., Stauffer, B., Stocker, T. F., Wahlen, M., 1999. Atmospheric CO_2 concentration from 60 to 20 kyr BP from the Taylor Dome ice core, Antarctica. Geophysical Research Letters, 27, 735-738.

Kirk, R. M., Komar, P. D., Allan, J. C., Stephenson, W. J., 2000. Shoreline erosion on Lake Hawea, New Zelaand, caused by high lake levels and storm-wave runup. Journal of Coastal Research 16(2), 346-356.

Klasen, N., Fiebig, M., Preusser, F., Reitner, J., Radtke, U., 2007. Luminescence dating of proglacial sediments from the Eastern Alps. Quaternary International 164-165, 21-32.

Kostic, B., Becht, A., Aigner, T., 2005. 3-D sedimentary architecture of a Quaternary gravel delta (SW-Germany): Implications for hydrostratigraphy. Sedimentary Geology 181, 143-171.

Lukas, S., Spencer, J. Q. G., Robinson, R. A. J., Benn, D. I., 2007. Problems associated with luminescence dating of Late Quaternary glacial sediments in the NW Scottish Highlands. Quaternary Geochronology 2, 243-248.

Mansergh, G. D. 1973. The New Zealand Quaternary; an introduction. In: Guidebook for Ninth INQUA Congress, Christchurch, New Zealand, p.63.

Marra, M. J., Leschen, R. A. B., 2004. Late Quaternary paleoecology from fossil beetle communities in the Awatere Valley, South Island, New Zealand. Journal of Biogeography 31, 571–586.

Marra, M. J., Shulmeister, J., Smith, E. G. C., 2006. Reconstructing temperature during the Last Glacial Maximum from Lyndon Stream, South Island, New Zealand using beetle fossils and maximum likelihood envelopes. Quaternary Science Reviews 25, 1841–1849.

Marra, M. J., Smith, E. G. C., Shulmeister, J., Leschen, R., 2004. Late Quaternary climate change in the Awatere Valley, South Island, New Zealand using a sine model with a maximum likelihood envelope on fossil beetle data. Quaternary Science Reviews 23, 1637–1650.

McCarthy, A., Mackintosh, A., Reiser, U., Fink, D., 2008. Mountain Glacier Chronology from Boulder Lake, New Zealand, Indicates MIS 4 and MIS 2 Ice Advances of Similar Extent. Arctic, Antarctic, and Alpine Research 40(4), 695-708.

McKellar, I. C., 1960, Pleistocene deposits of the upper Clutha valley, Otago, New Zealand. Journal of Geology and Geophysics 3, 432-460.

Menzies, J., Shilts, W. W., 1996. Subglacial environments. In: Past Glacial Environments Sediments, Forms and Techniques. Butterworth-Heinemann Ltd, Oxford, United Kingdom, p. 15-136.

Murray, A. S., Wintle, A. G., 2000. Luminescence dating of quartz using an improved single-aliquot regenerative-dose protocol, Radiation Measurements 32, 57-73.

Murray, A. S., Wintle, A. G., 2003. The single aliquot regenerative dose protocol: potential for improvements in reliability, Radiation Measurements 37, 377-381.

Newnham, R. M., Vandergoes, M. J., Hendy, C. H., Lowe, D. J., Preusser, F., 2007. A terrestrial palynological record for the last two glacial cycles from southwestern New Zealand. Quaternary Science Reviews 26, 517-535.

Otago Regional Council, Annual Rainfall – Median. GrowOTAGO Maps. Web. 16 Jan. 2013. <http://growotago.orc.govt.nz/scripts/mapserv.exe?imgxy=299.5 199.5>.

Paterson, W. S. B., 1994, *Physics of Glaciers*. Pergamon, Tarrytown, N. Y., 480.

Prescott, J. R., Hutton, J. T., 1994. Cosmic ray contributions to dose rates for luminescence and ESR dating: large depths and long-term time variations, Radiation Measurements 23, 497-500.

Preusser, F., Andersen, B. G., Denton, G. H., Schlüchter, C., 2005. Luminescence chronology of Late Pleistocene glacial deposits in North Westland, New Zealand. Quaternary Science Reviews 24, 2207-2227.

Preusser, F., Ramseyer, K., Schlüchter, C., 2006. Characterisation of low OSL intensity quartz from the New Zealand Alps. Radiation Measurements 41, 871-877.

Putnam, A. E., Schaefer, J. M., Denton, G. H., Barrell, D. J. A., Birkel, S. D., Andersen, B. G., Kaplan, M. R., Finkel, R. C., Schwartz, R., Doughty, A. M., 2013. The Last Glacial Maximum at 44°S documented by a ^{10}Be moraine chronology at Lake Ohau, Southern Alps of New Zealand. Quaternary Science Reviews 62, 114-141.

Ricker, K. E., Chinn, T. J. H., McSavney, M. J., 1992. A late Quaternary moraine sequence dated by rock weathering rinds, Craigieburn Range, New Zealand. Canadian Journal of Earth Sciences 30, 1861-1869.

Rother, H., Shulmeister, J., 2006. Synoptic climate change as a driver of late Quaternary glaciations in the mid-latitudes of the Southern Hemisphere. Climate of the Past 2, 11-19.

Rowan, A. V., Roberts, H. M., Jones, M. A., Duller, G. A. T., Covey-Crump, S. J., Brocklehurst, S. H., 2012. Optically stimulated luminescence dating of glaciofluvial sediments on the Canterbury Plains, South Island, New Zealand. Quaternary Geochronology 8, 10-22.

Schaefer, J. M., Denton, G. H., Barrell, D. J. A., Ivy-Ochs, S., Kubik, P. W., Andersen, B. G., Phillips, F. M., Lowell, T. V., Schlüchter, C., 2006. Near-synchronous interhemispheric termination of the last glacial maximum in mid-latitudes. Science 312, 1510-1513.

Shulmeister, J., Fink, D., Augustinus, P. C., 2005. A cosmogenic nuclide chronology of the last glacial transition in North-West Nelson, New Zealand—new insights in Southern Hemisphere climate forcing during the last deglaciation. Earth and Planetary Science Letters 233, 455-466.

Shulmeister, J., Fink, D., Hyatt, O. M., Thackray, G. D., Rother, H., 2010a. Cosmogenic 10Be and 26Al exposure ages of moraines in the Rakaia Valley, New Zealand and the nature of the last termination in New Zealand glacial systems. Earth and Planetary Science Letters 297, 558-566.

Shulmeister, J., Thackray, G. D., Rieser, U., Hyatt, O. M., Rother, H., Smart, C. C., Evans, D. J. A., 2010b. The stratigraphy, timing and climatic implications of glaciolacustrine deposits in the middle Rakaia Valley, South Island, New Zealand. Quaternary Science Reviews 29(17-18), 2362-2381.

Smith, H. J., Fischer, H., Mastroianni, D., Deck, B., Wahlen, M., 1999. Dual modes of the carbon cycle since the Last Glacial Maximum. Nature 400, 248-250.

Suggate, R. P., 1965. Late Pleistocene geology of the northern part of the South Island, New Zealand. New Zealand Geological Survey Bulletin 77, 91

Suggate, R. P., 1990. Late Pliocene and Quaternary Glaciations of New Zealand. Quaternary Science Reviews 9, 175-197.

Suggate, R. P., Almond, P. C., 2005. The Last Glacial Maximum (LGM) in western South Island, New Zealand: implications for the global LGM and MIS 2. Quaternary Science Reviews 24, 1923-1940.

Suggate, R. P., Moar, N. T., 1970. Revision of the chronology of the late Otira glacial. New Zealand Journal of Geology and Geophysics 13, 742-746.

Thackray, G. D., Shulmeister, J., Fink, D., 2009. Evidence for expanded middle and late Pleistocene glacier extent in northwest Nelson, New Zealand. Geografiska Annaler 91 A(4): 291-311.

Thomson, R., 2009. Field Trip 2 to the glacial history of the Upper Clutha. The 2009 New Zealand Snow and Ice Resaerch Group (SIRG) Annual Workshop.

Vandergoes, M. J., Fitzsimons, S. J., 2003, The Last Glacial-Interglacial Transition (LGIT) in south Westland, New Zealand: paleoecological insight into mid-latitude Southern Hemisphere climate change. Quaternary Science Reviews 22: 1461-1476.

Wallinga, J., Murray, A., Wintle, A., 2000, The single-aliquot regenerative-dose (SAR) protocol applied to coarse-grain feldspar. Radiation Measurements 32, 529-533.

Whittaker, T. E., Hendy, C. H., Hellstrom, J. C., 2011. Abrupt millennial-scale changes in intensity of Southern Hemisphere westerly winds during marine isotope stages 2-4. Geology 39, 455-458.

Williams, P. W., 1996. A 230 ka record of glacial and interglacial events from Aurora Cave, Fiordland, New Zealand. New Zealand Journal of Geology and Geophysics 39, 225-241.

Williams, P.W., King, D. N. T., Zhao, J.-X., Collerson, K.D., 2005. Late Pleistocene to Holocene composite speleothem ^{18}O and ^{13}C chronologies from South Island, New Zealand – did a global Younger Dryas really exist? Earth and Planetary Science Letters 230, 301-317.

Williams, P. W., Neil, H., Zhao, J.-X., 2010. Age frequency distribution and revised stable isotope curves for New Zealand speleothems: paleoclimatic implications. International Journal of Speleology 39(2),: 99-112.

Wintle, A. G., Murray, A. S., 2006. A Review of Quartz Optically Stimulated Luminescence Characteristics and Their Relevance in Single-aliquot Regeneration Dating Protocols, Radiation Measurements 41, 369-391.

CHAPTER 3

THE STRATIGRAPHY AND HISTORY OF GLACIAL ADVANCES IN THE SOUTH FORK HOH RIVER VALLEY, OLYMPIC MOUNTAINS, WASHINGTON, UNITED STATES

Abstract

The glacial stratigraphy exposed along the cutbanks of the South Fork Hoh River in the Olympic Peninsula, Washington allows reconstruction of MIS 2 ice, valley glacier dynamics, and sedimentary sequences. Age control was obtained from optically stimulated luminescence dating of quartz sand and radiocarbon dating of organic material. Glacial diamicton, outwash, and lacustrine sediments were deposited in association with four late Pleistocene ice-margin positions, the oldest of which extended beyond the South Fork valley into the main stem Hoh River valley (>23 ka). Three younger ice-margin positions were mapped as the SF 1-3 moraines (22-19 ka, <19 ka, and <19 ka) and were identified using stratigraphic records in cutbank exposures and geomorphic moraines. While the SF 1 and SF 3 positions were previously identified as the Twin Creek I and Twin Creeks II advances, the SF 2 position had not previously been recognized in this valley or other regional valleys. Notable sedimentologic observations of this wet-based glacier include few true tills, much water reworking, and moraines composed of stratigraphically poorly sorted sediment. The results of this study confirm that the South Fork Hoh valley is part of a unique setting in the Olympic and Cascade Mountains, in which the LGM is diminished in relation to MIS 4-3 ice positions. Additionally, this research provides a detailed reconstruction of LGM glacial conditions in the South Fork Hoh valley that show rapid ice-margin fluctuation.

1. Introduction

Glacial ice extent, as preserved in the geomorphic record by moraines, is modulated by glacier mass balance, which is primarily controlled by climate. More specifically, winter snow accumulation and cool temperatures during the ablation season typically control ice advance and retreat (e.g. Paterson, 1994). The relative roles of precipitation and temperature on ice dynamics in the late Pleistocene are debated, however, and especially regarding the western United States.

The Olympic Mountains hosted extensive valley glaciers during the last glaciation. Today, the region lies within a humid climate influenced primarily by Pacific Ocean sea-surface temperature and pressure variations. Reconstructions of ice dynamics based on glacial deposits may elucidate details about the responses of humid-region glaciers to precipitation and temperature forcing related to the Pacific Ocean. The glacial chronology of the Cascade Mountains, which extend north-south from southern British Columbia to northern California (Porter and Swanson, 2008), and the chronology of the Olympic Mountains in northwestern Washington (Thackray, 2008) suggest a strong temperature influence on Late Pleistocene glacial mass balance. In the Cascade Mountains, six late Pleistocene advances occurred coincident with MIS 5d, 5b, 4, and 2 northern hemisphere insolation minima (and therefore reduced summer ablation) (Porter and Swanson, 2008). Olympic Mountain glacial advances also occurred during MIS 5d, 4, and 2 (Thackray, 2008). Most importantly, the MIS 2/global last glacial maximum (LGM) advance does not mark greatest ice extent in both the Olympic and Cascade Mountains. MIS 4-3 glacier advances in the Cascade Mountains (Porter and Swanson, 2008) and Olympic Mountains (Thackray, 2008) of Washington were more extensive than those during the global LGM, and greatest ice extent occurred during MIS 4 in the Olympic Mountains (Thackray, 2008) and MIS 5 in the Cascade Mountains (Porter and Swanson, 2008). This is in contrast with non-

maritime glaciers of the western United States, which reached their maximum extents during or after the LGM (26-19 ka) (Clark et al., 2009). Thackray (2008) suggested that increased ice volume during MIS 5 and MIS 4 in these regions was due to increased precipitation.

Traditional glacial chronologies are primarily constructed using geomorphic mapping and dating of glacial landforms such as moraines, glacial lakes, and outwash terraces. Ice advance and retreat deposit sediments and construct landforms that are related to the influence of climate changes on glacial mass balance. Glacial sediment deposits can therefore be examined to elucidate details about ice dynamics and depositional settings at the time of their emplacement. The importance of understanding the sedimentology and stratigraphic architecture of glacio-geomorphic landforms has recently been emphasized, as these detailed studies can provide more information about processes of formation and interpretations of landform origin in relation to ice dynamics (e.g. Evans and Benn, 2004).

This study focuses on deposits of the South Fork Hoh River valley (SF Hoh), a formerly glaciated valley in the Olympic Mountains of northwestern Washington. The research originally conducted by Thackray (1996, 2001, 2008) was updated and significantly expanded by improving descriptions of glacial sediments and the age control on deposits. This study relies heavily upon the descriptions and interpretations of the sedimentology and stratigraphy of glacial sequences exposed within cutbanks of the SF Hoh to establish ice margins and constrain the style and chronology of glacial advance and retreat in the SF Hoh valley. Results suggest a dynamic ice margin during the global LGM, characterized by multiple ice retreats and re-advances, as opposed to a more static ice position during this notable global climatic period.

1.1 Background

Thackray (2001) provides a comprehensive summary of the major valley glacier advances on the western Olympic Peninsula. Named advances include of Lyman Rapids (MIS 4), Hoh Oxbow 1-3 (MIS 3-2), and Twin Creeks 1-2 (MIS 2) (Table 3.1). The Hoh Oxbow 3 advance most closely corresponds to the global LGM (26-19 ka). Landforms marking this ice-marginal position include terminal moraines at the lower Hoh and Queets valleys and broad outwash terraces extending to coastal bluffs (Figure 3.1). Current age constraints suggest the timing of the Hoh Oxbow 2 (~34-31 ka) is broadly contemporaneous with Heinrich event 3, suggesting a possible link between Olympic glacial advances and conditions in the North Atlantic Ocean (Thackray, 2001).

Florer (1972) and Heusser (1972) used pollen from peat sequences exposed in the Kalaloch sea cliffs between the Hoh and Queets Rivers to reconstruct vegetation of the region between 17 to > 48 ka (Figure 3.1). These studies suggest mean July temperatures in the region at the time ranged from 11 to 14°C (Florer, 1972; Heusser, 1972), in comparison to the modern mean July temperature of ~16°C (1931-2005, WRCC). While temperatures were cooler during the late Pleistocene, periods of maximum ice extent do not appear to correspond to the coldest temperatures, suggesting that variations in Pacific moisture delivery was a dominant influence on ice extent within the Olympic Mountains (Thackray, 2001). These mountain glaciers are therefore thought to be more sensitive to moisture balance, with periods of advance related to enhanced precipitation and periods of retreat during more arid conditions. Moreover, glacial advances in the Olympic Mountains correlate partly with northern hemisphere insolation maxima, when temperatures were presumably warmer (Thackray, 2008). Hemispheric contrasts in insolation could have driven enhanced moisture delivery through strengthened atmospheric and westerly circulation.

Table 3.1 Glacial advances of the western Olympic Peninsula and associated ages (Thackray, 2001). Ages were calibrated using the IntCal09 calibration curve (Reimer et al., 2009).

Name	Age (14C ka)	Age (cal. ka)	Isotope Stage
Twin Creeks 2	undated	undated	2
Twin Creeks 1	19.1-18.3	22.8-21.9	2
Hoh Oxbow 3	23-19	27.9-22.7	2 (LGM)
Hoh Oxbow 2	29-27	33.7-31.3	3
Hoh Oxbow 1	39-26	43.2-41.2	3
Lyman Rapids	≥54	n/a	4

Continental ice sheets interacted only marginally with the Olympic Peninsula. The Puget Lobe of the Cordilleran ice sheet flowed into the Puget Lowland, between the Olympic and Cascade Mountains. This lobe experienced similar climate influences as Olympic and Cascade Mountain glaciers and advanced twice to into the Puget Lowland, during MIS 4 and MIS 2 (Porter and Swanson, 1998; Borden and Troost, 2001). The MIS 2 advance of the Puget Lobe flowed onto the Olympic Peninsula and into the Sol Duc River catchment just north of the Hoh River, and therefore regional precipitation and the glacial chronology of the Sol Duc catchment were influenced by this lobe. Although the influence of the Puget Lobe on Olympic Mountain glaciers has not been assessed, the proximity of the two systems suggests that changes in regional precipitation and atmospheric circulation associated with the Cordilleran Ice Sheet would have influenced the Olympic Mountains.

1.2 Study area

The Olympic Mountains on the Olympic Peninsula of Washington lie on the northwestern-most edge of the contiguous United States (Figure 3.1). The Puget Sound bounds the peninsula to the east, the Pacific Ocean bounds the west, the Strait of Juan de Fuca bounds the north, and the Chehalis River Valley lowland bounds the south. The western Olympic

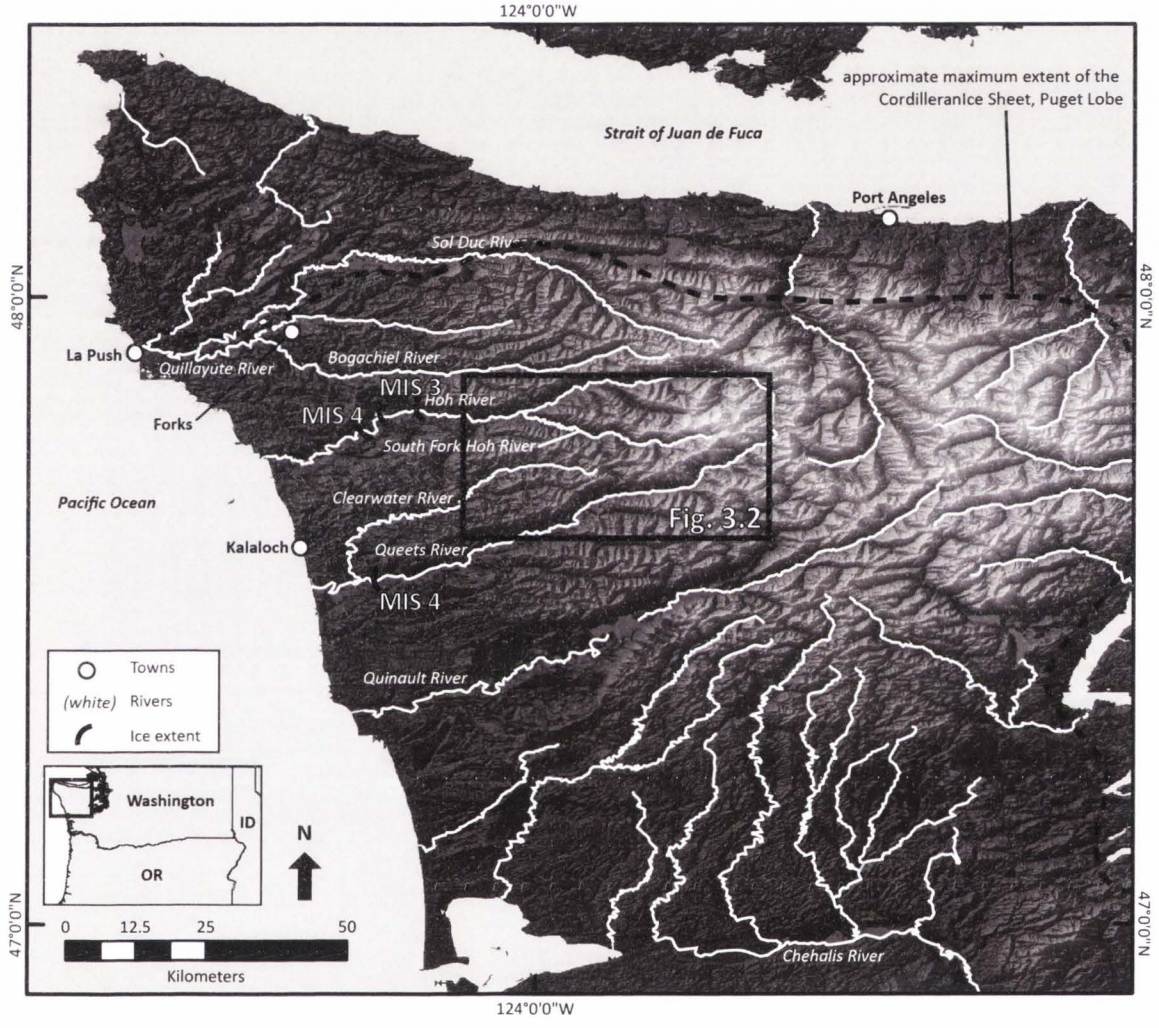

Figure 3.1 The Olympic Peninsula, Washington. Major rivers of the western peninsula and towns labeled. The approximate maximum extent of the Puget Lobe of the Cordilleran Ice Sheet is denoted by a blue border, and MIS 4 and MIS 3 ice extents in the Hoh River valley and Queets River valley are also labeled. Inset box shows the location of Figure 3.2. Hillshade derived from 30 m NED DEM data.

Peninsula has a maritime climate dominated by the influence of westerly atmospheric flow and Pacific Ocean sea surface temperature and pressure variability. Southwesterly and westerly winds deliver peak precipitation in the fall and winter, whereas northwesterly and westerly winds create a summer dry season (Spicer, 1986). These humid maritime conditions support the temperate rainforest of the western Olympic Peninsula. The mean annual precipitation in Forks, Washington, ~30 km northwest of the Hoh River and SF Hoh River confluence (Figure 3.1) is ~3 m/yr (Station: Forks 1 E, WRCC, 1931-2005) with the most precipitation delivered from November to January and the least from June to August. A strong orographic effect, however, delivers more precipitation inland, where modern precipitation in the mountains reaches as high as 5 m/yr (LaChapelle, 1959, 1960; Spicer, 1986). The mean annual temperature for Forks is ~10°C with warmest temperatures from July to September and coldest temperatures from December to February (WRCC, 1931-2005).

Cirque glaciers dominate the 266 modern glaciers and permanent ice fields in the Olympic Mountains (Spicer, 1986). Blue glacier is the largest in volume (0.016 km^3), whereas Hoh Glacier is the longest (4.93 km). Blue Glacier is one of the mountain glaciers in the U.S. that has been extensively studied from a mass balance perspective (e.g. Conway et al., 1999; Rasmussen et al., 2000). Pleistocene radial valley glaciers flowed from the high peaks of the Olympic Mountains to the coastal lowlands and beyond the modern shoreline (Thackray, 2008). The equilibrium line altitudes (ELA) during the global LGM were ~640 m for the Hoh River and ~650 m for the SF Hoh (Thackray, 1996). Ice extended nearly 25 km down-valley of the Hoh and SF Hoh confluence during MIS 4, and the SF Hoh ice merged with the mainstem Hoh valley ice at their confluence. The ice of these two valleys also merged at the confluence during the early stages of MIS 2, as discussed further in the text.

The SF Hoh (~30 km long, ~140 km^2 catchment area) joins the main Hoh River (~90 km long, ~770 km^2), which flows roughly west-southwest before entering the Pacific Ocean (Figure 3.2). The elevation within the SF Hoh catchment ranges from ~125-2,427 m. Mount Olympus is the highest peak and there are no faults mapped in the lower portion of the valley (Tabor and Cady, 1978).

The uplift of the Olympic Mountains is created by accretionary wedge processes of the Cascadia Subduction Zone approximately 80 km offshore, which accounts for much of the modern tectonic activity of the region. The Olympic Peninsula experiences long-term uplift rates of ~1 mm/yr in the center and ~0.1 mm/yr along the flanks (Brandon, 2004). Elevations of resulting peaks extend higher than 2,400 m (Mount Olympus) and decrease to the west to a low-relief coastal plain. Eocene through Miocene age accretionary wedge rocks of the Olympic Subduction Complex compose the core of the Olympic Mountains.

2. Methods

This study uses both field and laboratory methods to provide details of glacial deposits, geomorphology, and ultimately, ice advance and retreat cycles in the SF Hoh. Fieldwork included describing the stratigraphy and sedimentology of ten cutbank exposures along the SF Hoh and geomorphic mapping of an ~25 km reach of the valley. Topographic maps and aerial photographs aided geomorphic mapping. Samples were collected for optically stimulated luminescence (OSL) and radiocarbon dating to provide chronologic constraints on individual packages within the sedimentary exposures, especially to provide ages of sequences associated with identified ice-margin positions.

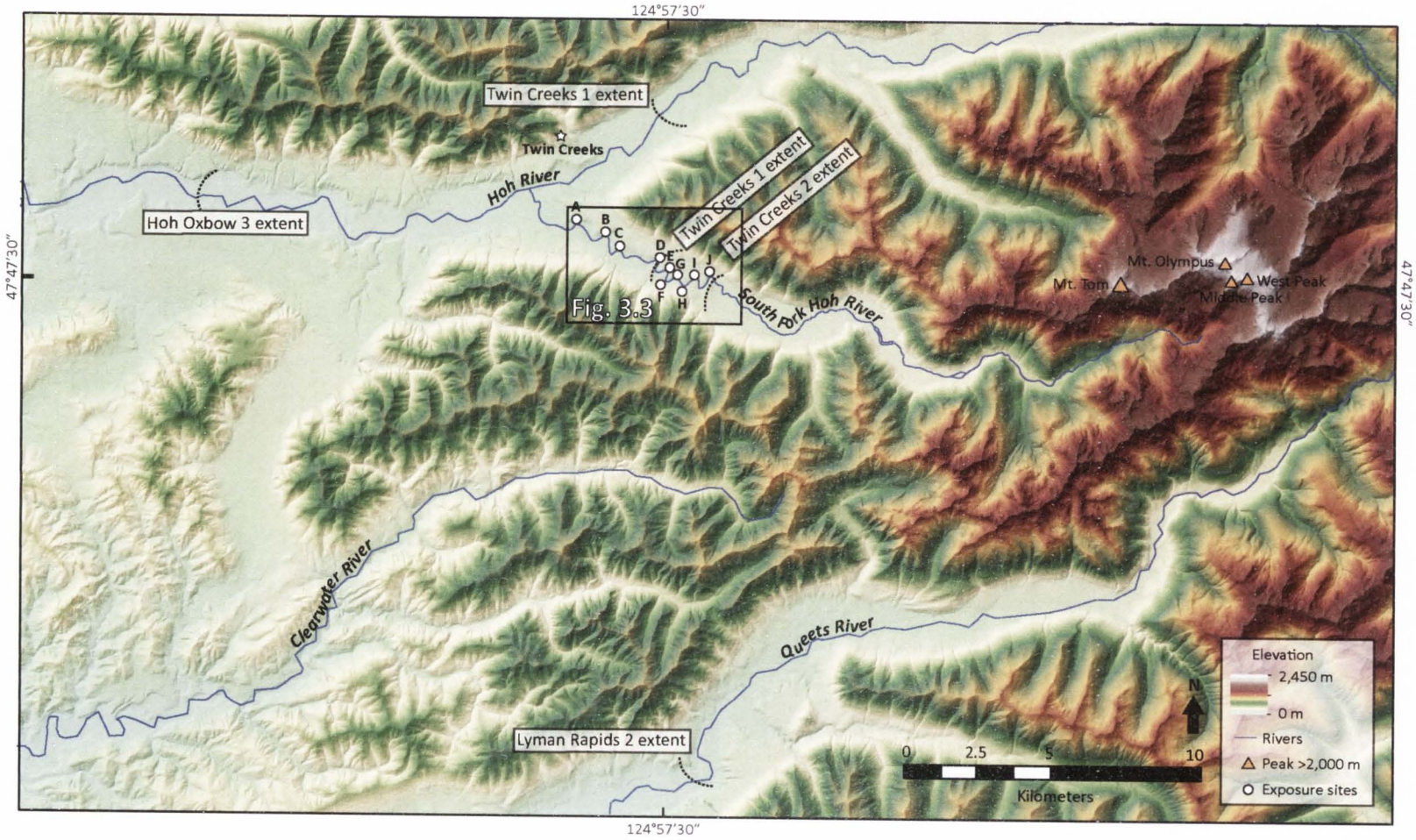

Figure 3.2 The SF River valley and surrounding area. Exposures studied are labeled as Sites A-J, with Site A being the farthest down-valley and Site J the farthest up-valley. Dashed lines indicate ice extent relevant to this study as mapped by Thackray (2001). Elevations derived from 30 m NED DEM data.

2.1 Geomorphology and stratigraphy

Geomorphic mapping was conducted using field observations and assessment of topographic maps and stereo-paired air photos. Geomorphic mapping was overlain on a portion of the 1:24 000 scale Owl Mountain USGS quadrangle. The map extent was chosen based on sites visited during fieldwork and focuses on the SF Hoh valley; this includes Site A as the furthest down-valley reach and extends slightly up-valley of Site J (Figure 3.2). Pleistocene glacial landforms in the map area include moraines and outwash terraces. More recent Quaternary features include the floodplain of the SF Hoh, and other alluvial and colluvial landforms. These younger landforms were not mapped due to scale and vegetative cover.

Outcrops of Pleistocene sediment along cutbanks of meander bends of the SF Hoh were chosen for detailed study due to accessibility and outcrop quality. Ten exposures were studied, labeled Sites A-J, from down- to up-valley (Figure 3.2). Exposures were logged and detailed sedimentary and stratigraphic measurements were made, including description of unit thickness and geometry, sedimentary facies and structures, bedding, grain size, fabric, and color. Due to the large size and height of the outcrops, photographs were stitched together to aid in production of outcrop-scale stratigraphic panels.

This study relies not only on geomorphic relations, but also heavily upon the descriptions and interpretations of the internal sedimentology and stratigraphy exposed in the SF Hoh to provide information on the style and sequence of MIS 2 ice advances and deglaciation in the valley. Facies descriptions are especially important, as the physical characteristics of individual facies are related to their processes of formation. The interpretations of their origins therefore comprise an important step in unraveling the history of glacial deposits, as facies may connect glacial environments to the same advance and retreat events and/or provide detail crucial to reconstructions of sediment transport- and depositional-dynamics. Table 3.2 lists

facies codes used in unit descriptions following Evans and Benn (2004). This level of detail is especially important and novel in comparison to previous western U.S. glacial studies during the LGM. This research consequently helps better understand the nature of Olympic Mountain ice dynamics during a globally important glacial and climatic period.

In this study, the term diamicton is used to refer to poorly sorted sediments with a wide range of grain/clast sizes in a finer matrix. These deposits are interpreted to represent rapid sedimentation associated with glacial ice. Many of these deposits appear similar to subglacial tills, but lack the compaction of a true till; the distinction between the two terms therefore provides refinement to interpretations of depositional settings of diamictons (Evans and Benn, 2004). The term 'till' is used in this study only for subglacially deposited, compacted, non-water sorted diamicton. Stratified (as opposed to massive) diamictons are typically recognizable at outcrop scale, but still retain their poorly sorted nature and suggest the influence of water at or immediately following deposition. Stratification is especially important in differentiating diamicton deposition in various ice-proximal settings from subglacial till in the humid glacial environment of the Olympic Mountains, where the influence of meltwater on sedimentary facies is likely. Proximal and distal outwash were differentiated based primarily on clast size and sorting; proximal outwash contained larger clasts that were more poorly sorted and less sand, whereas distal outwash contained smaller clasts that were better sorted and more sand.

Samples were collected for particle size analysis from silt and diamicton facies and measured using a laser particle-size analyzer on the <1000 μm fraction to aid differentiation of diamicton units from silt-rich units of other depositional facies. An ice-proximal stratified diamicton and matrix-rich unit of fluvial or lacustrine origin may appear similar in field observations and may represent a continuum of facies distinguished by degree of sorting. The sediment-size analysis conducted here therefore seeks to determine if a difference in matrix size

Table 3.2 Facies codes and descriptions found in the stratigraphy of the SF Hoh River valley exposures. Codes adapted from Evans and Benn (2004).

Code	Description	Interpretation
Fm	Silt and clay, massive	glaciolacustrine deposition or deposition in abandoned outwash channel
Fl	Silt and clay, fine lamination often with minor fine sand and very small ripples	glaciolacustrine deposition or deposition in abandoned outwash channel
F(w)	Silt and clay, dewatering structures and/or deformation features	glaciolacustrine deposition or deposition in abandoned outwash channel
Sm	Sand, massive	glacial outwash
Suc	Sand, upward coarsening	glacial outwash
Suf	Sand, upward fining	glacial outwash
Sh	Sand, horizontally bedded or laminated	glacial outwash
St	Sand, trough cross-bedded	glacial outwash
Sr	Sand, ripple cross-laminated	glacial outwash
Sfo	Sand, foresets	glaciolacustrine deltaic deposition
Sd	Sand, deformed bedding	glacial outwash
Sr(w)	Sand, ripple cross-laminated with dewatering structures	glaciolacustrine deposition or deposition in abandoned outwash channel
Gm	Gravel, clast supported massive	glacial outwash
Go	Gravel, openwork	glacial outwash
Gh	Gravel, horizontally bedded	glacial outwash
Gt	Gravel, trough cross-bedded	glacial outwash
Gfo	Gravel, deltaic foresets	glaciolacustrine deltaic deposition
Bcm	Boulders, clast supported massive	glacial outwash
Bl	Boulder lag or pavement	glacial outwash
Dmm	Diamicton, massive	sub-aqueous deposition at an ice margin with no water re-working
Dml	Diamicton, laminated	sub-aqueous deposition at an ice margin with water re-working

is detectable between glacial diamicton and other silt-rich facies. Four diamicton samples were collected, and these include Site A Unit 1 (a over- compacted, weakly stratified diamicton), Site G Unit 1 (a diamicton that is stratified in some places and massive in others), Site I Unit 1 (a massive diamicton), and Site I Unit 3 (a weakly stratified diamicton). Three matrix or silty-facies samples were collected, and these include Site F Unit 2 (fine sediment infilling pores of a clast-supported gravel outwash), Site G Unit 2 (a channel form containing laminated silt and sand), and Site I Unit 4 (silt within in a sand lens in a gravel outwash package).

Information on clast characteristics (texture; shape, roundness, and size) can elucidate details about provenance, flow regimes, and mechanisms of erosion and transportation. Ternary diagrams display clast shapes based on the length of the three major axes, and end member shapes include block, slab, and elongate clasts. The C40 index records clasts with c:a axis ratios ≤0.4 and can help distinguish between actively- and passively-transported glacial sediment (Evans and Benn, 2004). However, neither this index nor the ternary diagrams assist in differentiating between subglacially- and glaciofluvially-transported sediment, as neither environment readily preserves angular clasts and shape may be dominated by clast lithology. Clast roundness is more useful to distinguish between these two environments, as fluvially-transported clasts are generally better rounded than glacially-transported (Evans and Benn, 2004). For these purposes, histograms depicting clast roundness and ternary diagrams depicting clast shape were created (see supplemental material).

2.2 Radiocarbon dating

Samples for radiocarbon dating were collected wherever organic material was present. Four samples (one from Site A, two from Site F, and one from Site G) were collected during fieldwork and dated at the Center for Accelerator Mass Spectrometry at the Lawrence

Livermore National Laboratory. Four additional radiocarbon samples (three from Site A and one from Site D) were previously collected by Thackray (1996) and analyzed at the University of Arizona AMS Facility. The IntCal09 calibration curve was used for calibration (Reimer et al., 2009) and ages are reported at 2-sigma error. Ages in the text and on figures are reported using the mid-point of the calibrated age range for simplicity.

2.3 Optically stimulated luminescence

Optically stimulated luminescence dating (OSL) is based on the premise that the sediment was exposed to sufficient sunlight (or heat) to zero (bleach) any residual luminescence signal prior to deposition (Huntley et al., 1985). Upon burial, the sediment is removed from sunlight and the luminescence signal begins to accumulate due to exposure to radiation from the surrounding sediment and incoming cosmic rays. The intensity of the luminescence signal measured in the lab is related to the length of burial and dose-rate environment that the sediment is exposed to. The most widely used and accepted method to determine the equivalent dose (or "paleodose") of the sediment is the single-aliquot regenerative-dose (SAR) protocol using quartz sand (Murray and Wintle, 2000, 2003; Wintle and Murray, 2006).

The age of a sample is calculated by dividing the equivalent dose (De) by the dose rate (DR).

$$\text{Age (ka)} = \text{De (Gy)} / \text{DR (Gy ka}^{-1}\text{)}$$

where 1 Gray (Gy) = 1 joule/kilogram (J/kg) (Aitken, 1998). The dose rate is a measure of the dose per unit time received by a sample while buried, defined as the flux of radiation measured directly in the field or indirectly determined by chemical composition of surrounding sediments, more specifically the radioactive elements Uranium (U), Potassium (K), Thorium (Th), and Rubidium (Rb) and cosmic contribution. The equivalent dose (De) is the dose of radiation

needed to induce a luminescence signal equal to the natural luminescence signal acquired by a sample subsequent to its most recent bleaching event. The dosage should therefore be approximately equivalent to the paleodose, or the radiation dose a sample received during burial.

Although OSL dating has been successfully applied in many glacial settings, glacial sediments have proven challenging (e.g. Fuchs and Owen, 2008). Problems specific to OSL dating of glaciofluvial and glaciolacustrine deposits include incomplete bleaching (e.g. Klasen et al., 2007), poor luminescence properties (e.g. Preusser et al., 2006), enhanced thermal transfer creating extra luminescence (e.g. Alexanderson, 2007), and feldspar contamination (e.g. Lukas et al., 2007).

Eleven OSL samples were obtained by pounding a steel tube into targeted sand layers after the outcrop face was scraped to obtain a fresh surface. A representative sample from a 30 cm radius around the sample tube was collected for dose-rate analysis and water content. Samples for dose-rate determination were split to obtain a representative sample and the concentrations of K, Rb, Th, and U were analyzed using ICP-MS and ICP-AES at ALS Chemex in Elko, NV. Moisture content was determined by weighing samples while moist and again when dry. Raiodelemental concentration (Guerin et al., 2011), moisture content, and cosmic contribution (Prescott and Hutton, 1994) were used to calculate the dose-rate to the sediment.

OSL sample preparation and analyses were conducted at the Utah State University Luminescence Laboratory under ambient amber light (590 nm) conditions. Samples were sieved to the grain sized listed in Table 4.1 and treated with hydrocloric acid and bleach to dissolve carbonates and organic material. Sodium polytungstate (2.7 g/cm^3) was used to separate quartz and feldspar from heavy minerals, and was followed by concentrated hydrofluoric and

hydrochloric acids to remove feldspars and etch the quartz grains. This fraction was then sieved to <75 μm to remove any partially dissolved feldspar grains.

The single-aliquot regenerative-dose method (SAR) (Murray and Wintle, 2000) on small-aliquots (2 mm diameter, ~50 grains per disk) and central age model (CAM; Galbraith et al., 1999) or minimum age model (MAM; Galbraith et al., 1999) were used to calculate ages. More specific details regarding analysis procedures can be found in Chapter 4 and Table 4.1. All OSL results are currently preliminary.

3. Results and interpretations

3.1 Geomorphology

The lower SF Hoh River valley contains extensive outwash and fill terraces and evidence for two, and possibly three, ice positions marked by moraines, hereafter referred to as South Fork 1-3 (SF 1-3), oldest to youngest (Figure 3.3). The SF 1 and SF 3 moraines were previously mapped by Thackray (1996) as the Twin Creeks 1 and Twin Creeks 2 end moraines, respectively. The SF 2 position is more tenuous, as more work will be needed to confirm this position, however, this position is included here in the numbering scheme of ice positions.

The moraines are identified based on observations from aerial imagery and topographic maps; however, they cannot be easily identified in the field due to extensive tree cover. These three recessional moraines of the SF 1-3 ice-margin positions (Qm1, Qm2, and Qm3) form ridges that cross the valley in roughly arcuate shapes. Additionally, the alluvial corridor of the modern river is narrowest where constrained between the three moraines. An alluvial fan appears to have been deposited over a portion of the SF 2 moraine on the southern side of the river, causing the moraine to be less geomorphically distinguishable than the others. LiDAR data may be helpful for further detail documenting the SF 2 position. The outwash plain is distinguishable into inset

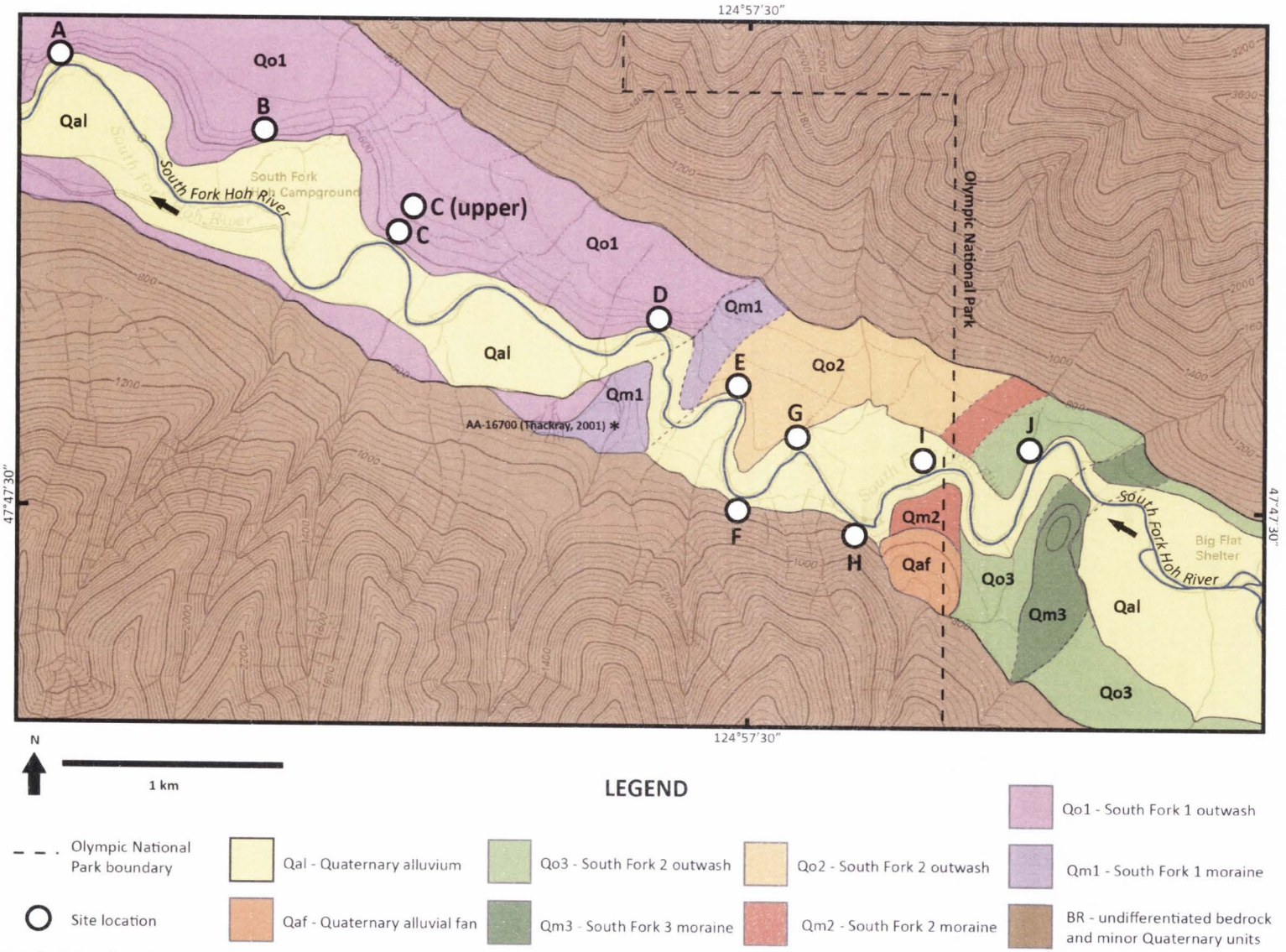

Figure 3.3 Surficial map of the SF Hoh River valley. The extent was chosen to reflect areas visited in the field, and exposure sites are labeled from down- to up-valley, A-J. The valley contains three moraines that represent stable ice positions during the late Pleistocene.

terrace levels by surface elevation and capping units in stratigraphy discussed in Section 3.3.

3.2 Particle size analysis and identification of glacial deposits

The results of particle size analysis (Figure A1.1 and Table A1.1) suggest a potentially useful tool in differentiating ice-contact diamicton and other sediment in this system based on the grain-size distribution of the <1,000 μm fraction of the matrix. Units identified as diamicton (Site A Unit 1, Site G Unit 1, Site I Units 1 and 3) have matrix predominantly composed of clay to medium silt grain-size fractions, whereas the other samples collected from fine-grained facies (Site F, Site G Unit 2, Site I Unit 4) have coarser overall matrix. Additionally, the grain-size distribution curves are strikingly similar in the diamicton samples and are characterized by peaks in the finest grain size fractions (clay-medium silt), with a decline to some steady value typically in the coarse silt-very fine sand fraction, and a subsequent steep decline to the 1,000 μm upper limit. Although we tested few samples, these results may be useful in supporting interpretations of diamicton and silty units in the study area. No differences were seen between units interpreted as true till and those interpreted as diamicton.

3.3 Sedimentology, stratigraphic descriptions, and interpretations

The facies and stratigraphic architecture of the ten exposures studied are described here from down-valley to up-valley, Site A to Site J. Detailed information on unit descriptions, facies photographs, and clast count data are in Appendix A1. All chronologic data are in Table 3.3, with radiocarbon ages presented as the mid-point of the 2-sigma calibrated age range, and preliminary OSL ages are also reported at 2-sigma error.

Site A is composed of over-compacted (lower part) and weakly stratified (upper part) diamicton (Unit 1, Dml) overlain by interbedded silt and sand (Unit 2, Sh and Fl) and sand and

gravel foresets (Sfo, Gfo) and horizontal bedding (Sh, Gh) (Unit 3) (Figure 3.4). Three radiocarbon samples from Unit 2 (Fl) produced a mean age of 22.5-23.5 ka (Thackray, 2001), and an OSL sample from the same unit (Sh) produced a preliminary age of 19.2 ± 3.9 ka (USU-989; Table 3.3). A preliminary OSL age from Unit 3 is 21.3 ± 4.6 ka. Three horizontally bedded gravel deposits (Gh) cap the lower units (Units 4-6) and are differentiated by clast size. Unit 4 and Unit 6 are both reverse-graded pebble-cobble gravel, and are separated by the coarser Unit 5, a cobble-boulder gravel. A discontinuous silty-sandy clay bed (Fl) in Unit 4 yielded mean ^{14}C ages of 18.5-19.0 ka (beetle) and 19.2-19.6 ka (plant). Beetle fragments from this clay bed are currently being analyzed for paleoecological and paleotemperature inferences. The over-compacted basal diamicton is interpreted to represent a true subglacial till, and the two overlying units are interpreted as lacustrine and deltaic sediments that have formed in ponded water, likely due to damming of the SF Hoh valley by ice or a moraine in the mainstem Hoh valley. Upper gravel units are interpreted as glacial outwash.

Site B was not studied in detail due to the limited exposure of sediment. However, in 1994, Thackray noted that this site was composed of a single coarsening-upward glacial outwash deposit (personal communication, 2012). The clast sizes and characteristics during fieldwork confirmed that this is glacial outwash.

Site C is an exposure of two horizontally bedded gravel units (Figure 3.5, Gh). Unit 1 was described at the foot of a bluff exposed at river-level, whereas Unit 2 was described in an excavated gravel pit above and slightly (~130 m) behind the cut-bank exposure. Both units are composed of horizontally bedded pebble-cobble gravel with sand lenses; however Unit 1 is generally coarser, with rare boulders and Unit 2 contains more sand lenses. Preliminary OSL ages from Unit 1 (Sh) and Unit 2 (Sm) are 18.6 ± 3.7 ka (USU-1243) and 12.4 ± 5.3 ka (USU-991), respectively (Table 3.3). These two units are interpreted to represent glacial outwash, the lower

Table 3.3 Age constraint for the SF Hoh valley exposures. Methods include radiocarbon dating and preliminary optically stimulated luminescence results of quartz sand grains. Age constraint exists for all sites except Site B and Site H. More detailed information about OSL ages can be found in Chapter 4.

Sample ID	Site	Unit	Sample Type	Material	^{14}C Age[2]	δ^{13}C	Number of Aliquots Accepted (Run)	Equivalent Dose (Gy)	Dose rate (Gy/ka)	Age (ka) ± 2σ	Study
AA-18406	A	2	radiocarbon	wood	19,169 ± 162	-26	-	-	-	22.4-23.4	Thackray, 2001
AA-18407	A	2	radiocarbon	wood	19,324 ± 165	-26.7	-	-	-	22.5-23.5	Thackray, 2001
AA-18408	A	2	radiocarbon	wood	19,274 ± 154	-27.1	-	-	-	22.5-23.5	Thackray, 2001
USU-989	A	2	OSL	quartz	-	-	25 (69)	24.53 ± 4.26[4]	1.28 ± 0.06	19.2 ± 3.9	this study
USU-990	A	3	OSL	quartz	-	-	21 (69)	25.08 ± 4.81[4]	1.18 ± 0.05	21.3 ± 4.6	this study
CAMS#156404	A	4	radiocarbon	plant	16,210 ± 60	-25[3]	-	-	-	19.2-19.6	this study
CAMS#159920	A	4	radiocarbon	beetle	15,520 ± 160	-25[3]	-	-	-	18.5-19.0	this study
USU-1243	C	1	OSL	quartz	-	-	18 (33)	20.85 ± 3.56[4]	1.12 ± 0.07	18.59 ± 3.7	this study
USU-991	C	2	OSL	quartz	-	-	23 (61)	19.40 ± 8.51[5]	1.57 ± 0.07	12.4 ± 5.3[6]	this study
AA-18405	D	0	radiocarbon	wood	19,067 ± 329	-29.8	-	-	-	22.0-23.7	Thackray, 2001
AA-16700[1]	-	-	radiocarbon	wood	18,274 ± 195	-25	-	-	-	21.4-22.3	Thackray, 2001
USU-1242	D	2	OSL	quartz	-	-	23 (52)	39.95 ± 15.22[5]	1.02 ± 0.07	39.2 ± 15.5[6]	this study
USU-1241	E	1	OSL	quartz	-	-	12 (24)	43.43 ± 11.12[5]	1.00 ± 0.06	43.4 ± 12.0[6]	this study
USU-1240	E	2	OSL	quartz	-	-	9 (24)	27.20 ± 11.91[4]	1.36 ± 0.06	20.0 ± 9.0	this study
USU-1285	F	1	OSL	quartz	-	-	17 (36)	24.46 ± 4.32[5]	1.29 ± 0.07	18.9 ± 3.8	this study
CAMS#159911	F	1	radiocarbon	wood	18,130 ± 70	-25[3]	-	-	-	21.4-22.1	this study
CAMS#159912	F	1	radiocarbon	wood	18,090 ± 60	-25[3]	-	-	-	21.3-22.0	this study
CAMS#159913	G	2	radiocarbon	wood	16,940 ± 60	-25[3]	-	-	-	19.9-20.4	this study
USU-1282	G	2	OSL	quartz	-	-	18 (32)	40.73 ± 8.95[4]	1.80 ± 0.09	22.7 ± 5.4	this study
USU-1283	I	4	OSL	quartz	-	-	15 (31)	21.75 ± 9.15[5]	1.08 ± 0.07	20.1 ± 8.8	this study
USU-1284	J	1	OSL	quartz	-	-	12 (24)	31.50 ± 8.80[5]	1.08 ± 0.06	29.8 ± 8.9[6]	this study

[1] across the river from Site D (Thackray, 2001)
[2] IntCal09 (Riemer et al., 2009) used for calibration
[3] assumed δ^{13}C value
[4] based on CAM (Galbraith et al., 2009)
[5] based on MAM (Galbraith et al., 2009)
[6] sample and associated age estimate considered unreliable

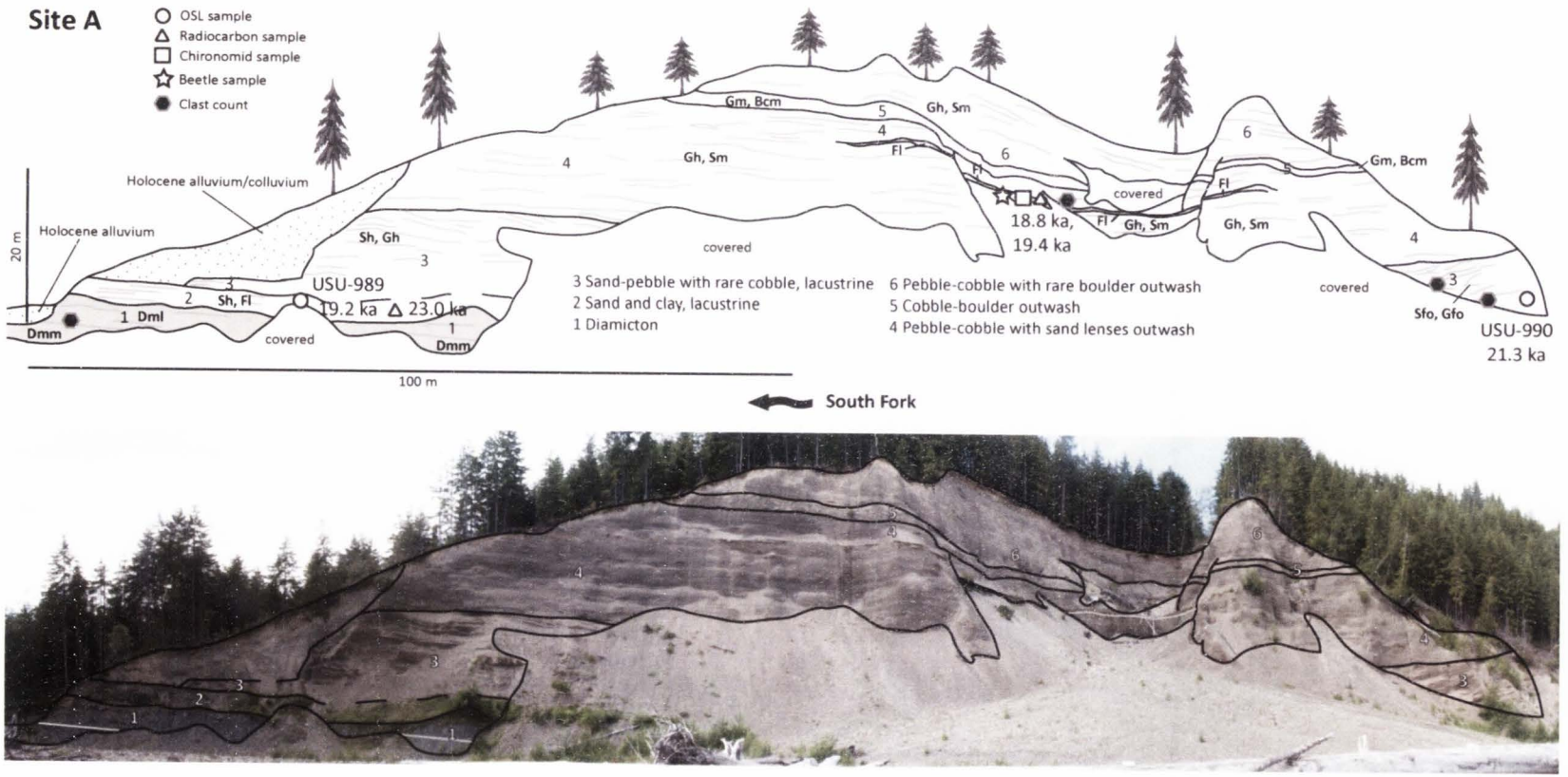

Figure 3.4 Stratigraphic panel and photograph of the Site A exposure. Numbers represent unit labels. Open circles and ages represent OSL sample locations. Triangles and ages represent radiocarbon sample locations. Filled hexagons represent clast count locations. The open square represents a chironomid sample location. The open star represents a beetle sample location. Facies codes (Table 2) are present on the panel. Detailed unit descriptions, photos, and clast counts can be found in the supplemental material (Figures A1.2-1.4).

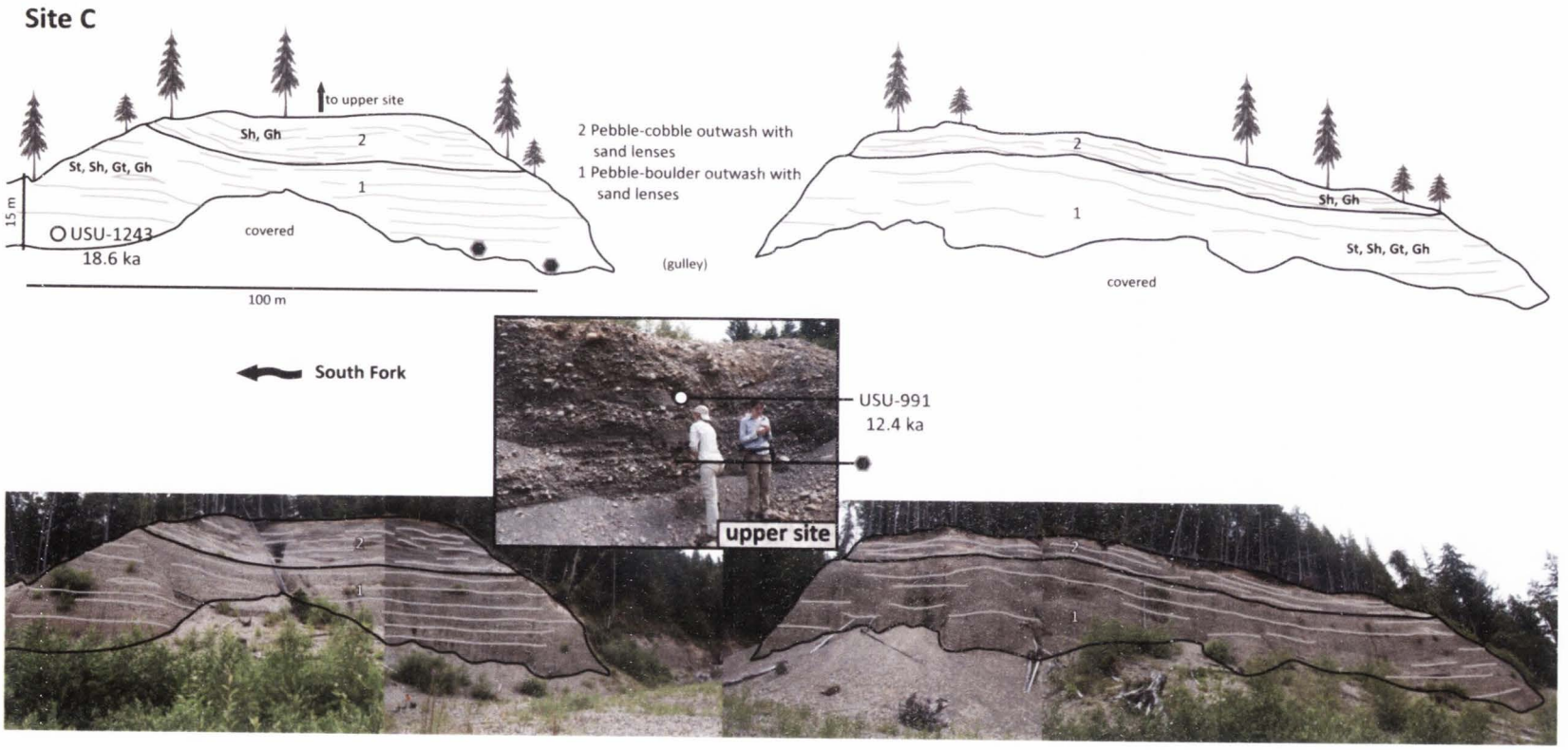

Figure 3.5 Stratigraphic panel and photographs of the Site C exposure. Numbers represent unit labels. Open circles and ages represent OSL sample locations. Filled hexagons represent clast count locations. See Figure 3.4 for a key to symbols. Facies codes (Table 3.2) are present on the panel. Detailed unit descriptions, photos, and clast counts can be found in the supplemental material (Figures A1.5-1.6).

being more ice-proximal and the upper more distal based primarily on overall grain size and relative concentration of sand lenses.

Site D is composed of five units (Figure 3.6). The two lower gravel units (Units 1, finer and 2, coarser; Gh) are overlain by a wedge of gravel (Unit 3, Gh) that interfingers with a moderately stratified diamicton (Unit 4, Dml), and another gravel sequence (Unit 5, Gh). Separate gravel packages were identified based on clast size and subtle color differences (Figure A1.7-1.8). Age constraint on this exposure includes a ^{14}C age of 22.0-23.7 ka from an underlying unit that was not exposed at the time of this study but was described as pebble-rich lacustrine sediment (AA-18405; Thackray, 2001). A preliminary OSL age from near the base of Unit 2 (Sm) is 39.2 ± 15.5 ka (USU-1242) (Table 3.3), although this age is likely unreliable due to partial bleaching (see Chapter 4). Thackray (1996, 2001) presents another ^{14}C age on a sample collected by another worker from "till" in this area (AA-16700, 21.4-22.3 ka; from a location across the river noted on Figure 3.3). However, its relation to the stratigraphy presented here is not clear, as Thackray originally projected its location across the river back to Unit 4 in this exposure, which may not be accurate. The gravel units (Unit 1-3, Unit 5) are interpreted as glacial outwash. The lowest outwash is interpreted as more ice-distal, that is capped by a coarser, more proximal outwash of Unit 2. These units are overlain by finer outwash (Unit 3) that interfingers with diamicton (Unit 4), which is interpreted to represent subaqueous deposition at an ice margin. These lower units are interpreted to represent an ice re-advance sequence, which is capped by another more distal outwash unit (Unit 5).

Site E is composed of a stratified diamicton (Dml) with sand (Sh) and gravel (Gh) lenses (Unit 1) overlain by horizontally bedded gravel (Gh) with sand lenses (Sh) (Unit 2) and ultimately by inset Holocene terrace alluvium (Figure 3.7 and Figures A1.9-1.10). A preliminary OSL sample from a sand lens within Unit 1 (Dml) produced an age of 43.4 ± 12.0 ka (USU-1241) and an OSL

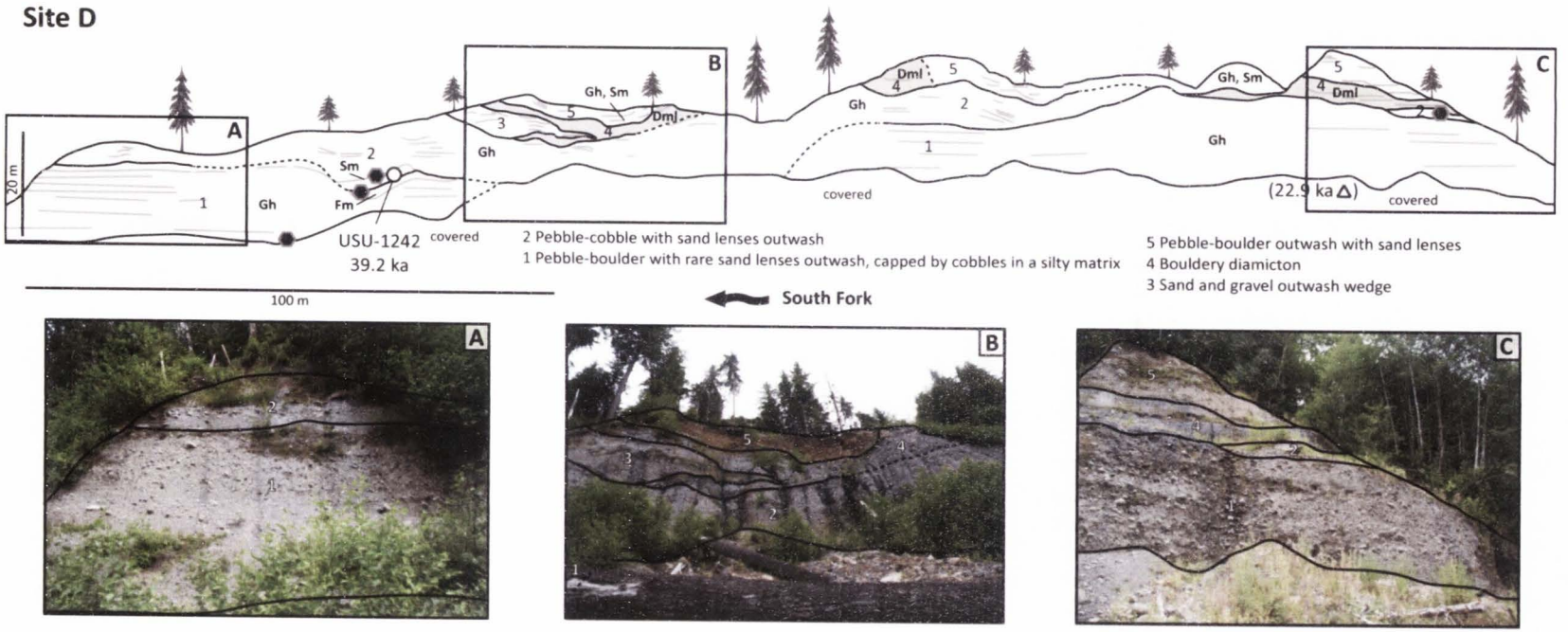

Figure 3.6 Stratigraphic panel and photographs of the Site D exposure. Numbers represent unit labels. Open circles and ages represent OSL sample locations. Triangles and ages represent radiocarbon sample locations. Filled hexagons represent clast count locations. See Figure 3.4 for a key to symbols. Facies codes (Table 3.2) are present on the panel. Detailed unit descriptions, photos, and clast counts can be found in the supplemental material (Figures A1.7-1.8).

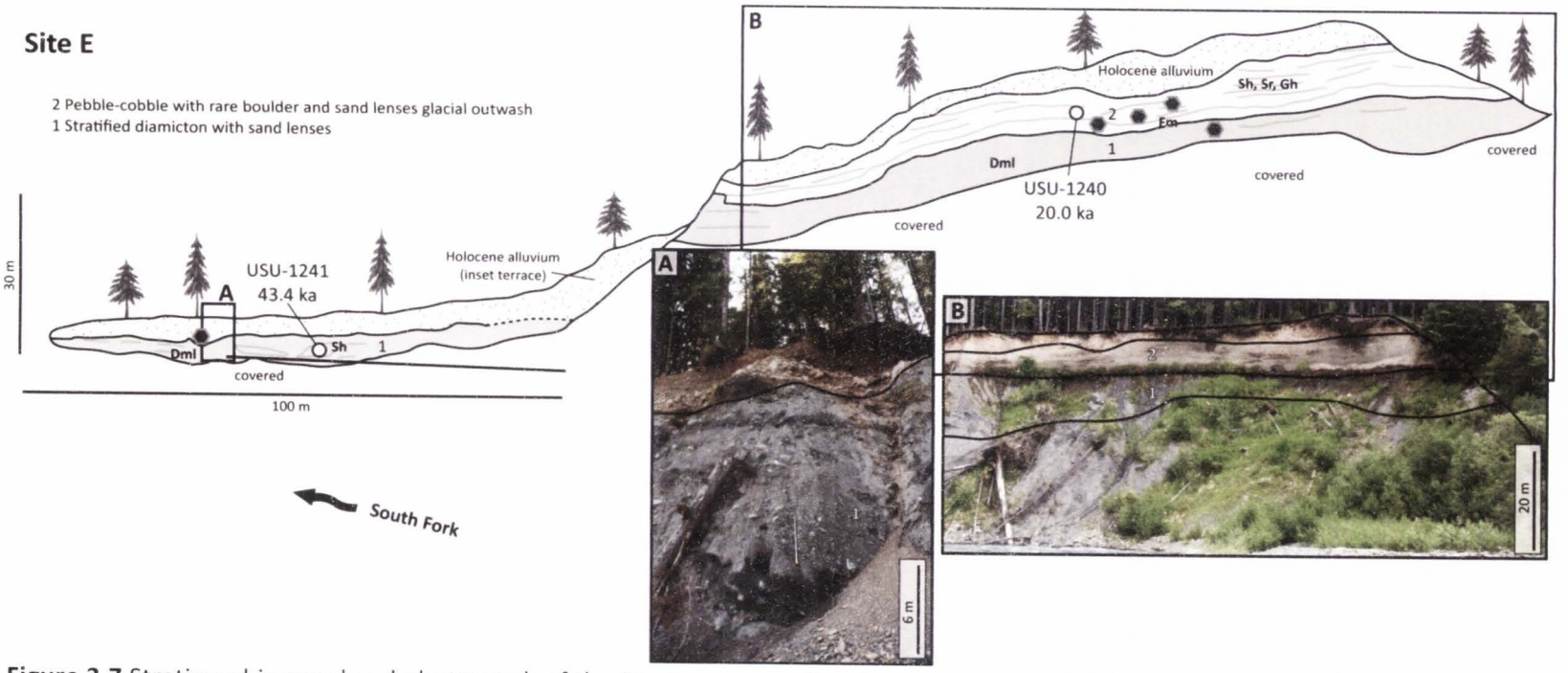

Figure 3.7 Stratigraphic panel and photograph of the Site E exposure. Numbers represent unit labels. Open circles and ages represent OSL sample locations. Filled hexagons represent clast count locations. See Figure 3.4 for a key to symbols. Facies codes (Table 3.2) are present on the panel. Apparent dipping of horizontal beds on outcrop panel is a relic of the photomosaic on which it was drawn. Bedding is in fact horizontal, as can be seen in photo B. Detailed unit descriptions, photos, and clast counts can be found in the supplemental material (Figures A1.9-1.10).

sample from near the base of Unit 2(Sr) is 20.0 ± 9.0 ka (USU-1240) (Table 3.3). OSL dating of Unit 1 was not likely to produce reliable age estimates based on the turbid, ice proximal depositional environment, and this sample may show an age from a previous depositional cycle (see Chapter 4). The basal unit represents an ice-proximal, water-reworked diamicton, which is capped by younger outwash as an inset terrace. The glacial deposits and the Holocene terrace alluvium are separated by near-horizontal, erosional unconformities.

Site F is composed of three horizontally bedded gravel units (Gh) differentiated by clast size (Figure 3.8). The lowest unit (Unit 1) contains pebble-cobble gravel and sand lenses (Sm) that coarsen upward and is overlain by a pebble-boulder gravel with sand lenses (Sm) and a prominent boulder lag (BL) (Unit 2). These units are capped by a third unit composed of pebble-cobble gravel and sand lenses (Sm) (Unit 3) (Figures A1.11-1.12). Two trees (~30 cm diameter) protruded from the outcrop face near the base of Unit 3. Radiocarbon samples collected from the outer rings of the trees produced ages of 21.4-22.1 ka and 21.3-22.0 ka (Table 3.3). Additionally, a preliminary OSL age from a sand lens (Sm) near the base of this exposure suggests deposition at 18.9 ± 3.8 ka (USU-1285) (Table 3.3). These three units are interpreted to represent more ice-distal outwash overlain by coarser and only moderately-sorted proximal outwash, capped by finer-grained, more distal outwash, and are addiotionally interpreted to record an ice-readvance and retreat sequence.

Site G contains a stratified diamicton (Dml) that is massive in places (Dms) (Unit 1) overlain by horizontally bedded gravel (Gh) with sand lenses (Sm) and channel forms (Gt, St, Sh, Fl) (Unit 2) (Figure 3.9 and Figures A1.13-1.14). A ^{14}C sample from a channel form near the base of the gravel (Unit 2, Sh and Fl) yielded an age of 19.9-20.4 ka (Table 3.3). A preliminary OSL age from this same channel form has produced an age of 22.7 ± 5.4 ka (USU-1282) (Table 3.3). The diamicton is interpreted to represent a subglacial and ice-proximal environment, and is overlain

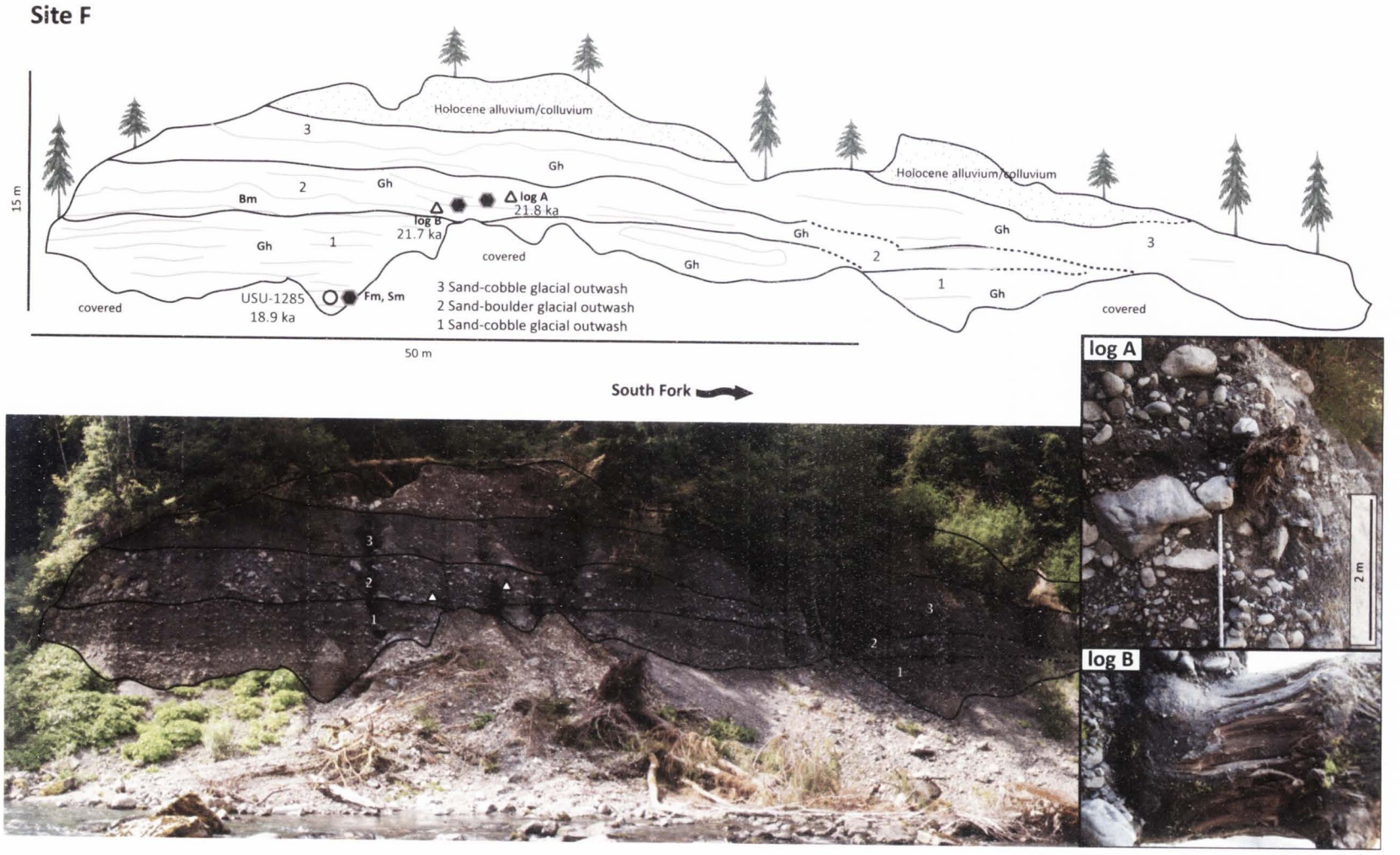

Figure 3.8 Stratigraphic panel and photograph of the Site F exposure. Numbers represent unit labels. Open circles and ages represent OSL sample locations. Triangles and ages represent radiocarbon sample locations. Filled hexagons represent clast count locations. See Figure 3.4 for a key to symbols. Facies codes (Table 3.2) are present on the panel. Detailed unit descriptions, photos, and clast counts can be found in the supplemental material (Figures A1.11-1.12).

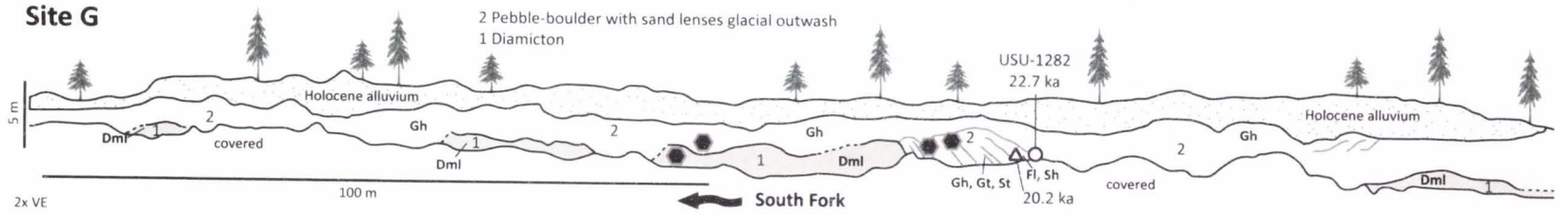

Figure 3.9 Stratigraphic panel and photograph of the Site G exposure. Numbers represent unit labels. Open circles and ages represent OSL sample locations. Triangles and ages represent radiocarbon sample locations. Filled hexagons represent clast count locations. See Figure 3.4 for a key to symbols. Facies codes (Table 3.2) are present on the panel. Detailed unit descriptions, photos, and clast counts can be found in the supplemental material (Figures A1.13-1.14).

by gravel that is interpreted as glacial outwash.

Site H contains two horizontally bedded gravel units (Gh) (Figure 3.10 and Figures A1.15-1.16). Unit 1 is finer, more sorted, and contains more rounded clasts than the overlying unit. Unit 2 is coarser, less well-sorted, and contains more angular clasts, likely representing more ice-proximal deposition, and coarsens upward overall. These two gravel units are interpreted as outwash, and the sequence is interpreted to represent an ice re-advance towards the site.

Site I is composed of a massive diamicton (Dms) (Unit 1) overlain by a horizontally bedded gravel unit (Gh) (Unit 2) and a stratified diamicton (Dml) (Unit 3). Two horizontally bedded gravel units (Gh) (Units 4 and 5) overlay these lower deposits (Figure 3.11). The upper unit (Unit 5) contains smaller clasts than Unit 4 (Figures A1.17-1.18). A preliminary OSL age from a sand lens near the base of Unit 4 (Sh) suggests deposition at 20.1 ± 8.8 ka (USU-1283) (Table 3.3). The basal diamicton (Unit 1) is interpreted to be a true glacial till that represents subglacial deposition, because of its compaction and lack of structure. This is overlain by gravel interpreted as outwash (Unit 2). The upper diamicton (Unit 3) is interpreted to represent an ice re-advance and an ice-proximal or water reworked setting, as its stratification implies some water-sorting. This is overlain by gravel interpreted as ice-proximal outwash (Unit 4) and a more ice-distal outwash (Unit 5), as differentiated by relative clast size and abundance of sand lenses.

The base of Site J (Unit 1) is composed dominantly of horizontally bedded gravel (Gh) with large boulders at the base, with some trough cross-bedded gravel (Gt), finely laminated silt (Fl), and massive (Sm) and trough cross-bedded (St) sand. This is overlain by horizontally bedded silt (Fl) and sand (Sm) that coarsen upwards to horizontally bedded pebble gravel (Gh) (Unit 2) and a horizontally bedded pebble-boulder gravel unit (Gh) (Unit 3) (Figure 3.12; Figures A1.19-1.20). A preliminary OSL age from a sand bed near the middle of Unit 1 (Sm) is 29.8 ka ± 8.9 (USU-1284) (Table 3.3), although this age is considered unreliable due to potential partial

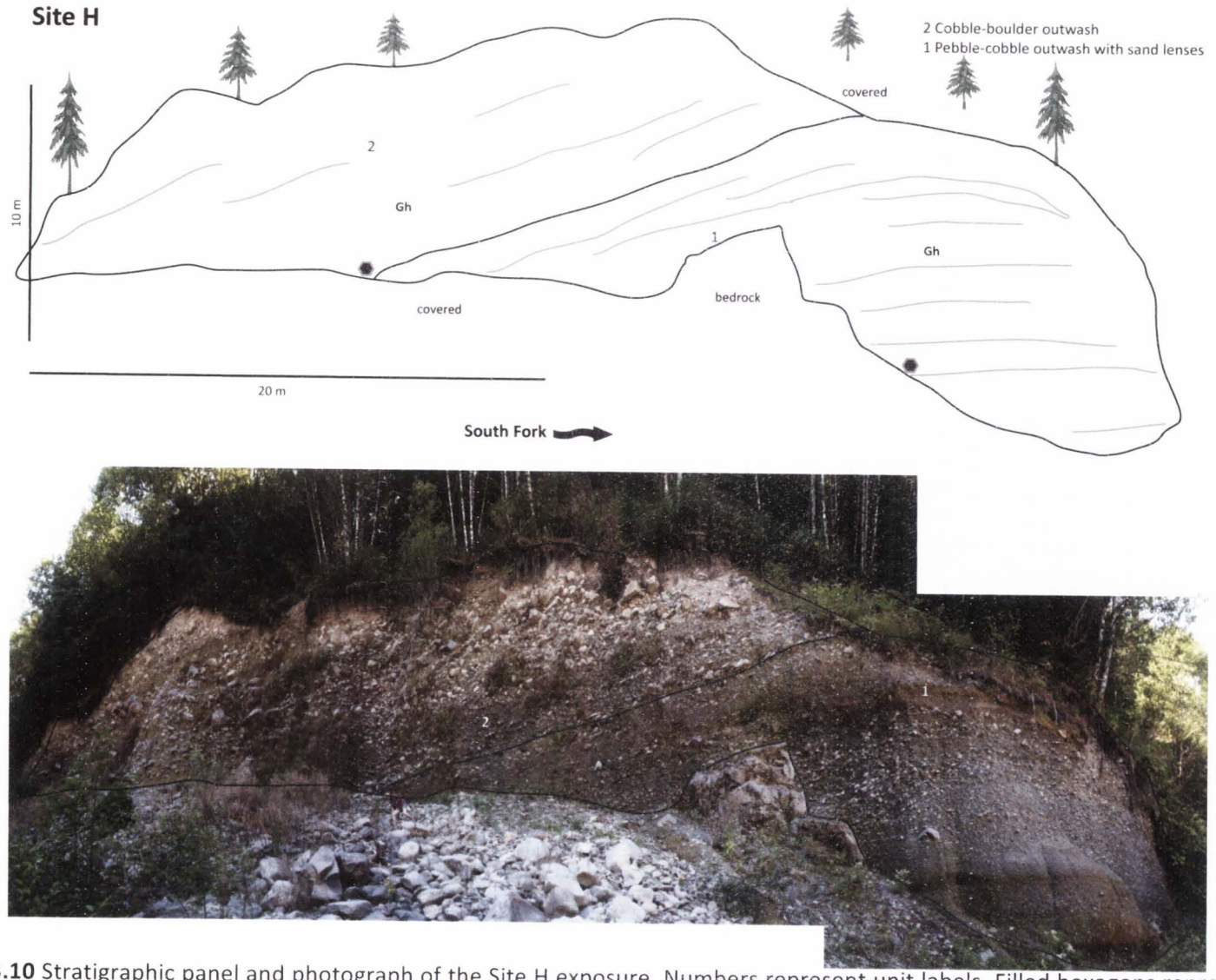

Figure 3.10 Stratigraphic panel and photograph of the Site H exposure. Numbers represent unit labels. Filled hexagons represent clast count locations. See Figure 3.4 for a key to symbols. Facies codes (Table 3.2) are present on the panel. The apparent tilt of the contact between Unit 1 and Unit 2 and horizontal beds of both units are relic of the photomosaic. These are horizontal in reality. Detailed unit descriptions, photos, and clast counts can be found in the supplemental material (Figures A1.15-1.16).

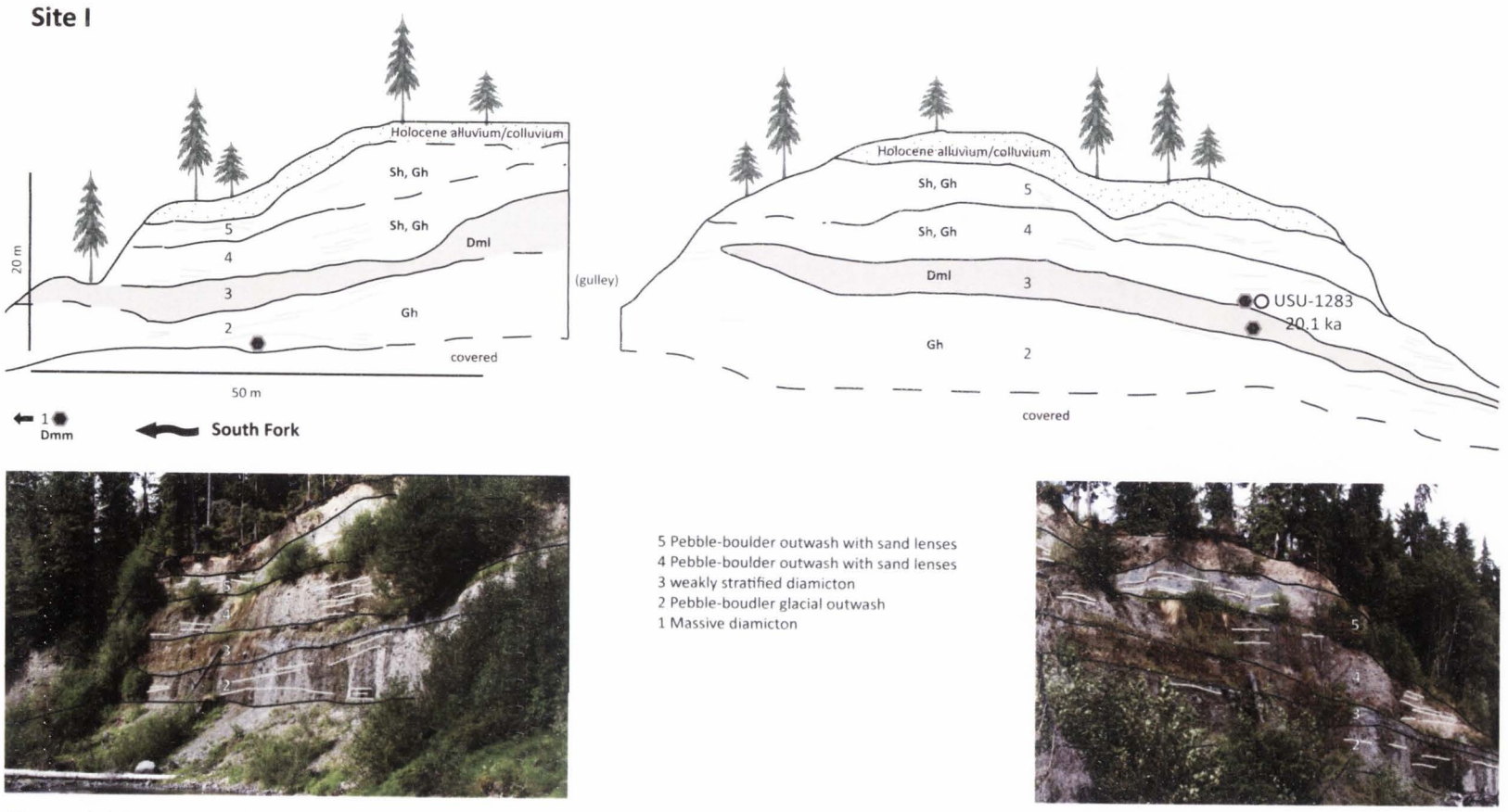

Figure 3.11 Stratigraphic panel and photograph of the Site I exposure. Numbers represent unit labels. Open circles and ages represent OSL sample locations. Filled hexagons represent clast count locations. See Figure 3.4 for a key to symbols. Facies codes (Table 3.2) are present on the panel. Detailed unit descriptions, photos, and clast counts can be found in the supplemental material (Figures A1.17-1.18).

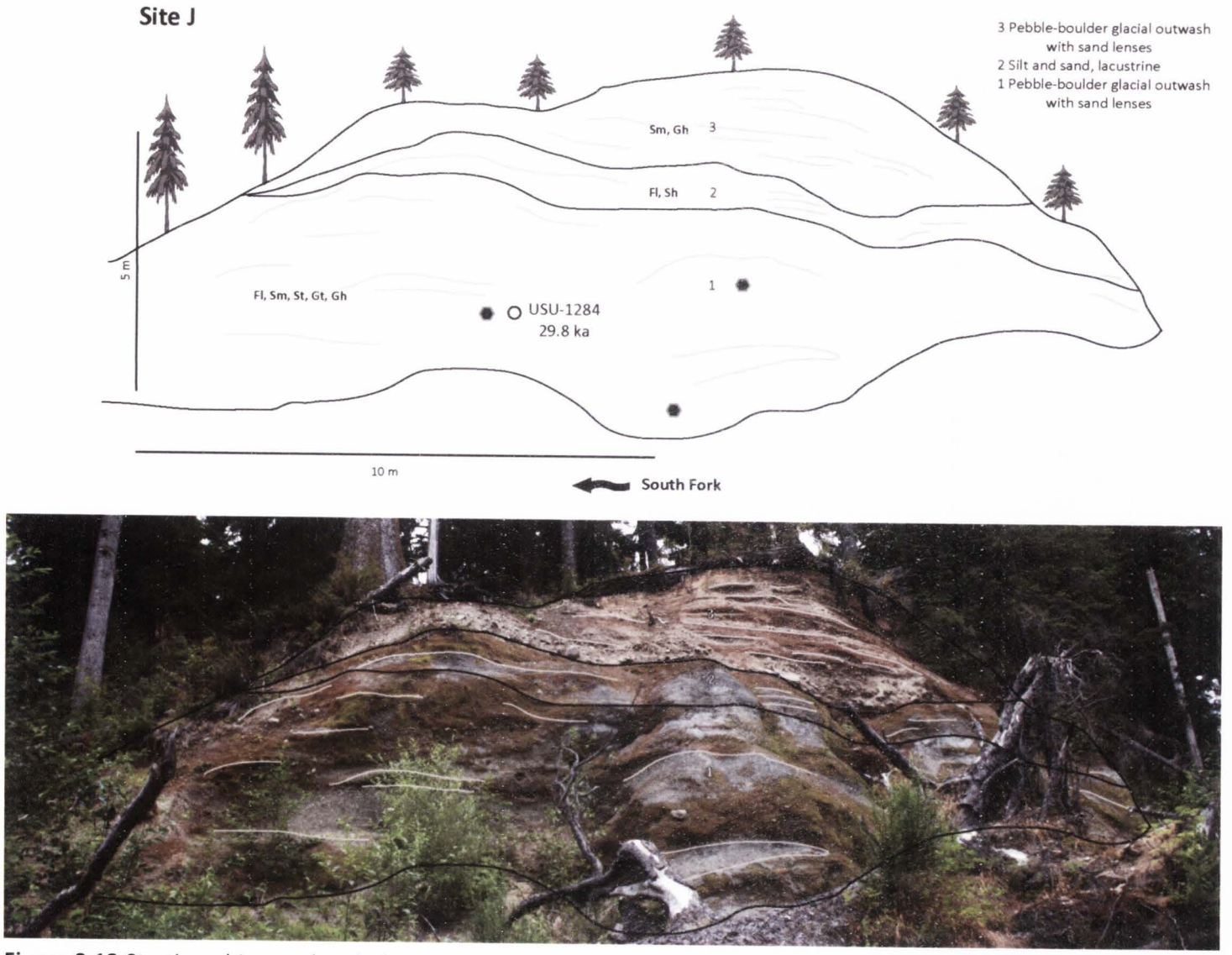

Figure 3.12 Stratigraphic panel and photograph of the Site J exposure. Numbers represent unit labels. Open circles and ages represent OSL sample locations. Filled hexagons represent clast count locations. See Figure 3.4 for a key to symbols. Facies codes (Table 3.2) are present on the panel. Detailed unit descriptions, photos, and clast counts can be found in the supplemental material (Figures A1.19-1.20).

bleaching. This sequence is interpreted to represent proglacial deposition at a moraine (Unit 1), followed by localized ponding and deposition of glaciolacustrine sediment (Unit 2), and gravel interpreted as outwash of the final phase of ice retreat out of the study area.

4. Reconstruction of glacial advances in the SF Hoh River valley

The relations between the stratigraphy of the ten study sites in the SF Hoh River valley are presented with stratigraphic columns plotted by elevation and distance along a downstream profile (Figure 3.13). These exposures are interpreted to preserve deposits associated with four glacial positions, referred to here as Hoh Oxbow 3 (from the chronology developed by Thackray, 2001), SF 1, SF 2, and SF 3, however the the Hoh Oxbow 3 terminal position is found in the mainstem Hoh River valley. The SF 1 position corresponds to the Twin Creeks I advance, and the SF 3 position corresponds to the Twin Creeks II advance of Thackray (2001). The SF 2 advance is an ice position not previously recognized but has been interpreted here primarily from the sequence of glacial deposits in the valley and the presence of a moraine-like landform. The discovery of this advance advocates for detailed sedimentologic and stratigraphic analyses.

4.1 The Hoh Oxbow 3 position

Site A and Site D contain sediment deposited following retreat from the Hoh Oxbow 3 ice position (Thackray, 2001). The till unit at Site A suggests that either the ice front was down-valley of this exposure and potentially joined with the main Hoh Valley glacier at the time of its emplacement or that it was deposited during retreat from this position. This interpretation is derived from the over-compacted nature of the deposit and association of till with subglacial deposition. The subsequent deposits in this exposure, Unit 2 and Unit 3, indicate a glaciolacustrine setting beginning ~23 ka that persisted following ice retreat up-valley of Site A

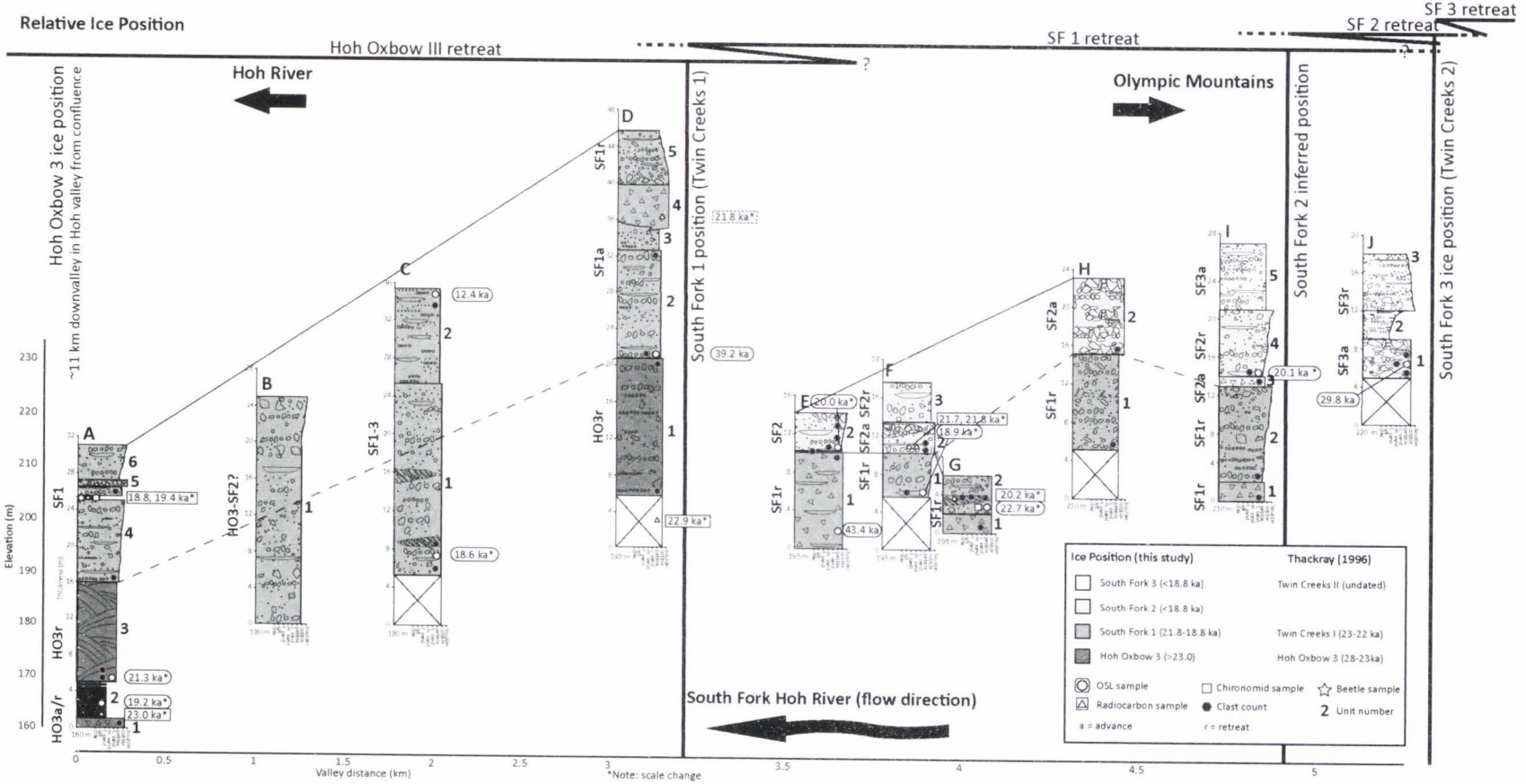

Figure 3.13 Stratigraphic columns representative of stratigraphy of all ten SF Hoh River valley exposures. All sample and clast count locations represented with the same symbology from stratigraphic panels. Ages considered somewhat reliable and used for interpretation in the text are denoted with '*'.The base of each site is represented here at the elevation of the river at each site. Each individual stratigraphic column also shows thickness on the y-axis. The color designation refers to the favored interpretation for correlation to each ice position. The upper lines depict the history of ice positions, between Hoh Oxbow 3 retreat and the SF3 ice position.

due to damming in the mainstem Hoh valley by either ice or sediment. This interpretation suggests that ice retreated faster up the SF valley than the mainstem Hoh valley during Hoh Oxbow 3 retreat. A sediment dam, conversely, may suggest rates of retreat in both valleys were similar. The sandy-pebbly deltaic foresets of Site A (Unit 3) suggest deposition of distal outwash into the lake, conformably overlying the finer glaciolacustrine deposit. The lacustrine sediment at Site A are ~15 m thick total, extending to ~178 m elevation.

The age constraints on this glaciolacustrine sediment are in stratigraphic order, but also within error of each other, suggesting rapid deposition. There is no evidence that the lacustrine environment extended far up-valley of Site A, as is expected due to the slope of the valley. The base elevation of the Site A exposure is ~160 m. The elevation of Site B at its base, in contrast, is ~180 m. This 20 m difference in elevation shows that the lacustrine sediment preserved at Site A would not have extended up-valley to what is currently exposed in Site B, but may be underlying the Site B outwash.

Site D exposes one unit of outwash at its base (Unit 1) interpreted to represent deposition during the up-valley retreat from the Hoh Oxbow 3 position, based on chronologic constraint and stratigraphic relationships. The 22.0-23.7 ka radiocarbon age from an underlying unit that is not currently exposed (see Thackray, 2001) suggests that this lacustrine sediment may be contemporaneous with the glaciolacustrine sediment of Site A (Units 2 and 3, within error). The basal outwash gravels at this site may represent the up-valley fluvial system feeding into the deltaic system at Site A. Other sedimentary packages related to retreat from the Hoh Oxbow 3 and older positions have not been identified, perhaps because these sediments may have been removed by erosion or are still buried. In summary, the stratigraphy and age control from the SF Hoh valley suggests retreat from the Hoh Oxbow 3 position was underway by 23 ka.

4.2 The South Fork 1 position

Stratigraphic evidence of the SF 1 advance is recorded at Site D, just downstream of the SF 1 moraine, as inter-bedded outwash and weakly stratified diamicton and possibly by coarsening upward outwash sequences at Sites A-C. Age control for these correlations is limited (Figure 3.13). Site D contains a weakly stratified diamicton (Unit 4) interbedded with glacial outwash (Unit 3) that is interpreted to have been deposited during the SF 1 re-advance. The stratification of this diamicton suggests a proglacial or ice-contact environment, and therefore provides evidence the location of the ice margin at this time. This unit and the interbedded outwash was probably sediment shed from the SF 1 moraine (Qm1). Thackray (1996, 2001) reports a 21.4-22.3 ka age from wood collected from a "till" across the river from Site D and projects this unit to a diamicton deposit in Site D, likely Unit 4 here. Although there is some uncertainty in the exact stratigraphic position, this age provides a maximum age constraint for the SF 1 ice position and moraine.

Several other glacial outwash units are interpreted to have been deposited during the SF 1 advance and retreat. These include the coarsening upward outwash sequences observed in Sites A, B, and C (Figure 3.13). Chronology of these deposits is limited; however, the upper radiocarbon dates from Site A (Unit 4) suggest deposition of this outwash 19.6-18.5 ka. These packages can only be broadly interpreted as having been deposited sometime during SF 1-3.

The coarsening outwash in Site A (Unit 4-6) and at Site B suggests an advancing ice front, and the relative elevation of Site B and Site C compared to Site A and Site D suggests that these outwash packages are related (Figure 3.13). Other outwash packages (Site C, D, F-I) and diamicton (Site I) units, as seen in Figure 3.13, are interpreted to mark a period of retreat from the SF 1 position. The outwash generally fines down-valley. We expect this pattern, as boulders

will be deposited closest to the ice front, while finer outwash can be transported farther. The SF 1 ice position is constrained to 22.7-18.8 ka based on age constraint from Site G and Site A.

4.3 The South Fork 2 position

A previously unidentified moraine and ice position has been mapped ~6.5 km upstream of the confluence of the Hoh and SF Hoh rivers. This has been labeled SF 2 and lies between the Twin Creeks 1 and Twin Creeks 2 moraines identified by Thackray (2001).

Four stratigraphic units are interpreted to be related to this advance, as preserved in Site E (Unit 2), Site F (Unit 2), Site H (Unit 2), and Site I (Unit 3) (Figure 3.13). Outwash preserved in Site F and Site H contain finer-grained more well-sorted pebble-gravel outwash overlain by coarser, less well-sorted and more angular cobble-boulder outwash, suggesting a transition from ice-distal to ice-proximal conditions. These changes in outwash packages are interpreted to represent an ice re-advance sequence. Site I contains a diamicton (Unit 3) interpreted to have been deposited during the SF 2 advance. This diamicton suggests ice-proximal or ice-contact deposition.

Outwash interpreted to represent retreat from the SF 2 position is preserved in two sites. Unit 3 of Site F contains finer, more sorted clasts than the underlying outwash package, suggesting the transition from SF 2 advance to SF 2 retreat. Although coarsening upwards slightly, Unit 4 of Site I is also interpreted to have been deposited during retreat, as it overlays the diamicton deposited during the SF 2 advance.

The sequence of deposits and presence of a moraine (Qm2) suggest that ice during the SF 2 advance reached Site I or just up-valley of the current exposure. Although the extent of SF 2 retreat is unknown, the moraines representative of SF 1 and SF 2 advances are separated by ~1.6 km. Due to limited age control in the upper portion of the field area, the timing of the Qm2

moraine and SF 2 ice position are limited to <18.8 ka. This is based on a radiocarbon sample at Site A (Unit 4) that relates to the SF 1 position.

4.4 The South Fork 3 position

The SF 3 ice position is marked by a moraine (Qm3) directly up-valley of Site J, which was mapped as the Twin Creeks 2 terminal moraine by Thackray (2001). The coarse basal boulder-gravel of Site J (Unit 1) was likely deposited in an ice-proximal environment during SF 3 advance to the Qm3 moraine immediately up-valley of this site. The uppermost packages at Site I (Unit 5) and Site J (Unit 3) may represent retreat from the SF 3 position. The lacustrine deposition at Site J (Unit 2) is interpreted to represent local ponding in abandoned outwash channel.

Diamicton associated with the SF 3 advance was not found in the valley. Site J was the farthest up-valley exposure studied, and a survey of air photos suggests that there are no additional exposures. Similarly, there is no topographic or geomorphic evidence for other moraines or glacial landforms up-valley. An area known as "Big Flat" on topographic maps and Olympic National Park guides begins ~1 km up-valley of Site J. Here, the river flows through a ≥1 km wide , broad and flat, meander plain for ~8 km before its confinement to the narrowest reaches of the valley as it is joined by tributaries and gullies originating in the high peaks of the Olympic Mountains. Although no chronologic constraint for these sediments exist, the constraint on the next oldest advance (SF 2) constrains the timing of the SF 3 advance to <18.8 ka.

5. Discussion

This study records three ice positions in the South Fork Hoh River valley, as well as earlier retreat from an older position when ice of the SF Hoh joined with ice in the mainstem Hoh valley. Radiocarbon and OSL age constraints on the oldest sediment in the SF Hoh constrain the occupation of the Hoh Oxbow 3 position to >23 ka. Retreat from this position was followed by advance to the SF 1 position. Radiocarbon ages constrain occupation of the SF 1 position to between 22.7 and 18.8 ka. The subsequent SF 2 advance and retreat are constrained to <18.8 ka based on few radiocarbon and OSL ages. Lastly, the SF 3 period can only be constrained to <18.8 ka as derived from the ages of SF 1 and SF 2 sediment. Although some of these ages have evidence of reworked older carbon and incomplete resetting of luminescence signals, they provide the best constraints on the glacial history of the valley.

The importance of detailed stratigraphic analysis in glacial environments is echoed by the discovery of the SF 2 ice position, which was not previously recognized. This research extended the data collected by Thackray (2001) by revisiting old sites, whose exposures have since changed, and updating the analyses and interpretations of their sedimentology and stratigraphy, as well as describing entirely new exposures. This study therefore provided both refinement of previous work in the same valley, allowing for more detailed interpretations of the sequence of glaciation, and new discoveries, further extending knowledge of SF Hoh glacial history.

Thackray (2001) previously mapped two ice positions in the SF Hoh River valley (Twin Creeks 1 and Twin Creeks 2) and interpreted some sedimentary packages to be related to retreat from an older ice position that reached, and probably joined with, ice in the mainstem Hoh River valley (Hoh Oxbow 3). These ice positions correspond to the Hoh Oxbow 3, SF 1, and SF 3 ice positions identified here. Additionally, the age constraint on ice advance periods is

consistent between the two studies. These three positions (or some combination of them) are also recorded in other western Olympic Peninsula valleys, including the Queets River valley, the main Hoh River valley, and the Sam's River valley as outwash terraces, end moraines, and/or undifferentiated dead-ice landforms (Thackray, 2001).

This study, however, specifically documents the SF Hoh as a unique valley in the Olympic Mountains that preserves three ice positions. Ice was restricted to the SF Hoh during the LGM period, suggesting that ice during this period in the Olympic Mountains ice was restricted to the upper valleys. This study shows that the ice margin fluctuated rapidly during this time, characterized by rapid valley cutting, glacial sedimentation, and valley filling. Three moraines were formed and three different ice positions recorded in less than ~3 ka. This research records a more detailed LGM record than those presented for most other valley glacier systems in the western United States.

This chronology in particular, as well as others in the Olympic Mountains, show significant differences from other regional and western United States mountain glacier systems, as summarized by Thackray (2008). In the Wallowa Mountains of Oregon (Licciardi et al., 2004), Wind River Range of Wyoming (Gosse et al., 1995), and perhaps the Sawtooth Mountains of Idaho (Thackray et al., 2004; Sherard, 2006), maximum ice extent corresponded to the global LGM and a prominent northern hemisphere insolation minimum. Glaciers in the Uinta Mountains (Munroe et al., 2006; Laabs et al., 2006, 2007; Refsnider et al., 2008) and Yellowstone Plateau (Sturchio et al., 1994; Licciardi et al., 2001; Pierce et al., 2007; Licciardi and Pierce, 2008) reached maximum extent slightly later (~19-17 ka), which may correspond to Heinrich Event 1. Glaciers in the Cascade Mountains of Washington advanced during northern hemisphere insolation minima; however, ice reached its greatest extent during MIS 4, not MIS 2 (Porter and Swanson, 2008). The Puget Lobe of the Cordilleran Ice Sheet, the closest other

glacial system to the Olympic Mountains, reflects the sequence of northern hemisphere continental glaciation and as such, is consistent with hemispheric insolation variations (Dethier et al., 1995; Porter and Swanson, 1998; Borden and Troost, 2001). These glacial systems were all influenced by major northern hemisphere climate events associated with orbital cycles.

Glaciers in the Olympic Mountains also reached maximum extent during MIS 4, similar to the Cascade chronology, however the glacial chronology of the Olympics varies from other western United States systems. Thackray (2001) suggests that the six major late Pleistocene advances, derived from the Hoh River and Queets River valley (and tributaries) sedimentary and geomorphic records, compared to paleoclimate records suggest that advances correlate with periods of sustained moisture delivery during insolation maxima *not* minima, thereby suggesting a dominant precipitation influence on ice advance and retreat.

The paleoclimate records from the western Olympic Peninsula are limited, however, and are interpreted in regards to temperature fluctuations. Those that relate specifically to the period recorded in the SF Hoh (~23-18 ka) are palynological studies that interpret pollen sequences (Florer, 1972; Heusser, 1972, 1974). The record of sea cliffs along the western Olympic coast presented by Florer (1972) extends to ~23 ka, at which time she notes a transition from non-glacial forest to tundra vegetation. Heusser (1972) presents a record from sea cliffs north of Kalaloch. He discusses a generally cold period from ~23-16 ka, which is punctuated by two periods of warmer temperatures, ~21.5-19 ka and ~18-17.5 ka. Heusser (1974) studied pollen in bog sediments in the Hoh River valley and shows that ice in this valley had begun retreat before 18.8 ka. The record also shows that temperatures were cold from ~18.8-10 ka, although a short (and not constrained) warm period began ~18 ka.

Several interpretations of these paleotemperature records may relate to the glacial history in the SF Hoh. The ~23 ka transition from non-glacial to tundra vegetation (Florer, 1972)

may mark the period of retreat from the Hoh Oxbow 3 ice position (<23 ka) and transition to the SF 1 advance (by 22.7 ka). The period of warmer temperatures from ~21.5-19.0 ka (Heusser, 1972) may relate to retreat from the SF 1 position, which spanned 22.7-18.8 ka. Retreat in the Hoh River valley that began prior to 18.8 ka (Heusser, 1974) supports this connection. Another period of warmer temperatures, ~18-17.5 ka (Heusser, 1972) and ~18 ka (Heusser, 1974), may represent a subsequent retreat, either from the SF 2 or the SF 3 position. Unfortunately, none of these records are interpreted in regards to precipitation and, therefore, inferences regarding temperature vs. precipitation influences cannot be drawn. The chronologic constraint and ice positions show that ice fluctuated rapidly in this valley during the LGM, providing a unique record of valley glaciation in the western United States.

Similar research to that conducted in the SF Hoh in other Olympic Mountain valleys could hold implications for the interpretation of local climate and how glaciers in this system may have responded to potential regional changes in temperature and/or precipitation. The progressively younger ice positions in the SF Hoh represent ice positions further and further up-valley; hence, the sequence of these positions suggests a broad period of increasing temperatures and/or decreasing precipitation. Each stable ice position, whether related to an ice re-advance or still-stand, may therefore represent a perturbation in climatic mechanism(s) influencing the broader period of deglaciation.

6. Conclusions

Ten exposures along cutbanks in the SF Hoh River valley reveal three stable ice positions and sediment deposited during retreat from the Hoh Oxbow 3 ice position in the main Hoh River valley. The system was dominated by several distinct glacial outwash channel systems, and glaciolacustrine deposition in the lower reaches of the valley. Three geomorphically expressed

moraines and outwash and diamicton stratigraphic sequences mark the positions of the last three stable ice positions in the SF Hoh, dated to 22.7-18.8 ka ka and two positions followed 18.8 ka. The oldest (SF 1) and youngest (SF 3) correlate to the Twin Creeks 1 and Twin Creeks 2 positions of Thackray (2001). Reassessment of the sediments in this valley has identified a previously unrecognized moraine between these two ice positions. In this study, we renamed these ice positions as SF 1, SF 2, and SF 3.

Although the climatic mechanisms of advance and retreat during this time period remain debated, the stratigraphy, timing, and history of the last glacial advance in the SF Hoh River valley presented here may aid in unraveling the paleoclimatology and glacial response of the Olympic Mountains. The overall period of retreat punctuated by stable ice positions as re-advances or still-stands likely reflect short-duration changes temperature, as related to pollen-based paleoclimate reconstructions from the western Olympic Mountains. A comparison to precipitation records is not currently available. Additionally, this research adds to a growing database of transport and depositional processes of valley glaciers in hyper-humid maritime climate zones, specifically pertaining to diamicton deposition and glacial outwash systems.

The turbid proglacial and diamicton depositional setting complicate obtaining chronological constraint due to issues associated with incomplete luminescence signal bleaching and lack of preservation and common re-deposition of organic material. Some of the OSL samples in this research, however, yield good results and expected ages, therefore showing the importance of sample site selection and/or that any environmental problems can be mitigated through laboratory procedures.

References

Aitken, M. J., 1998. An Introduction to Optical Dating: the Dating of Quaternary Sediments by the Use of Photon-stimulated Luminescence. Oxford University Press, Oxford.

Borden, R. K., Troost, K. G., 2001. Late Pleistocene Stratigraphy in the South-Central Puget Lowland, Pierce County, Washington. Washington State Department of Natural Resources, Division of Geology and Earth Resources Report of Investigations 33.

Brandon, M. T., 2004, The Cascadia subduction wedge: the role of accretion, uplift, and erosion. In: van der Pluijm, B. A., Marshak, S. (Eds.), 2004, Earth Structure: An Introduction to Structural Geology and Tectonics, 2nd Edition. WCB/McGraw Hill Press, New York, pp. 566-574.

Clark, P. U., Dyke, A. S., Shakun, J. D., Carlson, A. E., Clark, J., Wohlfarth, B., Mitrovica, J. X., Hostetler, S. W., McCabe, A. M., 2009. The Last Glacial Maximum. Science 325(5941), 710-714.

Conway, H., Rasmussen, L. A., Marshall, H. P., 1999. Annual mass balance of Blue Glacier, U.S.A.:1955097. Geografiska Annaler 81A(4), 509-520.

Dethier, D. P., Pessl Jr., F., Keuler, R. F., Balzarini, M. A., Pevear, D. R., 1995. Late Wisconsonian glaciomarine deposition and isostatic rebound, northern Puget Lowland, Washington. GSA Bulletin 107(11), 1288-1303.

Evans, D. J. A., Benn, D. I., 2004. A Practical Guide to the Study of Glacial Sediments. Hodder Education, London.

Florer, L. E., 1972. Quaternary Paleoecology and Stratigraphy of the Sea Cliffs, Western Olympic Peninsula, Washington. Quaternary Research 2, 202-216.

Fuchs, M., Owen, L. A., 2008. Luminescence dating of glacial and associated sediments: review, recommendations and future directions. Boreas 37(4), 636-659.

Galbraith, R. F., Roberts, R. G., Laslett, G. M., Yoshida, H., Olley, J. M., 1999. Optical dating of single and multiple grains of quartz from Jinmium rock shelter, northern Australia: Part I, experimental design and statistical models. Archaeometry 41, 339-364.

Gosse J. C., Klein J., Evenson E. B., Lawn B., Middleton R., 1995. Beryllium-10 dating of the duration and retreat of the last Pinedale glacial sequence. Science 268, 1329–1333.

Guérin G., Mercier, N., Adamiec, G., 2011. Dose-rate conversion factors: update. Ancient TL 29, 5-8.

Heusser, C. J., 1972. Palynology and phytogeographical significance of a Late-Pleistocene refugium near Kalaloch, Washington. Quaternary Research 2, 189-201.

Heusser, C. J., 1974. Quaternary Vegetation, Climate, and Glaciation of the Hoh River Valley, Washington. Geological Society of America Bulletin 85(10), 1574-1560.

Huntley, D. J., Godfrey-Smith, D. I., Thewalt, M. L. W., 1985. Optical dating of sediments. Nature 313, 105-107.

Klasen, N., Fiebig, M., Preusser, F., Reitner, J., Radtke, U., 2007. Luminescence dating of proglacial sediments from the Eastern Alps. Quaternary International 164-165, 21-32.

Laabs B. J. C., Plummer M. A., Mickelson D. M., 2006. Climate during the Last Glacial Maximum in the Wasatch and southern Uinta Mountains inferred from glacier modeling. Geomorphology 75, 300–317.

Laabs B. J. C., Munroe J. S., Rosenbaum J. G., Refsnider K. A., Mickelson D. M., Singer B. S., Caffee M. W., 2007. Chronology of the Last Glacial Maximum in the Upper Bear River Basin, Utah. Arctic, Antarctic, and Alpine Research 39, 537–548.

LaChapelle, E. R., 1959. Annual mass and energy exchange on the Blue Glacier, Journal of Geophysical Research 64(4), 443-449.

LaChapelle, E. R., 1960. The Blue Glacier Project, 1959 and 1960. University of Washington, Department of Meteorology and Climatology, Seattle.

Licciardi J. M., Clark P. U., Brook E. J., Pierce K. L., Kurz M. D., Elmore D., Sharma P., 2001. Cosmogenic ^{3}He and ^{10}Be chronologies of the late Pinedale northern Yellowstone ice cap, Montana, USA. Geology 29, 1095–1098.

Licciardi J. M., Clark P. U., Brook E. J., Elmore D., Sharma P., 2004. Variable responses of western US glaciers during the last termination. Geology 32, 81–84.

Licciardi J. M., Pierce K. L., 2008. Cosmogenic exposure age chronologies of Pinedale and Bull Lake glaciations in greater Yellowstone and the Teton Range, USA. Quaternary Science Reviews 27, 814–831.

Lukas, S., Spencer, J. Q. G., Robinson, R. A. J., Benn, D. I., 2007. Problems associated with luminescence dating of Late Quaternary glacial sediments in the NW Scottish Highlands, Quaternary Geochronology 2, 243-248.

Munroe, J. S., Laabs, B. J. C., Shakun, J. D., Singer, B. S., Mickelson, D. M., Refsnider, K. A., Caffee, M. W., 2006. Latest Pleistocene advance of alpine glaciers in the southwestern Uinta Mountains, Utah, USA: Evidence for the influence of local moisture sources. Geology 34(10), 841-844.

Murray, A. S., Wintle, A. G., 2000. Luminescence dating of quartz using an improved single-aliquot regenerative-dose protocol, Radiation Measurements 32, 57-73.

Murray, A. S., Wintle, A. G., 2003. The single aliquot regenerative dose protocol: potential for improvements in reliability, Radiation Measurements 37, 377-381.

Paterson, W. S. B., 1994. The Physics of Glaciers. Elsevier Science, Oxford.

Pierce K. L., Despain D. G., Morgan L. A., Good J. M., 2007. The Yellowstone hotspot, Greater Yellowstone ecosystem, and human geography. In: Morgan, L. A. (Ed.) Integrated Geoscience Studies in the Greater Yellowstone Area: Volcanic, Tectonic, and Hydrothermal Processes in the Yellowstone Geoecosystem, Morgan LA (ed.). USGS Professional Paper 1717. US Geological Survey: Reston, VA, pp. 1–39.

Porter, S. C., Swanson, T. W., 1998. Radiocarbon Age Constraints on Rates of Advance and Retreat of the Puget Lobe of the Cordilleran Ice Sheet during the Last Glaciation. Quaternary Research 50, 205-213.

Porter S. C., Swanson T. W., 2008. ^{36}Cl dating of the classic Pleistocene glacial record in the northeastern Cascade Range, Washington. American Journal of Science 308, 130–166.

Prescott, J. R., Hutton, J. T., 1994. Cosmic-ray contributions to dose rates for luminescence and ESR dating - Large depths and long-term time variations. Radiation Measurements 23, 497-500.

Preusser, F., Ramseyer, K., Schlüchter, C., 2006. Characterisation of low OSL intensity quartz from the New Zealand Alps. Radiation Measurements 41, 871-877.

Rasmussen, L. A., Conway, H., Hayes, P. S., 2000. Accumulation regime of Blue Glacier, U.S.A., 1914-96. Journal of Glaciology 46(153): 326-334.

Refsnider K. A., Laabs B. J. C., Plummer M. A., Mickelson D. M., Singer B. S., Caffee M. W., 2008. Last glacial maximum climate inferences from cosmogenic dating and glacier modeling of the western Uinta ice field, Uinta Mountains, Utah. Quaternary Research 69, 130-144.

Reimer, P. J., Baillie, M. G., Bard, E., Bayliss, A., Warren, B. J., Blackwell, P. G., Ramsey, C. B., Bruch, C. E., Burr, G. S., Edwards, R. L., Friedrich, M., Gootes, P. M., Guilderson, T. P., Hajdas, I., Heaton, T. J., Hogg, A. G., Hughen, K. A., Kaiser, K. F., Kromer, B., McCormac, F. G., Manning, S. W., Reimer, R. W., Richards, D. A., Southon, J. R., Ralamo, S., Turney, C. S.M., van der Plicht, J., Weyhenmeyer, C. E., 2009. IntCal09 and Marine09 Radiocarbon Age Calibration Curves, 0-50,000 Years cal BP. Radiocarbon 51(4), 1111-1150.

Sherard C., 2006. Timing of early Holocene Glacial advances in Idaho and Washington. M.S. thesis, Western Washington University, Bellingham.

Spicer, R. C., 1986. Glaciers in the Olympic Mountains, Washington: Present Distribution and Recent Variations. M.S. thesis, University of Washington, Seattle.

Sturchio N. C., Pierce K. L., Murrell M. T., Sorey M. L., 1994. Uranium-series ages of travertines and timing of the last glaciation in the northern Yellowstone area, Wyoming–Montana. Quaternary Research 41, 265–277.

Station: Forks 1 E, Washington (452914). Western U.S. Climate Historical Summaries: Western Regional Climate Center, http://www.wrcc.dri.edu/cgi-bin/cliMAIN.pl?wafork, Accessed 04/02/2012.

Tabor, R. W., Cady, W. M., 1978. Geologic map of the Olympic Peninsula, Washington. U.S. Geological Survey, Miscellaneous Investigations Series Map 1-994, scale 1:125,000.

Thackray, G. D., 1996. Glaciation and Neotectonic Deformation on the Western Olympic Peninsula, Washington. PhD dissertation, University of Washington, Seattle.

Thackray, G. D., 2001. Extensive Early and Middle Wisconsin glaciation on the western

Olympic Peninsula, Washington, and the variability of Pacific moisture delivery to the northwestern United States. Quaternary Research 55, 257-270.

Thackray, G. D., 2008. Varied climatic and topographic influences on Late Pleistocene mountain glaciation in the western United States. Journal of Quaternary Science 23(6-7), 671-681.

Thackray G. D., Lundeen K. A., Borgert J. A., 2004. Latest Pleistocene alpine glacier advances in the Sawtooth Mountains, Idaho, USA: reflections of midlatitude moisture transport at the close of the last glaciation. Geology 32, 225–228.

Wintle, A. G., Murray, A. S., 2006. A review of quartz optically stimulated luminescence characteristics and their relevance in single-aliquot regeneration dating protocols. Radiation Measurements 41, 369-391.

CHAPTER 4

LUMINESCENCE DATING OF LATE PLEISTOCENE PROXIMAL GLACIAL SEDIMENTS IN THE OLYMPIC MOUNTAINS, WASHINGTON AND SOUTHERN ALPS, NEW ZEALAND

Abstract

Late Pleistocene glacial sediments from the South Fork Hoh River valley in the Olympic Mountains, Washington, USA and the Lake Hawea valley in the Southern Alps, New Zealand were dated using optically stimulated luminescence (OSL) on quartz and infrared stimulated luminescence (IRSL) on feldspar sand. High sediment supply typical of glacial environments, short transport distances, and sediment newly eroded from bedrock sources were expected to pose problems for luminescence dating in these locations. Samples were collected from a variety of depositional environments and inferred distances from the ice-front to assess how luminescence signals may vary due to these factors and to determine which samples produce the most reliable age estimates. This study supports previous work that discusses limitations of quartz OSL dating of sediments from the Southern Alps and advocates for feldspar IRSL dating in the Hawea drainage. Additionally, results from the South Fork Hoh highlight the importance of transport environment and sedimentary facies on solar resetting. Samples from these glacial settings were collected as part of larger research goals of improved understanding the glacial history of the two study areas.

Introduction

Establishing chronologic constraint of glacial periods and ice advance and retreat cycles is imperative in understating the influence of climate on glaciation, ice dynamics, and bedrock erosion and sediment transport by glacial ice. However, organic material for radiocarbon (^{14}C)

dating is not commonly preserved in glacial deposits and appropriate boulders for cosmogenic nuclide (CRN) dating may not be present. Optically stimulated luminescence (OSL) dating provides an age estimate of the last time sediment was exposed to sunlight in a variety of depositional environments. OSL dating is therefore a potentially useful tool in dating glacial deposits if complications associated solar resetting can be overcome. This research seeks to refine age control on glacial sediments from the Olympic Mountains and Southern Alps and assess the viability of using OSL in various depositional facies associated with proglacial environments.

Researchers have successfully employed OSL dating in a number of settings, however glacial deposits pose particular challenges to luminescence dating. Problems include incomplete bleaching (e.g. Klasen et al., 2007; Alexanderson and Murray, 2012), poor luminescence properties (e.g. Preusser et al., 2006), high thermal transfer (e.g. Alexanderson, 2007), and feldspar contamination of quartz OSL samples (e.g. Lukas et al., 2007). Many proglacial environments are turbid and have high sediment loads, which may not allow sufficient sunlight exposure to completely bleach sediments. Additionally, many glacial sediments may be derived directly from bedrock due to glacial erosion (Lukas et al., 2007) and may have experienced short transport and deposition histories (Moska and Murray, 2006; Pietsch et al., 2008; Sawakuchi et al., 2011; Jeong and Choi, 2012), which may produce quartz with poor luminescence properties and sensitivity.

Problems with OSL dating on the South Island of New Zealand include poor luminescence sensitivity, short transport distances from the source, and direct erosion of sand from bedrock. Preusser et al. (2006) discuss problems with OSL dating of quartz from Westland, South Island of New Zealand. They found that standard laboratory protocols could not correct for sensitivity changes, low luminescence, and thermal transfer of quartz. The authors suggest

that these issues arise from the young history of the quartz grains, namely that they were freshly eroded from bedrock and have not been sensitized through the process of repeated exposure to sunlight and radiation from multiple cycles of transport and deposition.

These complications, however, have not fully thwarted researchers, and recent work has demonstrated success with quartz OSL dating on the eastern coast of the South Island (Rowan et al., 2012). However, this study may have been successful, due to the longer sediment transport distance (>50 km across the Canterbury Plains to the coast) than most other studies of glaciofluvial sediments on the South Island. This difference likely increased the bleaching potential and sensitivity of the quartz grains. Additionally, a study in North Westland, South Island compared radiocarbon, IRSL, and OSL age estimates from silt overbank deposits separating glacial outwash sequences and found that the IRSL and OSL signals showed no effects of partial bleaching (Hormes et al., 2003). Additionally, IRSL dating in the Rakaia River valley of the central South Island appears quite successful (Shulmeister et al., 2010).

Previous research using OSL dating on the Olympic Peninsula of Washington includes quartz OSL and feldspar IRSL in the Puget Lowland (Mahan, 2013, personal communication) and feldspar IRSL from a northwestern coastal dune (Feathers, 2013, personal communication). Due to complications with the quartz, much of the OSL in the Puget lowlands used feldspar IRSL dating methods (Mahan, 2013, personal communication). Current research projects in valleys originating in the Olympic Mountains (this study) and along the coastal cliffs (Marshall, 2013) used OSL and IRSL dating to enhance and revise chronologic constraint of Pleistocene glaciation of the Olympic Mountains.

OSL dating has also been used in several other glacial settings with variable success. Many of these studies discuss incomplete bleaching of quartz and/or feldspar grains prior to deposition as the primary complication with OSL dating (e.g. Duller et al., 1995 in Scotland;

Gemmell, 1999 in the European Alps; Berger and Doran, 2001 in Antarctica; Gemmell et al., 2007 in Scotland; Alexanderson and Murray, 2012 in Svalbard). Examples of additional complications include thermal transfer of quartz samples from the Himalaya (Spencer and Owen, 2004), changes in luminescence sensitivity of feldspar samples in the Hindu Kush (Owen et al., 2002), and anomalous fading of feldspar samples from Quebec, Canada (Lamothe et al., 1994).

This study presents quartz OSL dating results from the South Fork Hoh River valley of the Olympic Mountains, Washington and feldspar IRSL results from the Lake Hawea valley of the Southern Alps, New Zealand. The primary goal is to investigate the influence of depositional facies and relative distance from the ice front on OSL characteristics and equivalent dose (De) distributions in late Pleistocene proglacial sedimentary packages.

This research is part of a larger project that seeks to provide and refine age control on packages of outwash and glaciolacustrine sediment in two settings where previous age control is limited by lack of exposed boulders for cosmogenic dating and the limited range of radiocarbon dating of organic material within deposits. Broader goals include investigating glacial dynamics and responses of these glacial systems to climate forcings. The study areas collectively aid investigations of hyper-humid climates on glacial dynamics and sediment transport and depositional architecture.

1.1 Luminescence dating

Optically stimulated luminescence dating (OSL) of quartz and infrared stimulated luminescence dating (IRSL) of feldspar provide age estimates of the last time sediment was exposed to sufficient sunlight (or heat) to zero (bleach) the luminescence signal acquired during the previous burial history (Huntley et al., 1985). Upon deposition and burial, the sediment is

removed from sunlight and exposed to radiation from the surrounding sediment and incoming cosmic rays. The sediment acquires a stored charge dependent on the length of burial and dose rate environment. The most widely used and accepted method to determine the equivalent dose (or "paleodose") of the sediment is the single-aliquot regenerative-dose (SAR) method (Murray and Wintle, 2000, 2003; Wallinga et al., 2000; Wintle and Murray, 2006). The age of a sample is calculated by dividing the equivalent dose (De) by the dose rate (DR).

$$\text{Age (ka)} = \text{De (Gy)} / \text{DR (Gy ka}^{-1}\text{)}$$

where 1 Gray (Gy) = 1 joule/kilogram (J/kg) (Aitken, 1998). The dose rate is a measure of the dose per unit time received by a sample while buried, defined as the flux of radiation measured directly or indirectly in the field and/or determined by chemical composition (more specifically the radioactive elements Uranium (U), Potassium (K), Thorium (Th), and Rubidium (Rb)) and cosmic contribution. The equivalent dose (De) is the dose of radiation needed to induce a luminescence signal equal to the natural luminescence signal acquired by a sample subsequent to its most recent bleaching event. The dosage should therefore be approximately equivalent to the paleodose, or the radiation dose a sample received in nature during burial.

1.2 Study areas

1.2.1 South Fork Hoh River, Olympic Mountains, USA

The Olympic Mountains of Washington lie on the northwestern-most edge of the contiguous United States. The Olympic Peninsula is bound by the Puget Sound to the east, the Pacific Ocean to the west, the Strait of Juan de Fuca to the north, and the Chehalis River lowland to the south (Figure 4.1). Pleistocene radial valley glaciers that may have been confluent at their heads flowed from the high peaks of the Olympic Mountains to the coastal lowlands and beyond the modern shoreline (Thackray, 2008). Thackray (2001) provides the most comprehensive

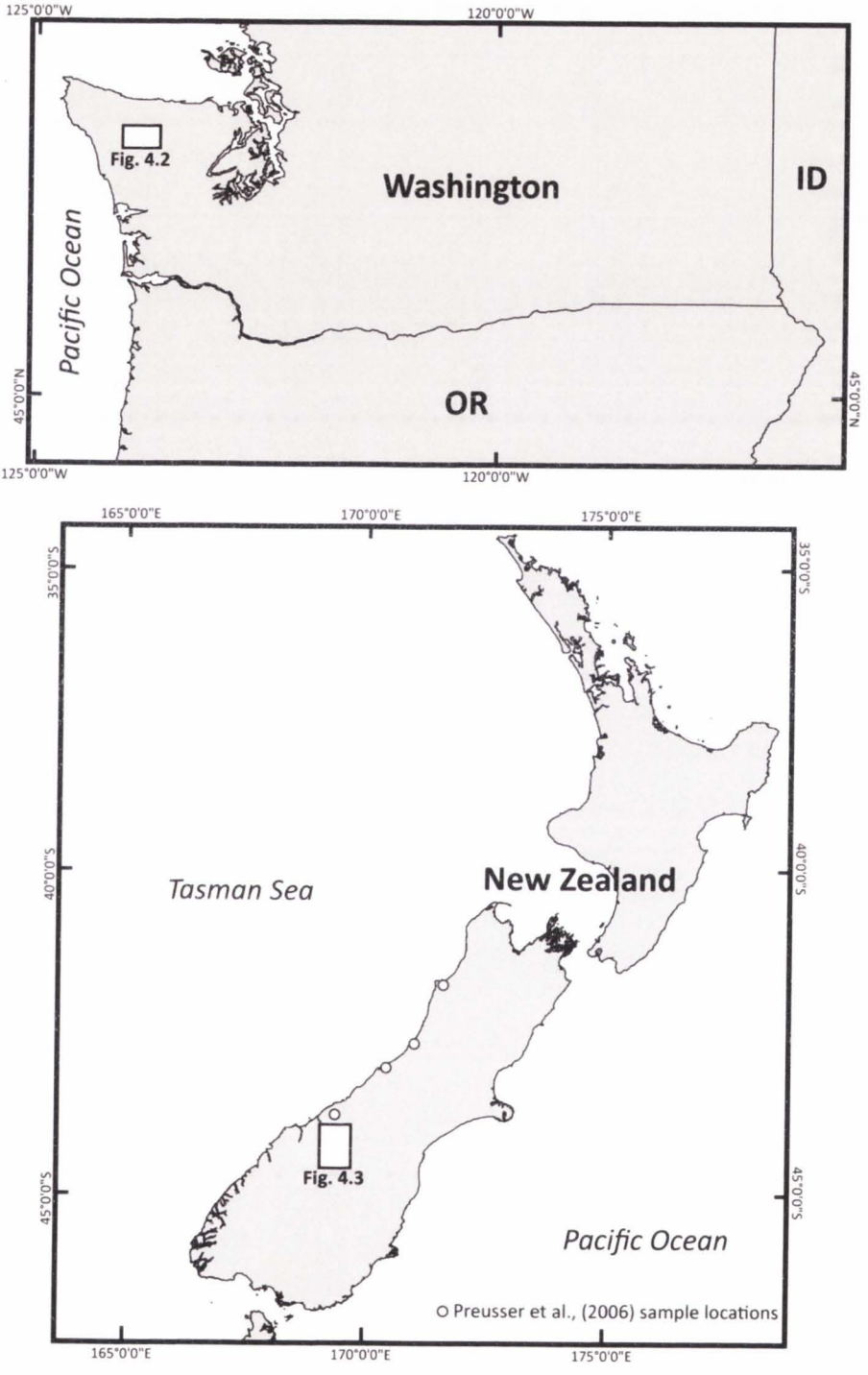

Figure 4.1 Locations of the South Fork Hoh River, Washington, USA (upper) and Lake Hawea, South Island, New Zealand (lower) catchments. Boxes show the locations of Figure 4.2 and Figure 4.3. Circles represent the locations of samples discussed in Preusser et al. (2006).

summary of the major valley glacier advances on the western Olympic Peninsula. Named advances consist of Lyman Rapids (MIS 4), Hoh Oxbow 1-3 (MIS 3-2), and Twin Creeks 1-2 (MIS 2). The Hoh Oxbow 3 advance most closely corresponds to the global LGM (26-19 ka; Clark et al., 2009). Landforms marking this ice-marginal position include terminal moraines at the mouth of the Hoh and Queets Rivers and broad outwash terraces extending to coastal bluffs, and outwash terraces.

Today, the remnants of these glaciers and their meltwater feed the Hoh River and the South Fork Hoh River (SF Hoh), which flow west out of the Olympic Mountains (Figure 4.2). The South Fork (~30 km long, ~140 km^2 catchment area) joins the main Hoh River (~90 km long, ~770 km^2), which flows roughly west-southwest before entering the Pacific Ocean. The elevation of the SF Hoh ranges from ~125-2,427 m, with Mount Olympus representing the highest elevation. Cut banks of meander bends along the SF Hoh produce numerous exposures of glacial sediment. Diamicton, glacial outwash, and lacustrine sediments were deposited around four late Pleistocene ice positions, the oldest of which extended beyond the South Fork valley into the main stem Hoh River valley (>23 ka) (Chapter 3). Three younger stable ice positions mapped as the South Fork 1-3 (SF 1-3) moraines (22-19 ka, <19 ka, and <19 ka) are preserved stratigraphically in cutbank exposures and geomorphically by moraines. One of these positions, SF 2, represents a stable ice margin during a period of overall retreat that has not previously been recognized in this valley or in the mainstem Hoh River valley. Five radiocarbon dates, three of which are from the same unit, from three exposures provided the only previous age control on these deposits within the SF Hoh (Thackray, 2001). Five additional radiocarbon samples from three exposures and three units were collected and presented as part of the current research project (see Chapter 3).

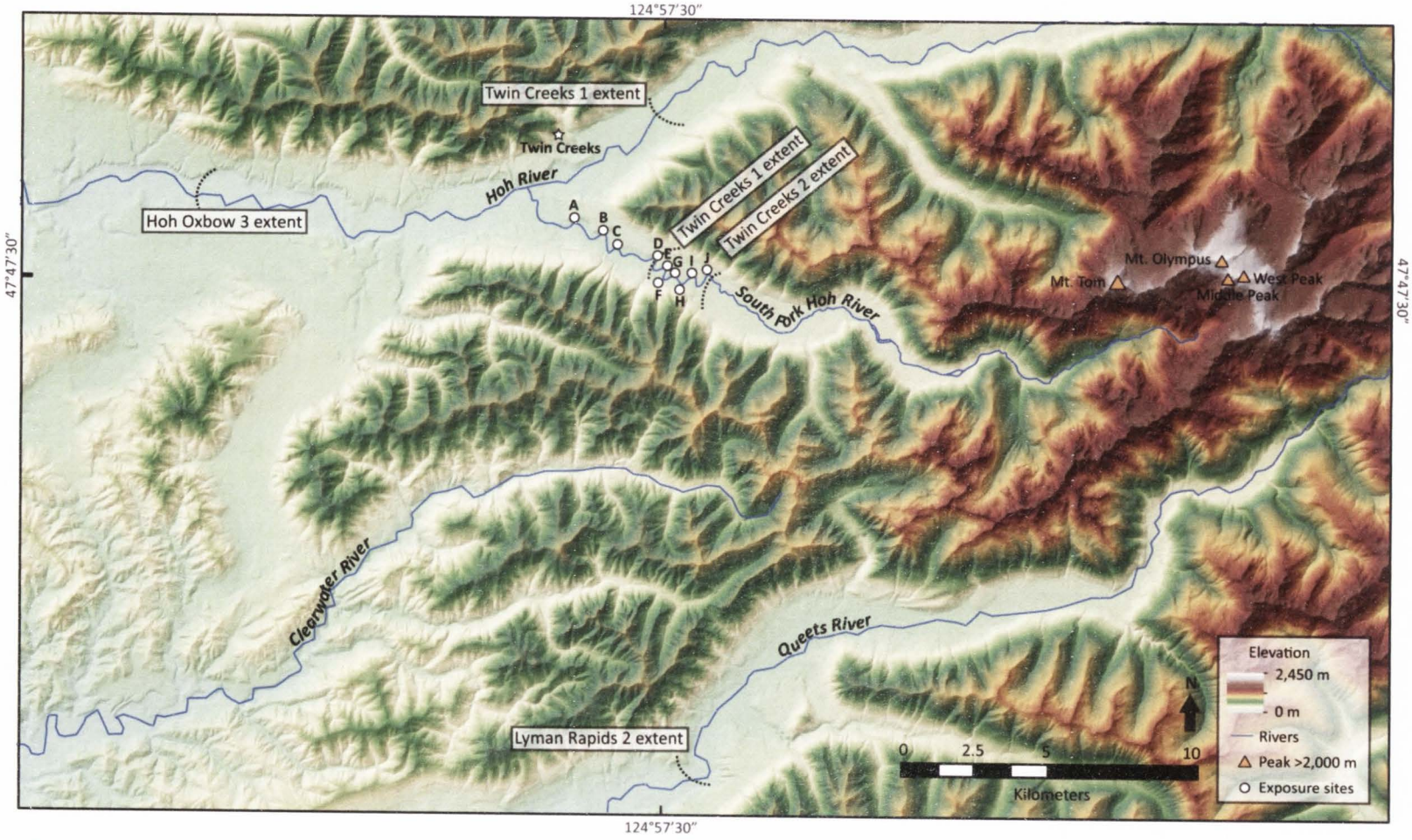

Figure 4.2 The South Fork Hoh River valley and surrounding area. Exposures studied are labeled as Sites A-J, with Site A being the farthest down-valley and Site J the farthest up-valley. Dashed lines indicate ice extent relevant to this study as mapped by Thackray (1996). Elevations derived from 30 m NED DEM data.

1.2.2 Lake Hawea, New Zealand

Lake Hawea lies on the eastern side of the Southern Alps drainage divide in northwestern Otago, South Island, New Zealand (Figure 4.1). The lake occupies ~140 km^2 of a northeast-southwest trending valley and is ~35 km long (Figure 4.3). Lake Hawea formed in the overdeepened trough excavated by glacial ice extending from the headwaters of the Hunter River and water impoundment from damming by glacial deposits and outwash at the southern margin of the basin. The Hunter River to the north feeds the lake, while the Hawea River on the southwestern shore drains the lake and becomes a tributary to the Clutha River ~15 km downstream. The bluffs along the southern shoreline of Lake Hawea, near the town of Gladstone, contain vertical, exposures of glacial sediment (~2-9 m tall, ~1.3 km long) of what is known as the Hawea moraine (see Chapter 2).

During the last glaciation, a regional ice cap extending along the ridgeline of the Southern Alps fed valley glaciers. One of these large valley glaciers, the Hawea glacier (McKellar, 1960), extended southward beyond the modern Lake Hawea margin. The glacial chronology of the Lake Hawea-Clutha River area is poorly constrained. Current age constraints are based on correlation of landforms and a limited number of radiocarbon (^{14}C) ages. Thomson (2009) identified the ice advances of the Lake Hawea-Lake Wanaka area as the Northburn (MIS 26), Lowburn (MIS 16), Lindis (MIS 12), Queensbury (MIS 10), Luggate (MIS 6), Albertown (MIS 4), Mt. Iron (MIS 2 early), and Hawea (MIS 2 late) advances, with moraines and heads of outwash marking most advances (Thomson, 2009). These advances represent progressively reduced ice positions. For example, the Albertown MIS 4 ice position reached farther down-valley than the MIS 2 (and global LGM) ice position(s). The Mt. Iron advance probably marks the LGM position in this area, although age control and geomorphic evidence of this advance are limited. The youngest advance is represented by a moraine at the southern margin of Lake Hawea.

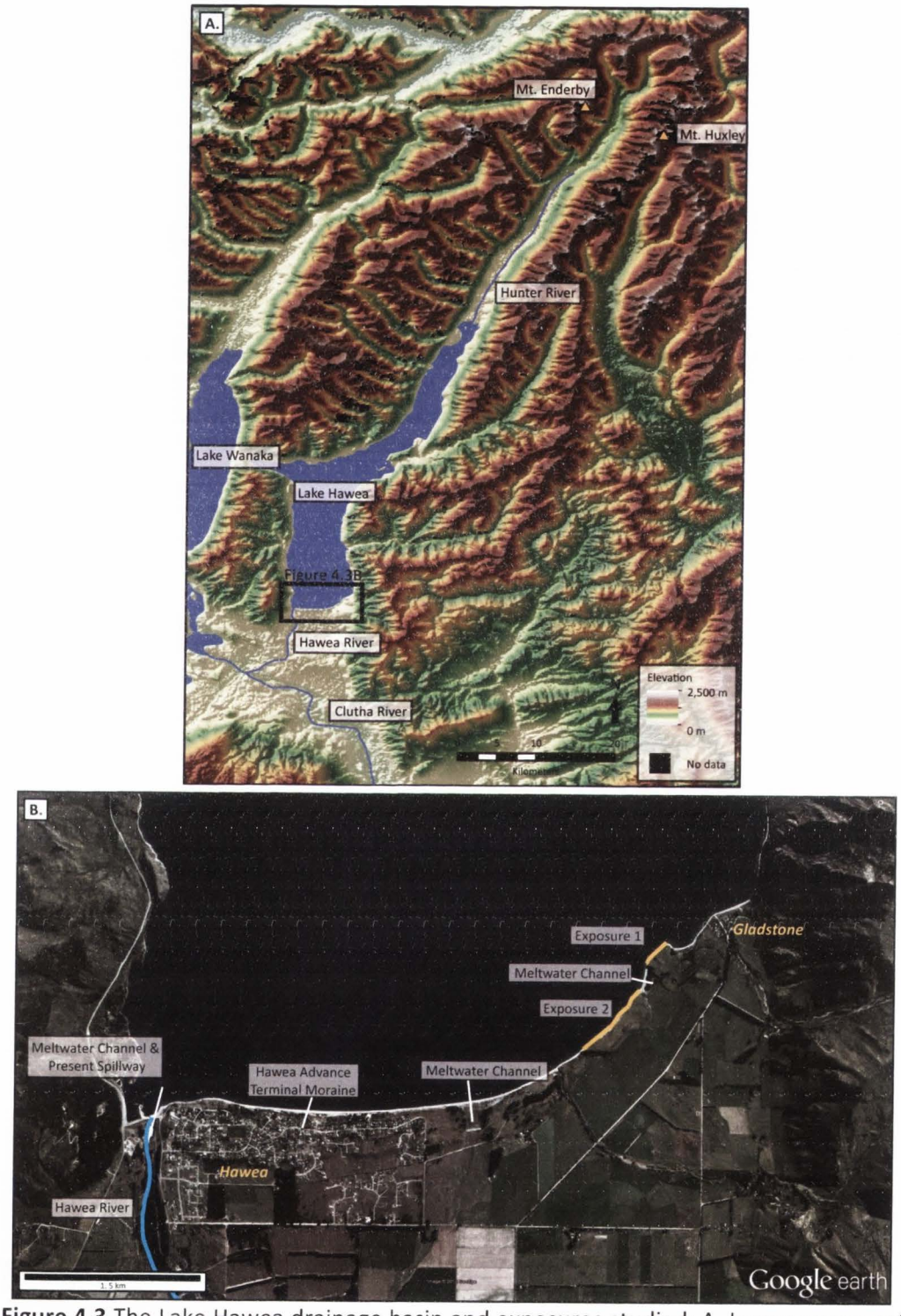

Figure 4.3 The Lake Hawea drainage basin and exposures studied; A. Image covers extent of the Hawea drainage basin and surrounding area, as bound and labeled in Figure 1. Black bounding box shows location of Figure B below. Elevations basen on 30 m SRTM data; B. Exposures studied labeled as Exposure 1 and Exposure 2. Blue line shows paths of the Hawea River. Imagery obtained from Google Earth, 2012 Digital Globe, 2012 GeoEye.

Radiocarbon ages from peat overlying outwash in an abandoned channel at the southern outlet of Lake Hawea constrain a broad minimum age of this moraine to 15.1 ± 0.2 ^{14}C ka (~17.8-18.7 ka cal. years, 2 σ error[1]) (McKellar, 1960). Cosmogenic surface exposure dating (^{10}Be) of a biotite schist with quartz veins exposed in the same outwash channel produced an age of ~17.5 ka (Graham et al., 1998). Additionally, samples have been collected for cosmogenic dating of boulders in the Wanaka and Hawea catchments; however, these results are not yet available (Rother, personal communication).

2. Methods

2.1. Descriptions of Pleistocene glacial deposits

Exposures within the SF Hoh and along the southern margin of Lake Hawea were logged and detailed sedimentary and stratigraphic measurements were made, including description of unit thickness and geometry, sedimentary facies, bedding, structures, grain size and shape, fabric, and color. Due to the large size of the outcrops, photographs were stitched together to aid in production of outcrop-scale stratigrapghic panels (see Chapter 2 and Chapter 3 for details).

2.2. Sample collection and preparation

Two samples for OSL dating were collected from the Lake Hawea bluffs and eleven samples were collected from the SF Hoh exposures. Samples were obtained by pounding an opaque steel tube into sandy layers after the outcrop face was scraped to obtain a fresh surface.

---

[1] Calibrated using IntCal09 calibration curve: Reimer, P. J., Baillie, M. G. L., Bard, E., Bayliss, A., Beck, J. W., Blackwell, P. G., Bronk Ramsey, C., Buck, C. E., Burr, G. S., Edwards, R. L., Friedrich, M., Grootes, P. M., Guilderson, T. P., Hajdas, I., Heaton, T. J., Hogg, A. G., Hughen, K. A., Kaiser, K. F., Kromer, B., McCormac, F. G., Manning, S. W., Reimer, R. W., Richards, D. A., Southon, J. R., Talamo, S., Turney, C. S. M., van der Plicht, J., Weyhenmeyer, C. E., 2009. Radiocarbon 51:1111-1150.

These samples were collected from sandy beds and lenses and targeted fine sand. A sample from a 30 cm radius around the sample tube was collected to gather a representative sample for dose-rate. A sample for water content was collected in an airtight container to maintain accurate water content at the time of sample collection.

OSL sample preparation and analyses were conducted at the Utah State University Luminescence Laboratory under ambient amber light (590 nm wavelength). Samples were sieved to the grain size ranges listed in Table 4.1. Hydrocloric acid and bleach were used to dissolve carbonates and organic material. For quartz separation and purification, sodium polytungstate (2.7 g/cm^3) was used to separate quartz and feldspar from heavy minerals. A portion of the light mineral fraction was then treated in concentrated hydrofluoric and hydrochloric acids to remove feldspars and etch quartz. Samples were then sieved to remove partially dissolved feldspar grains and sample purity of each aliquot was checked by IRSL responses. For potassium feldspar separation, the light mineral fraction from the heavy mineral separation step above was further separated using 2.58 g/cm^3 sodium polytungstate to separate potassium feldspar and quartz.

2.3. Dose rate determination

Samples for dose-rate determination were split to obtain a representative sample and the concentrations of K, Rb, Th, and U were analyzed using ICP-MS and ICP-AES at ALS Chemex in Reno, Nevada. Moisture content was determined by weighing samples while moist and again when dry. The dose rate conversion of Guérin et al. (2011), moisture content, and cosmic contribution (Prescott and Hutton, 1994) were used to calculate dose rate to the sediment.

Table 4.1 Quartz OSL and feldspar IRSL information. Quartz OSL samples discussed in detail in the text include USU-910 and USU-1090 from the Lake Hawea moraine and USU-989, USU-990, USU-991, and USU-1242 from the SF Hoh. "SF, Site x" refers to the SF Hoh exposure from which the sample was collected, as explained in Chapter 3. Feldspar IRSL samples include USU-910 and USU-1090 from the Lake Hawea moraine. Ages used in the interpretations of the glacial histories presented in Chapter 2 and Chapter 3 are denoted in bold. Significant overdispersion and positive skew are denoted by an asterisk.

USU Lab number	Material	Location	Facies Unit Type	Grain Size (μm)	OD (%)	Skew	Aliquots Accepted (Run)	Dose rate (Gy/ka)	Equivalent dose, De (Gy)	Method	Age (ka)	CAM/MAM
USU-910	quartz	Hawea	Sh	125-212	27.0 ± 7.6*	0.52 ± 0.51*	23 (47)	2.24 ± 0.11	39.18 ± 6.45	CAM	17.34 ± 3.33	-
	feldspar		p.g.o.		52.7 ± 8.2*	0.98 ± 0.51*	23 (32)	4.10 ± 0.21	72.47 ± 11.16	MAM-3	**25.64 ± 8.39**	-
USU-1090	quartz	Hawea	Sh	150-250	38.0 ± 12.1*	-0.63 ± 0.87	8 (25)	2.50 ± 0.13	48.08 ± 14.83	CAM	19.24 ± 6.08	-
	feldspar		p.g.o.		41.3 ± 12.6*	1.14 ± 0.74*	11 (40)	4.71 ± 0.29	150.81 ± 25.41	MAM-3	**32.42 ± 8.75**	-
USU-989	quartz	SF, Site A	Sh	150-212	36.1 ± 7.1*	0.39 ± 0.49	25 (69)	1.28 ± 0.06	24.53 ± 4.26	CAM	**19.21 ± 3.86**	1.63
			lac						15.03 ± 3.62	MAM-3	11.77 ± 3.07	
USU-990	quartz	SF, Site A	Sfo	150-212	35.0 ± 8.3*	1.10 ± 0.53*	21 (69)	1.18 ± 0.05	25.08 ± 4.81	CAM	**21.30 ± 4.59**	1.58
			lac						15.86 ± 5.83	MAM-3	13.47 ± 5.12	
USU-991	quartz	SF, Site C	Sh	150-212	47.5 ± 8.3*	0.51 ± 0.47*	27 (61)	1.57 ± 0.06	47.28 ± 9.95	CAM	30.14 ± 6.97	2.44
			d.g.o.						19.40 ± 8.15	MAM-3	**12.37 ± 5.33**	
USU-1240	quartz	SF, Site E	Sr	125-250	59.6 ± 16.9*	1.48 ± 0.82*	9 (24)	1.36 ± 0.06	27.20 ± 11.91	CAM	**19.97 ± 8.95**	1.54
			d.g.o.						17.70 ± 4.80	MAM-3	13.00 ± 3.74	
USU-1241	quartz	SF, Site E	Sh	125-250	25.6 ± 7.3*	0.72 ± 0.71*	12 (24)	1.00 ± 0.06	60.24 ± 10.59	CAM	60.24 ± 12.34	1.39
			Dml						43.43 ± 11.12	MAM-3	**43.43 ± 12.02**	
USU-1242	quartz	SF, Site D	Sm	125-250	30.3 ± 6.4*	0.22 ± 0.51	23 (52)	1.02 ± 0.07	72.04 ± 10.98	CAM	70.77 ± 13.21	1.80
			p.g.o.						39.95 ± 15.54	MAM-3	**39.25 ± 15.54**	
USU-1243	quartz	SF, Site C	Sh	125-250	29.1 ± 7.2*	1.31 ± 0.58*	18 (33)	1.12 ± 0.07	20.85 ± 3.56	CAM	**18.59 ± 3.73**	1.35
			p.g.o.						15.70 ± 2.75	MAM-3	14.01 ± 2.86	
USU-1282	quartz	SF, Site G	Sh	90-150	42.3 ± 8.4*	1.50 ± 0.58*	18 (32)	1.80 ± 0.09	40.73 ± 8.95	CAM	**22.65 ± 5.45**	1.70
			p.g.o.						23.90 ± 8.15	MAM-3	13.29 ± 4.72	
USU-1283	quartz	SF, Site I	Sh	125-212	35.3 ± 8.5*	-0.49 ± 0.63	15 (31)	1.08 ± 0.07	39.69 ± 8.38	CAM	36.77 ± 8.71	1.83
			p.g.o.						21.75 ± 9.15	MAM-3	**20.14 ± 8.75**	
USU-1284	quartz	SF, Site J	Sm	150-250	33.4 ± 7.9*	0.23 ± 0.71	12 (24)	1.06 ± 0.06	52.23 ± 10.87	CAM	49.43 ± 11.45	1.66
			p.g.o.						31.50 ± 8.80	MAM-3	**29.81 ± 8.86**	
USU-1285	quartz	SF, Site F	Sm	150-250	45.6 ± 9.7*	1.13 ± 0.59*	17 (36)	1.29 ± 0.07	41.20 ± 10.25	CAM	31.86 ± 8.55	1.68
			d.g.o.						24.46 ± 4.32	MAM-3	**18.91 ± 3.84**	

d.g.o. = ice-distal gravel outwash p.g.o. = ice-proximal glacial outwash

Dml = stratified diamicton lac = lacustrine

2.4. Optical measurements

Risø TL/OSL Model DA-20 readers were used to conduct optical measurements on quartz and feldspar grains following the single-aliquot regenerative protocol (SAR; Murray and Wintle, 2000 for quartz, Wallinga et al., 2000 for feldspar). These measurements were conducted using blue-green (470 ± 30 nm) light emitting diodes (LED) as stimulation. For quartz measurements, the luminescence signal was measured at 36 W/m^2 LED power and 125°C over40 s (250 channels), through 7.5 mm Hoya U-340 filters. A 12 Gy test-dose was administered, and samples were irradiated with ^{90}Sr β-irradiation (0.12 and 0.13 Gy/sec source dose rates). The preheat temperature was 240° for 10 seconds and cutheat temperatures were either 160°C or 220°C for 0 seconds. For USU-989, the SAR sequences were followed by a 280°C high temperature bleach (Wintle and Murray, 2006). Sample purity was checked for all aliquots using infrared stimulation at room temperature.

Due to weak signals, strong medium and slow components, and fast ratios below 20 (Durcan and Duller, 2011) and apparent quartz OSL age underestimates in comparison to other age control, New Zealand samples were analyzed using IRSL. IRSL mesurements and g-value fading rate determinations were performed on the two samples from Lake Hawea, USU-910 and USU-1090. Risø Tl/OSL Model DA-20 readers were used to conduct optical measurements on feldspar grains following the SAR protocol (Wallinga et al., 2000). These measurements were conducted using infrared (870 nm) diodes and the luminescence signal was measured using a 123 W/m^2 IR diode at 50°C over 100 s (250 channels), through Schott BG-39 and Corning 7-59 filters. Samples were preheated at 250°C for 60 s. A 12 Gy test-dose was administered, and samples were irradiated with ^{90}Sr β-irradiation (0.12 and 0.13 Gy/sec source dose rates).

All aliquots were corrected for anomalous fading (Huntley and Lamothe, 2001; Auclair et al., 2003). Anomalous fading refers to the loss of the luminescence signal over time and, if

uncorrected, will results in an age underestimate. The fading rate measurements followed the methods suggested by Huot (2011).

A preheat-plateau test was performed on sample USU-990 to determine the appropriate preheat temperature for this sample (and others from the field area estimated to be of the same approximate age and bedrock source) as suggested by Murray and Wintle (2003) (Figure 4.4). Four small-aliquots (2 mm) were used at each temperature step. Preheat temperatures ranged from 200-300°C in 20°C increments and held for 10 s. Results from this preheat plateau test suggest that a 240°C preheat temperature is appropriate for this sample (Figure 4.4). Preheat –plateau tests and dose-recovery tests will be performed on two of the Olympic Mountains samples. A dose-recovery test will determine if a known applied dose is recovered through the SAR protocol.

2.5. Equivalent dose (De) and error calculation

The SAR method (Murray and Wintle, 2000; Wallinga et al., 2000) on small-aliquots (2 mm diameter, ~50 grains per disk) and either the central age model (CAM) or minimum age model (MAM) (Galbraith et al., 1999) were used to calculate De values on idealy at least 20 accepted aliquots, although due to reporting of preliminary results, fewer aliquots are used in many samples and due to limited material for dating, 11 accepted aliquot for dating were used for USU-1090 IRSL results (Table 4.1). The quartz luminescence signal was calculated by subtracting the mean of the last 5 sec (the background signal) from the first 0.7 sec (or, 4 channels). The IRSL of potassium feldspar was calculated by subtracting the mean of the last 10 sec of the signal from the first 0.8 sec.

Aliquot rejection criteria of OSL data included evidence of feldspar contamination (for quartz samples), a recycling ratio <0.9 or >1.1, a poor dose response growth curve fit,

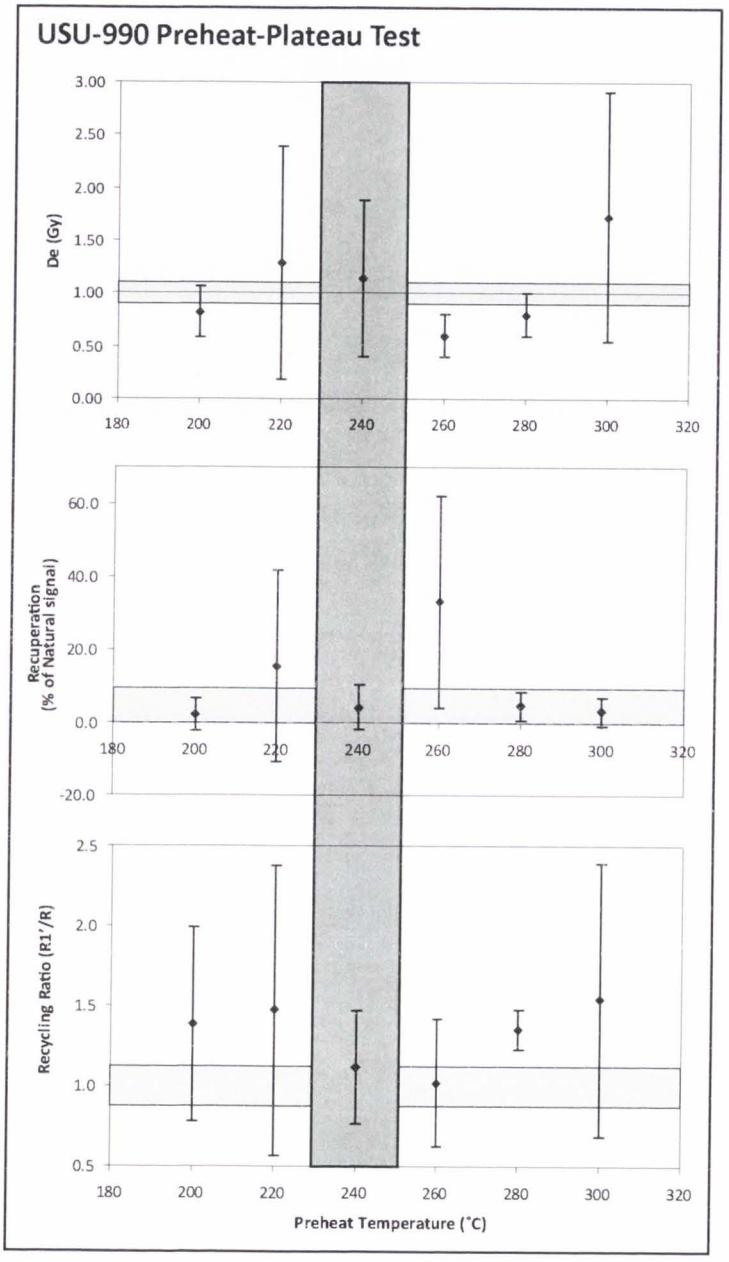

Figure 4.4 Preheat-plateau test results for sample USU-990. Results represent the average of four aliquots for each preheat temperature. Light gray bars represent ±10% error. Dark gray bar represent chosen preheat temperature of 240°C.

recuperation >10% of the natural signal, and/or a natural De greater than the highest regenerative dose give (similar to the rejection criteria discussed in Rittenour et al., 2005). Equivalent dose and age estimate errors are reported at 2-sigma standard error calculated using the methods of Aitken and Alldred (1972) and Aitken (1976, 1985). This considers errors associated with scatter in equivalent dose, dose rate calculations, and instrument calibration.

3. Results

At the writing of this chapter, analysis of many samples has not been completed. The amount of data will steadily increase and will be more thoroughly reported in future publication. This work currently presents the limited preliminary results and interpretations for the samples that have 10 or more aliquots accepted for quartz samples and all feldspar samples (see Table 4.1).

3.1 New Zealand samples

As previously mentioned, the use of quartz for luminescence dating was expected to be a limitation to OSL dating of New Zealand sediments due to low luminescence signals, thermal transfer effects, and sensitivity changes (i.e. Preusser et al., 2006; Rowan et al., 2012). The most noticeable issue with quartz samples of USU-910 and USU-1090 was the weak signal and presence of strong unstable medium decaying components of the signal decay curves (Figure 4.5), which can produce age underestimates due to increased regenerative doses (Steffen et al., 2009). A medium component that dominates the bulk of the luminescence signal may indicate recuperation of the medium component, thermal instability during the SAR protocol (Jain et al., 2003; Li and Li, 2006), or differential sensitization of the fast and medium components (Steffen

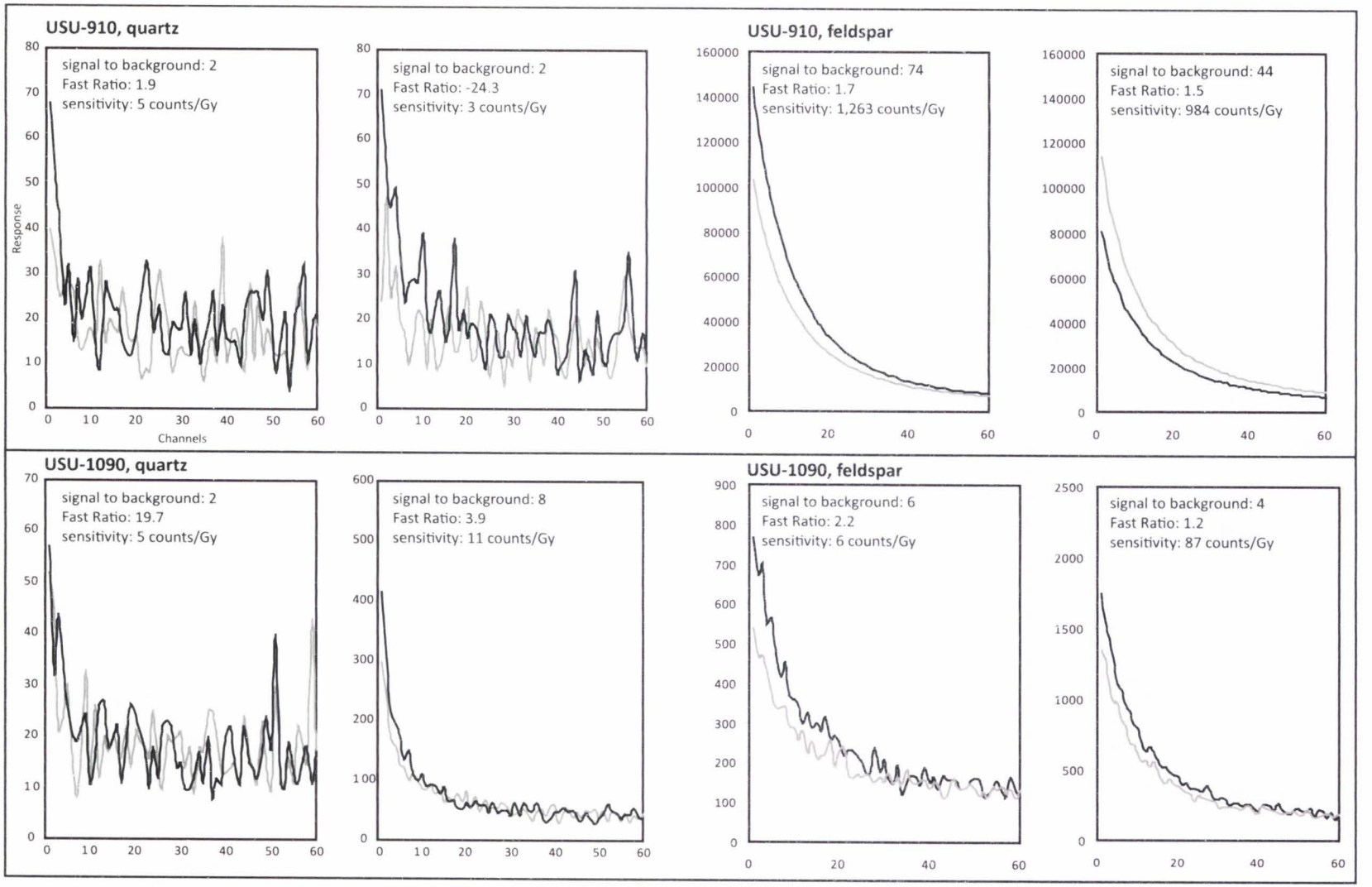

Figure 4.5 Examples of signal decay curves from the two New Zealand quartz and feldspar samples. Black lines shows the natural signal and grey lines show the Regen 2 signal. Note that only the first 60 channels (9.6 seconds) are shown.

et al., 2009). Additionally, the fast ratio is based on measurements of both the fast and medium components (Durcan and Duller, 2011) and provides a rapid test to determine if a sample is dominated by the fast component of the luminescence signal, i.e. providing an easy criterion to add to screening for accepted aliquots. Low fast ratios (all <20%) of the two New Zealand quartz samples therefore suggest a weak fast component. Future tests to define the presence of a dominant medium decay component with include linear modulation OSL (LM-OSL).

These complications with quartz OSL dating of the two Lake Hawea samples prompted the need for feldspar IRSL dating. The IRSL data for both samples produced higher equivalent doses, and therefore ages older, than the quartz OSL data (Figure 4.6). The only complication observed with feldspar samples occurred in sample USU-1090, which showed low signal intensity (Figure 4.5). The average sensitivity of the accepted aliquots of USU-910 when mounted on 2 mm masks was ~462 counts/Gy, whereas USU-1090 had a sensitivity of ~149 counts/Gy for accepted aliquots when mounted on 2 mm masks. The shine-down curves for USU-1090 additionally shows low signal intensity, as many of the counts/second measurements (i.e. response, y-axis) are quite low when compared to USU-910 (Figure 4.5). Problems associated with low feldspar signal intensity of this sample will be mitigated in the future by only using 5 mm masks so that more grains contribute to the overall luminescence signal, however these samples contained a minor fraction of potassium feldspar due to limited sediment available for dating, limiting the use of large aliquots.

IRSL dating produced preliminary ages of 25.6 ± 8.39 ka for USU-910 and 32.4 ± 8.75 ka for USU-1090, which are in stratigraphic order with a TCN sample (17.5 ka; Graham et al., 1998) and a ^{14}C sample (18.2 ka; McKellar, 1960) collected from a younger meltwater channel inset into the Hawea moraine (Table 4.2; Figure 4.7). It is important to note that both IRSL samples were collected from separate sand lenses within the same glacial outwash package, and should

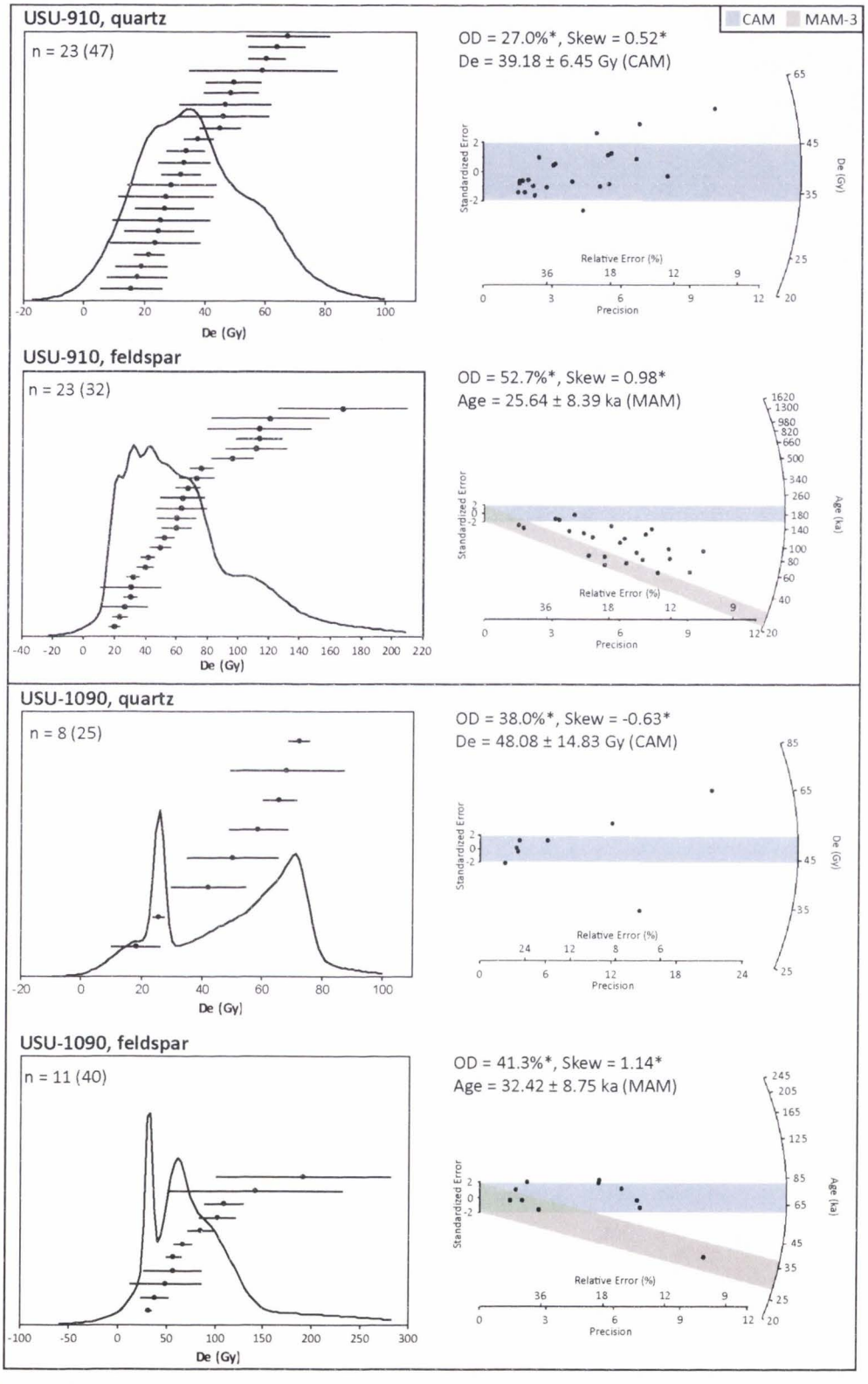

Figure 4.6 Equivalent dose distributions of New Zealand samples for quartz OSL and feldspar IRSL measurements. Significant overdispersion and positive skew are denoted by an asterisk.

Table 4.2 Radiocarbon and cosmogenic nuclide age constraint for Lake Hawea and SF Hoh study areas.

Sample ID	Site	Unit	Sample	Material	14C Calibration	14C Age	$\delta^{13}C$	Age (ka) ± 2σ	Study
S. 115/500, R36.	Hawea	-	radiocarbon	peat	IntCal09	15,100 ± 200	-25*	17.8-18.7	McKellar, 1960
-	Hawea	-	10Be SED	quartz	-	-	-	**17.5**	Graham et al., 1998
AA-18406	A	2	radiocarbon	wood	IntCal09	19,169 ± 162	-26	22.4-23.4	Thackray, 2001
AA-18407	A	2	radiocarbon	wood	IntCal09	19,324 ± 165	-26.7	22.5-23.5	Thackray, 2001
AA-18408	A	2	radiocarbon	wood	IntCal09	19,274 ± 154	-27.1	22.5-23.5	Thackray, 2001
CAMS#156404	A	4	radiocarbon	plant	IntCal09	16,210 ± 60	-25*	19.2-19.6	this study
CAMS#159920	A	4	radiocarbon	beetle	IntCal09	15,520 ± 160	-25*	18.5-19.0	this study
AA-18405	D	0	radiocarbon	wood	IntCal09	19,067 ± 329	-29.8	22.0-23.7	Thackray, 2001
AA-16700	**	**	radiocarbon	wood	IntCal09	18,274 ± 195	-25	21.4-22.3	Thackray, 2001
CAMS#159911	F	1	radiocarbon	wood	IntCal09	18,130 ± 70	-25*	21.4-22.1	this study
CAMS#159912	F	1	radiocarbon	wood	IntCal09	18,090 ± 60	-25*	21.3-22.0	this study
CAMS#159913	G	2	radiocarbon	wood	IntCal09	16,940 ± 60	-25*	19.9-20.4	this study

* assumed δ13C value

** across the river from Site D (Thackray, 2001)

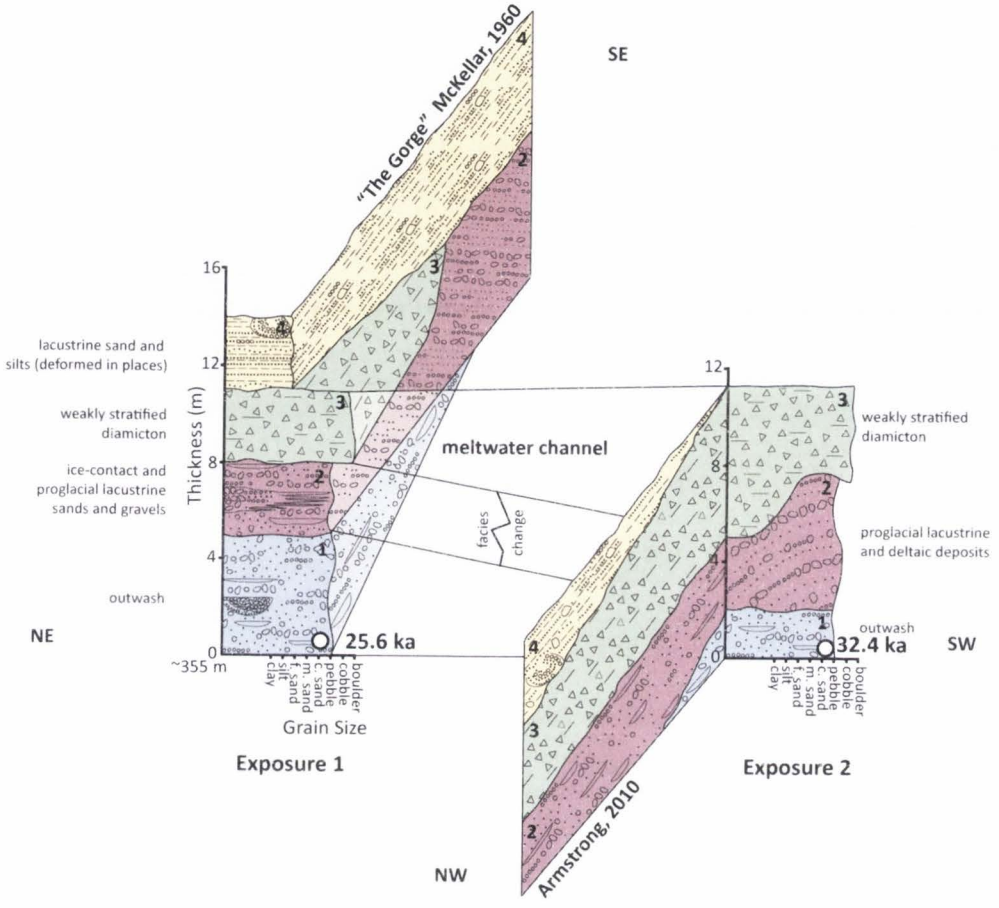

Figure 4.7 Stratigraphic columns representative of stratigraphy of the Hawea moraine. Tie lines show relationships between units of these two exposures. Open circles and associated ages show OSL sample locations. The triangle shows the ^{14}C sample presented by McKellar (1960), and the filled circle shows the TCN sample presented by Graham et al. (1998), although the exact locations of these samples in relation to the Hawea moraine stratigraphy is unknown. These samples were likely collected from an outlet channel inset into the moraine and younger material.

therefore yield the similar ages (Figure 4.7). These ages are indistinguishable considering error, and therefore provide a broad constraint on sediment age.

3.2 Olympic Mountains samples

More samples were collected from the SF Hoh in the Olympic Mountains than from Lake Hawea, New Zealand. Additionally, more external age control (^{14}C dating) exists in the drainage for comparison to OSL age estimates, although some of these may be reworked samples that provide maximum age constraints on deposition (Table 4.2). Nonetheless, the number of samples collected for OSL dating and other age constraint allow for more thorough analysis of luminescence signals and subsequent age results. Eleven samples total were collected fromexposures in the SF Hoh. One sample was collected from horizontally bedded sand (Sh) in diamicton (Dml) (USU-1241 Site E), two samples from massive sand (Sm) in proximal outwash (USU-1242 Site D and USU-1284 Site J), three samples from horizontally bedded sand (Sh) in proximal outwash (USU-1243 Site C, USU-1282 Site G, and USU-1283 Site I), one sample from massive sand (Sm) in distal outwash (USU-1285 Site F), one sample of ripple cross-bedded sand (Sr) in distal outwash (USU-1240 Site E), one sample of horizontally bedded sand (Sh) in distal outwash (USU-991 Site C), one sample from delta foresets (Sfo) in lacustrine sediment (USU-990 Site A), and one sample from horizontally bedded sand (Sh) in lacustrine sediment (USU-989 Site A).

The partial resetting (or "zeroing" or "bleaching") of the luminescence signal is the greatest concern for OSL dating of sediments deposited in glacial environments. Results from both a central age model (CAM) and a minimum age model (3-parameter MAM) are presented for all samples from the Olympic Mountains. Whereas the CAM produces a weighted mean of the De results, the MAM statistically selects those aliquots that were most likely sufficiently bleached

based on younger populations of equivalent doses (Galbraith et al., 1999). Figures 4.8-4.10 show the equivalent dose distributions for the South Fork Hoh River valley OSL samples, and radial plots show both CAM and MAM data. All samples show significant (>25%) overdispersion and many equivalent dose dispersions have positive skews (Table 4.1).

Several samples were collected from exposures with external age control. Sample USU-989 (19.2 ± 3.86 ka) and USU-990 (21.3 ± 4.59 ka) (Site A) were collected from the same exposure (Site A) and preliminary results are in stratigraphic order within error (Figure 4.11). These OSL samples are also in agreement with ^{14}C samples collected from the same exposure. Three samples from the same unit as USU-989 produce a mean calibrated ^{14}C age of 23.0 ka. Two ^{14}C samples collected from one fine bed in an upper unit of the exposure are 19.4 and 18.8 ka. Sample USU-1242 (39.2 ± 15.54 ka, Site D) is not in stratigraphic order with a ^{14}C sample (22.9 ka) collected from the now covered base of the exposure (Site D) (Figure 4.11). The significantly older preliminary OSL age of this sample suggests that the luminescence signal was not fully reset. Sample USU-1285 (18.9 ± 3.84 ka, Site F) was collected stratigraphically below two ^{14}C samples from the same exposure (Site F) (Figure 4.11). The resulting preliminary ages are in stratigraphic order within error (18.9 ka and 21.7-21.8 ka). Sample USU-1282 (22.7 ± 5.45 ka, Site G) was collected from the same bed as a ^{14}C sample (20.2), and the ages are indistinguishable within error.

Two exposures contained multiple OSL samples. Sample USU-991 and USU-1243 were collected from Site C (Figure 4.11). The preliminary ages are in stratigraphic order, 12.4 ± 5.33 ka and 18.6 ± 3.73 ka, respectively; however both samples show evidence of partial bleaching in their significantly high overdispersion values and positive skew (Table 4.1). The samples at Site E, USU-1240 (20.0 ka ± 8.95) and USU-1241 (43.4 ± 12.02 ka), are also in stratigraphic order (Figure 4.9), however the significant overdispersion and positive skew of both samples suggest

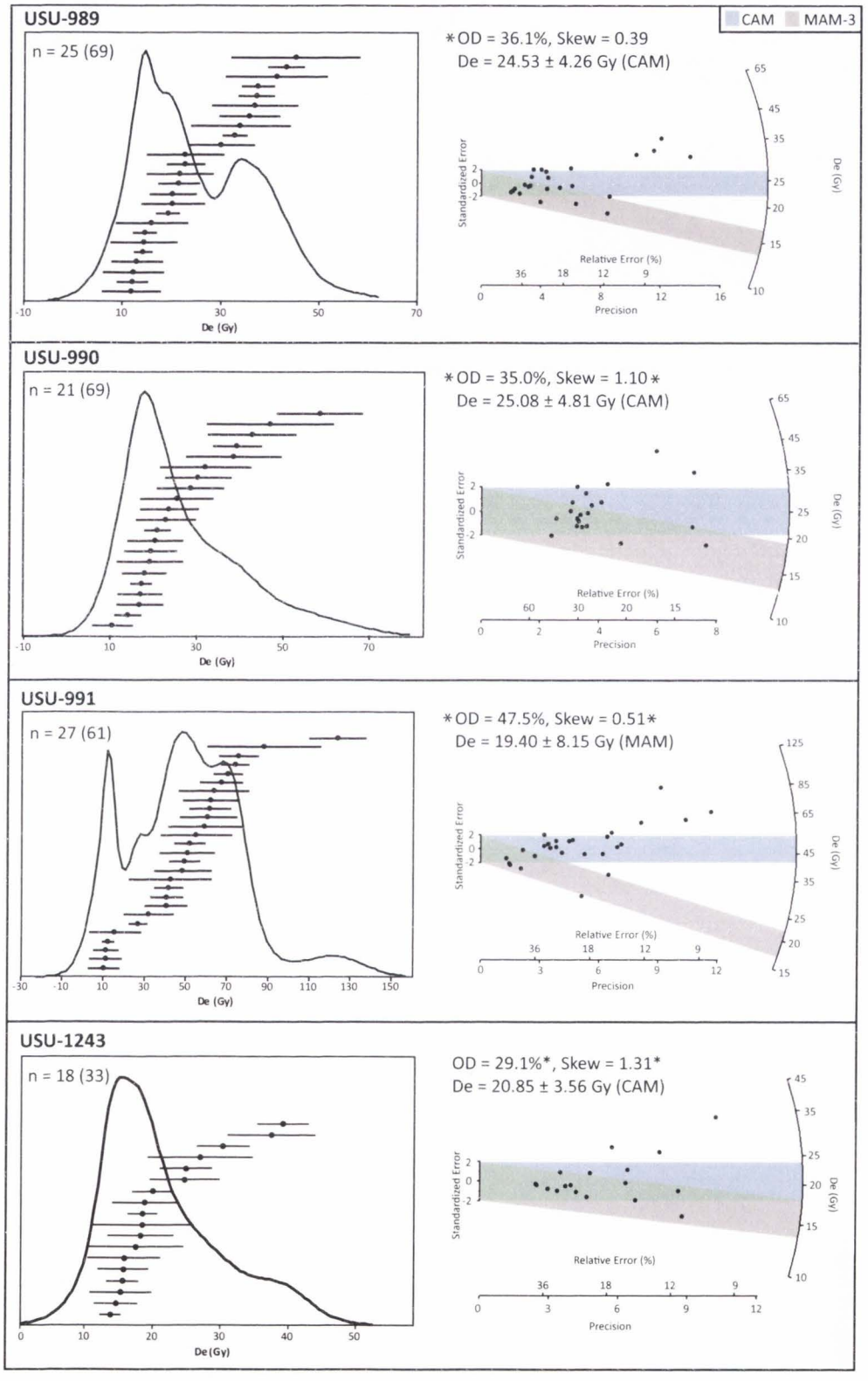

Figure 4.8 Equivalent dose distributions of SF Hoh samples USU-989, USU-990, USU-991, and USU-1243. Significant overdispersion and positive skew are denoted by an asterisk.

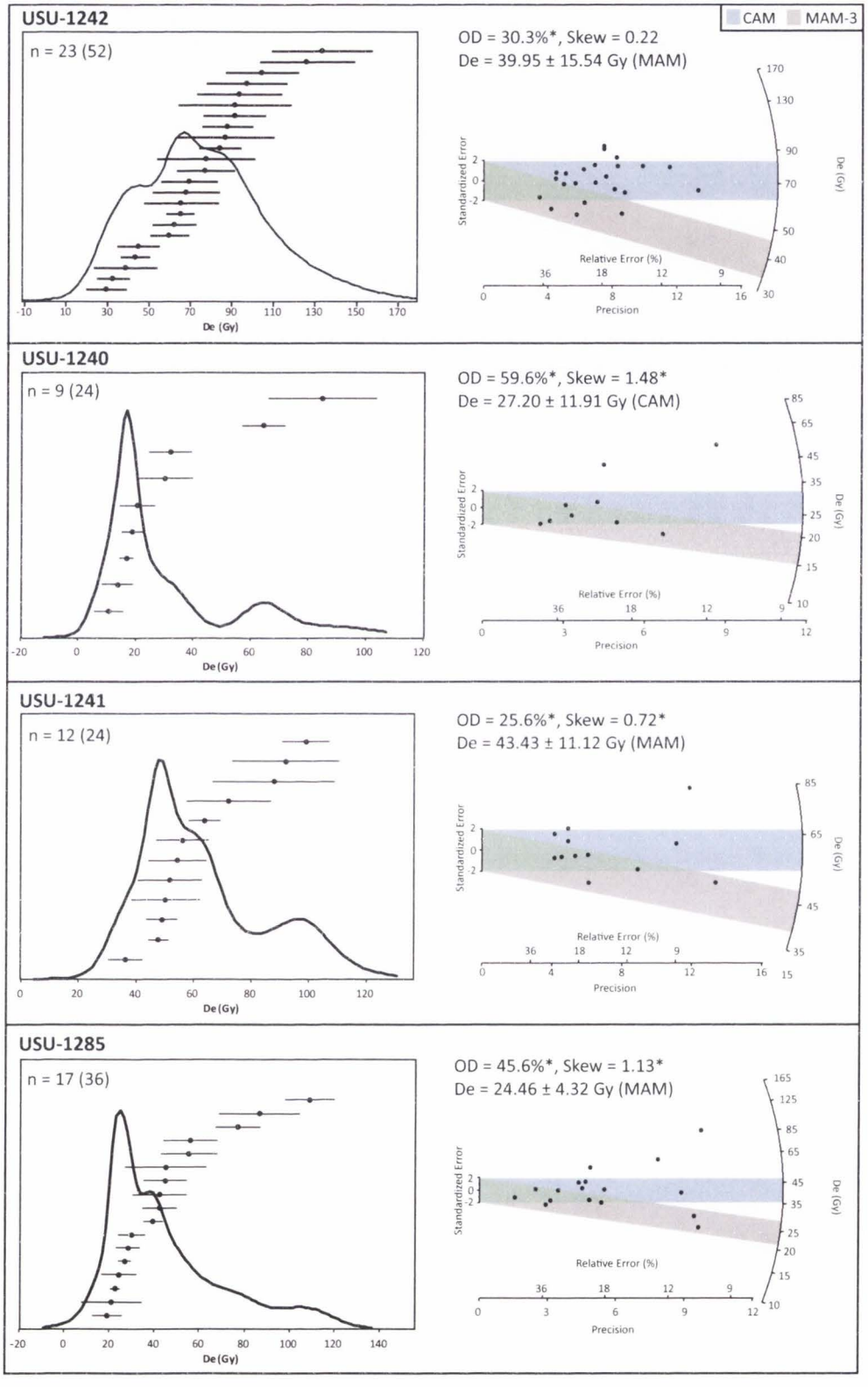

Figure 4.9 Equivalent dose distributions of SF Hoh samples USU-1242, USU-1240, USU-1241, and USU-1285. Significant overdispersion and positive skew are denoted by an asterisk.

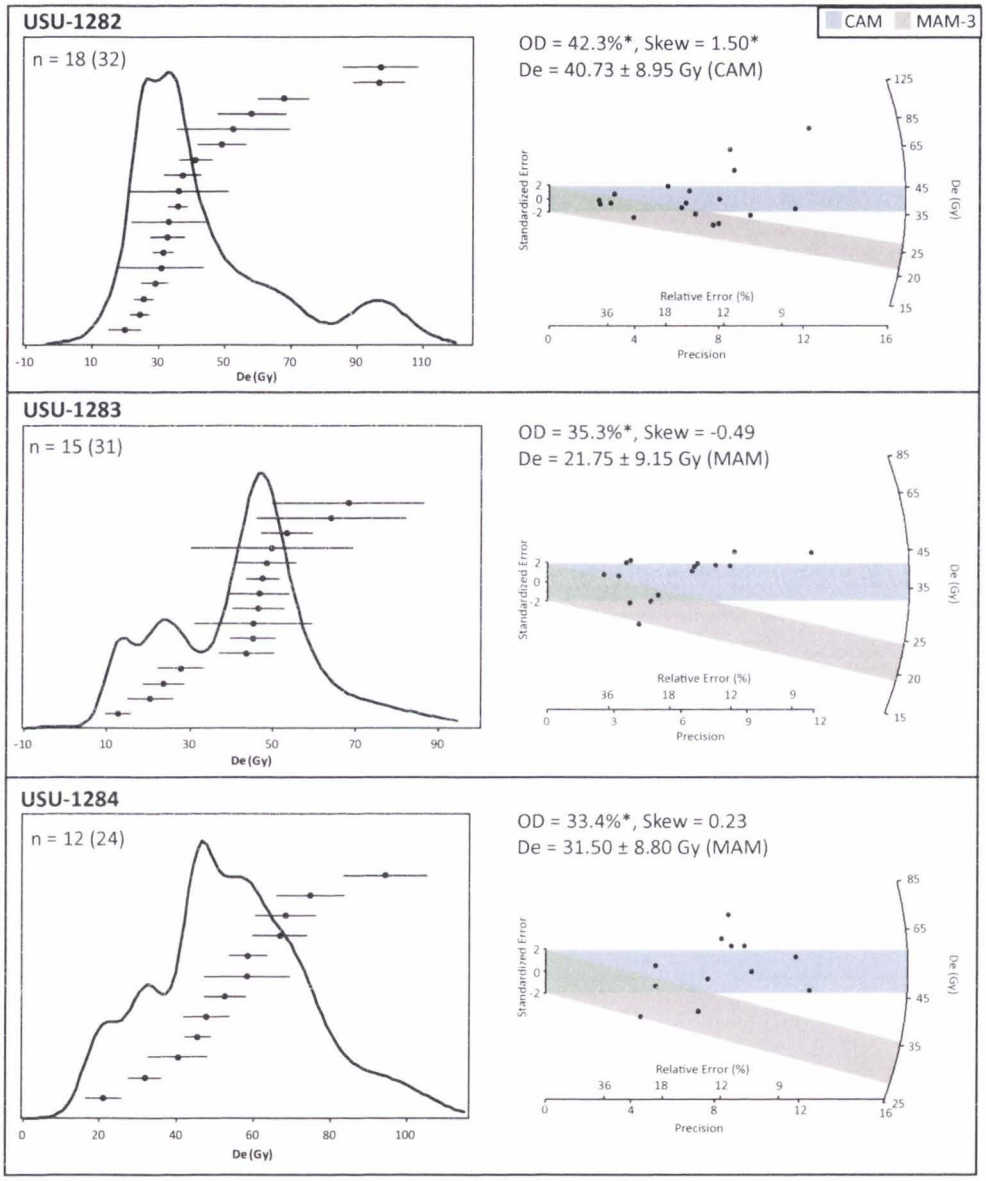

Figure 4.10 Equivalent dose distributions of SF Hoh samples USU-1282, USU-1283, and USU-1284. Significant overdispersion and positive skew are denoted by an asterisk.

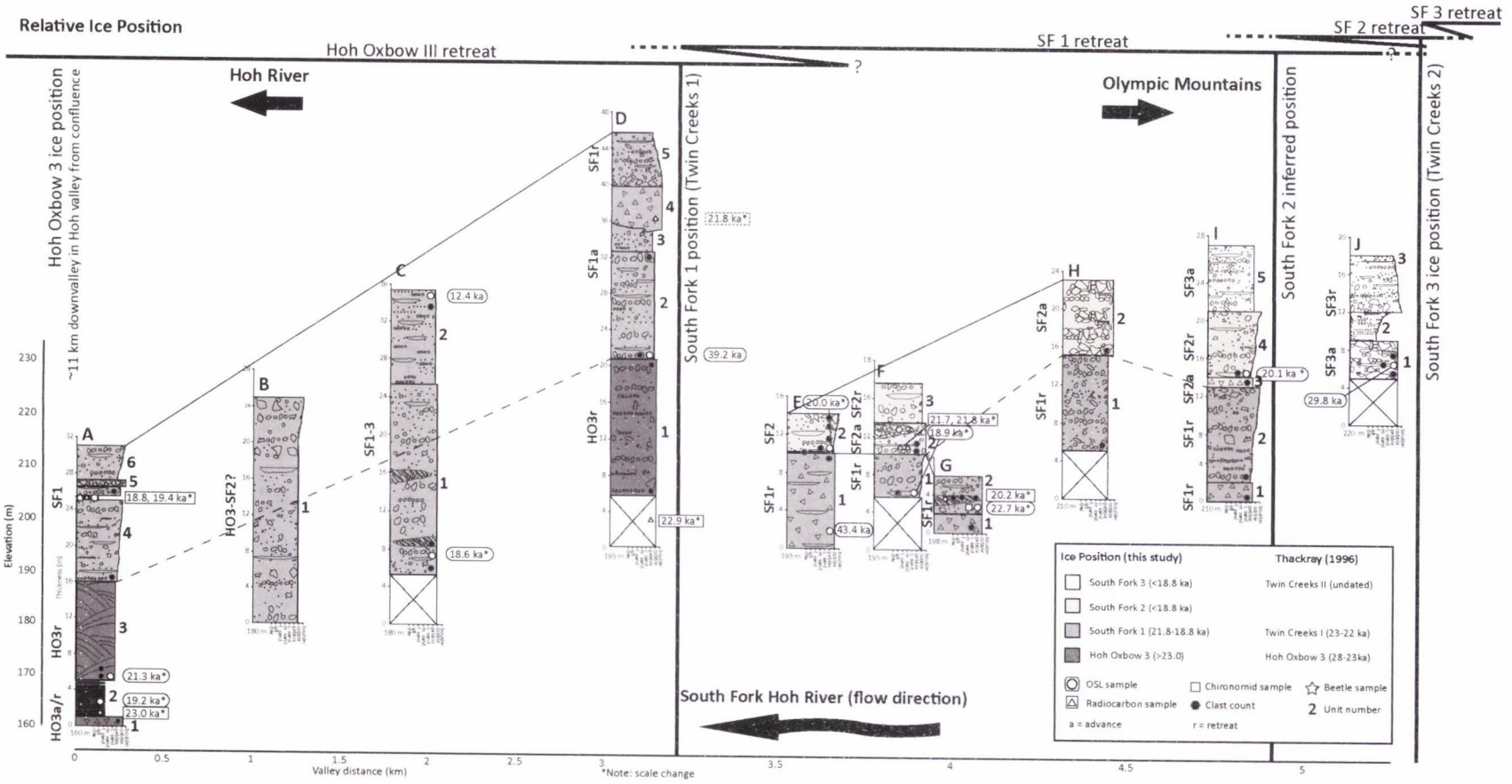

Figure 4.11 Stratigraphic columns representative of stratigraphy of all ten SF Hoh River valley exposures. Ages considered somewhat reliable and used for interpretation of the glacial history are denoted with '*' (see Chapter 3).The base of each site is represented here at the elevation of the river at each site. Each individual stratigraphic column also shows thickness on the y-axis. The color designation refers to the favored interpretation for correlation to each ice position. The upper lines depict the history of ice positions, between Hoh Oxbow 3 retreat and the SF3 ice position.

that the luminescence signals may not have been fully reset prior to deposition (Table 4.1).

Sample USU-1283 (Site I, Figure 4.11) and sample USU-1284 (Site J, Figure 4.11) provide the only age constraint on the two exposures. Both samples have high overdispersion and minimal positive skew (Table 4.1).

4. Discussion

4.1 New Zealand quartz

IRSL ages presented here are broadly consistent with interpretations of the glacial history of the Lake Hawea valley, discussed in Chapter 2. The glacial outwash package that was sampled was deposited during the retreat from the Mt. Iron, the second to last ice position prior to terminal deglaciation of the valley. Age control on the timing of ice retreat from the Hawea moraine comes from a ~18 ka radiocarbon age from sediment in a meltwater channel (McKellar, 1960) and ~17.5 ka TCN age from scoured bedrock in a meltwater channel (Graham et al., 1998). These ages provide a minimum constrain on retreat from the Hawea position, formation of Lake Hawea, and establishment of the current lake outlet. These ages are in stratigraphic agreement with the IRSL ages (25.6 ± 8.39 ka and 32.4 ± 8.75 ka) of sediment deposited during retreat from an older ice position.

Previous work (namely Preusser et al., 2006) has cautioned others from attempting OSL dating of quartz sediments from the Southern Alps. The data and results presented here echo concerns with quartz luminescence properties in the Hawea area, specifically by emphasizing a strong medium signal component that yields age underestimates. Although the exact cause of this medium component merits further attention and research, several possibilities exist. These include potential thermal instability and insufficient sensitization of quartz grains, both discussed by Preusser et al. (2006). This could reflect the possible influence of local bedrock

type. Quartz OSL samples from the Rangitata River and Rakaia River drainages to the north of Lake Hawea and on the eastern side of the Southern Alps seem to produce good luminescence signals and ages (Rowan et al., 2012; Rittenour,, 2013, personal communication). Nonetheless, the results presented here advocate for feldspar IRSL dating of sediments derived from the Southern Alps of New Zealand.

4.2 Applicability of OSL dating to glacial depositional facies

The data from different depositional settings of the Olympic Mountains merits discussion of the relationships between De distributions, OSL ages, and facies. All samples show high overdispersion (>25%) of De with varying degrees of skew of De distribution (-0.49-1.50) (Table 4.1; Figure 4.12). High over dispersion of sediments deposited in glacial environments can be expected due to the variability of bleaching associated with sediment transport processes. These high values may also suggest variable luminescence properties of the grains, arising from grains that have not yet been sensitized due to relatively recent erosion from bedrock.

Samples in stratigraphic order with each other and/or ^{14}C sample ages suggest high overdispersion may not be an indication of poor luminescence signals in this environment. The two samples collected from glaciolacustrine depositional settings (USU-989 and 990) were collected from the same exposure (Site A, Figure 4.11) and what is interpreted to represent a prograding shoreline of a locally ponded water body. USU-989 was collected from a sand bed in a package of alternating silt and sand beds, and USU-990 was collected from a sandy-pebbly delta facies. Although these two samples appear to be out of stratigraphic order, there is no reason to believe that this is due to major complications in the OSL dating. The samples are still indistinguishable, i.e. within error of each other, and are in stratigraphic order with three

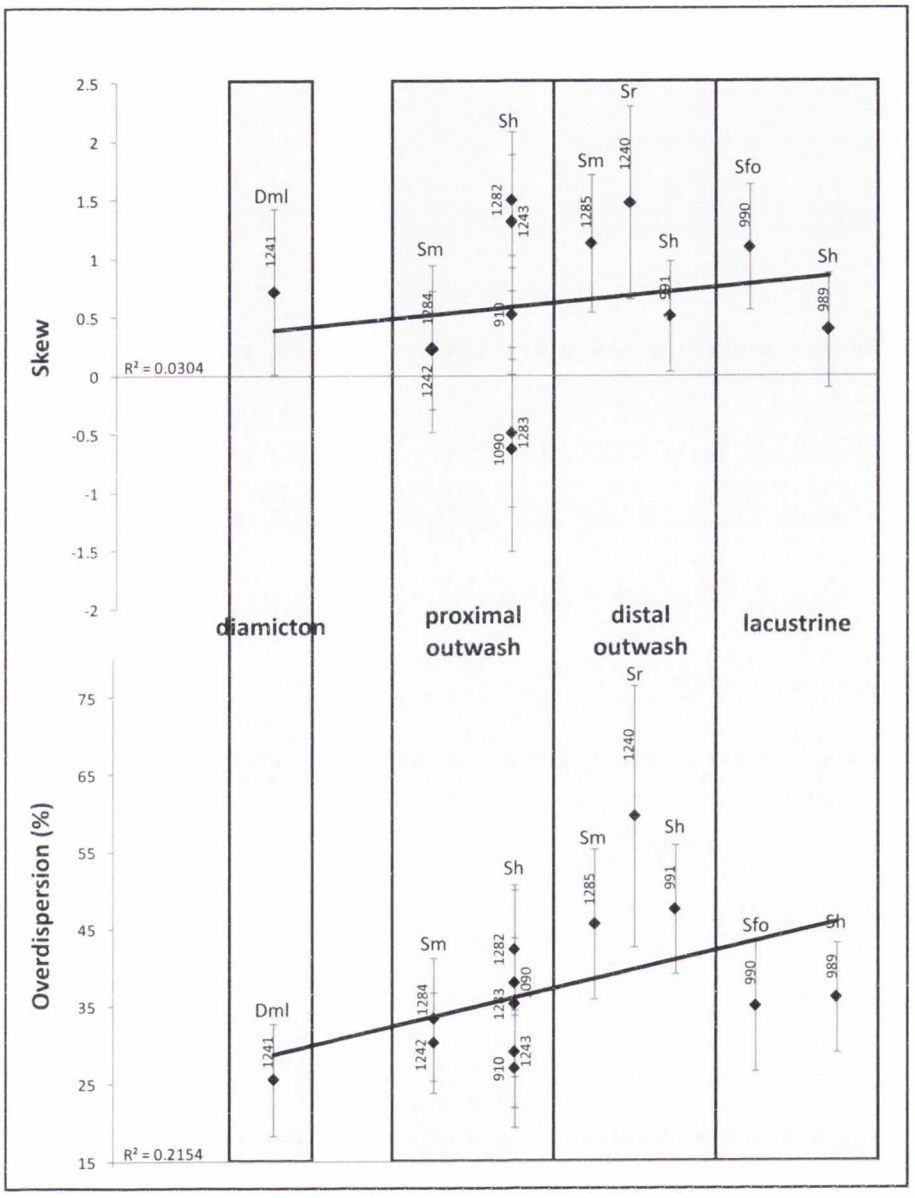

Figure 4.12 Plots of skew and overdispersion values in relation to depositional environment. All quartz OSL samples from New Zealand and the Olympic Mountains are plotted and indicated by sample number. Facies are also labeled.

radiocarbon samples collected from the same unit as USU-989 (~23 ka) and two radiocarbon samples collected from higher in sequence (18.8 ka and 19.4 ka). Additionally, these ages are consistent with interpretations of the glacial history of the valley presented in Chapter 3, which place these packages into a period of retreat from the Hoh Oxbow 3 ice position and advance to the SF1 position.

As mentioned, USU-991 (12.4 ± 5.33 ka) and USU-1242 (18.6 ± 15.54 ka) (Site C) were collected from gravelly outwash packages (Gh) with sand lenses (Sh) (Figure 4.11). No other age control was obtained from this exposure; however, the ages of these two OSL samples are consistent with stratigraphic order. These units are interpreted to represent deposition during advance to the SF 1 ice position (lower) and retreat from this position (upper) (Chapter 3). Due to poor age constraint of surrounding packages and in other exposures, however, this package can only be more definitively interpreted as having been deposited sometime during SF 1-3.

Samples USU-1240 (20.0 ± 8.95 ka) and USU-1241 (43.4 ± 12.02 ka) (Site E) were collected from different units of the same exposure and are in stratigraphic order. Sample USU-1240 is consistent with the interpretation that this outwash package was deposited during retreat from the SF 2 ice position, as discussed in Chapter 3. The significantly older age of sample USU-1241, however, suggests partial bleaching of this sediment. This sample was collected from a sand lens in a stratified diamicton, and its partial bleaching may therefore be expected due to ice-proximal deposition with only moderate water reworking. The turbid, sediment rich ice proximal environment and short transport distance interpreted to represent this unit do not favor exposure to sunlight.

Samples USU-1285 (18.9 ± 3.84 ka, Site F) and USU-1282 (22.7 ± 5.45 ka, Site G), although from different exposures, were both collected from outwash and are interpreted to represent retreat from the SF 1 ice position, as discussed in Chapter 3. These ages agree, within

error, and therefore suggest robust OSL data. Radiocarbon sample ages further support the accuracy of these OSL ages. Two radiocarbon samples collected above USU-1285 produce ages of 21.7 ka and 21.8 ka. These ages are indistinguishable within error from the OSL age collected lower in the stratigraphy. A ^{14}C sample collected from the same bed as USU-1282 is 20.2 ka, which is within error of the OSL age (22.7 ± 5.45 ka).

Independent age control is lacking for some of the exposures studied in the SF Hoh, however the stratigraphy of the exposures and surrounding sites can be used to interpret OSL results. Sample USU-1283 was collected from outwash overlying diamicton in Site I. The preliminary 20.1 ± 8.75 ka age is consistent with the interpretation that this outwash was deposited during retreat from the SF 2 ice position, as presented in Chapter 3 and suggests that this sample is producing an accurate age estimate. Sample USU-1284 (29.8 ± 8.86 ka) was collected from outwash at the base of Site J. The position of this site and its stratigraphy suggest that this outwash was deposited during advance to the SF 3 position. The preliminary OSL sample age, however, is too old to support this interpretation despite the use of the MAM-3 model, suggesting that the luminescence signal was not reset prior to deposition. This could have been expected due to its proximity to the ice margin and the presence of many large boulders in the deposit suggesting a relatively high energy deposition in a turbid environment capable of transporting high sediment loads. Alternatively, the age could accurately reflect the deposition of an older unit preserved in the valley. This explanation, however, is unlikely given the elevation of the deposit, its location furthest up-valley, and the interpreted glacial history.

Sample USU-1242 (39.2 ± 15.54 ka), collected from a glacial outwash unit at Site D, also is older than expected, as suggested foremost by its position in the stratigraphy. The preliminary age of this sample (39.2 ± 15.54 ka) is not in stratigraphic order with a ^{14}C sample, collected from a lower unit that provides a maximum age estimate of 22.9 ka. This ^{14}C age suggests that

this outwash package may be contemporaneous with the glaciolacustrine sediment from which USU-989 and USU-990 (Site A) were collected and may represent the up-valley fluvial system feeding into the lake and deltaic system. The high overdispersion (30.3%) and slightly positive skew (0.22) suggest that partial bleaching may be producing the older than expected age. The MAM-3 model was therefore used to calculate the most accurate equivalent doses and optical age for USU-1242.

These results suggest that the transport mechanisms and depositional environments associated with different facies are important in bleaching the luminescence signal prior to deposition (Figure 4.12). The sedimentary packages interpreted to have been deposited more distally from the ice front produced more reliable OSL ages, as expected. The glaciolacustrine sediments of USU-989 and USU-990 (Site A) were likely deposited in an aqueous environment with a high sediment load, as indicated by thick clay drapes over sandy layers of the glaciolacustrine sediment and the thickness of the overlying prograding delta foresets. The time of suspension in the water column before deposition may have increased the likelihood of sufficient solar resetting. Conversely, thick clay beds suggest a very turbid environment that would limit bleaching. The other ice-distal sediments were collected from a horizontally bedded sand lens (USU-991, Site C), a ripple cross-bedded sand bed (USU-1240, Site E), and a massive sand lens (USU-1285, Site F) in glacial outwash packages. More ice-proximal sediments that produced good OSL ages were deposited in horizontally bedded sand lenses within glacial outwash (USU-1243 Site C and USU-1282 Site G). These samples both produce age results consistent with stratigraphy, external age control, and/or the interpreted glacial history of the valley. These results suggest that longer transport distances and sandy facies deposited in lower energy environments with better sorting (i.e. horizontally bedded and ripple cross-bedded sand)

may expose sediment to more sunlight prior to deposition, enhancing the potential to reset the luminescence signals.

Conversely, some of the samples collected from ice-proximal environments produce apparently unreliable OSL ages (Figure 4.12). As previously discussed, the diamicton depositional environment (USU-1241, Site E) is not likely to expose sediment to sufficient sunlight to bleach sediments sufficiently. Samples USU-1242 (Site D) and USU-1284 (Site J) were collected from massive sand lenses within gravel outwash, which may have not allowed for sufficient bleaching due to the turbid transport and depositional environment associated with glacial outwash systems and/or the rapid deposition represented by the lack of depositional structures in the sand lens. These results echo suggestion of a lithofacies-based approach to OSL sampling, presented by Thrasher et al. (2009), which may identify sediments with increased bleaching potential.

The previously describe lithofacies-based approach seems to contradict the trends of skew and overdispersion with facies and interpreted relative distances from the ice front displayed on Figure 4.12. This figure shows that overdispersion and skew both increase somewhat from proximal to distal settings. Most notably, the diamicton sample (USU-1241, Site E) exhibits the lowest overdispersion of equivalent doses, which typically suggests a more precise age and less partial bleaching. As previously explained, however, this sample produces an age overestimate, likely due to partial resetting of the luminescence signal. A potential explanation is that the sediment was once well-bleached, then transported again and redeposited with little to no bleaching in the diamicton environment. Conversely, this sediment could be accurately dated, older sediment deposited during an earlier ice advance, although this contradicts the interpreted glacial history and stratigraphy throughout the valley.

Nevertheless, the ages that agree best with the stratigraphy, external age control, and interpreted glacial history support the previous interpretations relating facies in ice-proximal and ice-distal environments to higher luminescence dating potential.

5. Conclusions

Similar to Preusser et al. (2006), limitations to small-aliquot OSL dating of quartz sediments from the Southern Alps, New Zealand were encountered. These limitations were manifested in age underestimates, and although the cause has not been pinpointed, these underestimates could be attributed to a strong medium luminescence signal component due to thermal instability and insufficient sensitization of the quartz grains. Potassium feldspar IRSL analyzes encountered minimal complications. This research therefore cautions others from OSL dating of Pleistocene glacial sediments derived from the Hawea drainage, although this may be bedrock provence specific, and instead advocates for IRSL as a better method of chronologic constraint on these sediments.

Preliminary results from the Olympic Mountains suggest that bleaching potential of these glacial sediments is influenced by facies and depositional environment. The results advocate for a facies approach to OSL sampling of glacial sediments to obtain sediments that have been sufficiently bleached to reset the luminescence signal before deposition. This study suggests that lacustrine, horizontally-bedded sand, and ripple-crossbedded sand facies may be better to sample than massive sand and diamicton facies. Although complications do exist, this study also shows that there is good promise in OSL dating of glacial sediments if transport, depositional environments, and facies are considered.

References Cited

Aitken, M.J., 1976. Thermoluminescent age evaluation and assessment of error limits: revised system. Archaeometry 18, 233-238.

Aitken, M.J., 1985. Thermoluminescence Dating. Academic Press, New York.

Aitken, M. J., 1998. An Introduction to Optical Dating: The Dating of Quaternary Sediments by the Use of Photon-stimulated Luminescence. Oxford University Press, Oxford.

Aitken, M.J., Alldred, J.C., 1972. The assessment of error limits in thermoluminescent dating. Archaeometry 14, 257-267.

Alexanderson, H., 2007. Residual OSL signals from modern Greenlandic river sediments. Geochronometria 26, 1-9.

Alexanderson, H., Murray, A. S., 2012. Luminescence signals from modern sediments in a glaciated bay, NW Svalbard. Quaternary Geochronology 10:250-256.

Auclair, M., Lamothe, M., Huot, S., 2003. Measurement of anomalous fading for feldspar IRSL using SAR. Radiation Measurements 37, 487-492.

Berger, G. W. , Doran, P. T., 2001. Luminescence-dating zeroing tests in Lake Hoare, Taylor Valley, Antarctica. Journal of Paleolimnology 25, 519–529.

Brandon, M. T., 2004, The Cascadia subduction wedge: the role of accretion, uplift, and erosion. In: van der Pluijm, B. A., Marshak, S. (Eds.), 2004, Earth Structure: An Introduction to Structural Geology and Tectonics, 2nd Edition. WCB/McGraw Hill Press, New York, pp. 566-574.

Clark, P. U., Dyke, A. S., Shakun, J. D., Carlson, A. E., Clark, J., Wohlfarth, B., Mitrovica, J. X., Hostetler, S. W., McCabe, A. M., 2009. The Last Glacial Maximum. Science 325(5941), 710-714.

Duller, G. A. T., Wintle, A. G., Hall, A. M., 1995. Luminescence dating and its application to key pre-Late Devensian sites in Scotland. Quaternary Science Reviews 14, 495–519.

Durcan, J. A., Duller, G. A. T., 2011. The fast ratio: a rapid measure for testing the dominance of the fast component in the initial OSL signal from quartz. Radiation Measurements 46, 1065-1072.

Galbraith, R. F., Roberts, R. G., Laslett, G. M., Yoshida, H., Olley, J. M., 1999. Optical dating of single and multiple grains of quartz from Jinmium rock shelter, northern Australia: Part I, experimental design and statistical models. Archaeometry 41, 339-364.

Gemmel, A. M. D., 1999. IRSL from fine-grained glacifluvial sediment. Quaternary Science Reviews 18(2), 207-215.

Gemmell, A. M. D., Murray, A. S., Connell, E. R., 2007. Devensian glacial events in Buchan (NE Scotland): a progress report on new OSL dates and their implications. Quaternary Geochronology 2, 237–242.

Graham, I.J., Kim, K., McSaveney M.J., Zondervan, A., Webb, P., 1998. Establishment of surface exposure dating methods using ^{10}Be and ^{26}Al at GNS. Institute of Geological and Nuclear Science science report 98/30. Lower Hutt, New Zealand.

Guérin, G., Mercier, N., Adamiec, G., 2011. Dose-rate conversion factors: update. Ancient TL 29, 5-8.

Hormes, A., Preusser, F., Denton, G., Hajdas, I., Weiss, F., Stocker, T. F., Schlüchter, C., 2003. Radiocarbon and luminescence dating of overbank deposits in outwash sediments of the Last Glacial Maximum in North Westland, New Zealand. New Zealand Journal of Geology and Geophysics 46(1), 95-106.

Huntley, D. J., Godfrey-Smith, D. I., Thewalt, M. L. W., 1985, Optical dating of sediments. Nature 313, 105-107.

Huntley, D. J., Lamothe, M., 2001. Ubiquity of anomalous fading in K-feldspars and the measurement and correction for it in optical dating. Canadian Journal of Earth Science 38, 1093-1106.

Huot, S., 2011. A Recipe Book for Fading. Unpublished.

Jeong, G. Y., Choi, J.-H., 2012. Variations in quartz OSL components with lithology, weathering and transportation. Quaternary Geochronology 10, 320-326.

Klasen, N., Fiebig, M., Preusser, F., Reitner, J., Radtke, U., 2007. Luminescence dating of proglacial sediments from the Eastern Alps, Quaternary International 164-165, 21-32.

Lamothe, M., Balescu, S., Auclair, M., 1994. Natural IRSL intensities and apparent luminescence ages of single feldspar grains extracted from partially bleached sediments. Radiation Measurements 23, 555–561.

Lukas, S., Spencer, J. Q. G., Robinson, R. A. J., Benn, D. I., 2007. Problems associated with luminescence dating of Late Quaternary glacial sediments in the NW Scottish Highlands, Quaternary Geochronology 2, 243-248.

Marshall, K. J., 2013. Expanded late Pleistocene glacial chronology for western Washington, U.S.A. and the Wanaka-Hawea Basin, New Zealand, using luminescence dating of glaciofluvial outwash. M.S. thesis, Idaho State University, Pocatello.

McKellar, I. C., 1960. Pleistocene deposits of the upper Clutha valley, Otago, New Zealand. Journal of Geology and Geophysics 3, 432-460.

Moska, P., Murray, A. S., 2006. Stability of the quart fast-component in insensitive samples. Radiation Measurements 41, 878-885.

Murray, A. S., Wintle, A. G., 2000. Luminescence dating of quartz using an improved single-aliquot regenerative-dose protocol, Radiation Measurements 32, 57-73.
Murray, A. S., Wintle, A. G., 2003. The single aliquot regenerative dose protocol: potential for improvements in reliability, Radiation Measurements 37, 377-381.

Owen, L.A., Kamp, U., Spencer, J. Q., Haserodt, K., 2002. Timing and style of Late Quaternary glaciation in the eastern Hindu Kush Chitral, northern Pakistan: a review and revision of the glacial chronology based on new optically stimulated luminescence dating. Quaternary International 97-98, 41-55.

Pietsch, T. J., Olley, J. M., Nanson, G. C., 2008. Fluvial transport as a natural luminescence sensitizer of quartz. Quaternary Geochronology 3, 365-376.

Preusser, F., Ramseyer, K., Schlüchter, C., 2006. Characterisation of low OSL intensity quartz from the New Zealand Alps. Radiation Measurements 41, 871-877.

Rowan, A. V., Roberts, H. M., Jones, M. A., Duller, G. A. T., Covey-Crump, S. J., Brocklehurst, S. H., 2012. Optically stimulated luminescence dating of glaciofluvial sediments on the Canterbury Plains, South Island, New Zealand. Quaternary Geochronology 8, 10-22.

Sawakuchi, A. O., Blair, M. W., DeWitt, R., Faleiros, F. M., Hyppolito, T., Guedes, C. C. F., 2011. Thermal history versus sedimentary history: OSL sensitivity of quartz grains extracted from rocks and sediments. Quaternary Geochronology 6, 261-272.

Shulmeister, J., Thackray, G. D., Rieser, U., Hyatt, O. M., Rother, H., Smart, C. C., Evans, D. J. A., 2010. The stratigraphy, timing and climatic implications of glaciolacustrine deposits in the middle Rakaia Valley, South Island, New Zealand. Quaternary Science Reviews 29(17-18), 2362-2381.

Spencer, J. Q., Owen, L. A., 2004. Optically stimulated luminescence dating of Late Quaternary glaciogenic sediments in the upper Hunza valley: validating the timing of glaciation and assessing dating methods. Quaternary Science Reviews 23, 175-191.

Steffen, D., Preusser, F., Schlunegger, F., 2009. OSL quartz age underestimation due to unstable signal components. Quaternary Geochronology 4, 353-362.

Thackray, G. D., 2001. Extensive Early and Middle Wisconsin Glaciation on the Western Olympic Peninsula, Washington, and the Variability of Pacific Moisture Delivery to the Northwestern United States. Quaternary Research 55, 257-270.

Thackray, G. D., 2008. Varied climatic and topographic influences on Late Pleistocene mountain glaciation in the western United States. Journal of Quaternary Science 23(6-7), 671-681.

Thomson, R., 2009. Field Trip 2 to the glacial history of the Upper Clutha. The 2009 New Zealand Snow and Ice Research Group (SIRG) Annual Workshop.

Thrasher, I. M., Mauz, B., Chiverrell, R. C., Land, A., 2009. Luminescence dating of glaciofluvial deposits: a review. Earth-Science Reviews 97, 133-146.
Wallinga, J., Murray, A., Wintle, A., 2000, The single-aliquot regenerative-dose (SAR) protocol applied to coarse-grain feldspar. Radiation Measurements 32, 529-533.

Wintle, A. G., Murray, A. S., 2006. A Review of Quartz Optically Stimulated Luminescence Characteristics and Their Relevance in Single-aliquot Regeneration Dating Protocols, Radiation Measurements 41, 369-391.

CHAPTER 5

Conclusion

Thesis research investigated the late Pleistocene glacial history of the Lake Hawea valley, Southern Alps, New Zealand and the South Fork Hoh River valley, Olympic Mountains, Washington by reconstructing sequences of stable ice positions and the style of deposition associated with ice advance and retreat. Establishing chronologic constraint on these deposits was mostly successful, however complications based on scarcity of organic samples for radiocarbon dating and issues associated with luminescence dating of glacial sediments arose. Nonetheless, discussion of these hindrances is important for future research projects that seek to use luminescence techniques on glacial sediments, thus supporting the motivation for Chapter 4. Additionally, the glacial record from Lake Hawea was compared with paleoclimate data from the South Island because of the greater resolution of glacial and paleoclimate studies in the region.

This research adds to a growing suite of studies that may eventually be connected to examine the hypothesis that Pleistocene glacial advances are synchronous between the maritime, hyper-humid Olympic Mountains and Southern Alps, potentially due to interhemispheric climate transfer mechanisms (e.g. Lowell et al., 1995; Denton et al., 1999; Vandergoes et al., 2005; Thackray, 2008). Presently, more work is needed to test this hypothesis; this can be accomplished by future studies that also employ detailed sedimentologic, stratigraphic, geomorphic, and chronologic analyses, coupled with continued paleocliamatologic research, in other glacial valleys in the Southern Alps and the Olympic Mountains.

Future Work

The most immediate and tangible future work is continuing data collection on OSL and IRSL samples and subsequent analyses. Chapter 4, although presently preliminary, will eventually be expanded to a full manuscript for publication discussing each of the samples and what is inferred about their OSL signals based on depositional facies and relative transport distance from the ice front.

Geomorphic observations in the upper Hoh River valley catchment and Lake Hawea area could be appreciably extended through the analysis of LiDAR data. LiDAR was flown for the lower Hoh River catchment by the Puget Sound Lidar Consortium but postponed for the upper due to snow cover. Landforms here were difficult to recognized in the field and in aerial photographs due to extensive rainforest cover and the available DEM data was too coarse (30 m) to notice subtle differences in elevation that may be important in differentiating outwash plains. The budget of this project did not include purchase of LiDAR data for the Lake Hawea region, but this data could have helped in interpretations of landforms such as the Quaternary ice contact feature.

Work in Lake Hawea could be furthered by investigating geomorphic features further down-valley (i.e. south of the Hawea moraine) and up-valley (i.e. north of the Hawea moraine) to more extensively assess the glacial history of the valley and continue Pleistocene glacial research associated with the upper Clutha River catchment. Exposurse of glacial sediment and geomorphic landforms up-valley were noticed during fieldwork in February 2013, and should be studied in detail. Additionally, cosmogenic nuclide dating of glacially deposited boulders in the Lake Hawea and Lake Wanaka basins could provide more chronologic constraint on the last glacial advances in the region.

Future work in the Olympic Mountains should be aimed at a better age control on the SF 2 and SF 3 ice positions, as they are currently both constrained to <20 ka. Also, future research should contribute to an increased understanding of the paleoclimatology of the last glaciation in this area. Presently, the only two paleocliamatologic research papers that focus specifically on the Olympic Peninsula were published in 1972 (Florer, 1972; Heusser, 1972). These climate reconstructions could be aided by extended pollen sampling to provide higher resolution and by other paleoclimate proxies such as chironomid and beetle analyses, where these organisms are present in the stratigraphy.

Lessons Learned

Samples for luminescence dating should be floated for both quartz and feldspar at the outset. This would have expedited sample processing and data collection and analysis. This was overlooked, as the USU Luminescence Lab did not systematically consider feldspar analysis and routinely dedicate one of the Riso machines to these measurements. An early indication that feldspar analysis should have been considered early in New Zealand research projects includes the literature that scorns quartz OSL analysis from the South Island.

Interpretations can change significantly with added information. This may seem like an obvious statement, but was learned especially during research in the South Fork Hoh River valley. Interpretations of stratigraphic sequences and connections to stable ice positions were firstly formed used preliminary OSL ages and stratigraphic relationships. These ideas quickly changed with more definite chronologic constraint (radiocarbon dating) and continued OSL data collected that either solidified previous age estimates or greatly altered them. The initial ideas and interpretations were important in developing an understanding for how the glacial system of the valley may have worked, but additional information (and continually incoming additional

data) provided an exercise in patience; relying too heavily on initial interpretations may make newly discovered information that significantly changes interpretations frustrating and difficult to reconcile. It would have been most useful and efficient to rely firstly on foremost on field observations of sedimentology and stratigraphy, as the age constraints may not be accurate.

Referenced Cited

Denton, G. H., Lowell, T. V., Heusser, C. J., Moreno, P. I., Andersen, B. G., Heusser, L. E., Schlüchter, C., Marchant, D. R., 1999, Interhemispheric Linkage of Paleoclimate during the Last Glaciation. Geografiska Annaler 81(2), 107-153.

Florer, L. E., 1972, Quaternary Paleoecology and Stratigraphy of the Sea Cliffs, Western Olympic Peninsula, Washington. Quaternary Research 2, 202-216.

Heusser, C. J., 1972. Palynology and Phytogeographical Significance of a Late-Pleistocene Refugium Near Kalaloch, Washington. Quaternary Research 2, 189-201.

Lowell, T. V., Heusser, C. J., Andersen, B. G., Moreno, P. I., Hauser, A., Heusser, L. E., Schlüchter, C., Marchant, D. R., Denton, G. H., 1995, Interhemispheric Correlation of Late Pleistocene Glacial Events. Science 269, 1541-1549.

Thackray, G. D., 2008, Varied climatic and topographic influences on Late Pleistocene mountain glaciation in the western United States. Journal of Quaternary Science 23(6-7), 671-681.

Vandergoes, M. J., Newnham, R. M., Preusser, F., Hendy, C. H., Lowell, T. V., Fitzsimons, S. J., Hogg, A. G., Kasper, H. U., Schlüchter, C., 2005, Regional insolation forcing of late Quaternary climate change in the Southern Hemisphere. Nature 436, 242-245.

APPENDICES

APPENDIX A

Supplemental material to Chapter 3

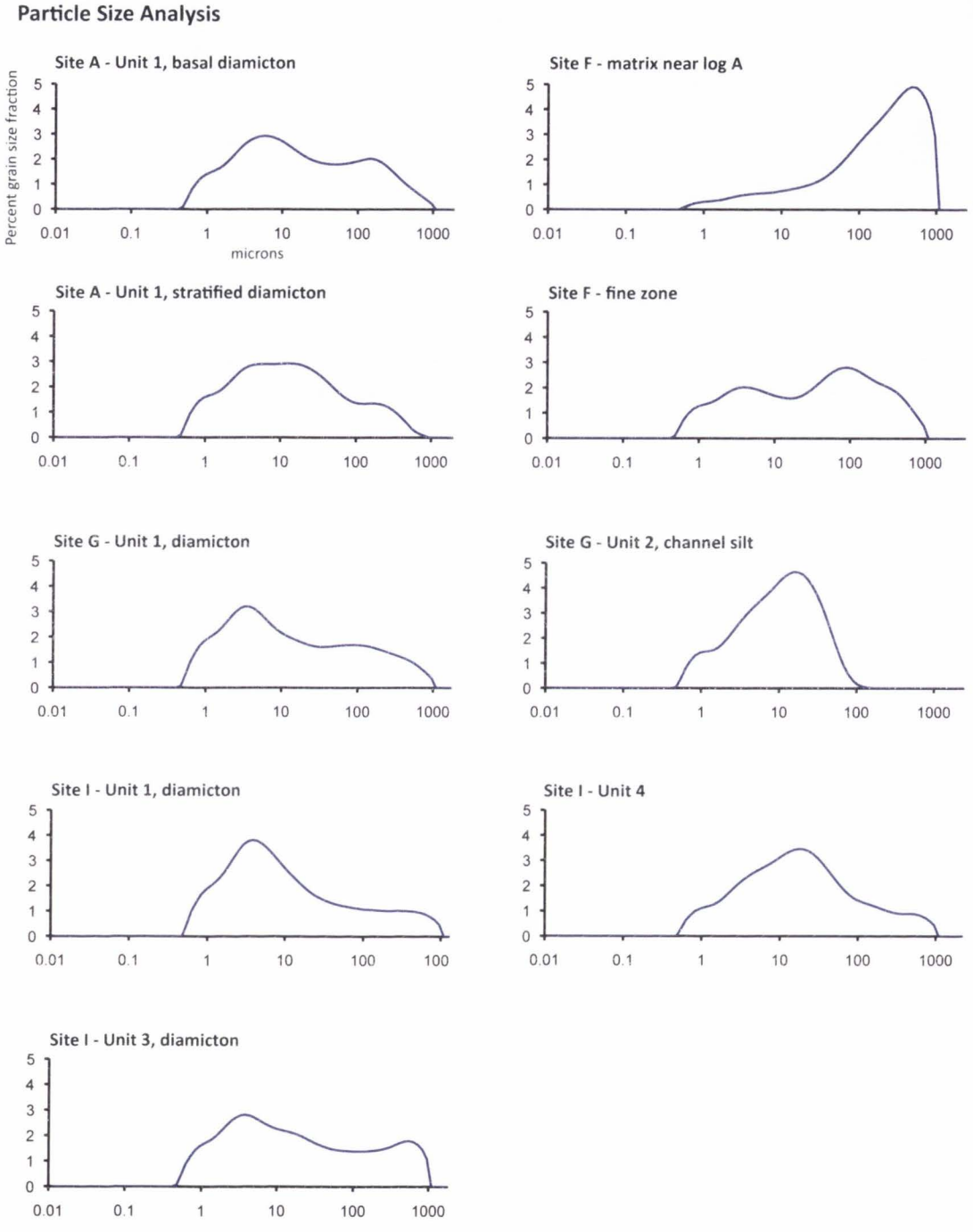

Figure A1.1 Results of particle size analysis for sediments <1,000 µm. Data can be found in Table 4. All units interpreted as diamicton are found on the left side of the figure, whereas those interpreted otherwise are on the right side of the figure.

Table A1.1 Grain size data to accompany Figure A1.1. This table contains the particle size analysis conducted using a Malvern Mastersizer on the <1,000 μm fraction of the samples collected.

Site A - Unit 1, basal diamicton

Size (μm)	Sediment	Percent fraction
0-2	clay	13.29
2 to 4	vf silt	12.26
4 to 8	f silt	14.47
8 to 16	med silt	12.95
16 to 31	coarse silt	10.17
31 to 62	vc silt	9.05
62 to 125	vf sand	9.51
125 to 250	fine sand	9.62
250 to 500	med sand	6.94
	microns	
	d(0.1)	1.49
	d(0.5)	12.73
	d(0.9)	215.89

Site A - Unit 1, stratified diamicton

Size (μm)	Sediment	Percent fraction
0-2	clay	14.86
2 to 4	vf silt	12.78
4 to 8	f silt	14.47
8 to 16	med silt	14.58
16 to 31	coarse silt	13.76
31 to 62	vc silt	10.45
62 to 125	vf sand	7.21
125 to 250	fine sand	6.64
250 to 500	med sand	4.85
	microns	
	d(0.1)	1.35
	d(0.5)	11.04
	d(0.9)	146.04

Site G - Unit 1, diamicton

Size (μm)	Sediment	Percent fraction
0-2	clay	17.78
2 to 4	vf silt	15.37
4 to 8	f silt	13.98
8 to 16	med silt	10.38
16 to 31	coarse silt	8.54
31 to 62	vc silt	8.19
62 to 125	vf sand	8.42
125 to 250	fine sand	7.68
250 to 500	med sand	7.12
	microns	
	d(0.1)	1.21
	d(0.5)	9.06
	d(0.9)	234.23

Site F - matrix near log A

Size (μm)	Sediment	Percent fraction
0-2	clay	2.87
2 to 4	vf silt	2.74
4 to 8	f silt	3.28
8 to 16	med silt	3.89
16 to 31	coarse silt	5.02
31 to 62	vc silt	7.75
62 to 125	vf sand	12.67
125 to 250	fine sand	17.87
250 to 500	med sand	27.97
	microns	
	d(0.1)	9.41
	d(0.5)	193.73
	d(0.9)	655.01

Site F - fine zone

Size (μm)	Sediment	Percent fraction
0-2	clay	11.78
2 to 4	vf silt	9.56
4 to 8	f silt	9.65
8 to 16	med silt	8.28
16 to 31	coarse silt	8.59
31 to 62	vc silt	11.82
62 to 125	vf sand	13.84
125 to 250	fine sand	11.98
250 to 500	med sand	11.03
	microns	
	d(0.1)	1.64
	d(0.5)	34.88
	d(0.9)	324.34

Site G - Unit 2, channel silt

Size (μm)	Sediment	Percent fraction
0-2	clay	12.91
2 to 4	vf silt	12.44
4 to 8	f silt	17.52
8 to 16	med silt	21.95
16 to 31	coarse silt	21.45
31 to 62	vc silt	11.77
62 to 125	vf sand	1.92
125 to 250	fine sand	0.04
250 to 500	med sand	0.00
	microns	
	d(0.1)	1.51
	d(0.5)	9.63
	d(0.9)	35.24

Site I - Unit 1, diamicton

Size (μm)	Sediment	Percent fraction
0-2	clay	18.20
2 to 4	vf silt	17.73
4 to 8	f silt	17.46
8 to 16	med silt	12.55
16 to 31	coarse silt	8.44
31 to 62	vc silt	6.36
62 to 125	vf sand	5.47
125 to 250	fine sand	5.10
250 to 500	med sand	5.92
	microns	
	d(0.1)	1.22
	d(0.5)	6.54
	d(0.9)	203.28

Site I - Unit 3, diamicton

Size (μm)	Sediment	Percent fraction
0-2	clay	15.30
2 to 4	vf silt	13.34
4 to 8	f silt	13.01
8 to 16	med silt	11.10
16 to 31	coarse silt	9.58
31 to 62	vc silt	7.67
62 to 125	vf sand	6.98
125 to 250	fine sand	7.08
250 to 500	med sand	10.00
	microns	
	d(0.1)	1.34
	d(0.5)	12.75
	d(0.9)	396.02

Site I - Unit 4

Size (μm)	Sediment	Percent fraction
0-2	clay	10.27
2 to 4	vf silt	10.16
4 to 8	f silt	13.36
8 to 16	med silt	16.12
16 to 31	coarse silt	16.65
31 to 62	vc silt	12.20
62 to 125	vf sand	7.58
125 to 250	fine sand	5.66
250 to 500	med sand	5.37
	microns	
	d(0.1)	1.86
	d(0.5)	15.22
	d(0.9)	193.14

SITE A (N 47°48'35" W 124°00'11")
Figure S2 shows facies photographs.

Unit 1 – over-compacted weakly stratified diamicton

- ≥3 m thick
- Blue-grey
- Very weakly and weakly stratified, consolidated gravel and rare boulders in a clayey-silt (with some very fine sand) matrix (Dml)
    - The basal portion (~1 m exposed) of the unit is over-compacted and contains clasts that are dominantly rounded but range from angular to well-rounded (Figure A1.3).
    - Particle size data from the matrix of the basal over-compacted portion and the matrix of the upper weakly stratified portion are shown in Figure A1.1 and Table A1.1.
- This over-compacted nature of the lower part of this unit likely represents subglacial deposition. The upper weakly stratified portion may represent either subglacial deposition with stratification due to the flow of the diamicton or immediately proglacial deposition with some minor fluvial reworking.

Unit 2 – lacustrine sediment

- 3-5 m thick
- Blue-grey
- Clear, conformable, planar basal contact
- Alternating horizontally bedded sand (Sh) and thinly laminated clay (Fl)
    - Sand beds range from 1-25 cm thick but are predominantly 4-6 cm thick. Some thicker sand beds are cross-bedded and draped by clay. The grain size of the sand ranges from fine-upper to medium upper, and is composed of poorly-moderately sorted, angular to sub-rounded sand.
    - Clay beds range from 1-35 cm thick and are thicker at the bottom of the unit. Clay beds contain dewatering and/or soft sediment deformation features in places (F(w)).
- Three ^{14}C ages provide a limiting age of 23.0 ka on deposition (Thackray, 1996). A preliminary OSL age collected from the middle of the unit suggests deposition at ~17.9 ka (USU-989) (Table 3.3).
- This unit represents sedimentation into a lacustrine environment.

Unit 3 – delta foresets

- 11 m thick
- Brown
- Clear, conformable, planar basal contact
- Horizontal beds (Sh, Gh) on the left of the exposure and trough cross-beds on the right of the exposure, representing a lateral facies shift
    - The cross-beds are composed of sand beds (Sfo) and pebble gravels with rare cobbles (Gfo). Bed thickness ranges from centimeter to tens-of-centimeter scale. Some sand beds contain millimeter to centimeter-scale ripple cross-beds (Sr). Sand size ranges from very fine lower to medium lower, and is composed of well sorted angular to sub-rounded grains. Pebble-sized clasts are dominantly sub-rounded but range from angular to rounded (Figure A1.3).

    - The horizontal beds were inaccessible.
- A preliminary OSL age from the cross-beds in this unit suggests deposition at ~21.3 ka (USU-990) (Table 3.3).
- The cross-beds of this unit represent deltaic sedimentation as delta foresets into a lacustrine environment, whereas the horizontally bedded sand and gravels represent lower-energy sedimentation further into the lacustrine environment.

Unit 4 – glacial outwash

- ~10 m thick
- Brown
- Clear, conformable, planar basal contact
- Stratified clast-supported pebble to cobble gravel (Gh) with some sand lenses (Sm)
    - Bed thickness of the gravel ranges from centimeter- to tens-of-centimeter-scale. The gravel package below the clay bed coarsens upwards, whereas no grading is seen in the upper package. Clasts in the lower gravel package are dominantly sub-angular, but range from angular to sub-rounded (Figure S4). Clasts in the upper gravel package are dominantly sub-angular, but range from angular to rounded (Figure A1.4).
    - Sand beds are 5-10 cm thick. The sand in these beds ranges from fine lower to very coarse upper in size, and is composed of poorly sorted angular to sub-angular grains.
    - A laterally discontinuous clay layer separates the bottom portion of this unit from the top portion of the unit. This clay layer is 50 cm thick at its maximum. The top half is brown clayey-silt grading upwards to silty sand. The sand in this layer ranges in size from very fine lower to medium upper sub-angular to sub-rounded grains and is moderately sorted. The bottom half is blue silty-clay with interfingering very fine-lower sized sand. Horizontal laminations of the clay (Fl) are millimeter-scale thickness and are folded and warped in some places, presumably due to soft-sediment deformation. This bed likely represents an abandoned channel of the outwash plain that in-filled with fine sediment and organic material after abandonment.
- Two ^{14}C ages from this clay bed suggest deposition at 18.4 ka and 19.4 ka (Table 3.3). The 19.4 ka age comes from a wood fragment found near the base of the bed. The 18.8 ka age comes from beetle fragments from the uppermost part of the channel fill. These ages and their stratigraphic locations suggest that this channel was abandoned from the main outwash plain and in-filling with finer sediment and organic material for ~600 years. It is possible, however, that the wood fragment is slightly older than the abandoned channel. We did not find and abundance of wood in this bed, suggesting that the wood fragment dated could be slightly older than the channel fill itself, as it was likely incorporated from elsewhere (i.e. not grown in situ).
- The clay bed additionally contains beetle fragments that will be analyzed for temperature signals. Additional sample was collected for future chironomid analysis.
- This unit represents glacial outwash.

Unit 5 – glacial outwash

- 50 to 80 cm thick
- Moderately clear, perhaps erosional, planar basal contact
- Clast-supported cobbles and boulders (Gm/Bcm)

    - A clast count was not conducted due to safety issues associated with removing boulder-sized clasts from the outcrop face, however the longest exposed axes of boulder-sized clasts reach 40 cm.
- This unit may represents more proximal glacial outwash than Unit 4 or a distinct change in channel dynamics and carrying capacity.

Unit 6 – glacial outwash

- 5-10 m thick
- Diffusive to moderately clear, planar, conformable basal
- Stratified, coarsening upward pebble-cobble gravels with rare boulders (Gh) and some massive sand lenses (Sm) with occasional pebbles
    - Beds are >10 cm thick. Clasts are dominantly sub-angular but range from angular to rounded (Figure A1.4).
    - The sand ranges from medium-upper to very coarse-upper in size and is composed of poorly sorted angular to sub-rounded grains.
- This unit represents glacial outwash.

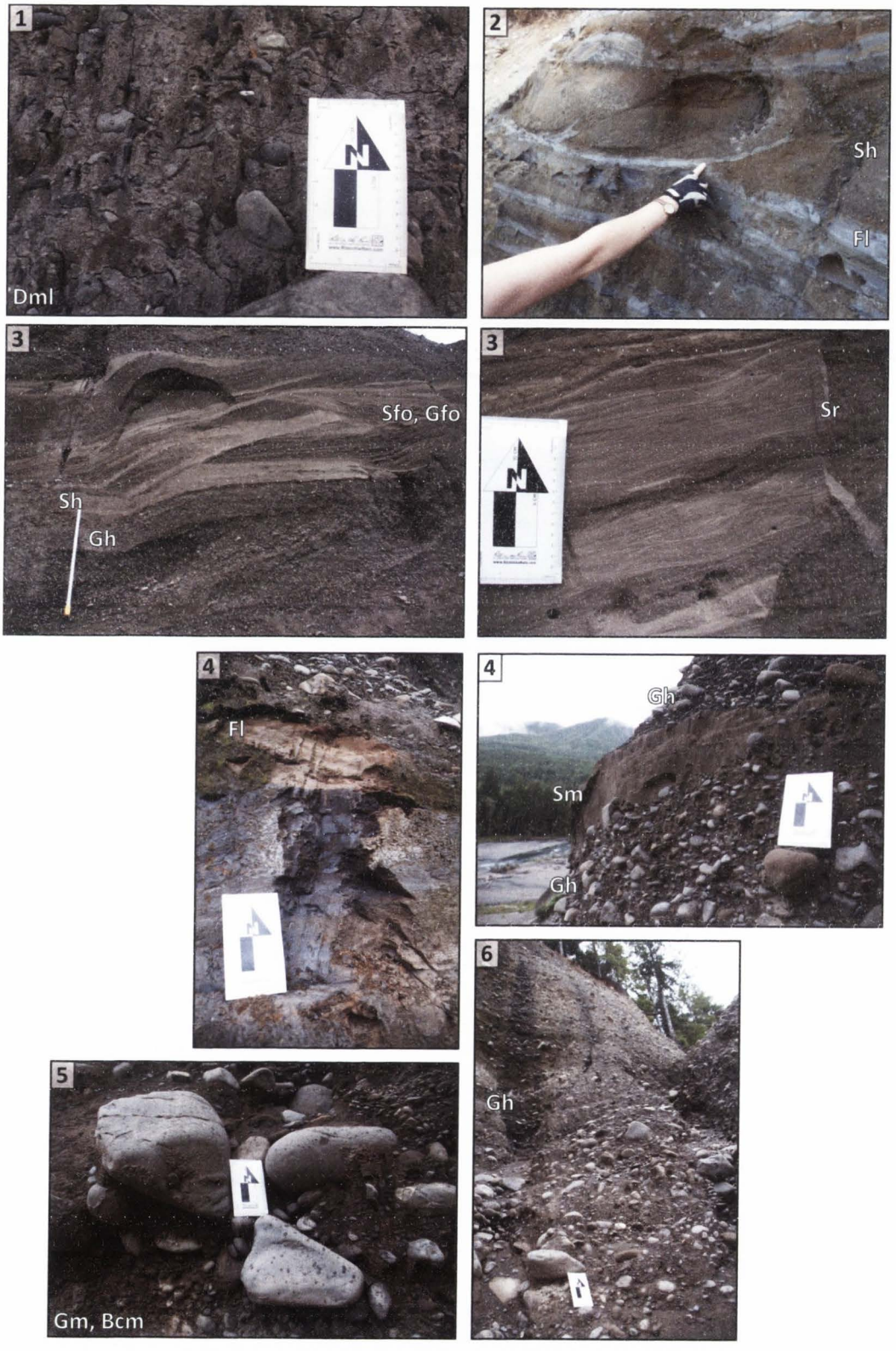

Figure A1.2 Facies photographs from Site A. Numbers represent unit designation, labels represent facies codes as found in Table 3.2.

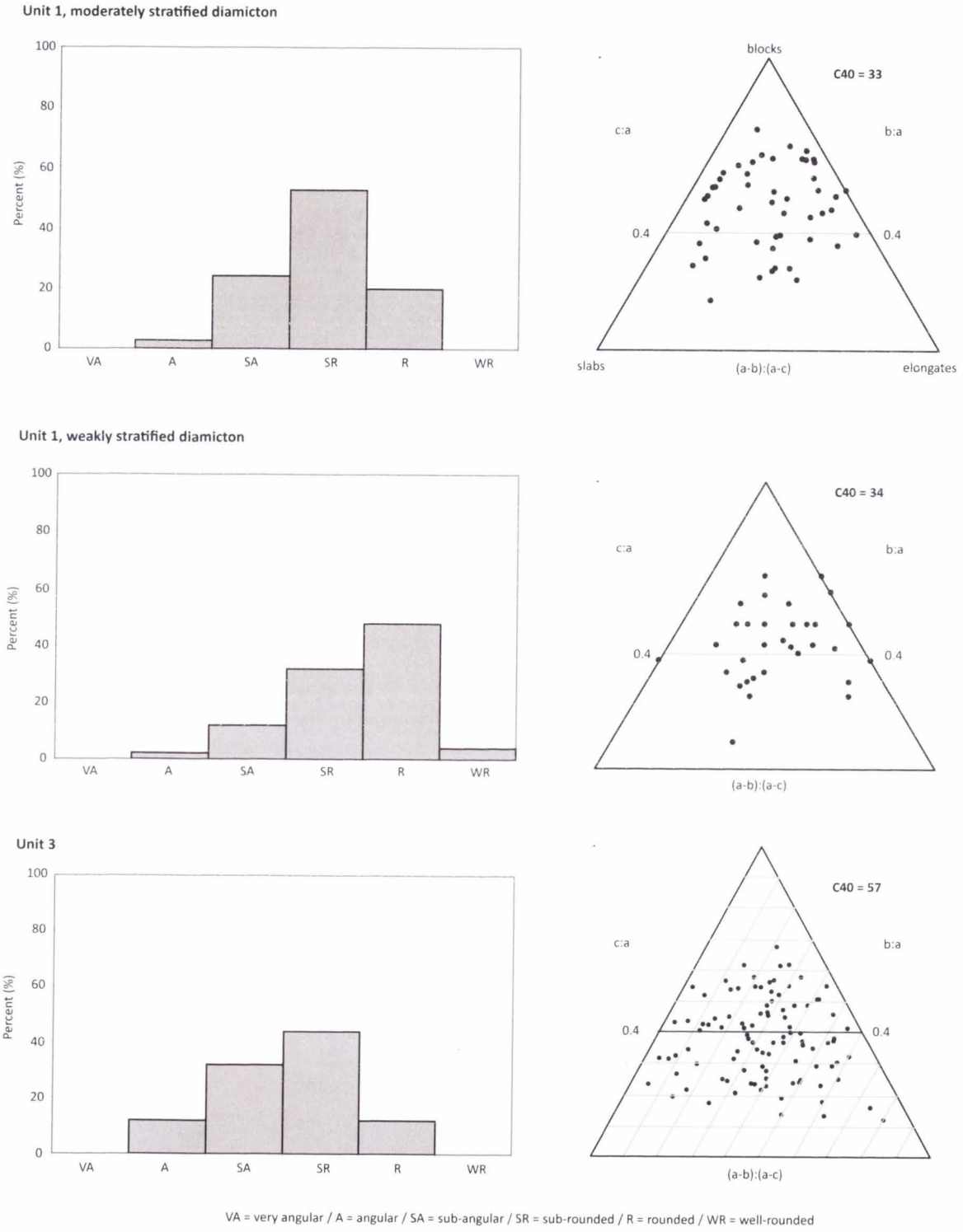

Figure A1.3 Clast shape data for Unit 1 and Unit 3 of Site A. Individual datasets composed of 50 pebble- to gravel-sized clasts, except for the 100 clasts in Unit 3. Although the ternary diagrams are of little to no use in distinguishing subglacial and fluvially transported sediments because neither environment is likely to contain many angular clasts, the diagrams are provided here for the sake of potential comparison to other environments.

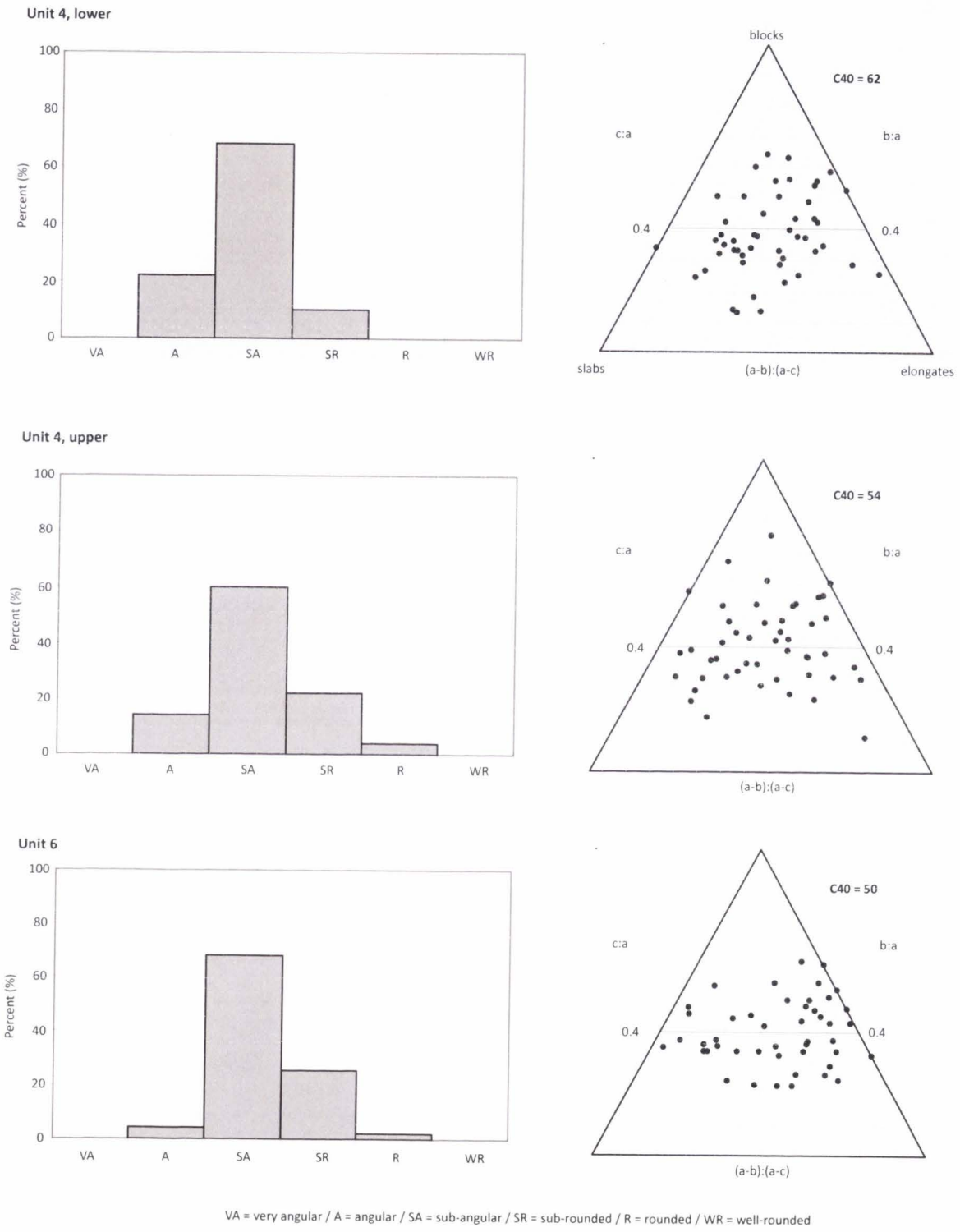

Figure A1.4 Clast shape data for Unit 4 and Unit 6 of Site A. Individual datasets composed of 50 pebble- to gravel-sized clasts. Although the ternary diagrams are of little to no use in distinguishing subglacial and fluvially transported sediments because neither environment is likely to contain many angular clasts, the diagrams are provided here for the sake of potential comparison to other environments.

SITE B (N 47°48'23" W 123°59'24")

Unit 1 – glacial outwash

- ~25 m
- Poorly sorted, weakly stratified, coarsening upwards, pebble-cobble gravel with rare boulders and sand lenses (Gh, Sm)
    - Boulders in the top 5 m reach 0.3-0.6 m along their longest axes

SITE C (N 47°48'11" W 123°58'56")

Figure S5 shows facies photographs.

Unit 1 – glacial outwash

- >20 m thick
- Horizontally stratified, clast-supported (Gh) and openwork (Go) pebble-cobble gravel with some massive sand lenses (Sm) and cross-bedded sands (St)
    - ~1 m thick gravel beds. Clasts are dominantly sub-angular, but range from angular to rounded (Figure A1.6).
    - The sand infilling void spaces ranges from very fine lower to very coarse upper in size and is composed of poorly sorted sub-angular to angular grains, with few sub-rounded grains.
    - The sand described in one lens (from which OSL sample USU-1243 was taken) ranges from very fine lower to very fine upper in size and is composed of horizontally bedded moderately sorted grains (Sh). This sand lens is ~15 cm thick and extends >3 m laterally.
- A preliminary OSL age from this unit suggests deposition at 17.4 ka (USU-1243) (Table 3.3).
- This unit represents glacial outwash sedimentation.

Unit 2 – glacial outwash

- ~5-14 m thick
- Clear, planar, conformable basal contact
- Stratified clast-supported pebble-cobble gravel (Gh) and a greater concentration of sand lenses than Unit 1
    - Horizontal gravel beds are decimeters thick. Clasts are dominantly rounded but range from sub-angular to rounded (Figure A1.6).
    - Sand lenses are ~50 cm thick and their lateral widths vary across the outcrop (<4 m to >15 m). Sand within these lenses ranges from very fine upper to very coarse upper in size and is composed of horizontally bedded moderately to well sorted angular to subangular grains (Sh).
- A preliminary OSL age from the upper reaches of this unit suggests deposition at 21.7 ka (USU-991) (Table 3.3).
- This unit represents more distal outwash than Unit 1.

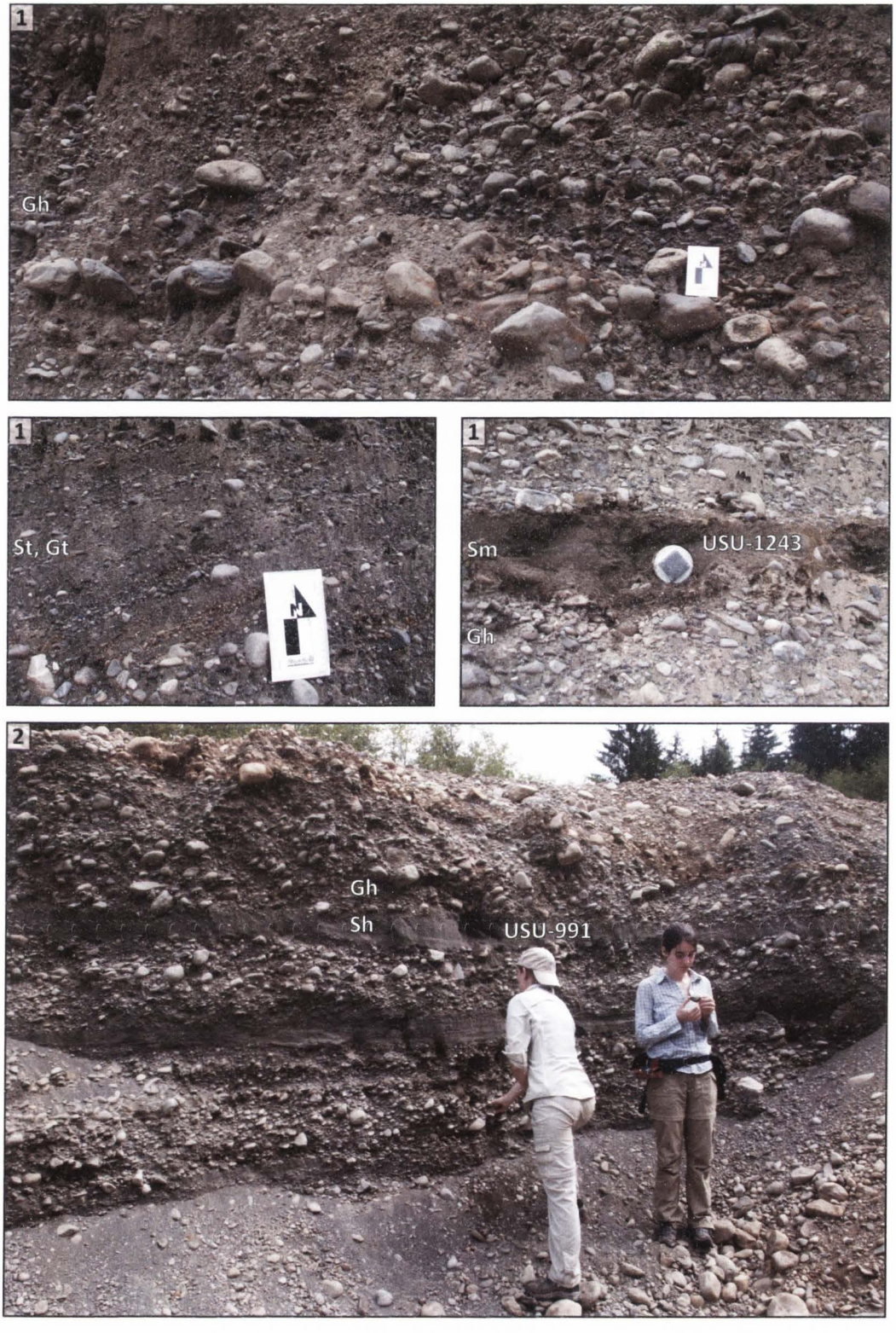

Figure A1.5 Facies photographs from Site C. Numbers represent unit designation, labels represent facies codes as found in Table 3.2.

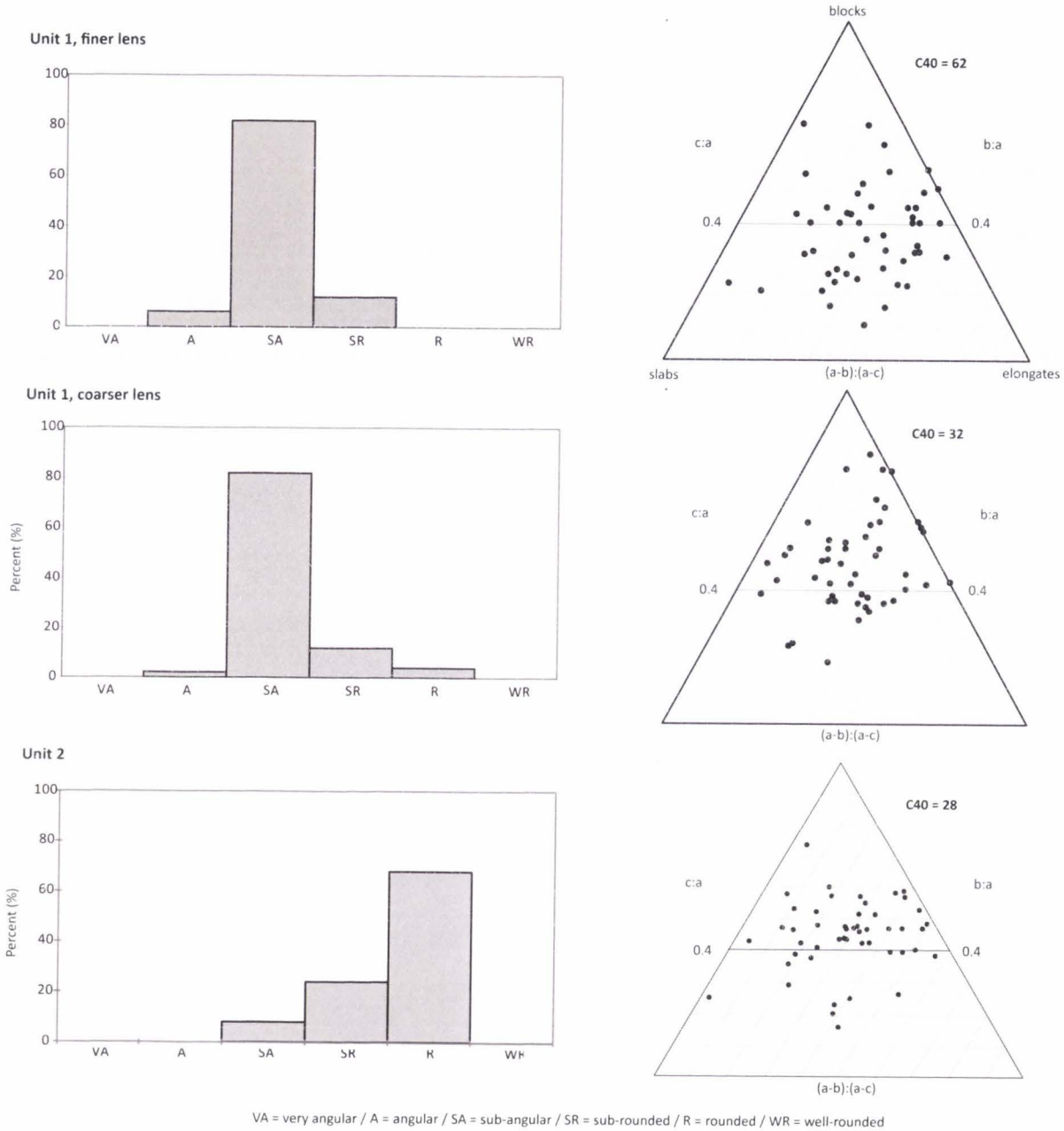

Figure A1.6 Clast shape data for Unit 1 and Unit 2 of Site C. Individual datasets composed of 50 pebble- to gravel-sized clasts. Although the ternary diagrams are of little to no use in distinguishing subglacial and fluvially transported sediments because neither environment is likely to contain many angular clasts, the diagrams are provided here for the sake of potential comparison to other environments.

SITE D (N 47°47'57" W 123°57'58")
Figure S7 shows facies photographs.

Previously exposed unit: A ^{14}C age collected from this package provides a limiting age of ~22.9 ka on deposition (Thackray, 2001).

Unit 1 – glacial outwash

- >14 m thick
- Clast-supported stratified pebble-cobble gravel with rare boulders (Gh)
    - Horizontal beds range from 10-90 cm thick. Clasts are dominantly sub-angular but range from angular to sub-rounded (Figure A1.8).
    - A discontinuous 75-80 cm thick, horizontal and planar, blue-grey clayey silt bed overlays the gravel below in places (Fm). This bed additionally contains pebble-sized and rare cobble-sized clasts that are dominantly sub-angular but range from angular to rounded (Figure A1.8).
- This unit represents glacial outwash sedimentation, with the clay cap likely representing channel abandonment and in-filling.

Unit 2 – glacial outwash

- ~1-12 m thick
- Moderately clear, planar, conformable basal contact
- Weakly stratified clast-supported pebble-cobble gravel (Gh) with sand lenses (Sm)
    - Clasts are dominantly sub-angular but range from angular to sub-rounded (Figure A1.8).
    - One sand lens at near the base of this unit was accessible for description. This lens contains horizontally laminated very fine lower- to medium upper-sized grains that are poorly rounded and angular to sub-angular.
- A preliminary OSL age in the described sand lens suggests deposition at 50.9 ka (USU-1242).
- This unit represents a second glacial outwash package, more distal than Unit 1.

Unit 3 – glacial outwash

- ~8 m thick (only present as a wedge on the left side of the exposure)
- Clear, irregular, lens-like basal
- Weakly stratified sand (Sh) and gravel (Gh).
- This unit represents third glacial outwash package.

Unit 4 – stratified diamicton

- ~7 m thick (maximum)
- Moderately clear, planar and horizontal, conformable basal contact
- Moderately stratified diamicton (Dml)
    - Although this unit is inaccessible, the matrix is blue-grey in color and clasts range from cobble- to boulder sized. Clasts that are distinguishable from afar are sub-angular and angular.
- The moderate stratification may represent either subglacial deposition with stratification due to the flow of the diamicton or immediately proglacial deposition with some minor fluvial reworking.

Unit 5 – glacial outwash

- ~1-7 m thick
- Clear, horizontal and planar, conformable basal contact
    - Although this unit is inaccessible, it is composed of what appears to be a fining upward stratified clast-supported pebble-boulder gravel (Gh) with some sand lenses (Sm).
- This unit represents the fourth glacial outwash package preserved at this site.

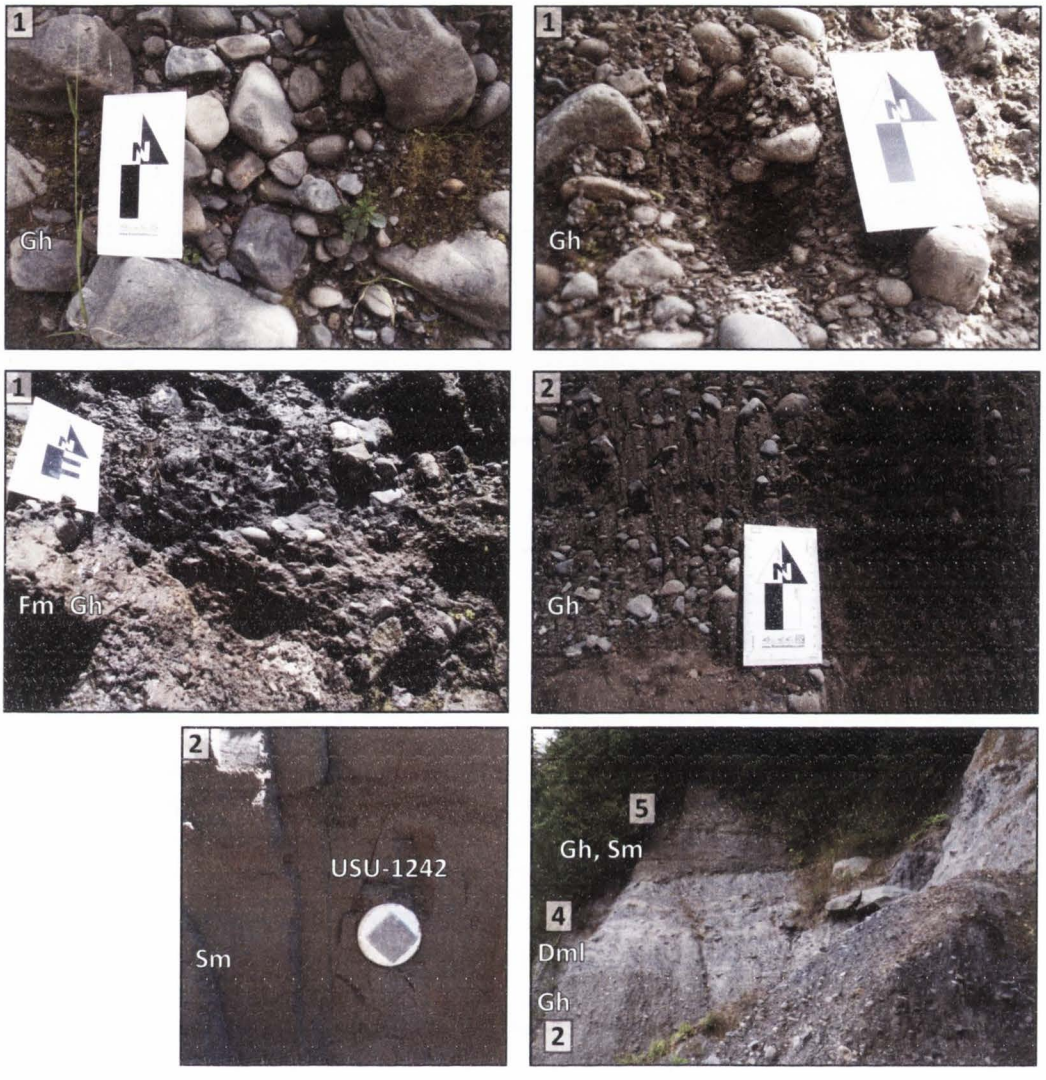

Figure A1.7 Facies photographs from Site D. Numbers represent unit designation, labels represent facies codes as found in Table 3.2.

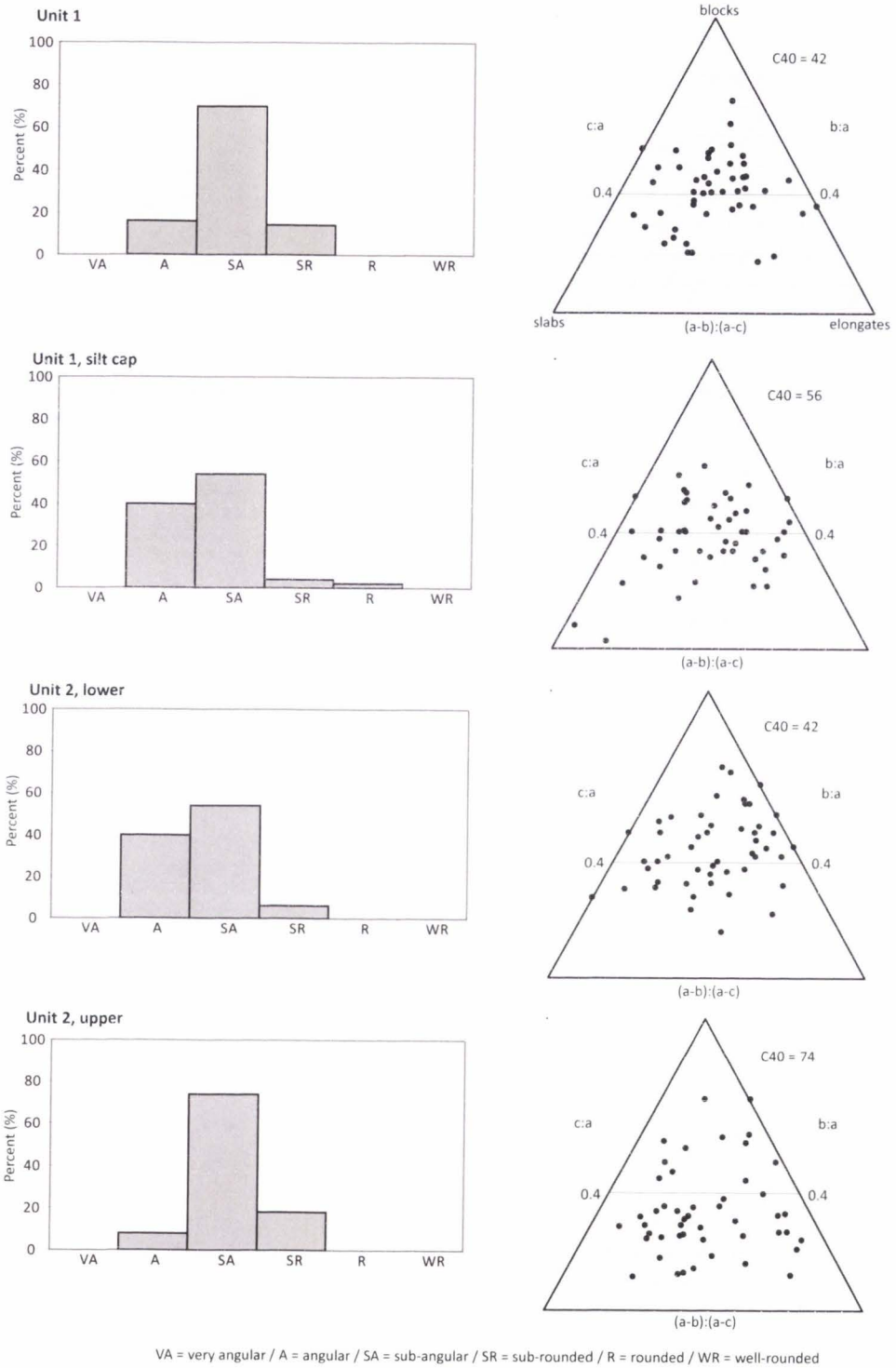

VA = very angular / A = angular / SA = sub-angular / SR = sub-rounded / R = rounded / WR = well-rounded

Figure A1.8 Clast shape data for Unit 1 and Unit 2 of Site D. Individual datasets composed of 50 pebble- to gravel-sized clasts. Although the ternary diagrams are of little to no use in distinguishing subglacial and fluvially transported sediments because neither environment is likely to contain many angular clasts, the diagrams are provided here for the sake of potential comparison to other environments.

SITE E (N 47°47'47" W 123°57'38")
Figure S9 shows facies photographs.

Unit 1 – stratified diamicton with gravel and sand lenses

- >10 m thick
- Blue-grey
- A complex mix of stratified diamicton (Dml) with common sand (Sh) and gravel (Gh) lenses
    - The diamicton matrix is composed of silty clay. In places, the silty matrix is thinly laminated.
    - Horizontal, planer gravel beds range in thickness from 2-3 m. Clasts are pebble- to boulder-sized and are dominantly angular but range from angular to sub-rounded (Figure A1.10).
    - Sand lenses range from 1 cm to 1 m thick and extend up to 8 m laterally. Sand lenses contain horizontal laminations (Sh), ripple cross-bedding (Sr), dewatering structures (Sr(w)), and both upward fining (Suf) and upward coarsening (Suc) beds.
    - The contact between the silt-matrix beds and sand lenses is undulatory and sometimes deformed by loading.
    - Additionally, ~2-3 m thick packages of this diamicton fine upwards (when assessing the gravel-sized fraction; several of these sequences are exposed, as seen in Figure A1.19.
- A preliminary OSL age form a sand lens in this unit suggests deposition at 60.2 ka (USU-1241).
- The stratification of this diamicton and the presence of common sand and gravel lenses likely represent immediately proglacial deposition with some fluvial reworking.

Unit 2 – glacial outwash

- ~4 m thick
- Clear, horizontal and planar, conformable basal contact
- Matrix- and clast-supported, coarsening upward, stratified pebble-cobble gravel with rare boulders (Gh) and some sand lenses (Sh)
    - The basal 30 cm of the unit on the upstream (right) side of the exposure, has a draping contact with Unit 1 below, and is composed of two distinct beds. The lower bed is 20-22 cm thick, brown, and is composed of pebble- and cobble-sized clasts tightly packed in a clay matrix (Fm). Clasts are dominantly sub-angular but range from angular to rounded (Figure A1.10). The upper bed is 8-10 cm thick, brown, and is a massive clay bed (Fm). This unit represents a very low-energy environment of a glacial outwash package. Horizontal beds range from ~10 cm to > 15 cm.
    - Clasts are dominantly sub-angular, but range from angular to rounded (Figure S10).
    - The sandy matrix, where present, contains medium to coarse sand, composed of poorly sorted mostly angular grains, with some sub-angular grains.
    - One sand lens at the base of this unit was measured as ~ 20 x 110 cm and consists of very fine to coarse grains that fine upwards (Suf). This sand lens also contains ripple cross-bedding (Sr).

- A preliminary OSL age from the measured sand lens suggests deposition at 20.0 ka (USU-1240) (Table 3.3).
- This unit represents glacial outwash deposition.

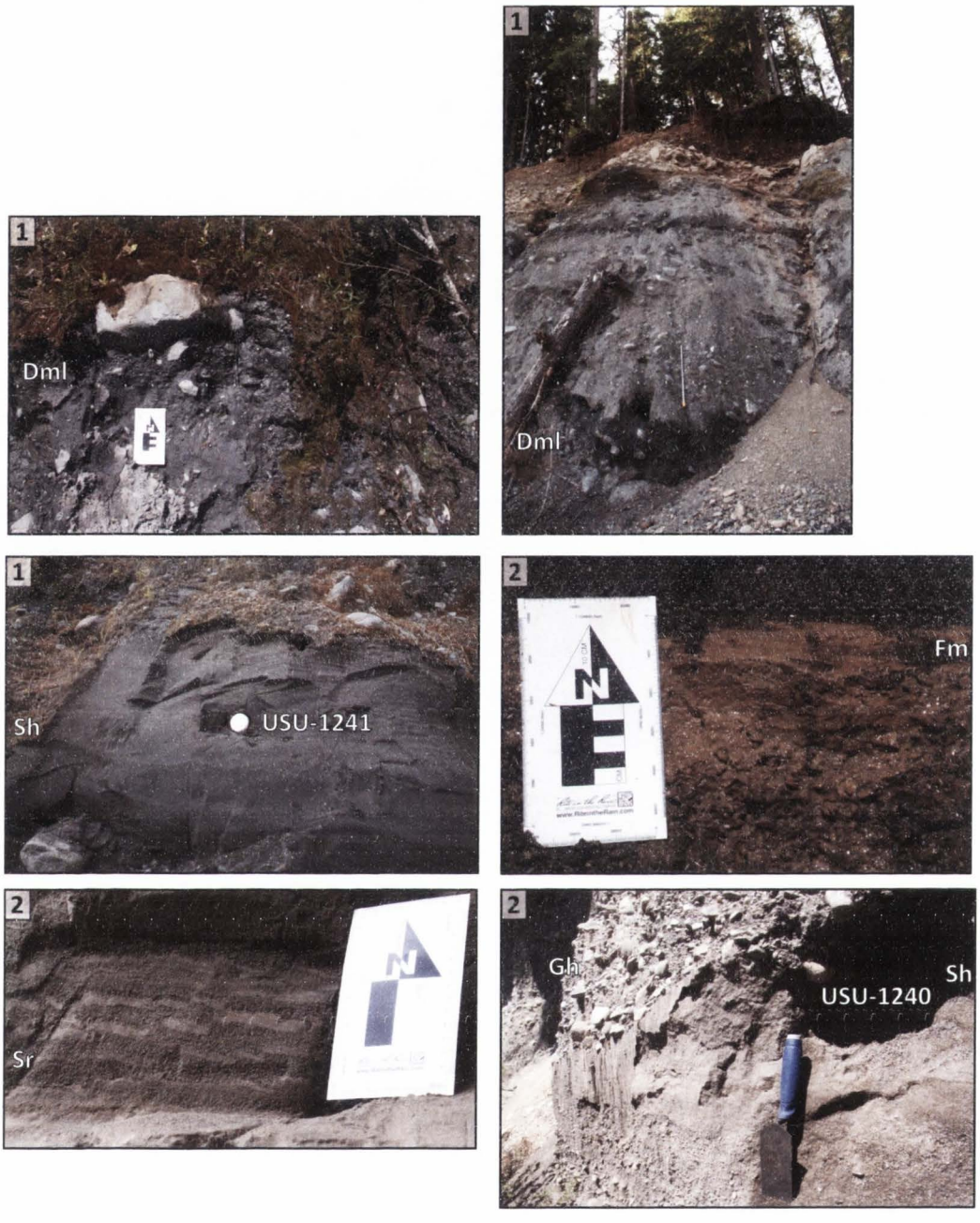

Figure A1.9 Facies photographs from Site E. Numbers represent unit designation, labels represent facies codes as found in Table 3.2.

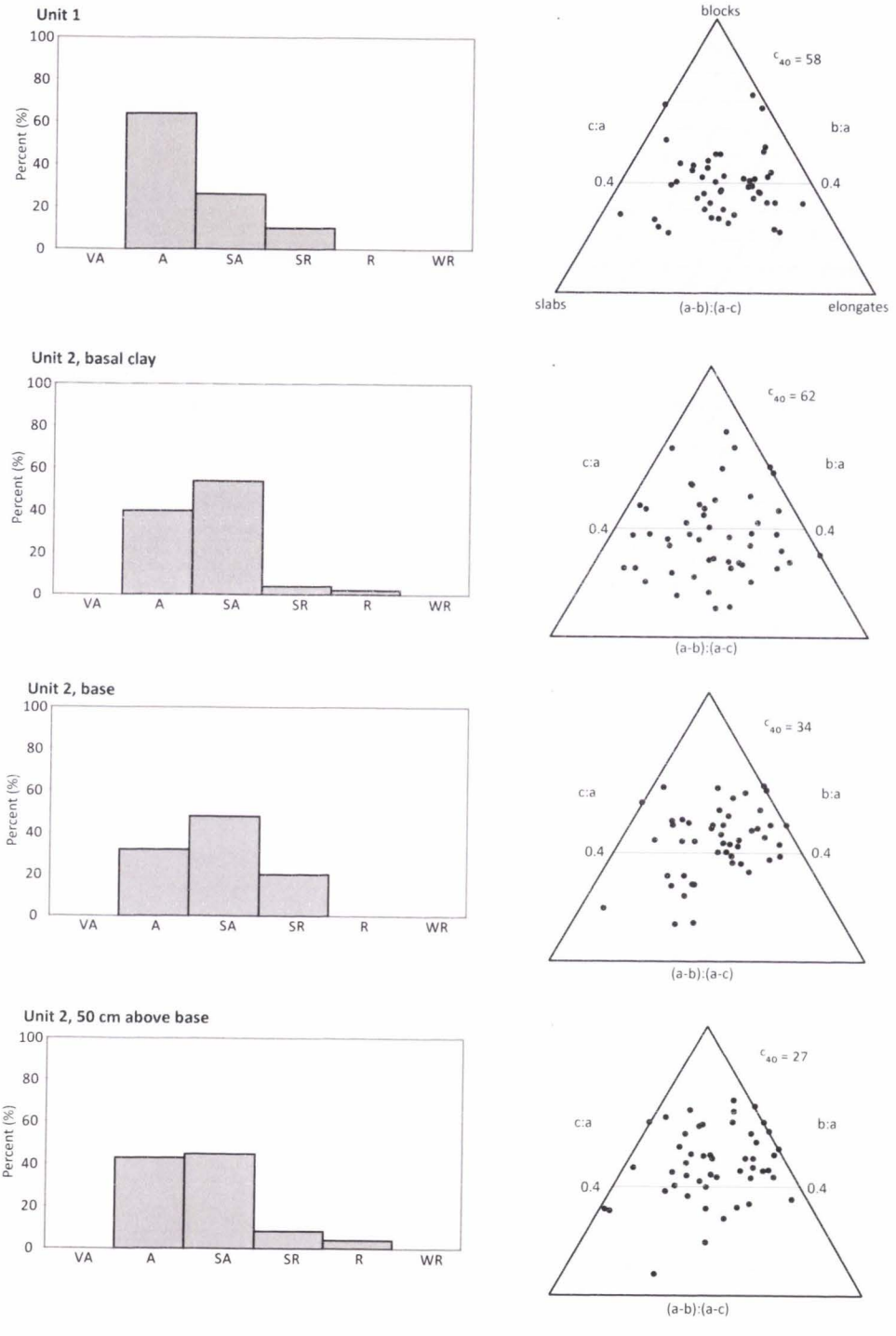

Figure A1.10 Clast shape data for Unit 1, Unit 2, and Unit 3 (on the up-river side of the exposure) of Site E. Individual datasets composed of 50 pebble- to gravel-sized clasts. Although the ternary diagrams are of little to no use in distinguishing subglacial and fluvially transported sediments because neither environment is likely to contain many angular clasts, the diagrams are provided here for the sake of potential comparison to other environments.

SITE F (N 47°47'31" W 123°57'40")
Figure S11 shows facies photographs.

Unit 1 – glacial outwash

- ~6 m thick (maximum)
- Stratified pebble-cobble gravel (Gh) with sand lenses (Sm)
    - This unit appears better sorted towards the base of the exposure, where sand lenses with some thin clays beds are exposed. There is then a transition to more gravel and less sorting upwards.
    - Horizontal gravel beds range from 3-10 cm thick. Clasts are dominantly sub-angular but range from angular to subangular with very few well-rounded clasts (Figure A1.12). Several striated clasts were seen in the deposit.
    - Sand lenses are ~15 cm thick maximum. Sand is mostly fine to medium in size, with some very fine grains and is composed of moderately sorted angular to sub-angular grains.
- A preliminary OSL age from a sand lens near the base of this exposure suggests deposition at 31.9 ka (USU-1285).
- This unit represents more distal glacial outwash sedimentation and ice re-advance.

Unit 2 – glacial outwash

- ~3 m thick (maximum)
- Stratified pebble-boulder gravel (Gh) with sand lenses (Sm)
    - Horizontal gravel beds range from 3-10 cm thick. Clasts are dominantly sub-angular but range from angular to subangular (Figure A1.12). Several striated clasts were seen in the deposit.
    - Sand lenses are ~15 cm thick maximum. Sand is mostly fine to medium in size, with some very fine grains and is composed of moderately sorted angular to sub-angular grains.
    - This unit also contains a wedge (~2 m maximum thickness) of cobble-boulder gravel that fines to the right (downstream) of the exposure (BL).
    - Particle size data of the matrix near log A (the downstream log, as seen in Figure 8, are shown in Figure A1.1 and Table A1.1.
- Two trees (~30 cm diameter) protrude perpendicularly from the middle of the exposure. Log A is 21.8 ka and log B is 21.7 ka based on ^{14}C dating.
- This unit represents proximal glacial outwash sedimentation.

Unit 3 – glacial outwash

- ~3 m thick (maximum)
- Stratified pebble-boulder gravel (Gh) with sand lenses (Sm)
    - Horizontal gravel beds range from 3-10 cm thick. Some gravel beds towards the top of the unit have low-angle cross-bedding.
    - Sand lenses are ~15 cm thick maximum. Sand is mostly fine to medium in size, with some very fine grains and is composed of moderately sorted angular to sub-angular grains.
    - Particle size data of a silty lens towards the top of the exposure are shown in Figure A1.1 and Table A1.1.
- This unit represents proximal glacial outwash sedimentation.

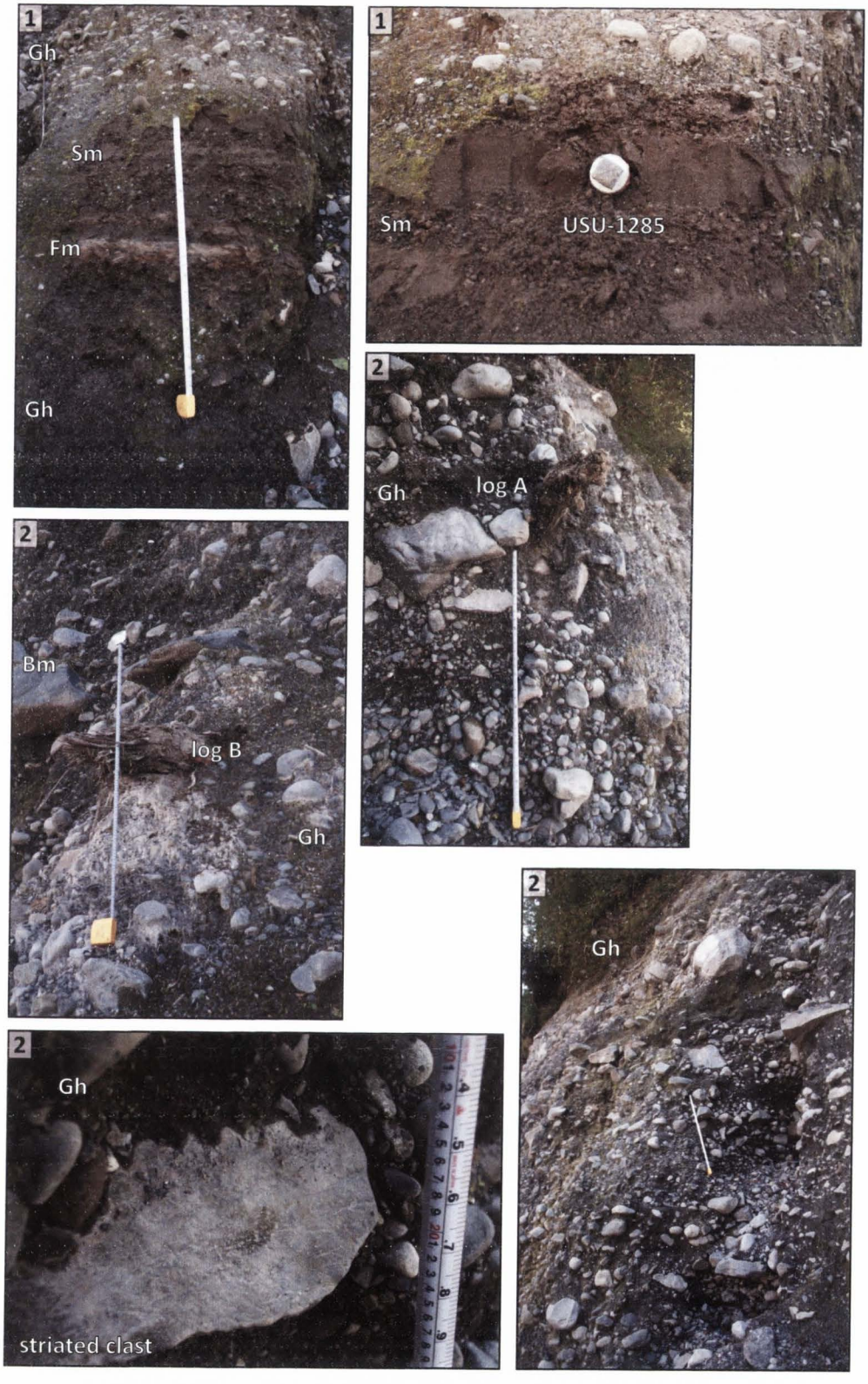

Figure A1.11 Facies photographs from Site F. Numbers represent unit designation, labels represent facies codes as found in Table 3.2.

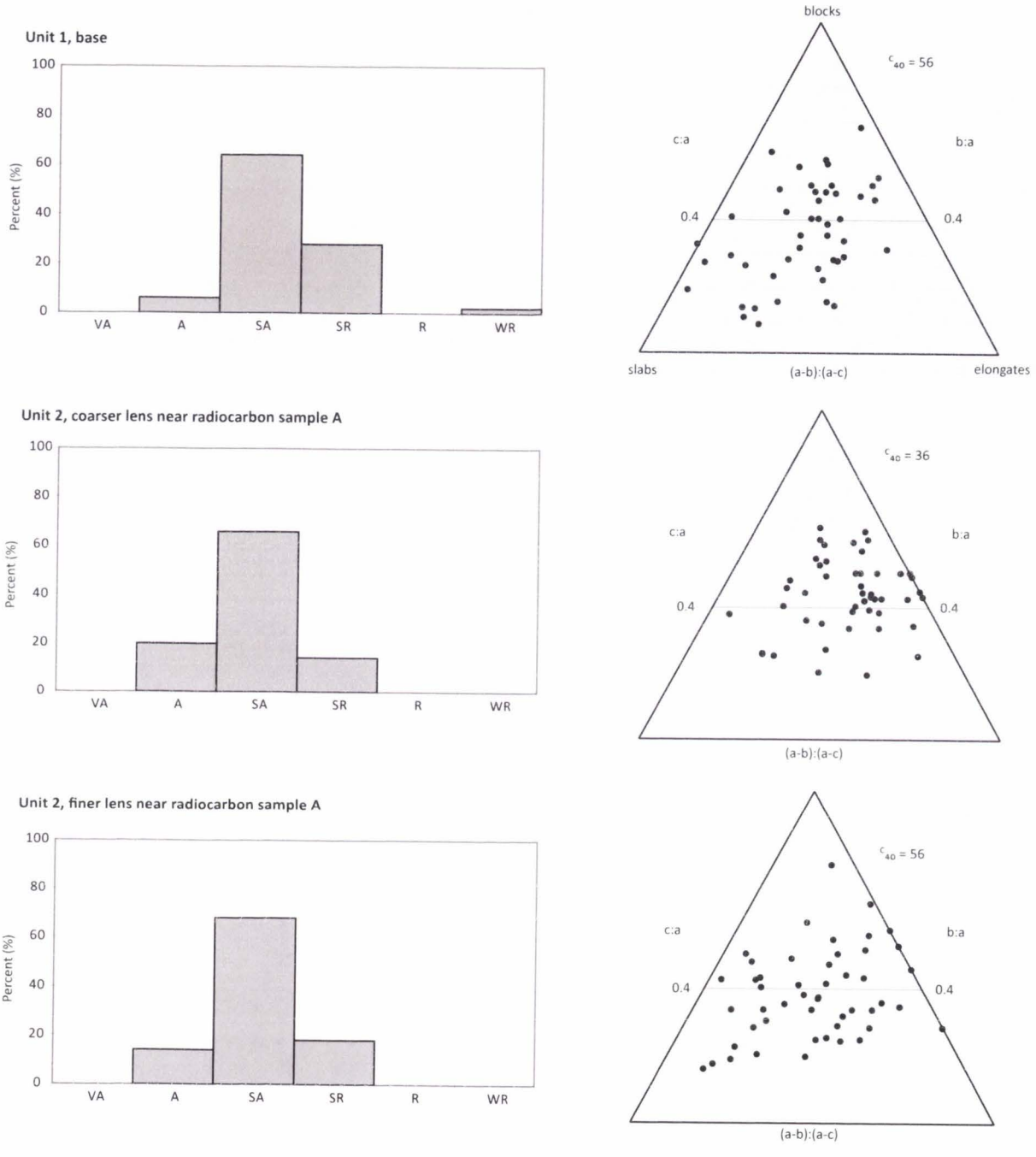

Figure A1.12 Clast shape data for Site F. Individual datasets composed of 50 pebble- to gravel-sized clasts. Although the ternary diagrams are of little to no use in distinguishing subglacial and fluvially transported sediments because neither environment is likely to contain many angular clasts, the diagrams are provided here for the sake of potential comparison to other environments.

SITE G (N 47°47'38" W 123°57'27")
Figure S13 shows facies photographs.

Unit 1 – stratified and massive diamicton

- >2 m thick
- Blue-grey
- Weakly stratified (Dml) and massive (Dms), well consolidated diamicton
    - This unit contains pebble-boulder-sized clasts in a silty matrix. The longest exposed axis of boulders approach 1 m. Clasts are dominantly angular and sub-angular but range from angular to rounded (Figure A1.14).
    - The silty matrix is thinly laminated in some clast-poor zones. Particle size data of this matrix are shown in Figure A1.1 and Table A1.1.
- This unit represents subglacial deposition.

Unit 2 – glacial outwash

- ~4 m thick
- Irregular (but generally horizontal) and typically covered basal contact
- Stratified clast-supported (Gh) and openwork (Go) pebble- boulder gravel with sand lenses (Sm) and channel forms with internal cross-bedding (Gt, St)
    - Horizontally bedded gravels are dominantly sub-rounded but range from sub-angular to well-rounded (Figure A1.14).
    - The prominent channel form contains cross-beds differentiated by clast size. Clasts in these crossbeds are dominantly sub-angular but range from angular to sub-rounded (Figure A1.14). This channel form is bordered by laminated brown and blue-grey silt (Fl) with some sand (Sh) that is a maximum of 60 cm thick. Horizontal laminations have a maximum thickness of 1 cm. The sand size is very fine lower to coarse lower and consists of moderately sorted sub-angular to sub-rounded (and rare angular) grains. Particle size data of the silt in this unit are shown in Figure A1.1 and Table A1.1.
- A ^{14}C sample from a piece of woods in the laminated silts yields an age of 20.2 ka. A preliminary OSL age from the laminated silt and sand suggests deposition at 22.7 ka (USU-1282).
- This unit represents glacial outwash deposition.

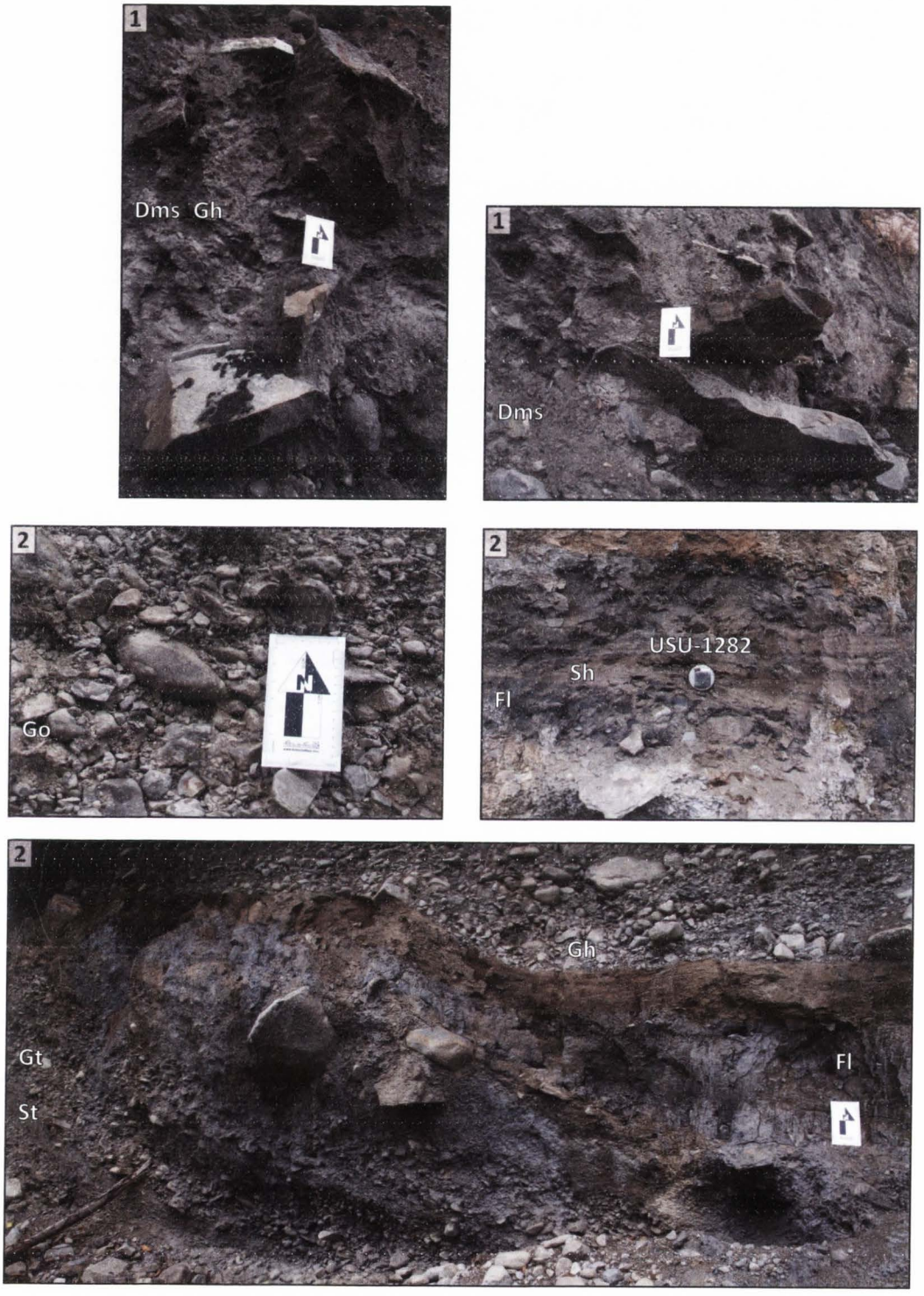

Figure A1.13 Facies photographs from Site G. Numbers represent unit designation, labels represent facies codes as found in Table 3.2.

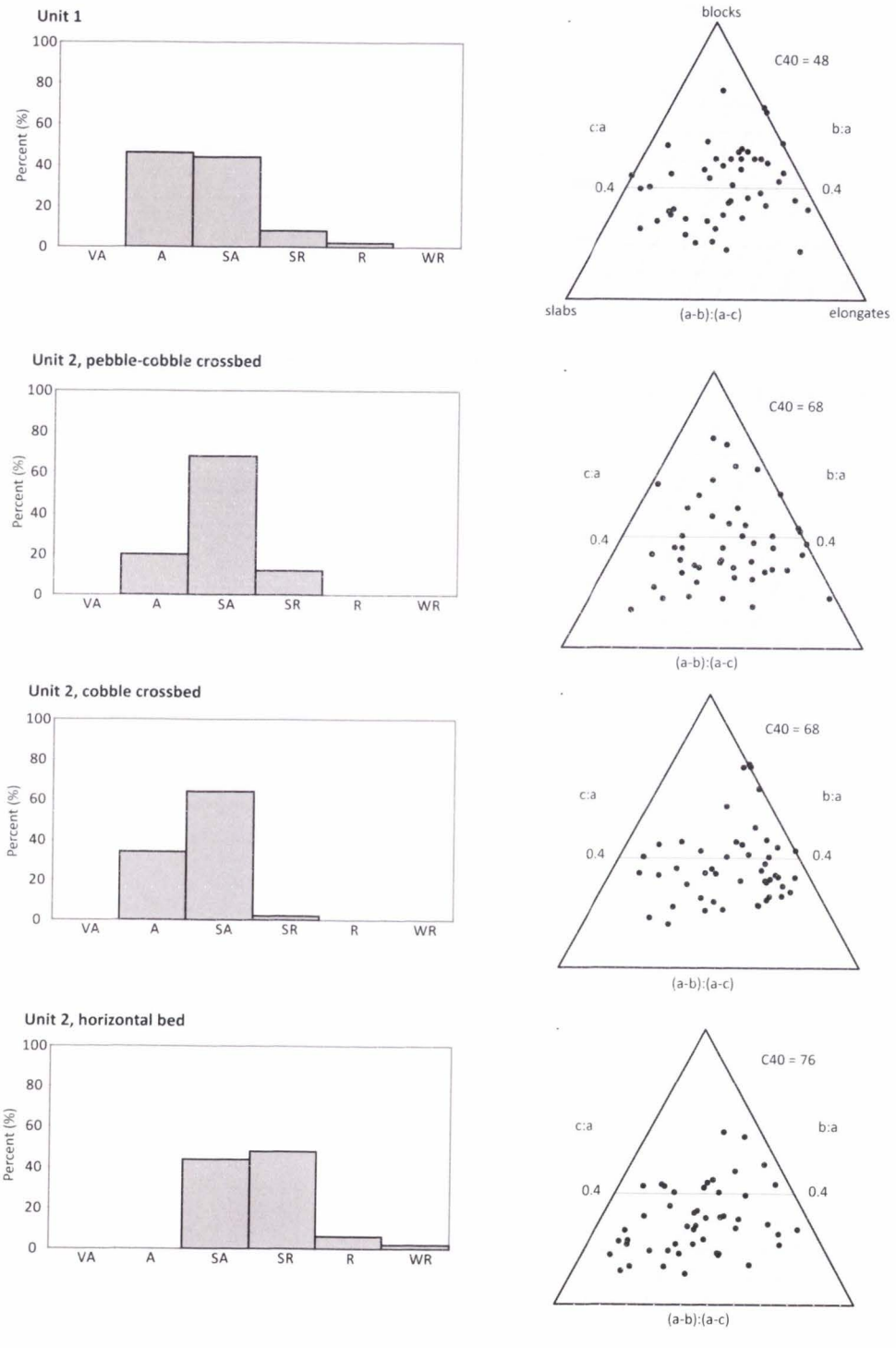

VA = very angular / A = angular / SA = sub-angular / SR = sub-rounded / R = rounded / WR = well-rounded

Figure A1.14 Clast shape data for Unit 1 and Unit 2 of Site G. Individual datasets composed of 50 pebble- to gravel-sized clasts. Although the ternary diagrams are of little to no use in distinguishing subglacial and fluvially transported sediments because neither environment is likely to contain many angular clasts, the diagrams are provided here for the sake of potential comparison to other environments.

SITE H (N 47°47'26" W 123°57'10")
Figure S15 shows facies photographs.

Unit 1 – glacial outwash

- >10 m thick
- Horizontally bedded, coarsening upwards, stratified clast- and matrix-supported pebble-cobble gravel (Gh)
    - Horizontal beds are 5-20 cm thick. Gravel is dominantly sub-angular but ranges from angular to rounded (Figure A1.16).
    - Where present, the matrix is composed of medium to very coarse lower sand that is moderately sorted and most sub-angular in shape (although some angular grains are present).
- This unit represents glacial outwash deposition.

Unit 2 – glacial outwash

- > 8 m thick
- Clear, horizontal and planar, conformable basal contact (where exposed)
- Weakly bedded, horizontally stratified clast-supported cobble-boulder gravel (Gh)
    - Horizontal bedding is very weak and was therefore not measured. Clasts are dominantly sub-angular but range from angular to rounded (Figure A1.16).
- This unit coarsens upwards overall and represents a second glacial outwash package more proximal than Unit 1.

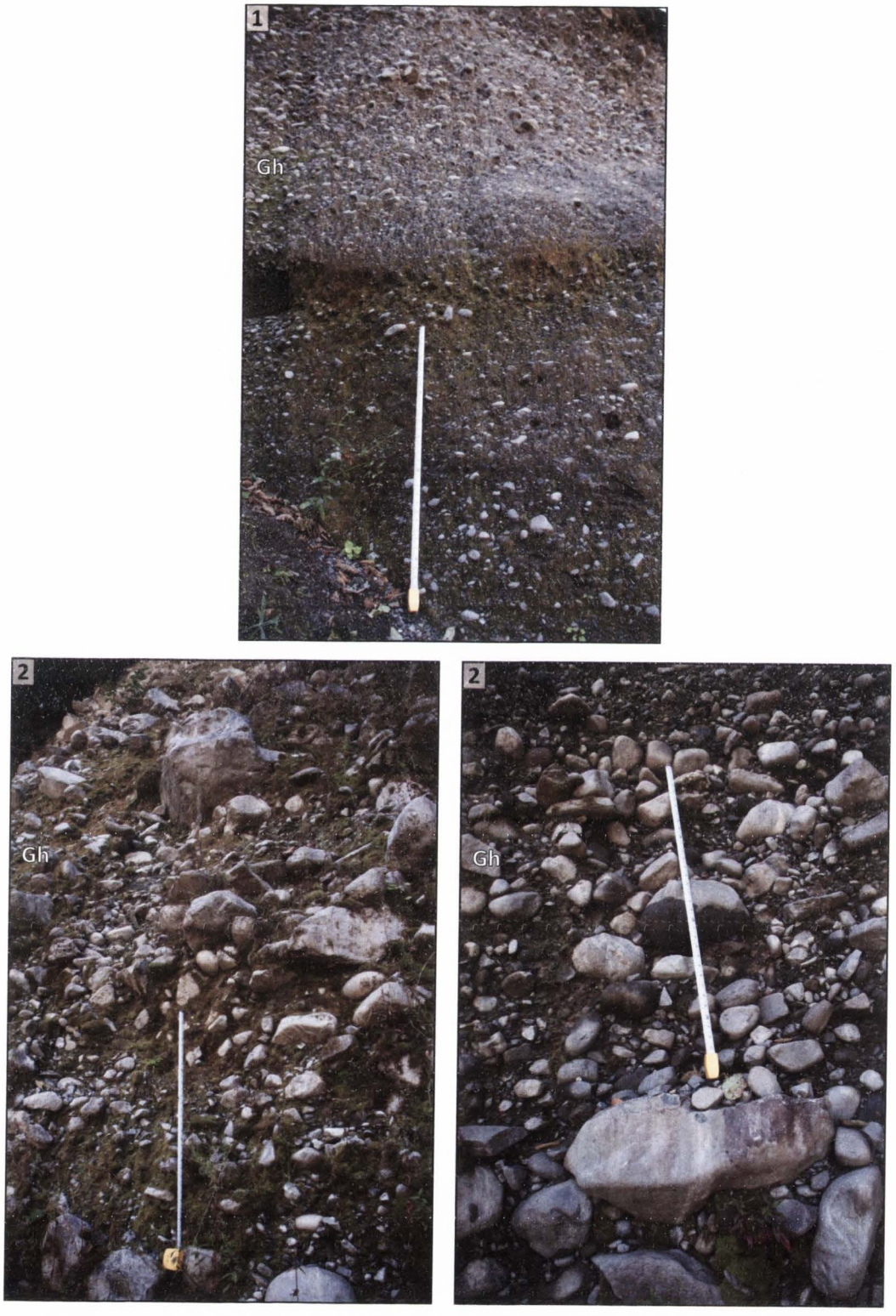

Figure A1.15 Facies photographs from Site H. Numbers represent unit designation, labels represent facies codes as found in Table 3.2.

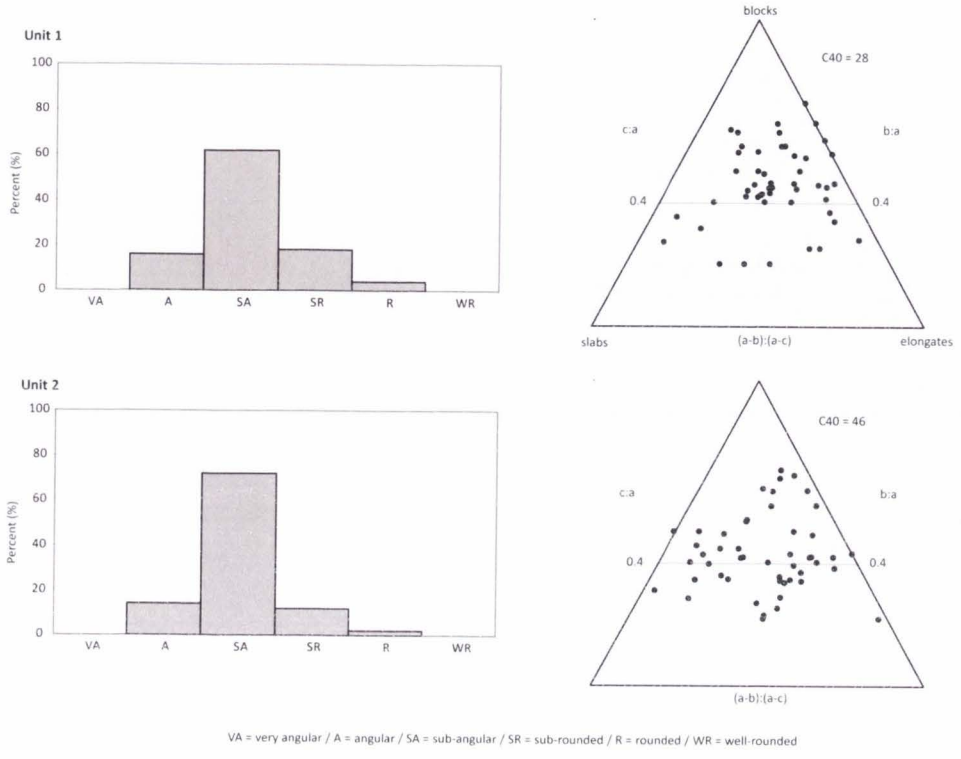

Figure A1.16 Clast shape data for Unit 1 and Unit 2 of Site H. Individual datasets composed of 50 pebble- to gravel-sized clasts. Although the ternary diagrams are of little to no use in distinguishing subglacial and fluvially transported sediments because neither environment is likely to contain many angular clasts, the diagrams are provided here for the sake of potential comparison to other environments.

SITE I (N 47°47'36" W 123°56'48")
Figure S17 shows facies photographs.

Unit 1 – massive diamicton

- >2 m thick
- Blue-grey
- Well consolidated massive diamicton (Dms) with pebble- to cobble-sized clasts and rare boulders in a silty matrix.
    - Clasts are dominantly sub-angular but range from angular to very few rounded (Figure A1.18).
    - Particle size data of this matrix are shown in Figure A1.1 and Table A1.1.
- This unit represents subglacial deposition during ice advance.

Unit 2 – glacial outwash

- <10 m thick
- The basal contact is covered.
- Coarsening upward, stratified, clast-support pebble-boulder gravel (Gh) with a zone of sandy matrix supported clasts
    - Horizontal beds range from 20 cm to 1 m thick. Clasts are dominantly sub-angular but range from angular to sub-rounded (Figure A1.18).
    - The sand matrix, where present, is composed of very fine upper to medium upper grains that are poorly sorted and angular to sub-angular.
- The unit represents glacial outwash deposition.

Unit 3 – stratified diamicton

- 50 cm to 2 m thick
- Blue-grey
- Clear, horizontal and planar, conformable basal contact
- Weakly stratified, moderately consolidated diamicton (Dml) with pebble- to cobble-sized clasts with some boulders
    - The silt matrix is thinly laminated in some places. Particle size data of this matrix are shown in Figure A1.1 and Table A1.1.
    - The clasts are dominantly sub-angular but range from angular to rounded (Figure A1.18).
- This unit may represent subglacial deposition or very ice proximal deposition with some fluvial reworking.

Unit 4 – glacial outwash

- ~7 m thick
- Clear, planar and horizontal, conformable basal contact
- Coarsening upwards, crudely stratified clast-supported pebble- boulder gravel (Gh) with some sand lenses (Sh)
    - The thicknesses of horizontal beds were too diffuse to measure. Clasts are dominantly angular and sub-angular but range from angular to rounded (Figure A1.18).
    - One accessible sand lens measures 50 cm thick and ~2 m wide and contains thin, horizontal laminations. The sand size is very fine upper to medium lower and contains horizontally bedded poorly sorted angular to sub-rounded grains.

This and lens also contained some thinly bedded silt (Fl), although this silt was only seen in this one lens. Particle size data of this silt are shown in Figure A1.1 and Table A1.1.

- A preliminary OSL age from this sand lens suggests deposition at 36.8 ka (USU-1283) (Table 3.3).
- This unit represents glacial outwash deposition.

Unit 5 – glacial outwash

- ~7 m thick
- Clear, horizontal and planar, conformable basal contact
- Clast-supported pebble- boulder gravel (Gh) with sand lenses (Sm)
    - Clasts appear poorly sorted and dominantly sub-angular.
    - Sand lenses appear to be ~50 cm-1 m thick.
- This unit represents a third glacial outwash package more distal than Unit 4.

Figure A1.17 Facies photographs from Site I. Numbers represent unit designation, labels represent facies codes as found in Table 3.2.

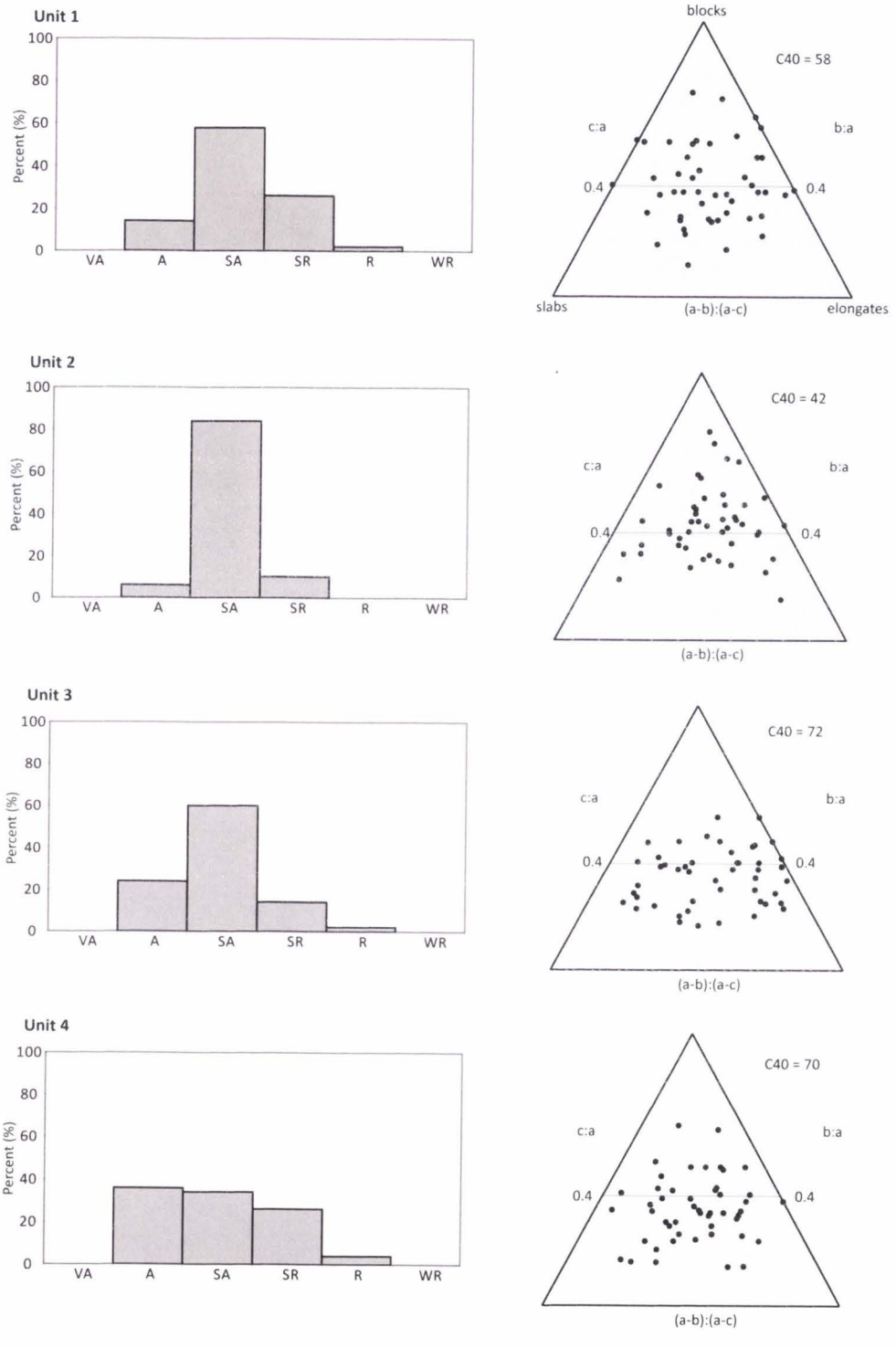

VA = very angular / A = angular / SA = sub-angular / SR = sub-rounded / R = rounded / WR = well-rounded

Figure A1.18 Clast shape data for Unit 1, Unit 2, Unit 3, and Unit 4 of Site I. Individual datasets composed of 50 pebble- to gravel-sized clasts. Although the ternary diagrams are of little to no use in distinguishing subglacial and fluvially transported sediments because neither environment is likely to contain many angular clasts, the diagrams are provided here for the sake of potential comparison to other environments.

SITE J (N 47°47'39" W 123°56'31")
Figure S19 shows facies photographs.

Unit 1 – glacial outwash

- >4 m thick
- Stratified clast-supported pebble-boulder gravel (Gh) with sand lenses (Sm) that fine upwards into interbedded pebbles, sand, and silt (Fl)
    - Horizontal beds are 15-30 cm thick, except where larger boulders are present and disrupt bedding. The longest exposed axis of one boulder reaches ~4 m. Clasts are dominantly sub-angular but range from angular to sub-rounded with very few rounded clasts (Figure A1.20). Large boulders are angular and sub-angular.
    - The horizontal sand and silt beds range from 1-15 cm thick. Sand size ranges from very fine lower to very coarse upper and consists of poorly and moderately sorted angular to sub-angular (with some sub-rounded) grains. Some areas contain trough cross-bedded pebbles (Gt) and sand (St). Pebbles are dominantly subangular but range from angular to sub-rounded (Figure A1.20).
- A preliminary OSL age from a sand bed towards the middle of the unit suggests deposition at 53.0 ka (USU-1284) (Table 3.3).
- This unit represents a glacial outwash package with changing channel dynamics upwards through the sequence. The fining upwards may represent ice retreat.

Unit 2 – lacustrine sediment

- ~3 m thick
- Clear, horizontal and planar, conformable basal contact
- Horizontally bedded sand and silt (Sh) that coarsens upwards to a pebble gravel (Gh).
- This unit represents glaciolacustrine sedimentation.

Unit 3 – glacial outwash

- ~6 m thick
- Clear, horizontal and planar, conformable basalt contact
- Fining upwards, stratified pebble-boulder gravel (Gh) with sand lenses (Sm).
    - Boulders are dominantly angular to sub-angular
- This unit represents a return to glacial outwash deposition.

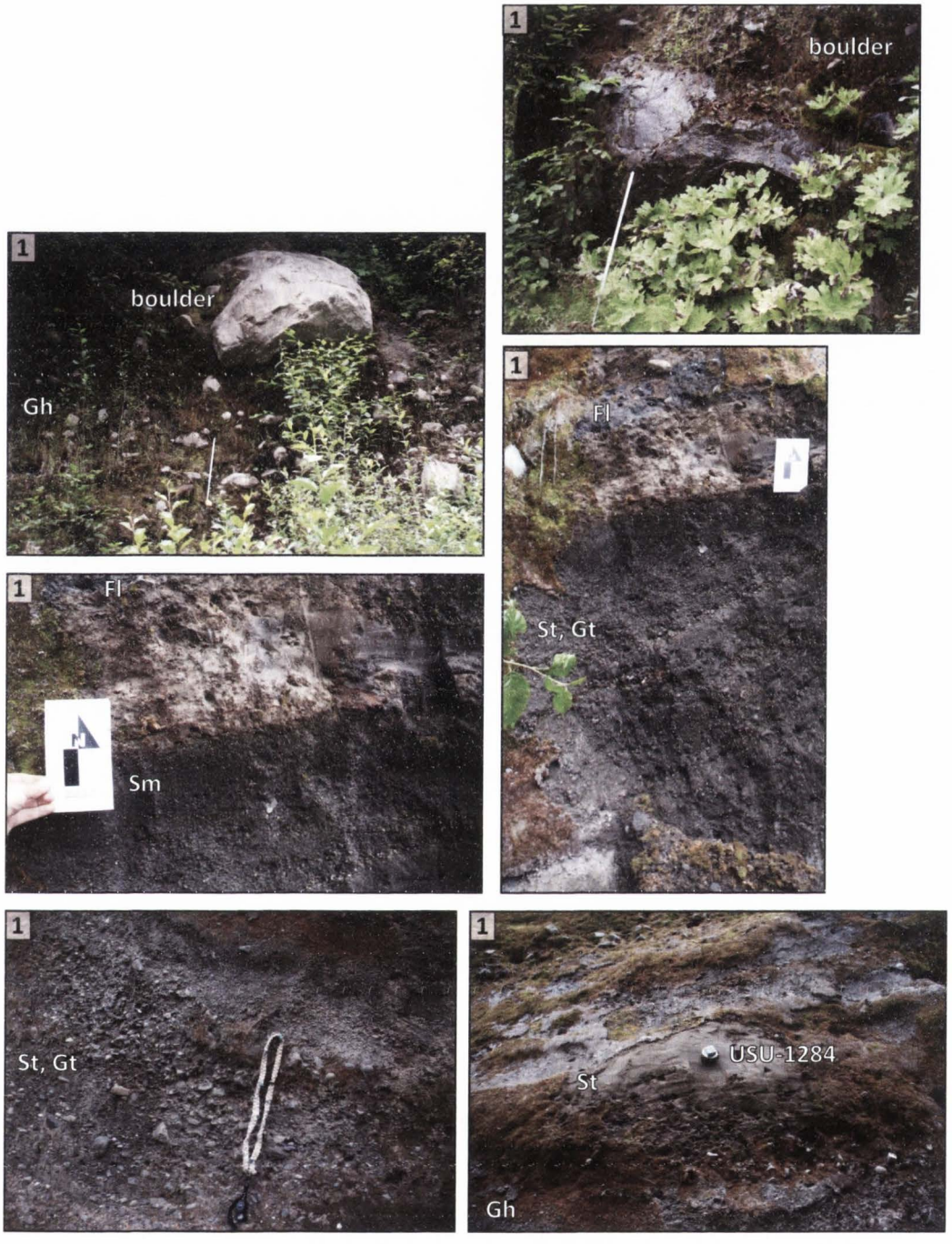

Figure A1.19 Facies photographs from Site J. Numbers represent unit designation, labels represent facies codes as found in Table 3.2.

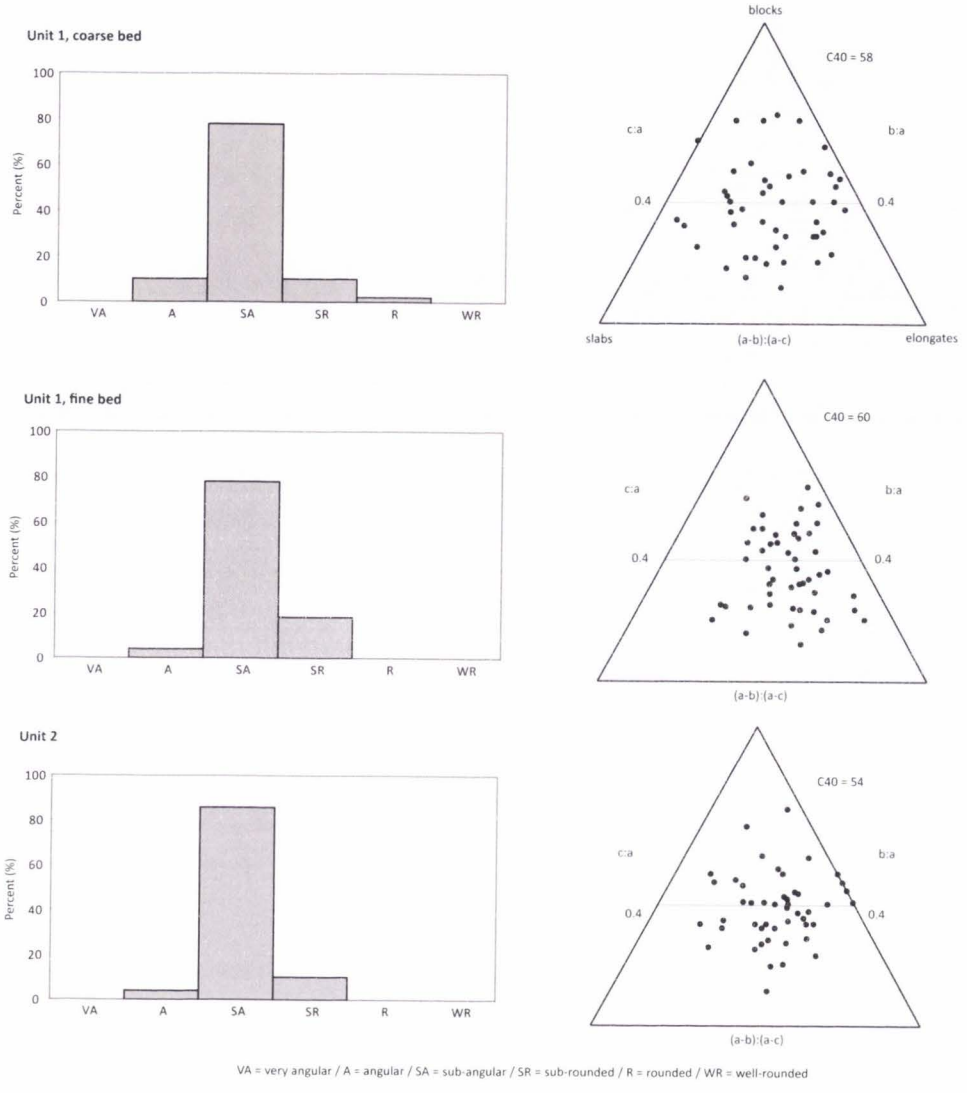

Figure A1.20 Clast shape data for Unit 1 and Unit 2 of Site J. Individual datasets composed of 50 pebble- to gravel-sized clasts. Although the ternary diagrams are of little to no use in distinguishing subglacial and fluvially transported sediments because neither environment is likely to contain many angular clasts, the diagrams are provided here for the sake of potential comparison to other environments.

APPENDIX B

OSL run details

Table A2.1 OSL run details. Table contains detailed information about OSL and IRSL runs from the Lake Hawea, New Zealand and South Fork Hoh River valley, Washington samples

USU Lab number	Location	Grain size (μm)	Irradiation (s) Regen 1	Regen 2	Regen 3	Regen 1'	Preheat (°C)	Preheat (sec)	Cutheat (°C)	Cutheat (sec)	USU Riso	Diode Power (%)	Additional Information
USU-910	Hawea	125-212	100	200	300	100	240	10	160	10	B	70	
			100	350	600	100	240	10	160	10	B	70	
			100	400	200	100	240	10	160	10	A	90	double SAR
			200	400	600	200	240	10	160	10	A	90	
USU-1090	Hawea	150-250	200	600	1000	200	240	10	160	10	B	70	
			200	400	600	200	240	10	160	10	A	90	
			100	200	300	100	240	10	160	10	A	90	
USU-989	SF, Site A	150-212	100	300	500	100	240	10	220	10	A	90	280 SD
			200	500	800	200	240	10	220	10	A	90	
			200	300	400	200	240	10	220	10	B	70	280 SD
			200	300	400	200	240	10	220	10	B	70	280 SD
			100	300	500	100	240	10	220	10	A	90	280 SD
			100	300	500	100	240	10	220	10	A	90	280 SD
			200	600	1000	200	240	10	220	10	A	90	280 SD
USU-990	SF, Site A	150-212	100	300	500	100	240	10	220	10	B	90	
			200	500	800	200	240	10	220	10	A	90	
			200	300	400	200	240	10	220	10	B	70	280 SD
			100	300	500	100	240	10	160	10	A	90	
			100	300	500	100	240	10	220	10	A	90	
			200	600	1000	200	240	10	220	10	A	90	280 SD
			100	300	500	100	240	10	160	10	B	70	
USU-991	SF, Site C	150-212	100	300	500	100	240	10	220	10	B	70	
			200	500	800	200	240	10	220	10	A	90	
			200	500	800	200	240	10	220	10	B	70	
			200	600	1000	200	240	10	160	10	A	90	

			200	500	800	200	240	10	220	10	A	90	
			200	600	1000	200	240	10	160	10	A	90	
USU-1240	SF, Site E	125-250	150	250	350	150	240	10	160	10	B	70	
			100	300	500	100	240	10	160	10	A	90	
			200	600	1000	200	240	10	160	10	A	90	
USU-1241	SF, Site E	125-250	200	500	800	200	240	10	220	10	A	90	
			100	300	500	100	240	10	160	10	A	90	
			200	600	1000	200	240	10	160	10	A	90	
USU-1242	SF, Site D	125-250	150	250	350	150	240	10	220	10	B	70	
			100	300	500	100	240	10	160	10	A	90	
			100	300	500	100	240	10	160	10	B	70	
			200	600	1000	200	240	10	160	10	A	90	
			400	800	1200	400	240	10	160	10	A	90	
USU-1243	SF, Site C	125-250	100	200	300	100	240	10	220	10	A	90	
			100	300	500	100	240	10	160	10	A	90	
			100	300	500	100	240	10	160	10	B	70	
			200	400	600	200	240	10	160	10	A	90	
USU-1282	SF, Site G	90-150	150	250	350	150	240	10	220	10	B	70	
			100	300	500	100	240	10	160	10	A	90	
			200	600	1000	200	240	10	160	10	A	90	280 SD
			100	300	500	100	240	10	160	10	B	70	
USU-1283	SF, Site I	125-212	100	300	500	100	240	10	160	10	A	90	
			200	400	600	200	240	10	160	10	A	90	
			200	600	1000	200	240	10	160	10	A	90	
USU-1284	SF, Site J	150-250	200	500	800	200	240	10	220	10	A	90	
			100	300	500	100	240	10	160	10	A	90	
			400	800	1200	400	240	10	160	10	A	90	

USU-1285	SF, Site F	150-250	100	300	500	100	240	10	160	10	A	90
			200	600	1000	200	240	10	160	10	A	90
			100	300	500	100	240	10	160	10	B	70
			200	600	1000	200	240	10	160	10	A	90

USU Lab number	Location	Grain size (μm)	Irradiation (s) Regen 1	Regen 2	Regen 3	Regen 1'	Preheat (°C)	Preheat (sec)	Cutheat (°C)	Cutheat (sec)	USU Riso	Diode Power (%)	Additional Information
USU-910	Hawea	125-212	500	1250	2000	500	250	60	250	60	A	90	+ fading test
			500	1500	2500	500	250	60	250	60	A	90	+ fading test
			1000	2000	3000	1000	250	60	250	60	B	85	+ fading test
USU-1090	Hawea	150-250	500	1250	2000	500	250	60	250	60	A	90	+ fading test
			500	1500	2500	500	250	60	250	60	A	90	+ fading test
			1000	2000	3000	1000	250	60	250	60	B	85	+ fading test

APPENDIX C

Dose rate data for all OSL samples

Table A3.1 Dose rate data for all OSL samples collected in this research.

SAMPLE: USU-910								
U, Th, Water:	U (ppm)=	2.1	+/-	0.15				
	Th (ppm)=	11	+/-	0.99		Assumed Errors (%):		
	% H2O =	3.5	+/-	1.05		K_2O /K =	2.5	
						U =	7	
	Mean Atten Coeff. b=		0.89			Th =	9	
	%K =	1.04	+/-	0.03		Rb_2O =	4	
	Rb (ppm) =	49.9	+/-	2.0		H_2O =	30	
						Cosmic =	10	
Cosmic:	Fract. of rate to use=		1			Calibration =	7	(Calculated, Aug 2012)
	Cosmic doserate=		0.040	+/-	0.00	DR Conversion =	3	(Assumed)
DATA CALCULATED FROM ABOVE								
Total Doserate=	4.10	+/-	0.21	Gy/ka				
	Alpha	Beta	Gamma					
U:	0.5578	0.2524	0.2254	Gy/ka				
Th:	0.7709	0.2363	0.5067	Gy/ka				
%K:		0.7450	0.2492	Gy/ka				
Rb:		0.0062		Gy/ka				
Cosmic:			0.0387	Gy/ka				

SAMPLE: USU-1090								
U, Th, Water:	U (ppm)=	2.5	+/-	0.18				
	Th (ppm)=	13.6	+/-	1.22		Assumed Errors (%):		
	% H2O =	3.0	+/-	3.00		K_2O /K =	2.5	
						U =	7	
	Mean Atten Coeff. b=		0.86			Th =	9	
	%K =	0.96	+/-	0.02		Rb_2O =	4	
	Rb (ppm) =	50.2	+/-	2.0		H_2O =	100	
						Cosmic =	10	
Cosmic:	Fract. of rate to use=		1			Calibration =	7	(Calculated, Aug 2012)
	Cosmic doserate=		0.101	+/-	0.01	DR Conversion =	3	(Assumed)
DATA CALCULATED FROM ABOVE								
Total Doserate=	4.71	+/-	0.29	Gy/ka				
	Alpha	Beta	Gamma					
U:	0.6687	0.2963	0.2698	Gy/ka				
Th:	0.9598	0.2863	0.6299	Gy/ka				
%K:		0.6828	0.2312	Gy/ka				
Rb:		0.0054		Gy/ka				
Cosmic:			0.0973	Gy/ka				

SAMPLE: USU-989

U, Th, Water:	U (ppm)=	0.9	+/-	0.10				
	Th (ppm)=	2.3	+/-	0.21		Assumed Errors (%):		
	% H2O =	11.2	+/-	3.35		K_2O /K =	2.5	
						U =	11	
	Mean Atten Coeff. b=		0.91			Th =	9	
	%K =	1.08	+/-	0.03		Rb_2O =	4	
	Rb (ppm) =	27.5	+/-	1.1		H_2O =	30	
						Cosmic =	10	
						Calibration =	7	(Calculated, April 09)
Cosmic:	Fract. of rate to use=		1			DR Conversion =	3	(Assumed)
	Cosmic doserate=		0.00	+/-	0.00			

Total Doserate=	1.28	+/-	0.06	Gy/ka
	Alpha	Beta	Gamma	
U:	0.0000	0.0983	0.0891	Gy/ka
Th:	0.0000	0.0448	0.0977	Gy/ka
%K:		0.7050	0.2387	Gy/ka
Rb:		0.0030		Gy/ka
Cosmic:			0.0003	Gy/ka

SAMPLE: USU-990

U, Th, Water:	U (ppm)=	1	+/-	0.10				
	Th (ppm)=	2.6	+/-	0.23		Assumed Errors (%):		
	% H2O =	4.8	+/-	3.00		K_2O /K =	2.5	
						U =	10	
	Mean Atten Coeff. b=		0.90			Th =	9	
	%K =	0.83	+/-	0.02		Rb_2O =	4	
	Rb (ppm) =	27.2	+/-	1.1		H_2O =	62	
						Cosmic =	10	
						Calibration =	7	(Calculated, April 09)
Cosmic:	Fract. of rate to use=		1			DR Conversion =	3	(Assumed)
	Cosmic doserate=		0.00	+/-	0.00			

DATA CALCULATED FROM ABOVE				
Total Doserate=	1.18	+/-	0.05	Gy/ka
	Alpha	Beta	Gamma	
U:	0.0000	0.1174	0.1058	Gy/ka
Th:	0.0000	0.0544	0.1181	Gy/ka
%K:		0.5823	0.1960	Gy/ka
Rb:		0.0031		Gy/ka
Cosmic:			0.0006	Gy/ka

SAMPLE: USU-991

U, Th, Water:	U (ppm)=	1	+/-	0.10			
	Th (ppm)=	3.2	+/-	0.29		Assumed Errors (%):	
	% H2O =	4.7	+/-	3.00		K_2O /K =	2.5
						U =	10
	Mean Atten Coeff. b=		0.90			Th =	9
	%K =	1.04	+/-	0.03		Rb_2O =	4
	Rb (ppm) =	37.3	+/-	1.5		H_2O =	64
						Cosmic =	10
						Calibration =	7 (Calculated, April 09)
Cosmic:	Fract. of rate to use=		1			DR Conversion =	3 (Assumed)
	Cosmic doserate=		0.16	+/-	0.02		

DATA CALCULATED FROM ABOVE				
Total Doserate=	1.57	+/-	0.07	Gy/ka
	Alpha	Beta	Gamma	
U:	0.0000	0.1176	0.1060	Gy/ka
Th:	0.0000	0.0671	0.1455	Gy/ka
%K:		0.7309	0.2460	Gy/ka
Rb:		0.0043		Gy/ka
Cosmic:			0.1512	Gy/ka

SAMPLE: USU-1240

U, Th, Water:	U (ppm)=	0.9	+/-	0.10			
	Th (ppm)=	2.7	+/-	0.24		Assumed Errors (%):	
	% H2O =	3.8	+/-	3.00		K_2O /K =	2.5
						U =	11
	Mean Atten Coeff. b=		0.90			Th =	9
	%K =	0.9	+/-	0.02		Rb_2O =	4
	Rb (ppm) =	30.4	+/-	1.2		H_2O =	80
						Cosmic =	10
						Calibration =	7 (Calculated, Aug 2012)
Cosmic:	Fract. of rate to use=		1			DR Conversion =	3 (Assumed)
	Cosmic doserate=		0.13	+/-	0.01		

DATA CALCULATED FROM ABOVE				
Total Doserate=	1.36	+/-	0.06	Gy/ka
	Alpha	Beta	Gamma	
U:	0.0000	0.1065	0.0963	Gy/ka
Th:	0.0000	0.0569	0.1240	Gy/ka
%K:		0.6377	0.2150	Gy/ka
Rb:		0.0034		Gy/ka
Cosmic:			0.1222	Gy/ka

SAMPLE: USU-1241

U, Th, Water:	U (ppm)=	0.8	+/-	0.10				
	Th (ppm)=	2.5	+/-	0.23		Assumed Errors (%):		
	% H2O =	20.7	+/-	6.20		K_2O /K =	2.5	
						U =	13	
	Mean Atten Coeff. b=		0.90			Th =	9	
	%K =	0.8	+/-	0.02		Rb_2O =	4	
	Rb (ppm) =	26.9	+/-	1.1		H_2O =	30	
						Cosmic =	10	
								(Calculated,
						Calibration =	7	Aug 2012)
Cosmic:	Fract. of rate to use=		1			DR Conversion =	3	(Assumed)
	Cosmic doserate=		0.09	+/-	0.01			

DATA CALCULATED FROM ABOVE				
Total Doserate=	1.00	+/-	0.06	Gy/ka
	Alpha	Beta	Gamma	
U:	0.0000	0.0788	0.0723	Gy/ka
Th:	0.0000	0.0438	0.0969	Gy/ka
%K:		0.4717	0.1613	Gy/ka
Rb:		0.0025		Gy/ka
Cosmic:			0.0727	Gy/ka

SAMPLE: USU-1242

U, Th, Water:	U (ppm)=	0.9	+/-	0.10				
	Th (ppm)=	2.8	+/-	0.25		Assumed Errors (%):		
	% H2O =	25.0	+/-	7.49		K_2O /K =	2.5	
						U =	11	
	Mean Atten Coeff. b=		0.90			Th =	9	
	%K =	0.8	+/-	0.02		Rb_2O =	4	
	Rb (ppm) =	26.7	+/-	1.1		H_2O =	30	
						Cosmic =	10	
								(Calculated,
						Calibration =	7	Aug 2012)
Cosmic:	Fract. of rate to use=		1			DR Conversion =	3	(Assumed)
	Cosmic doserate=		0.12	+/-	0.01			

DATA CALCULATED FROM ABOVE				
Total Doserate=	1.02	+/-	0.07	Gy/ka
	Alpha	Beta	Gamma	
U:	0.0000	0.0850	0.0782	Gy/ka
Th:	0.0000	0.0471	0.1044	Gy/ka
%K:		0.4522	0.1551	Gy/ka
Rb:		0.0024		Gy/ka
Cosmic:			0.0935	Gy/ka

SAMPLE: USU-1243

U, Th, Water:	U (ppm)=	0.9	+/-	0.10	
	Th (ppm)=	2.8	+/-	0.25	
	% H2O =	17.8	+/-	5.34	
	Mean Atten Coeff. b=		0.90		
	%K =	0.95	+/-	0.02	
	Rb (ppm) =	30.5	+/-	1.2	
Cosmic:	Fract. of rate to use=		1		
	Cosmic doserate=		0.01	+/-	0.00

Assumed Errors (%):		
K_2O /K =	2.5	%
U =	11	%
Th =	9	%
Rb_2O =	4	%
H_2O =	30	%
Cosmic =	10	% (Calculated,
Calibration =	7	Aug 2012)
DR Conversion =	3	(Assumed)

DATA CALCULATED FROM ABOVE				
Total Doserate=	1.12	+/-	0.07	Gy/ka
	Alpha	Beta	Gamma	
U:	0.0000	0.0912	0.0835	Gy/ka
Th:	0.0000	0.0505	0.1115	Gy/ka
%K:		0.5765	0.1967	Gy/ka
Rb:		0.0030		Gy/ka
Cosmic:			0.0083	Gy/ka

SAMPLE: USU-1282

U, Th, Water:	U (ppm)=	1.35	+/-	0.10	
	Th (ppm)=	3.75	+/-	0.34	
	% H2O =	13.5	+/-	4.04	
	Mean Atten Coeff. b=		0.93		
	%K =	1.33	+/-	0.03	
	Rb (ppm) =	43.9 ave of 2 samples	+/-	1.8	
Cosmic:	Fract. of rate to use=		1		
	Cosmic doserate=		0.15	+/-	0.01

Assumed Errors (%):		
K_2O /K =	2.5	%
U =	7.4	%
Th =	9	%
Rb_2O =	4	%
H_2O =	30	%
Cosmic =	10	% (Calculated,
Calibration =	7	Aug 2012)
DR Conversion =	3	(Assumed)

DATA CALCULATED FROM ABOVE				
Total Doserate=	1.80	+/-	0.09	Gy/ka
	Alpha	Beta	Gamma	
U:	0.0000	0.1496	0.1306	Gy/ka
Th:	0.0000	0.0753	0.1557	Gy/ka
%K:		0.8679	0.2872	Gy/ka
Rb:		0.0064		Gy/ka
Cosmic:			0.1260	Gy/ka

SAMPLE: USU-1283

U, Th, Water:	U (ppm)=	1.1	+/-	0.10	
	Th (ppm)=	3.5	+/-	0.32	
	% H2O =	23.5	+/-	7.04	
	Mean Atten Coeff. b=		0.90		
	%K =	0.81	+/-	0.02	
	Rb (ppm) =	30.3	+/-	1.2	
Cosmic:	Fract. of rate to use=		1		
	Cosmic doserate=		0.07	+/-	0.01

Assumed Errors (%):		
K_2O /K =	2.5	%
U =	9.1	%
Th =	9	%
Rb_2O =	4	%
H_2O =	30	%
Cosmic =	10	% (Calculated,
Calibration =	7	Aug 2012)
DR Conversion =	3	(Assumed)

DATA CALCULATED FROM ABOVE

Total Doserate= 1.08 +/- 0.07 Gy/ka

	Alpha	Beta	Gamma	
U:	0.0000	0.1067	0.0969	Gy/ka
Th:	0.0000	0.0607	0.1323	Gy/ka
%K:		0.4683	0.1592	Gy/ka
Rb:		0.0031		Gy/ka
Cosmic:			0.0524	Gy/ka

SAMPLE: USU-1284

U, Th, Water:	U (ppm)=	1.1	+/-	0.10	
	Th (ppm)=	3	+/-	0.27	
	% H2O =	19.9	+/-	5.97	
	Mean Atten Coeff. b=		0.89		
	%K =	0.72	+/-	0.02	
	Rb (ppm) =	26.7	+/-	1.1	
Cosmic:	Fract. of rate to use=		1		
	Cosmic doserate=		0.13	+/-	0.01

Assumed Errors (%):		
K_2O /K =	2.5	%
U =	9.1	%
Th =	9	%
Rb_2O =	4	%
H_2O =	30	%
Cosmic =	10	% (Calculated,
Calibration =	7	Aug 2012)
DR Conversion =	3	(Assumed)

DATA CALCULATED FROM ABOVE

Total Doserate= 1.06 +/- 0.06 Gy/ka

	Alpha	Beta	Gamma	
U:	0.0000	0.1083	0.1001	Gy/ka
Th:	0.0000	0.0525	0.1171	Gy/ka
%K:		0.4255	0.1462	Gy/ka
Rb:		0.0024		Gy/ka
Cosmic:			0.1047	Gy/ka

SAMPLE: USU-1285

U, Th, Water:	U (ppm)=	1.3	+/-	0.10	
	Th (ppm)=	3.5	+/-	0.32	
	% H2O =	15.2	+/-	4.55	
	Mean Atten Coeff. b=		0.89		
	%K =	0.96	+/-	0.02	
	Rb (ppm) =	35.6	+/-	1.4	
Cosmic:	Fract. of rate to use=		1		
	Cosmic doserate=		0.03	+/-	0.00

Assumed Errors (%):		
K_2O /K =	2.5	%
U =	7.7	%
Th =	9	%
Rb_2O =	4	%
H_2O =	30	%
Cosmic =	10	% (Calculated,
Calibration =	7	Aug 2012)
DR Conversion =	3	(Assumed)

DATA CALCULATED FROM ABOVE

Total Doserate= 1.29 +/- 0.07 Gy/ka

	Alpha	Beta	Gamma	
U:	0.0000	0.1344	0.1237	Gy/ka
Th:	0.0000	0.0643	0.1429	Gy/ka
%K:		0.5955	0.2039	Gy/ka
Rb:		0.0033		Gy/ka
Cosmic:			0.0254	Gy/ka